A Wave Climate Study of the Northern British Columbia Coast

Final Report

Volume II: Wave Properties and Wave Prediction

D.O. Hodgins, P.H. LeBlond,
D.S. Dunbar and C.T. Niwinski*

Marine Environmental Data Services Branch
Department of Fisheries and Oceans
Ottawa, Ontario K1A 0E6

March 1988

Canadian Contractor Report of Hydrography and Ocean Sciences No. 22

* Seaconsult Marine Research Ltd., Vancouver, B.C.

Fisheries and Oceans   Pêches et Océans

Canada

Canadian Technical Report of Hydrography and Ocean Sciences

These reports contain scientific and technical information of a type that represents a contribution to existing knowledge but which is not normally found in the primary literature. The subject matter is generally related to programs and interests of the Ocean Science and Surveys (OSS) sector of the Department of Fisheries and Oceans.

Technical Reports may be cited as full publications. The correct citation appears above the abstract of each report. Each report will be abstracted in Aquatic Sciences and Fisheries Abstracts. Reports are also listed in the Department's annual index to scientific and technical publications.

Technical Reports are produced regionally but are numbered and indexed nationally. Requests for individual reports will be fulfilled by the issuing establishment listed on the front cover and title page. Out of stock reports will be supplied for a fee by commercial agents.

Regional and headquarters establishments of Ocean Science and Surveys ceased publication of their various report series as of December 1981. A complete listing of these publications and the last number issued under each title are published in the *Canadian Journal of Fisheries and Aquatic Sciences*, Volume 38: Index to Publications 1981. The current series began with Report Number 1 in January 1982.

Rapport technique canadien sur l'hydrographie et les sciences océaniques

Ces rapports contiennent des renseignements scientifiques et techniques qui constituent une contribution aux connaissances actuelles mais que l'on ne trouve pas normalement dans les revues scientifiques. Le sujet est généralement rattaché aux programmes et intérêts du service des Sciences et Levés océaniques (SLO) du ministère des Pêches et des Océans.

Les rapports techniques peuvent être considérés comme des publications à part entière. Le titre exact figure au-dessus du résumé du chaque rapport. Les résumés des rapports seront publiés dans la revue Résumés des sciences aquatiques et halieutiques et les titres figureront dans l'index annuel des publications scientifiques et techniques du Ministère.

Les rapports techniques sont produits à l'échelon régional mais sont numérotés et placés dans l'index à l'échelon national. Les demandes de rapports seront satisfaites par l'établissement auteur dont le nom figure sur la couverture et la page de titre. Les rapports épuisés seront fournis contre rétribution par des agents commerciaux.

Les établissements des Sciences et Levés océaniques dans les régions et à l'administration centrale ont cessé de publier leurs diverses séries de rapports depuis décembre 1981. Vous trouverez dans l'index des publications du volume 38 du *Journal canadien des sciences halieutiques et aquatiques*, la liste de ces publications ainsi que le dernier numéro paru dans chaque catégorie. La nouvelle série a commencé avec la publication du Rapport n° 1 en janvier 1982.

Canadian Contractor Report of

Hydrography and Ocean Sciences 22

March 1988

A WAVE CLIMATE STUDY OF THE NORTHERN BRITISH COLUMBIA COAST

FINAL REPORT

VOLUME II: WAVE PROPERTIES AND WAVE PREDICTION

by

D.O. Hodgins, P.H. LeBlond, D.S. Dunbar and C.T. Niwinski

Seaconsult Marine Research Ltd.

405 - 1200 West 73rd Avenue

Vancouver, British Columbia

Canada V6P 6G5

Marine Environmental Data Services Branch

Department of Fisheries and Oceans

Ottawa, Ontario

K1A 0E6

This report was prepared by:

Seaconsult Marine Research Ltd., Vancouver, British Columbia, under DSS Contract OSS82-00053.

Scientific Authority - J.R. Wilson, MEDS.

Correct citation for this publication:

Hodgins, D.O., P.H. LeBlond, D.S. Dunbar and C.T. Niwinski. 1985. A wave climate study of the northern British Columbia coast, final report, volume II: Wave properties and wave prediction. Can. Contract. Rep. Hydrogr. Ocean Sci. 22:69 p. + app.

Canadian Contractor Report of Hydrography and Ocean Sciences No. 22 consists of two volumes.

Volume I: Wave Observations

Volume II: Wave Properties and Wave Prediction

Cat. No. Fs 97-17/22E ISSN 0711-6748

ABSTRACT

Hodgins, D.O., P.H. LeBlond, D.S. Dunbar and C.T. Niwinski. 1985. A wave climate study of the northern British Columbia coast, final report, volume II: Wave properties and wave prediction. Can. Contract. Rep. Hydrogr. Ocean Sci. 22:69 p. + app.

Key results from two years of wave measurements in Queen Charlotte Sound, Dixon Entrance and Hecate Strait are discussed in this report. Directional wave analysis following Long's (1980) approach has been investigated. It has been concluded that the method of determining the goodness-of-fit of spreading models proposed by Long is inappropriate. Use of the full set of data equations was found not to improve the algorithm and further research of this problem is warranted. Properties of the Wallops spectrum have been investigated with the new wave period-slope measurements. This has confirmed many of the essential features, indicating that the Wallops form is a verifiable alternative to total energy-period spectral models. The data set was limited and further tests are recommended as more direct measurements of sea surface slope become available. The data base collected in the present study is useful for specifying normal wave criteria; however, it is too short for a reliable prediction of extreme wave heights, and wave hindcasting is recommended. A discrete spectral model, incorporating shallow water effects, would be best suited to the area. Small scale, rapidly moving storms appear to cause the most severe sea states in the coastal waters. Present knowledge of their frequency, size, speed of advance and trajectory is inadequate for wave hindcasting, and detailed study of these storms, prior to finalizing hindcast/forecast model design, is recommended. Wind correlations between McKenney Rock and Cape St. James have also shown that reliable overwater winds cannot be inferred with confidence from that coastal station. The wind station on McKenney Rock thus appears necessary for predicting or verifying overwater winds in Queen Charlotte Sound-Hecate Strait.

RÉSUMÉ

Hodgins, D.O., P.H. LeBlond, D.S. Dunbar and C.T. Niwinski. 1985. A wave climate study of the northern British Columbia coast, final report, volume II: Wave properties and wave prediction. Can. Contract Rep. Hydrogr. Ocean Sci. 22:69 p. + app.

Le présent rapport examine les résultats les plus importants découlant de deux années de mesures des vagues dans les détroits de la Reine-Charlotte et d'Hecate ainsi que dans l'entrée Dixon. L'analyse directionnelle des vagues suivant la méthode de Long (1980) a été étudiée. La méthode proposée par Long pour déterminer la précision de l'ajustement pour les modèles de propagation ne convient pas. L'utilisation de l'ensemble des équations n'améliore pas l'algorithme et d'autres recherches concernant ce problème sont justifiées. Les propriétés du spectre de Wallops ont été étudiées au moyen des nouvelles mesures période-pente; cela a confirmé un grand nombre des caractéristiques essentielles, et indique que la forme de Wallops constitue une solution de remplacement vérifiable aux modèles spectraux énergie total - période. L'ensemble de données était restreint et il est recommandé d'effectuer d'autres essais lorsque des mesures plus directes de la pente de la surface de la mer deviendront disponibles. La base de données recueillies dans le cadre de la présente étude est utile pour la spécification des critères normaux des vagues; toutefois elle porte sur une durée trop courte pour permettre des prévisions fiables des hauteurs extrêmes des vagues et l'on recommande la prévision a posteriori des vagues. Un modèle spectral discret incorporant les effets des eaux peu profondes serait le mieux adapté à la région. Les tempêtes à petite échelle se déplaçant rapidement semblent soulever les plus mauvaises mers dans les eaux côtières. Les connaissances actuelles sur la fréquence, les dimensions, la vitesse de progression et les trajectoires de ces tempêtes sont inadéquates pour la prévision a posteriori des vagues et l'on recommande une étude détaillée de ces tempêtes avant le parachèvement de la conception du modèle de prévision a posteriori / prévision. Des corrélations sur les vents entre le rocher McKenney et le cap St. James ont également montré que l'on ne peut établir avec un niveau de confiance élevé des valeurs fiables pour les vents soufflant sur l'eau à partir des données provenant de cette station côtière. La station de mesure des vents sur le rocher McKenney semble donc nécessaire pour la prévision ou la vérification des vents soufflant sur l'eau dans les détroits de la Reine-Charlotte et d'Hecate.

TABLE OF CONTENTS

LIST OF TABLES

Table

LIST OF FIGURES

Figure

Figure

Figure

List of Acronyms

CSJ - Cape St. James (wind station)

GF - Groupiness Factor

METOC - Meteorological and Oceanographic Centre - Department of National Defense, Canada

MR - McKenney Rock (wind station)

NDBO - National Data Buoy Office (U.S.)

NEDN - Naval (U.S.) Environmental Data Network

SOWM - Spectral Ocean Wave Model (U.S. Navy)

SSMO - Summary of Synoptic Meteorological Observations

WAVEC - Directional wave buoy manufactured by Datawell, b.v.

WRIPS - Waverider buoy modified for satellite data transmission

SIWEH - Smoothed Instantaneous Wave Energy History

A note on notations

Three different symbols are used in the text for significant wave height, with the following meanings:

1) H_s - derived from wave hindcast models or measurements; used interchangeably with Hm_o

2) Hm_o - derived as 4 times the square root of the total energy in the wave spectrum; spectrum may be measured or hindcast

3) $H_{1/3}$ - strictly defined as the average height of the $1/3$ highest waves in a record, as determined by a zero-upcrossing analysis.

Other symbols are defined in the test where they first appear.

1.0 INTRODUCTION

Between the fall of 1982 and spring 1984 an extensive program of wave measurements was made in Dixon Entrance, Hecate Strait and Queen Charlotte Sound. The program aimed at documenting wave conditions for the first time at six distinct locations, some exposed directly to Pacific Ocean storms and some more sheltered in the inner waters (Fig. 1.1). Differing buoy types were used, including two directional instruments, and two Waveriders modified for satellite data transmission (WRIPS buoys). All aspects of the field program, including an evaluation of instrument performance, are described in Volume I of this report, prepared by Seakem Oceanography Ltd.

The purpose of this volume is to discuss some of the key results, and to present original findings concerning methods of analyzing directional wave measurements, factors governing wave directionality, and strategies for hindcasting normal and extreme sea states in the coastal waters. The report is divided into three principal chapters. The first of these (Chapter 2) presents basic wave climate statistics derived from the measurements. These are standard data products used for planning marine operations, and as they are rather self-explanatory, they are given without much discussion. Chapter 2 includes estimates of extreme wave heights derived both from offshore buoy measurements (not made in this program) and from the new measurements, together with some preliminary results on wave grouping.

Chapter 3 deals with directional wave studies. New results on the effects of bathymetric refraction are given, both to illustrate areas of wave convergence (severe conditions) near the coastline, and to examine factors that play an important role in observed wave directions at the measurements locations. One of the key questions in directional wave data processing is how to represent energy spreading about the mean wave direction in the spectrum. Long (1980) and others have proposed methods for estimating the goodness-of-fit of the cosine-power model for spread: these methods are examined in detail in this chapter, and with application to the new data are shown to be unsatisfactory. This does not cast doubt on the cosine-power model but rather on present algorithms for the goodness-of-fit test. Finally we examine relations between measured slopes and wave heights with a view to testing the validity of predictions from the Wallop's spectrum. This spectral form differs from more conventional parametric equations in that it is defined in terms of a significant wave slope and dominant wave period. This leads to support for the Huang et al. (1984) joint probability model for slope and surface elevation.

In Chapter 4 the question of extreme wave height prediction is examined. This is done by first assessing available measurements which demonstrates that existing data bases are too short in duration and too limited in coverage to give reliable estimates. This leads to the requirement for wave hindcasting: the factors governing accurate hindcast results in the coastal waters are then discussed in detail. The chapter concludes with a recommended strategy for an extreme wave hindcast.

2.0 THE WAVE CLIMATE OF B.C. COASTAL WATERS

2.1 Summary of Earlier Measurements

Before the program described in this report was undertaken, only two instrumental wave measuring stations had been regularly operated in B.C. waters; one was located off Tofino, well to the south of the area of interest, the other in Prince Rupert Harbour, in sheltered waters. Neither of these stations could provide information on wave conditions in exposed areas of the northern B.C. coast. Measurements were also made for short periods (a few days to 1½ months) at five well locations drilled by Shell Canada in 1968-69, as reported by Watts and Faulkner (1968) and Hafer (1970). While these latter measurements were not sufficiently long-lasting to make a significant contribution to the knowledge of local wave climatology, they indicated occurrences of very severe winter wave conditions, with combined sea and swell wave heights of up to 58 ft.

Visual observations are usually considered less reliable than instrumental data. They do nevertheless provide information which may be useful to mariners. Phillips (1977) compiled ship-based wave observations in a preliminary marine climatology of the area of interest. Ships tend to avoid storms and may tend to give sea state reports that are biased towards lower values. A drilling rig is less mobile, and in the fall of 1968 the SEDCO 135F, drilling for Shell, encountered a 95-ft wave in Hecate Strait. The wave height was visually estimated from the lowest and highest water levels observed on the structure of the platform.

These occasional observations of severe seas provided much of the impetus for the observational program described here.

2.2 Assessment of New Measurements

It is possible to give an overall appraisal of the quality of the new data through comparisons with independent sources of wave data (visual estimates and Defense Department wave analysis charts), through correlations of measurements from adjacent instruments, and through wave height and direction correlations with wind. The results of this type of assessment, using some of the data measured early in the field program, are discussed below.

a) Comparison With Other Data

METOC Wave Height Charts

The Canadian Forces Meteorological and Oceanographic Centre (METOC) in Esquimalt, B.C. produces wave analyses based on a combination of visual observations, instrumental measurements (from U.S. National Data Buoy Office 10 m discus buoys in the Pacific Ocean) and elementary forecasts of wave conditions. Experience in the North Atlantic (Neu, 1982; 1984) has shown that the METOC products give a reasonably good indication of the spatial and temporal character of significant wave heights. Fig. 2.1 shows a comparison of significant wave height measured in the mouth of Queen Charlotte Sound (Station 216) with the 12-hourly METOC chart wave heights for October through December 1982. Six moderately severe storms were predicted by METOC in close agreement with the measured values, and the variations in wave height generally agree well also. The similarity between the two time series serves mainly to verify the METOC procedures, but provides reassurance that nothing is seriously wrong with the measurements.

Visual Observations

A preliminary comparison of wave height exceedances in October through December 1982, as measured at Stations 215 (inner Queen Charlotte Sound) and 213 (Bonilla Island), with SSMO (Summary of Synoptic Meteorological Observations) is given in Table 2.1. The instrumental wave height exceedances, based only on one month of data compared with the much longer time span of visual observations, vary in the degree of agreement with the visual data. The December data at both stations are in reasonable agreement, although the October (at Station 215) - November (at Station 213) results at low wave heights show a less severe measured climate than given by visual observations. Considering the limitations of the data sets (visual estimates on one hand, and the short sample period on the other) we conclude that the measured wave data are consistent with other information available for the coastal waters.

b) Comparison of Adjacent Instruments

The dimensions of wave-generating storms are so much larger than the spacing between the instruments deployed in this program that one should expect a considerable degree of similarity between the outputs of adjacent wave-measuring buoys. Without expecting exact coincidences in time series of significant wave height (H_s) and peak period (T_p) there should certainly appear a resemblance in their variations over the time scales of storms, i.e. a few days. Such a resemblance is quite evident in the comparison of data at Stations 215 and 216 (Fig. 2.2a). Time series from more widely separated station pairs (212 and 216) still show considerable similarity (Fig. 2.2b) although time lags, probably associated with both storm movement and wave propagation, are evident between the two time series. The close coincidence in T_p values at the station pair (212 - 216), exposed to offshore swell provides reassurance that those instruments are faithfully registering the same events.

c) Directional Verification

The consistency of directional wave information obtained by the Endeco (Station 213) and WAVEC (Station 214) buoys was verified in two ways. The direction of high frequency waves was compared to that of the wind at the nearest meteorological station; it is expected that waves near the peak of the spectrum will run in the same direction as the wind. The direction of swell propagation, on the other hand, is largely independent of that of the wind, and is governed by the offshore incident direction and the refraction to which swell is subjected in shallow water.

Bonilla Island

Fig. 2.3 shows a comparison between wind, and waves measured with the Endeco buoy at Bonilla Island. The mean wave direction at the peak frequency is plotted here. Wave directions are more variable than those of the wind, although there is a tendency for the two to align when the significant wave height exceeds 2 m. This is illustrated in more detail for the storm on November 26, 1982 (Fig. 2.4). A comparison of onshore wave direction occurrences with those of onshore winds (i.e. excluding winds from the north, northeast and east octants) shows a reasonable correspondence at the highest sampled frequency (f = 0.417 Hz; T = 2.4 s) when the significant wave height exceeds 2 m (Fig. 2.5). Nevertheless, the overall seasonal statistics of wave direction are expected to show much more scatter than those of wind directions.

Swell directions at Bonilla Island are constrained by refraction in Hecate Strait. At a period of 16 s for typical swell, the refraction analysis given below (Section 3.1) restricts directions of arrival to a range of angles 150° to 170° true. Allowing for deflection by tidal currents of speeds of the order of 2 m/s would broaden the cone by 25° on each side, i.e. from 125° to 195° true at extreme limits. Inspection of the distribution of low-frequency arrival direction (Fig. 2.6) shows that swell directions measured by the Endeco buoy do not fall within the expected sector. Selecting a wave height threshold level of Hm_o = 2 m does not improve the situation. Repeating the test at an adjacent frequency band (f = 0.075 Hz; T = 13.3 s) confirms the picture.

Further analysis of directionality using the model fitting algorithms discussed in Section 3.2 also confirms the inadequacy of the Endeco buoy for detecting swell directions. These results indicate that this particular instrument is capable of responding to the direction of high-frequency locally-generated wind waves of sufficient energy, but that it may not be relied upon as an indicator of swell direction.

McInnes Island

Comparisons of wind directions at McKenney Rock, where a weather station was installed as part of this program, and mean wave directions at the peak of the spectrum at McInnes Island (Station 214) show reasonable agreement (Fig. 2.7a,b). In contrast to the Endeco buoy, wave directions here are less variable than the wind directions, despite the relatively low sea states. Comparisons with winds obtained on an hourly basis at the Atmospheric Environment Services station at McInnes Island itself (cf. below, Section 3.2, Fig. 3.12) indicate a very close agreement with the directions of locally-generated wind waves (periods 5 to 10 s). Swell directions (Fig. 2.8) are seen to gather about the SSW direction, as would be expected from the location of the station and refractive effects.

Our conclusion is that directional wave measurements at Station 214 appear reliable at all wave frequencies.

2.3 Wave Statistics Based On New Data

The data available from each measurement station have been analyzed to give a number of standard statistical distributions and parameter values useful for marine operations. The time span of data collection was too short to provide monthly distributions; however, where possible four seasonal categories:

Fall	Sept.,Oct.,Nov., 1982,1983
Winter	Dec., 1982,1983; Jan.,Feb., 1983,1984
Spring	Mar.,Apr.,May, 1983,1984
Summer	Jun.,Jul.,Aug., 1983

have been used. Annual statistics have been computed for the calendar year 1983.

a) Wave Height Exceedance

Exceedance diagrams for significant wave height are presented in Fig. 2.9 and 2.10 for annual and seasonal categories. Each curve is plotted from the cumulative distribution of 3-hourly or hourly (Langara East and West) measurements of Hm_o.

The seasonal diagrams for Queen Charlotte Sound, and to a lesser extent, Langara West, show clearly the changing conditions from summer to winter in the swell wave range, as well as in the large wave height range.

b) Joint Statistics of Wave Heights and Periods

Joint histograms of significant wave height and peak period are shown in Fig. 2.11 for all stations and all four seasons (except at Bonilla Island where no summer data were available). Yearly joint histograms for each station are shown in Fig. 2.12. These figures clearly show the presence of swell at periods of 14 to 22 s and its relative frequency of occurrence and strength at different stations and seasons. A comparison of winter to summer statistics at Langara West (Station 211), for example, illustrates the marked difference in wave heights at all periods, and the much larger swells seen on the outer coast during the winter months. A comparison of conditions at Stations 211 and 212, on opposite sides of Learmonth Bank, illustrates the relative decrease in swell intensity at the latter station due to the shadowing effect of the Bank. This point is examined in more detail in the refraction analysis presented in Section 3.1.

c) Operational Wave Criteria

The most frequent joint occurrence of significant wave height and peak period defines the operational wave criterion for each station in a given seasonal or annual category. These values are listed in Table 2.2.

It is important to note that in contrast to other areas (e.g. Scotian Shelf) operational criteria at some stations here appear to result from swell rather than locally generated seas, both on a seasonal and annual basis. This emphasizes the relative importance of long period swell for planning operations in these waters.

d) Spatial Distributions of Height and Period

The distribution of mean and maximum values of significant wave height H_s and spectral peak period T_p are shown in Fig. 2.13 for the year 1983. There is a clear decrease in both mean and maximum H_s from the more exposed stations (216 - Queen Charlotte Sound; 211 - Dixon Entrance) towards shore. The mean and maximum peak period values are less spatially dependent, indicating that swell from offshore (responsible for the larger T_p values) reaches the nearshore Stations 213, 214 and 215.

Tables 2.3 and 2.4 compare annual and seasonal estimates of mean and extreme values of H_s and T_p at the measuring stations. No summer data were collected at Station 213 (Bonilla Island). These tables show that wave heights are largest during winter and fall seasons and lowest during summer. As for annual statistics, the differences in peak period values are less pronounced than those of wave heights. Peak periods show a slight maximum during winter.

e) Wave Height and Period Persistence

The average and the maximum number of consecutive days over which were observed waves of a significant height greater than an assigned value are plotted in the bottom panel of Fig. 2.14 for each season at each station. Also shown, in the top panel of the same figure, are the number of days of favourable conditions, over which waves had a significant height smaller than an assigned value. The relative severity of wave conditions at different stations and during different seasons is a function of the duration as well as of the height of the waves observed. A comparison of summer and winter conditions at all stations reveals clearly that big waves last longer in the winter. Persistences also appear to depend much more strongly on season than on location.

Annual persistence diagrams are presented in Fig. 2.15.

The average and maximum persistences of wave periods are shown for each station and season in Fig. 2.16. Annual statistics appear in Fig. 2.17. We note that the average persistence is remarkably flat across the range of periods observed. Variations in average, and particularly maximum persistences, are apparent between stations and seasons.

f) Directional Wave Statistics

The directional statistics of wave heights and periods at McInnes Island (Station 214) are shown in joint histograms in Fig. 2.18 and 2.19 on seasonal and annual bases.

Wave directions at McInnes Island are almost exclusively from quadrants between SSE and WNW, i.e. from the ocean side of the compass, with a preponderance of up-coast (i.e. from SSE - SW) rather than down-coast (i.e. from WNW - N) directions at all seasons. These wave directions are consistent with those of the wind at these stations (Phillips, 1977). Swell directions, with peak periods of 14 s and above, are not noticeably different from those of higher-frequency locally generated waves; this feature is a consequence of refraction in Hecate Strait and Queen Charlotte Sound. Directional persistence tables on a seasonal and annual basis are shown in Fig. 2.20 and Fig. 2.21 for McInnes Island.

g) Extreme Wave Heights

Available databases from which one may derive extreme wave height estimates are all limited. In deeper waters offshore, data spanning 7 to 8 years are obtainable from the NDBO buoys, particularly Station 46004 in the Eastern Gulf of Alaska, (Fig. 4.1) and from the Naval Environmental Data Network (NEDN) based on hindcast sea states using the U.S. Navy Spectral model (SOWM). Data from the NDBO buoys are considered in detail in Section 4.1 below, including extremes estimated from fitting a Weibull distribution function to the cumulative distribution of all measured wave heights. The only other independent set is the SOWM hindcast data, available at 49.9°N 132.1°W. We have not considered the METOC chart data in this study.

In the coastal waters the only data are those measured in the present study. As with the NDBO data, these are treated in detail in Section 4.1 dealing with wave height prediction.

The predicted extreme values from each data set are given in Table 2.5. The SOWM extremes agree well with the Queen Charlotte Sound data giving, perhaps, a more plausible variation of severe wave heights across the offshore waters than suggested by the differences between Station 216 and NDBO Station 46004. This evidence indicates that the 100-year return H_s-value off the mouth of Queen Charlotte Sound is about 17 to 17.5 m with a statistical uncertainity no smaller than ± 2 m.

The maximum values of H_s for 1983 (Fig. 2.13) indicate, very roughly, that wave heights observed off the mouth of Queen Charlotte Sound decrease about 37% into McInnes Island, and above 23% in to Bonilla Island. Similarly, comparison of the extreme wave heights between Queen Charlotte Sound (216), Hecate Strait (215) and Langara West (211) gives reduction factors of about 5% and 15% respectively. Using these factors and the values averaged for Queen Charlotte South and the SOWM hindcast point as applicable to the offshore waters, the extreme values shown in Table 2.6 are provided for preliminary estimates.

2.4 Wave Grouping

a) Theory

"Wave groups" refer to sequences of large waves that occur in natural seaways. Common practice defines a group when its constituent waves exceed the significant wave height for the measured record; in general groups are two or three waves long, although lengths of 6 waves have been observed rarely, during severe Atlantic seaboard storms. Methods for identifying wave groups include simple counting procedures based on zero-crossing wave analyses of each record, and integral properties of continuous functions derived from the measured time series of sea level displacement η. Falling into this second category is the "Groupiness Factor" -GF- defined by Funke and Mansard (1978) as

$$GF = \left[\frac{1}{T_n} \int_0^{T_n} (E(t) - \overline{E})^2 dt \right]^{1/2} / \overline{E} \qquad (2.1)$$

where E(t) is the SIWEH (Smoothed Instantaneous Wave Energy History) function for a record of length T_n; this function is proportional to η^2 and hence to wave energy. GF ranges from about 0.4 to 1.2 for natural sea states with the larger values indicating records that are well grouped.

It is well established that wave groups have bound long waves associated with them; these are related to the set-up and set-down of the mean sea level resulting from variations in the radiation stress between individual waves. These effects are most pronounced in shallow water. The theory for reconstructing the bound long wave is known (Ottesen Hansen, 1978; Sand, 1982) and has been linked directly to the GF proposed by Funke and Mansard as a group-characterizing parameter.

Presently, little is known about the frequency of wave group occurrence and the variations in frequency from ocean to ocean. It has been shown (see e.g. Hodgins, 1983) that the number of waves in groups exceeds that predicted using the conventional Rayleigh distribution function for wave heights. This suggests that group formation may not be purely random, and hence is not predictable with existing distribution models for wave height.

Groups of waves are important for breakwater design and the motion response analysis of tethered, floating platforms. In this latter case the natural periods of heave and sway may range from 30 to 60 seconds, matched much more closely to the bound long wave periods than to the short wave periods. Thus near-resonant responses are possible, related directly to the grouped character of the wind waves.

Because bound long wave amplitudes are proportional to the energy of the associated wind waves, grouping is primarily a problem in storms, not in low energy conditions. In this study we have calculated the groupiness factor, GF, for a number of storms, both continuously monitored and with 3-hourly measurements, to examine the occurrence of groupy records. Relationships between GF and other wave properties were also investigated to see if obvious correlations could be found. Finally, selected records having high GF-values were used to reconstruct the bound long wave to give a graphical impression of the grouping character in individual 17 min. or 34 min. records.

b) Data Selection

Seven storms, listed below, were selected for the wave group analysis. These events represent the most suitable compromise between large wave heights and simultaneous monitoring at as many sites as possible. The Langara East and Bonilla Island data have been excluded.

	Site Names and Numbers			
	Queen Charlotte Sound	Langara West	Hecate Strait	McInnes Island
	216	211	215	214
Storm Dates	No. of records processed			
14-16 DEC 82	15	49	9	0
25-26 DEC 82	9	48	5	0
24-27 JAN 83	28	96	23	0
5- 7 NOV 83	13	65	6	0
26-27 FEB 84	10	48	7	77
18-19 MAR 84	12	48	1	18
27-28 MAR 84	9	48	6	31

The primary parameters of interest in each storm are the significant wave height and period, $H_{1/3}$ and $T_{1/3}$, largest individual wave height H_{max}, the groupiness factor GF and the ratio $H_{max}/H_{1/3}$. Time series plots showing the variation of these parameters at Langara West and Queen Charlotte Sound are presented in Fig. 2.22 and 2.23.

c) Discussion of Results

As shown in these time series plots, the GF values range from about 0.3 to 0.9, a slightly lower range than observed, for example, over the Grand Banks, although some storms examined there (e.g. February 14-15, 1982) were considerably more severe than the seven available in the study area. There is little justification to treat the three outer stations separately for grouping in terms of physical processes that could give rise to groups; therefore, all parameter values at Stations 211, 215 and 216 have been combined. The observed marginal distribution of GF is shown in Fig. 2.24. It is a narrow distribution with the most frequent values lying between 0.6 and 0.7 (weakly grouped); large values, exceeding 0.9 indicating large groups, are comparatively rare.

The marginal distribution does not indicate whether or not GF varies in proportion to some other measure of sea state intensity, such as $H_{1/3}$. Inspection of the time series plots suggests that such a correlation, if it exists at all, would be very weak; this is borne out by the joint frequency histogram in Fig. 2.25. The largest GF values correspond with $H_{1/3}$ ranging from 3 to 8 m; $H_{1/3}$ values between 9 and 12 m had observed GF values of 0.6 to 0.8, with no discernible trend to increasing GF with increasing wave height, as one might suspect at first.

The ratio $H_{max}/H_{1/3}$ is of great engineering concern since while $H_{1/3}$ is the conventional wave parameter for sea state intensity, H_{max} and its associated period, are required for fluid loading calculations. Inspection of individual wave traces often shows that the largest waves are found in groups: thus if one record contains more groups than another, there is a higher chance of observing a large $H_{max}/H_{1/3}$ ratio in that sequence. It is logical to inquire, then, if a correlation exists between GF and $H_{max}/H_{1/3}$. The joint frequency histogram is shown in Fig. 2.26. A weak trend showing the ratio $H_{max}/H_{1/3}$ to be proportional to GF is evident, although the scatter is large. It is interesting to note that, following conventional practice and assuming wave heights are Rayleigh distributed, one obtains the ratio of the <u>most probable</u> maximum wave height $\mu(H_{max})$ to $H_{1/3}$ as 1.57 for a 24 min record (weighted average of sample intervals for the present data base) and an average zero-crossing wave period of about 11 s. As Fig. 2.26 shows, at the 63% chance of exceedance for $\mu(H_{max})$, the observed ratio is about 1.53, in close agreement with Rayleigh theory.

As the joint distribution of $H_{max}/H_{1/3}$ and $H_{1/3}$ (Fig. 2.27) shows, however, the largest $H_{1/3}$ wave heights had ratios between 1.6 and 2.0 often enough to suggest that $\mu(H_{max})$ is not a particularly good design value.

The marginal distribution of GF at McInnes Island is shown superimposed on that for the other 3 sites in Fig. 2.24. It indicates that wave records may be slightly less grouped on average nearer the inner coast than at the more exposed locations, although values of GF exceeding one were observed. The sample size (121 values) is still too small to draw more definitive conclusions.

A sequence of time series plots showing the original wave trace (amplitude and phase corrected) with the bound long wave superimposed, the SIWEH function, and the bound long wave by itself, are presented in Fig. 2.28. These graphs are reproduced here for visual inspection to show the nature of wave groups and how large waves tend to occur in them. The SIWEH is useful for pointing at the groups - a peak in SIWEH points to the group in the upper panel η-trace and to larger amplitude long waves in the lower panel. Note that the amplitude of the measured sea level displacement ranges from 0 to 5 or more metres, but from 0 to about 20 to 30 cm for the bound long wave.

Some well grouped sequences are evident in the Queen Charlotte Sound data, a few of which extend to 5 waves.

Examination of wave traces such as these, and attempts to correlate GF with other wave properties, suggest that GF may not be a particularly fine discriminator of group properties, and this makes it difficult to compare group parameters from region to region. Future studies could profitably follow two different routes to arrive at a supplementary parameterizations to GF:

1) establish frequency of group occurrence and statistics of group non-occurrence (interval between groups), in addition to the density function for the number of waves in groups, using counting methods on zero-crossing wave heights and periods,

2) establish wave statistics (heights, periods, and clusters of large waves) for the group bound long wave in each η-trace.

These statistics would give meaningful parameters, related to wave theory, for comparison purposes.

3.0 DIRECTIONAL WAVE STUDIES

3.1 Wave Refraction

a) Importance

Waves are refracted, ie. change their amplitude and direction of propagation, in the presence of depth or current inhomogeneities. Because of refraction, waves may be focussed to locations where conditions will be more severe than elsewhere; the converse is also possible, where divergence of wave energy results in quieter areas. As a result, wave climate statistics in the coastal waters will be governed to a certain extent by refraction, particularly the directional properties of the low-frequency tail of the wave spectrum. For this reason, refraction of long-period waves has been considered here in some detail, concentrating on certain bottom features that are expected to play a significant role in affecting observed directional properties at the measurement sites.

b) Methods

Refraction By Bottom Relief

Spatial inhomogeneities in water depth are expected to be the major cause of refraction, and will be most effective for long waves with periods exceeding 14 s. For this reason, the influence of bottom topography on swell with periods of 16, 18.3 and 21.3 s (these values corresponding with spectral analysis frequencies) has been investigated to determine potential areas of wave focussing/defocussing, the influence of Learmonth Bank on waves inside Dixon Entrance, and possible swell sources at Bonilla Island in northern Hecate Strait.

The methods of analysis follow conventional practice. The coastal waters have been divided into two regions (Fig. 3.1) in which landforms and bathymetry have been resolved on grids of 2 and 5.25 km for Dixon Entrance and Hecate Strait - Queen Charlotte Sound respectively. The model domains and bathymetries as resolved by these grids are shown in Fig. 3.2; subjective smoothing of depth contours was used in a few points to remove unrealistically rapid changes in relief. Seaconsult applied its ray tracing program (forward and reverse modes) REFRACT on these grids; the program is based on the method first put forward by Munk and Arthur (1952) using a numerical procedure similar to that of Worthington and Herbich (1971). The program outputs maps of ray paths with cross-ticks at specified multiples of wave length. Shoaling and refraction coefficients are calculated at one-wavelength intervals on each ray. In the reverse tracing mode, the ticks are omitted.

Refraction by Tidal Currents

A horizontally sheared flow, such as produced by tidal currents in Hecate Strait, also refracts waves. The relative effect of current to bathymetric variations is most simply deduced in the case of unidirectional flow, where Snell's Law applies in the form (c.f. LeBlond and Mysak, 1978, p 334):

$$\frac{c}{\cos\phi} + U = \text{constant} \tag{3.1}$$

where ϕ is the angle which the wave propagation vector makes with the current U, and c is the phase speed. Differentiating (3.1) along a ray yields

$$\frac{c\sin\phi}{\cos^2\phi}\frac{d\phi}{ds} = -\left\{\frac{1}{\cos\phi}\frac{dc}{ds} + \frac{dU}{ds}\right\} \tag{3.2}$$

where ds is an element of distance along the ray. The relative contribution of current and wave speed to changes in wave direction are then in the ratio

$$dU: \frac{dc}{\cos\phi} \tag{3.3}$$

Current variations have no effect on waves that are perpendicular to the flow; in that case $\cos\phi \to 0$. Apart from this directional effect, the refractive influence of current changes relate to wave speed changes in the ratio dU to dc. Assuming the long wave speed $c = \sqrt{gd}$, (d = depth), we find

$$\frac{\Delta U}{\sqrt{gd}} : \frac{1}{2 \cos \phi} \frac{\Delta d}{d} \tag{3.4}$$

Typical currents, mainly due to the tides, are at most 1 or 2 knots, i.e. less than 1 m/sec. In water depths of the order of 100 m, such as over Learmonth Bank, $\Delta U/\sqrt{gh} \lesssim 0.03$, so that a relative depth variation of more than 3% (i.e. 3 m) is sufficient to dominate the refraction process. It is clear from (3.4) that current refraction will be important only in very shallow areas where the flow speed is a significant fraction of the wave speed. One such area is clearly that of Rose Spit, at the extreme northeast tip of Graham Island, which is so shallow at low tide that long swell might actually break over it. Current refraction may also be of some relevance in other very shallow areas of eastern Graham Island, or in similar shallow banks on the east side of Morseby Island.

However, over the greatest portion of the coastal waters bathymetric refraction will dominate, and current effects are of secondary importance. For this reason currents have not been treated further here.

c) Dixon Entrance

The principal refractive feature in Dixon Entrance is Learmonth Bank, a large shoal just north of Langara Island. This bank acts as a convergent lens, focussing swell onto various points depending on the period of the waves. Three reverse ray patterns shown in Fig. 3.3, originating at the Langara East measurement site (Station 212), for periods of 16, 18.3 and 21.3 s, demonstrate just how effective the focussing may be.

Fig. 3.4 compares forward ray diagrams for 16 s waves originating from three westerly directions, WNW, W, and WSW; Fig. 3.5 compares similar forward ray patterns for two different periods. While it is clear that Learmonth Bank focusses wave energy, the precise position where waves combine is very sensitive to the angle of incident swell in the open ocean, and to the period. Thus one cannot conclude, for example, that Station 212 will always exhibit more swell than Station 211, since many times 212, in the lee of the bank, lies in a zone of wave divergence.

Examples of the differences in observed swell energy levels between Stations 212 and 211, on either side of Learmonth Bank are illustrated in the spectra shown in Fig. 3.6. The spectra on Dec. 15, 1982, formed under active storm generation, are virtually identical at the peak frequencies (period ~ 18.1 s) while those on Nov. 24, 1982, at a much lower energy level, differ substantially at the same peak periods. Later in that same event, 21Z, Nov. 25, 1982 sheltering behind Learmonth Bank appears to be so effective as to remove most of the low frequency energy. We note, however, that because the Waveriders at these two locations did not measure wave directions, one cannot link the observed differences directly to refraction patterns (Fig. 3.4 and 3.5), but only surmise that refraction play an important role.

Hecate Strait-Queen Charlotte Sound

As pointed out in the preliminary analysis of directional wave data from Bonilla (Station 213) (Seaconsult, 1983b; pp 20-23) low-frequency energy was observed there. A refraction analysis for 16 s waves was carried out to see if these measurements correlated well with expected wave directions for swell originating in the open ocean. Fig. 3.7 shows the reverse-ray pattern for bathymetric refraction. It indicates an admittance angle of about 150°T to 170°T at the site, which corresponds with southerly to south southeasterly swells beyond Queen Charlotte Sound; for other directions no swell would be expected to reach the site.

This is confirmed by the forward ray diagrams as shown in Fig. 3.8. A similar diagram nor northwesterly swells incident from Dixon Entrance is shown in Fig. 3.9. These both show that Bonilla is well sheltered from swell aside from the narrow SSE angle of about 20°. It appears that the low-energy level information on direction at about 16 s periods at Bonilla was the result of measurement error (noise) in the Endeco Wave Trak system, rather than a wave property.

The forward ray refraction diagram for 10 s waves originating in the SE is shown in Fig. 3.10 for Hecate Strait. Such waves could result from storm winds over the Queen Charlotte Sound fetch. It shows that these waves will reach Bonilla (Station 213) virtually unmodified by refraction. Further west, however, refractive effects become increasingly important over the banks in shallow water. There, very definite areas of convergence (severe conditions) and divergence (mild conditions) are evident. Although, one must bear in mind, that the response at any one location is very sensitive to incident wave direction. The diagrams presented above do show, however, that spatial variations in wave climate are to be expected in Hecate Strait, particularly at swell periods.

The reverse ray diagram for McInnes Island (Station 214) in Fig. 3.11 shows that unlike Bonilla it has a wide exposure to swell, notably from the south and from southwest through to west (see also Fig. 3.8). Between south and southwest, the seaward bathymetry places Station 214 in a region of weak wave divergence; thus, its reponse to ocean swell in this sector will be slightly lower than the other directions to either side.

e) Consequences of Refraction

Three main consequences follow from the strong focussing of wave energy shown above in each region:

1) Spatial variations in wave climate will be large, particularly at low frequencies; this means even fairly close sites may exhibit differences in energy distribution and directional properties.

2) Near shore wave response will be sensitive to the periods and directions of incident waves in the open ocean. Calculations to transform ocean wave properties into coastal sites must account for refraction (including wave hindcast models).

3) As swell from distant sources reaches the coast, its frequency will gradually increase due to normal dispersion, and there will be a corresponding decrease in wavelength. Refraction is sensitive to this change in wave period. As the incoming wavelength changes, focussed waves will shift in direction; this results in a beam that will sweep past a point near the coastline on a time scale that is quite short (an hour or two) compared to that over which the swell event occurs (about one or two days). Such transient swell events would contribute little to the average wave climate, but could result in relatively severe, and generally short lived but unexpected conditions. This kind of phenomenon has been reported further south in the Barkeley Sound area, and may be expected in many regions with a complex offshore bathymetry.

3.2 Modelling the Directional Distribution of Wave Energy

a) Directional Spreading Functions

The directional properties of ocean waves are commonly expressed in terms of a parametric spectral function that represents mean wave direction, and the "spreading" or distribution of energy about this mean direction, in terms of a pair of frequency-dependent parameters. Mathematically, the directional spectrum is thus written as

$$F(\theta,f) = E(f)S(\theta,f) \tag{3.5}$$

for direction θ ($0 \leq \theta \leq 2\pi$) and frequency $f > 0$. E is an amplitude function and S a normalized spreading function obeying

$$\int_0^{2\pi} S(\theta,f)d\theta = 1 \tag{3.6}$$

The most conventional form for S has been the "cos-power" function

$$S(\theta,f) = K(f)\ \cos^{2p(f)}\{\tfrac{1}{2}(\theta - \theta_o(f))\} \tag{3.7}$$

where K(f) is chosen to satisfy (3.6). The parameters $\theta_o(f)$ and p(f) represent respectively the mean direction and angular spread as a function of frequency. A number of authors (Mitsuyasu et al., 1975; Hasselmann et al., 1980; Holthuizen, 1983) have described the directional properties of wind waves in terms of p and θ_o. They have found in particular that θ_o follows the wind direction closely (with some lag when the wind veers) and that p(f) is largest at the peak of the spectrum and increases with fetch and wind duration as the spectrum approaches equilibrium. This last observation is often summed up in the statement that p increases with "wave age", defined as the ratio of wave speed c to wind speed U.

The values of θ_o and p are obtained from co- and quadrature spectra of wave elevation and slopes following methods originally developed by Longuet-Higgins et al. (1963). Borgman (1969) has shown how the method may be used for other combinations of directional wave information. The quality of the fit provided by (3.7) to the measured directional spread has been discussed by Hasselmann et al. (1980), Holthuizen (1983), and especially by Long (1980) and Lawson and Long (1983). Since so much of the information related to wave directionality is contained in the two functions p(f) and $\theta_o(f)$, it is important to verify that relation (3.7) actually provides a good fit to the data. In this section we examine this question for the McInnes Island measurements, extending the earlier work of Long, and Lawson and Long, to reach some unexpected, but reasonable conclusions.

b) Theory

Following Long (1980), a set of four data equations is considered:

$$\underset{\sim}{d}(\underset{\sim}{x}) = \int_0^{2\pi} S(\theta)\underset{\sim}{b}(\theta)d\theta \qquad (3.8)$$

where

$$\underset{\sim}{x} = [\, C_{11}, C_{22}, C_{33}, Q_{12}, Q_{13}, C_{23}\,]^T \qquad (3.9)$$

$$\underset{\sim}{d}(\underset{\sim}{x}) = \begin{bmatrix} Q_{12}/[C_{11}(C_{22}+C_{33})]^{\frac{1}{2}} \\ Q_{13}/[C_{11}(C_{22}+C_{33})]^{\frac{1}{2}} \\ (C_{22}-C_{33})/(C_{22}+C_{33}) \\ 2C_{23}/(C_{22}+C_{33}) \end{bmatrix} \qquad (3.10)$$

$$\underset{\sim}{b}(\theta) = [\cos\theta, \sin\theta, \cos 2\theta, \sin 2\theta]^T \qquad (3.11)$$

The transpose symbol, T, is used to show that $\underset{\sim}{x}$ and $\underset{\sim}{b}$ are actually column vectors, the transposes of the row vectors written for typographic convenience. Subscripts 1, 2, and 3 correspond respectively to vertical displacement, North-South slope and East-West slope; C_{ij} are co-spectra, Q_{ij} quadrature spectra.

The spectral estimates C_{ij} and Q_{ij} are subject to statistical error. The data vector $\underset{\sim}{\tilde{x}}$ obtained from any specific realization is thus an estimate of the "true" value $\underset{\sim}{x}$ plus a random error $\delta\underset{\sim}{x}$:

$$\underset{\sim}{\tilde{x}} = \underset{\sim}{x} + \delta\underset{\sim}{\tilde{x}} \qquad (3.12)$$

The estimate of $\underset{\sim}{d}$ also contains random error:

$$\underset{\sim}{\tilde{d}} = \underset{\sim}{d} + \delta\underset{\sim}{d} \qquad (3.13)$$

To fit a model spectrum such as (3.5) to observed data, one attempts to minimize the difference between the observed estimate $\tilde{\underset{\sim}{d}}$ and the value of of $\underset{\sim}{d}$ given by the model. For the cosine-power spreading model, substitution of (3.7) into (3.8) gives

$$\begin{bmatrix} d_1 \\ d_2 \end{bmatrix} = \frac{p}{p+1} \begin{bmatrix} \cos \theta_o \\ \sin \theta_o \end{bmatrix} \tag{3.14a}$$

$$\begin{bmatrix} d_3 \\ d_4 \end{bmatrix} = \frac{p(p-1)}{(p+1)(p+2)} \begin{bmatrix} \cos 2\theta_o \\ \sin 2\theta_o \end{bmatrix} \tag{3.14b}$$

The parameters p and θ_o are then to be chosen to minimize $\tilde{\underset{\sim}{d}} - \underset{\sim}{d} = \delta\underset{\sim}{d}$. A measure of <u>lack</u> of fit is

$$\rho^2 = \delta\tilde{\underset{\sim}{d}}^T M \, \delta\underset{\sim}{d} \tag{3.15}$$

where M is a symmetric matrix of weights (cf. the discussion in Long, 1980). If the elements of $\tilde{\underset{\sim}{d}}$ are jointly Gaussian then $M = V^{-1}$ is an appropriate choice, with

$$V_{ij} = \text{cov}\{\delta\tilde{d}_i, \delta\tilde{d}_j\} \tag{3.16}$$

ρ^2 is distributed as χ_4^2 (4 degrees of freedom); thus, an 80% confidence level for ρ^2 is 6.2; that is, 80% of data realizations should result in a value of ρ^2 which is <u>less than</u> 6.2 if the model is correct.

c) <u>Long's (1980) Approach</u>

The cosine-power model includes only two parameters, p and θ_o. There are, however, four equations (3.8) relating $\underset{\sim}{d}$ to these parameters. Long (1980) used a method that assumes

$$\delta d_1 = \delta d_2 = 0 \tag{3.17}$$

$$\theta_o = \tan^{-1}(\tilde{d}_2/\tilde{d}_1) \tag{3.18a}$$

$$p = \tilde{K}_1/(1-\tilde{K}_1) \tag{3.18b}$$

where

$$\tilde{K}_1 = (\tilde{d}_1^2 + \tilde{d}_2^2)^{1/2} \tag{3.19}$$

The choice (3.17) is, of course, completely arbitrary, and another equivalent choice is

$$\delta d_3 = \delta d_4 = 0 \tag{3.20}$$

which yields

$$\theta_o = \tfrac{1}{2}\tan^{-1}\left(\frac{\tilde{d}_4}{\tilde{d}_3}\right) \tag{3.21a}$$

$$p = \frac{1 + 3\tilde{K}_2 + (\tilde{K}_2 + 14\tilde{K}_2 + 1)^{1/2}}{2(1 - \tilde{K}_2)} \tag{3.21b}$$

with

$$\tilde{K}_2 = (\tilde{d}_3^2 + \tilde{d}_4^2)^{1/2} \tag{3.22}$$

The error values ρ^2 found by using estimates (3.18) were all greater than 6.2: none of the fitting performed by Long (1980) were acceptable at the 80% confidence level.

A similar estimation method was used by Cardone et al. (1981) based on two integral properties of $S(\theta)$:

$$\theta_o = \arg \int_0^{2\pi} d\theta e^{i\theta} S = \tan^{-1}\left(\frac{d_2}{d_1}\right) \tag{3.23}$$

$$\theta_s = \left\{ \int_0^{2\pi} d\theta \; 4\sin^2[(\theta - \theta_m)/2] S \right\}^{1/2}$$

$$= [2 - 2(d_1^2 + d_2^2)^{1/2}]^{1/2} \tag{3.24}$$

These parameters were estimated by assuming $\delta d_1 = \delta d_2 = 0$. Thus, as in Long's (1980) method, only half the data were used.

A more refined technique discussed by Long and Hasselmann (1979) involves the minimization of a "nastiness" function describing the departure of the model from the data. The error ρ^2 is then constrained to remain below a prescribed level (e.g. 6.2). The analysis was applied to five and six element arrays, for which there are more degrees of freedom than for a pitch-roll buoy.

Lawson and Long (1983) also applied this method to pitch-roll buoy data. The best spectrum was thus that which minimized the "nastiness" function while keeping ρ^2 below a prescribed value. The coefficient λ of an additional term of the form $\underset{\sim}{b}^T \underset{\sim}{\lambda}$, were determined to find the optimal model spectrum

$$S_m = S(\theta,f) + \underset{\sim}{b}^T\underset{\sim}{\lambda} \qquad (3.25)$$

with $S(\theta,f)$ as given by (3.7). The coefficients of $S(\theta,f)$, i.e. p and θ_o were found by putting $\delta d_1 = \delta d_2 = 0$, again ignoring half the data.

None of these methods appear entirely satisfactory since many spectra fail to achieve acceptable fits over their most energetic portions. Either there exists a defficiency in the method, or natural seaway spectra are, in general, poorly represented with unimodal directional models having a cosine form. The consequences of the latter assumption proving true are profound: much engineering analysis, of loading on fixed structures for example, assumes the model given by (3.7) and its "failure" would necessitate quite a fundamental shift in thinking about parameterizing directional properties.

To examine the fitting of (3.7) with measured heave-pitch-roll data further, the line of reasoning presented by Long and others has been extended here to include all four data equations. This leads to a new optimization method, presented in the following section.

d) A New Optimization Procedure

In order to use all the available data to find the best values of p and θ_o in (3.7), we seek the minimum of $\rho^2(\underset{\sim}{\alpha})$, with $\underset{\sim}{\alpha} = [p, \theta_m]^T$, over variations of both p and θ_m. We thus set

$$\frac{\partial \rho^2}{\partial \alpha_k} = 0, \quad k = 1,2 \tag{3.26}$$

These equations will then yield values of p and θ_m that minimize ρ^2 and will use all the information available in (3.13), rather than discarding half of it. The procedure is a priori more direct than that required by Long and Hasselmann's (1979) "nastiness" function.

To solve (3.26), we express V^{-1} as $V^{-1} = T^T DT$, where $D = [D_{ij}]$ is diagonal and T is an orthogonal transformation. Thus,

$$\begin{aligned} \rho^2 &= (T\underset{\sim}{\delta\tilde{d}})^T D (T\underset{\sim}{\delta\tilde{d}}) = t^T\, Dt \\ &= \sum_{i=1}^{4} D_{ii} t_i^2 \end{aligned}$$

where

$$t_i = \sum_{j=1}^{4} T_{ij} \delta\tilde{d}_j$$

Hence,

$$\frac{\partial \rho^2}{\partial \alpha_k} = 2 \sum_{i=1}^{4} D_{ii} t_i \frac{\partial t_i}{\partial \alpha_k}$$

Using

$$\frac{\partial t_i}{\partial \alpha_k} = \sum_{j=1}^{4} T_{ij} \frac{\partial \delta\tilde{d}_j}{\partial \alpha_k} \quad ,$$

we have

$$\frac{\partial \rho^2}{\partial \alpha_k} = 2 \sum_{i=1}^{4} D_{ii} \left(\sum_{j=1}^{4} T_{ij} \delta\tilde{d}_j \right) \left(\sum_{j=1}^{4} T_{ij} \frac{\partial \delta\tilde{d}_j}{\partial \alpha_k} \right)$$

For brevity, let $J_{ij} = -\dfrac{\partial \delta \tilde{d}_j}{\partial \alpha_k}$, i.e.

$$J = \begin{bmatrix} \dfrac{1}{(p+1)^2} \cos \theta_o & , & \dfrac{-p}{p+1} \sin \theta_o \\ \dfrac{1}{(p+1)^2} \sin \theta_o & , & \dfrac{p}{p+1} \cos \theta_o \\ \dfrac{[4p(p+1)-2]}{(p+1)^2 (p+2)^2} \cos 2\theta_o & , & \dfrac{-2p(p-1)}{(p+1)(p+2)} \sin 2\theta_o \\ \dfrac{[4p(p+1)-2]}{(p+1)^2 (p+2)^2} \sin 2\theta_o & , & \dfrac{2p(p-1)}{(p+1)(p+2)} \cos 2\theta_o \end{bmatrix}$$

Then,

$$\frac{\partial \rho^2}{\partial \alpha_k} = -2 \sum_{i=1}^{4} D_{ii} \left[\sum_{j=1}^{4} T_{ij} \ \delta \tilde{d}_j \right] \left[\sum_{j=1}^{4} T_{ij} J_{jk} \right] = 0 \qquad (3.27)$$

which is a pair of equations for two unknowns, p and θ_o. T_{ij} is determined by finding the two independent eigenvectors of V^{-1}; the diagonal of D is then made up of the corresponding eigenvalues. A non-linear equation solver is used to obtain p and θ_o from (3.27) and values of ρ^2 are determined from (3.15). The results of this method will be compared to those of the less computationally demanding method of Long (1980) below.

e) Discussion of Preliminary Results

Coincident directional wave data were measured at Bonilla Island (Endeco Buoy) and McInnes Island (WAVEC Buoy) during a 6-day period from 18-23 October 1983. At that time two storms generated moderately severe sea states for these locations. Some of the basic directional properties are examined first, followed by a dicusssion of the fitting of spreading models as outlined above.

Co- and quad spectra were obtained using conventional procedures including Bartlett smoothing and Fast Fourier Transform techniques.

Measured Directional Wave Properties

Time series plots of wind speed and direction (as vectors), wave energy at 16 equally spaced frequencies (as vectors indicating magnitude and mean wave direction θ_o), and significant wave height are shown in Fig. 3.12 and 3.13 for McInnes Island and Bonilla Island respectively. Sequences of spectrum plots (Fig. 3.14 and 3.15) are then presented for selected events, corresponding with one column of energy vectors in the time series graphs. These show the power density in the upper panel, the ρ^2 value in the middle, and the directional spreading predicted by (3.7) fitted using Long's (1980) method (lower panel).

McInnes Island - The period includes two storm events with maximum significant wave heights H_s at 21:00, Oct. 18 and 09:00, Oct. 21. The first storm has peak winds of 24 m/s and peak wave energy densities of 33 m^2/Hz. Over the course of the preceding nine hours, the peak of the spectrum is seen to shift from 4.5 s to 9.7 s. Wave vectors are aligned reasonably well with the wind, although there is a small clockwise rotation of wave direction in the later stages of the storm. This shift in orientation is evident at longer periods (longer than 8 sec) and is interpreted as resulting from arrival of swell from the Pacific Ocean through Queen Charlotte Sound. Continuing arrival of swell from the southwest is evident in the day following the strong winds.

The second storm exhibits features very similar to those described above; the gradual rotation of the mean wave direction at low frequencies and the arrival of strong swell about a day and a half after the peak of the storm are also prominent.

The individual 3-hourly spectra clearly show the growth of the locally generated seas in the first storm, followed by the arrival of the low frequency swell, particularly between 21:00 on Oct. 19 and 15:00 on Oct. 20. In almost all instances the ρ^2 value exceeds the 90% confidence band suggesting that (3.7) is inapplicable, although the refraction analysis indicates that no strong wave crossing is expected for westerly swell. It is interesting to note, however, that at 21:00 on Oct. 19, a definite swell peak at 17 s contains a very broad distribution of energy, compared with rather tighter spreading associated with wind sea earlier in the storm. A cause for this is not immediately apparent, although swell occurring later also exhibit wider spreads of energy than the higher frequency waves.

Bonilla Island - The main features described above for McInnes Island are found in Fig. 3.13 as well: two peaks in H_s at 18:00 on Oct. 18 and 09:00 on Oct. 21 corresponding with local winds of 35 to 38 m/s and 25 to 30 m/s. An apparently spurious peak is evident at 03:00 on Oct. 22; it is due to very low frequency contamination, at periods below the range included in the directional analysis. In both storms, wave directions are about 45° westward of those noted at McInnes Island, corresponding to a similar difference in wind direction between the two locations. Very little swell is visible at Bonilla Island consistent with the refraction results presented earlier.

Fig. 3.13 shows an important difference in measurement from the WAVEC data at McInnes Island in the lowest frequency bands. Energy here is present at significant levels, during the storms, but is erratic in direction. This contrasts sharply with the WAVEC results and appears to be an instrumental problem (see also Seaconsult, 1983b).

The 3-hourly spectra also differ in appearance from those measured at McInnes Island, indicating much greater energy spreads at similar sea state intensities. This may reflect natural processes (wind variability) or instrument response characteristics. Exact causes of these differences are not readily explained without side-by-side measurements using both instruments, but seem most likely to be related to instrumental design of the Endeco Wave-Track. The more detailed analysis of directional wave data from the Endeco Buoy, discussed in Section 2.2c), showed that this instrument did not respond well at low frequencies.

Spreading Model Fitting

The error associated with model fitting using Long's (1980) method, where the parameters of the cosine-power model (3.7) are formed from (3.18), is shown in the central panel of individual spectra from McInnes and Bonilla Islands. What is most remarkable in the plots of ρ^2 against frequency is that the error is usually largest, and indeed large enough to dictate rejection of the model at the 80% confidence level, where the spectral energy is highest. Long's (1980) analysis thus shows that the favoured cosine-power spreading model is <u>not</u> a good fit to observed directional data precisely in those parts of the spectrum where all field measurements have shown the directionality to be greatest (cf. Mitsuyasu et al., 1975; Holthuizen, 1983).

It is also significant that the optimal fitting method presented above (Section d) decreases the error somewhat, but not enough to change the above conclusions. The comparison of Long's (1980) method with the new optimization method is shown in Fig. 3.16. Clearly, the ρ^2 values are very high near the spectral peak in both calculations. Similar high values are reported by Long (1980), so that there is nothing exceptional with our results. The cosine-power model is a poor fit to the measured directional information near the peaks of the spectrum, where the p values are largest, as evident from the narrowness of the angular spread in the lower panels of Fig. 3.14 and 3.15. In light of these results it is necessary to either reject the cosine-power model or re-interpret the goodness-of-fit estimator ρ^2.

Let us consider the nature of the directional information provided by a pitch-roll buoy and the process of fitting it with a cosine-power model. As shown first by Longuet-Higgins et al. (1961), the directional information yielded by simultaneous measurements of heave and of two orthogonal slopes consists of the coefficients to the four angular Fourier components (3.11): $\cos\theta$, $\sin\theta$, $\cos 2\theta$, $\sin 2\theta$. The degree of angular resolution provided by a Fourier series made up of only these four terms is very low; the peakiest curve will at best resolve a 45° angular spread. It is not surprising then to find that fits to Fourier series by the model function (3.7) will not be very good when p is large, which is commonly found to be the case near the peak of the spectrum. A large value of p gives a narrow angular distribution which will necessarily differ from the four-term Fourier series over most of the angular range. The error ρ^2, which is just the sum of the squares of the differences between the two curves, will thus also be large. One then expects large values of ρ^2 for large values of p, i.e. for highly directional seas. The large "error" value is thus an unavoidable consequence of the fitting technique rather than a true measure of how well the model represents wave directionality. This situation is sketched roughly below.

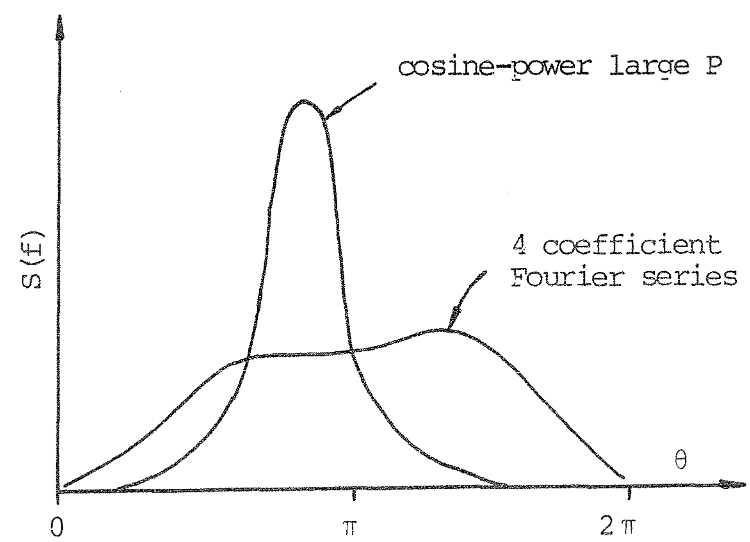

The method suggested by Long and Hasselmann (1979) does not, in our view, inprove the situation. The error, ρ^2, is indeed lowered by adding to the cosine-power model a supplementary quartet of Fourier terms, so that the differences between the original series and the cosine-power peak are minimized. However, this approach yields no more information on the actual directionality of the waves: all it does is to fill the gaps by introducing an error-compensating component that does not tell us any more about how good the cosine-power relation was in the first place.

f) Conclusions

The principal finding of this work is that the adequacy of the cosine-power model for angular spreading cannot be established by the methods proposed by Long and Hasselmann (1979) or Long (1980). The new optimization method proposed here also does not remedy the basic problem of angular resolution. Thus one must still accept the cosine-power law on intuitive grounds and empirical evidence, but reject the methods of establishing its veracity as outlined in preceding sections. In many respects, this is a retrogressive conclusion. Wherever refraction or other localized effects modify waves in shallow water so that a simple unimodal spreading model may not apply, one would like to have a test of goodness-of-fit and a sound basis for acceptance or rejection. The wave climate around Sable Island is, for example, one case in Canadian waters where this situation may obtain. Thus, since this whole problem of modelling directional spread, and mean wave direction, is of such fundamental importance further research in this area is strongly recommended.

3.3 Wave Slope Statistics

Recent laboratory and theoretical studies of wave slope statistics (Huang et al., 1984) have provided some confirmation for a simple model of the non-gaussian statistics of the joint probability distribution function of wave height and slopes. The importance of wave slopes has also been incorporated into a spectral model of the sea-state (the Wallops spectrum, as described by Huang and Long, 1981 and Huang et al., 1983; 1984) where the significant slope S (defined below) plays an important role. Wave slopes are of great practical importance in determining the effect of the sea state, and in many circumstances it is the steepness of the waves rather than their height which makes them particularly dangerous. Huang's studies indicate statistical relations between wave slopes and wave heights which may refine our understanding of wind waves.

Most of the results obtained by Huang and his collaborators have been based on laboratory experiments; the availability of simultaneous time series of heave and orthogonal slope components offers an opportunity to examine the applicability of some of these results to natural sea-states. This is done in following sections using data collected at McInnes Island during the present study.

a) Spectral Comparisons

Time series of sea level displacement η and of the two slope components S_E, S_N (in the east-west and north-south directions respectively) have been used to obtain estimates of the root-mean-square wave elevation $\sigma = (\overline{\eta^2})^{1/2}$ and slope $\sum = (\overline{S_E^2 + S_N^2})^{1/2}$. We recall that the significant wave height is defined as $H_s = 4\sigma$. The significant slope is however not currently defined in the same way in terms of $\sum$, but as $S = \sigma/\lambda_o$, where λ_o is the wave length at the spectral peak, deduced from the linear dispersion relation.

A relation between S and $\sum$ has been sought using the data from Station 214 (WAVEC) for the time period 14-25 October, 1983. Fig. 3.17 shows $\sum$ as a function of H_s. Although there is a considerable amount of scatter in the data, $\sum$ is found to increase monotomically with H_s at low values, but levelling off for larger H_s at $\sum \simeq 0.145 \pm 0.05$ (by visual estimation). This behaviour is quite consistent with the estimate of the mean slope of the wave of maximum steepness as $^1/_7 \simeq 0.143$ (LeBlond and Mysak, 1978). The slope statistics thus behave as would be expected from earlier knowledge, increasing with wave height and tending to limiting maximum average value.

The relation between S and $\sum$ depends on the shape of the wave spectrum. A wave spectrum of the form $\phi(\omega)$ [with units of $m^2/(rad/sec)$] has moments

$$m_i = \int_0^\infty \omega^i \phi(\omega) d\omega \tag{3.28}$$

The significant wave height is related to the zeroth moment,

$$H_s = 4\sigma = 4m_o^{1/2} \tag{3.29}$$

whereas the root-mean-square slope is given by

$$\textstyle\sum^2 = \int_0^\infty k^2 \phi(\omega) d\omega \tag{3.30}$$

which is related, via the dispersion relation $\omega^2 = gk$ to the fourth moment of the spectrum:

$$\textstyle\sum^2 = \frac{m_4}{g^2} \tag{3.31}$$

The distinguishing feature of the Wallops spectrum is that it is entirely defined, in shape as well as in level, in terms of internal variables: S (the significant wave slope) and ω_o, the peak frequency. The Wallops spectrum is written (Huang et al., 1981)

$$\phi_W(\omega) = \frac{\beta g^2}{\omega^m \omega^{5-m}} \exp\left\{\frac{-m}{4}\left[\frac{\omega_o}{\omega}\right]^4\right\} \tag{3.32}$$

with

$$\beta = (2\pi S)^2 / \{\Gamma(\frac{m-1}{4}) 4^{(\frac{m-5}{4})}\} \tag{3.33}$$

and the high-frequency spectral slope m given by

$$m = \left| \log(\sqrt{2}\pi S)^2 / \log 2 \right| \qquad (3.34)$$

With the data in hand on S, $\sum$ and the level of the spectral peak $\phi_W(\omega_o)$, it is thus possible to test the applicability of the Wallops spectrum in two ways: by comparing measured values of $\sum$, and $\phi_W(\omega_o)$, with values calculated on the basis of the Wallops spectrum.

The fourth moment of the Wallops spectrum as expressed in Huang et al. (1981) gives the following relation between $\sum$ and S:

$$\frac{\sum^2}{S^2} = m\pi^2 \Gamma\left(\frac{m-5}{4}\right) / \Gamma\left(\frac{m-1}{4}\right) \qquad (3.35)$$

This ratio $\sum/S$ is plotted in Fig. 3.18 for values of $\sum$ and S obtained from the WAVEC data, and compared with the value predicted by the Wallops spectrum (3.35) with m obtained from (3.34). Measured values of $\sum/S$ are generally smaller than Wallops values for $\sum/S > 6$ and greater for smaller $\sum/S$. A generally poor correspondence between measured and theoretical values is suggested by these data.

However, comparison of time series of $\sum/S$ (measured) with $\sum/S$ (Wallops), shown in Fig. 3.19, indicates that the greatest differences between the two values occur for low values of S, i.e. for low sea states; whenever $S \gtrsim 20 \times 10^{-3}$, the Wallops spectral prediction of the ratio $\sum/S$ is reasonably close to measurements, with $\sum/S$ (measured) $\simeq 5$ and $\sum/S$ (Wallops) $\simeq 6.5$. It is perhaps not surprising, although still far from conclusive, to discover that the Wallops spectrum, whose formulation is anchored on the importance of wave slopes in determining the spectral shape and level, is found to agree most closely with observations made at times of larger significant wave slopes.

The other test of the Wallops spectrum is a comparison of the maximum spectral level observed at the peak ($\phi(\omega_o)$) with that expected of a Wallops spectrum of the measured significant slope $\phi_W(\omega_o)$ given by

$$\phi_W(\omega_o) = \frac{\beta g^2 e^{-m/4}}{\omega_o^5} \tag{3.36}$$

with β and m as calculated above from S, using (3.33) and (3.34). The comparison is shown in Fig. 3.20, and is much closer than for the $\sum/S$ ratio, most likely because a comparison of spectral peaks is much less sensitive to the shape of the spectrum than a comparison of fourth moments.

Although this comparison of the measured slopes with those predicted by the Wallops spectrum indicates some similarity only for larger sea states, the comparison of spectral levels is much more favourable and indicates the need for further and more detailed evaluation of the Wallops spectrum.

b) Slope-Elevation Statistics

Laboratory studies by Huang et al. (1984) have shown that a relatively simple model of the probability density function of slope and elevation corresponded closely to observations. Fig. 3.21 shows a comparison between observed and model slope statistics for uni-directional waves. As a simple test for field data, we have plotted normalized magnitudes of the slope $(S_E^2 + S_N^2)^{1/2}/\sum$ against normalized sea level displacement $\eta' = \eta/\sigma$. Huang's theoretical model for the magnitude of the slopes is simply the upper half of the probability contour plots shown in Fig. 3.22. A simple qualitative interpretation of the Huang et al. (1984) results is that

1) the most likely slopes and elevations are both zero: the contours of the joint probability density function peak at $\eta/\sigma = 0$, slope = 0;

2) higher slopes are more probable for low elevations;

3) higher elevations are more probable at low slopes;

4) for large waves, there is a significant asymmetry: large negative elevations are more probable for small slopes, reflecting a well known asymmetry of surface gravity waves, with sharp crests and flat troughs.

The scatter plots shown in Fig. 3.21 exhibit many of the features of the Huang et al. probability density functions. Each point shown on the scatter plots represents one realization of an elevation-slope pair. The density of points in these plots is thus a measure of the joint probability density of slopes and elevations. In all scatter plots the density of points is highest just above the origin, near where the Huang et al. theory predicts it. Point densities are roughly symmetric about mean sea level for small slopes (Fig. 3.21a; $\Sigma = 0.085$, $S = 0.007$) but exhibit a concentration of points at negative elevations for larger significant slopes (Fig. 3.21b; $\Sigma = 0.141$, $S = 0.024$).

c) Conclusions

The spectral comparisons, and the apparent corroboration of of the joint probability density model, suggest that the "Wallops" approach relating elevations and slopes may indeed be a practical and useful way of parameterizing sea state parameters. Comparisons undertaken here are based on too few data to draw more definite conclusions; the results suggest, however, that further work in this area is warranted.

4.0 WAVE PREDICTION IN COASTAL B.C. WATERS

Coastal engineering developments related to harbour construction, mining, or oil and gas exploration will require design wave criteria. The principal needs include a knowledge of wave height exceedances and persistences, joint distributions of heights and periods, and of heights and directions, as well as estimates of extreme wave heights and associated periods. These criteria may be derived from instrumental data, such as those collected in the present study, or they may be hindcasted from historical wind fields. Seaward of the outer coast instrumental data are extremely sparce; those that do exist are reviewed in Section 2.2 and in the following section. Conventional spectral wave hindcasting, as one means of predicting sea state conditions to supplement measurements, is expected to be successful here since the waves are in deep water, generated by storm systems moving generally onto the coast from the open ocean. In the coastal waters of Queen Charlotte Sound, Hecate Strait and Dixon Entrance conditions are, however, much more complicated, and hindcast wave accuracy will depend on a number of factors particular to this region.

These factors are reviewed in Section 4.2, together with a discussion of overwater wind prediction, spectral resolution, spatial coverage and strategies for hindcasting the coastal waters. Conclusions and recommendations on model design and application are then presented.

4.1 Normals and Extremes Based on Instrumental Data

a) Data Sources and Methods

We consider here the problem of parameterizing the distribution function for significant wave height at offshore locations, and at the coastal measurement sites, for the purpose of estimating normal and extreme exceedances. These functions also reveal expected variations in wave climate severity over the Gulf of of Alaska and B.C. waters. The data examined here are comprised of the United States NDBO North Pacific measurements (National Climate Data Centre, 1983) at three stations (Fig. 4.1):

		Years
46003	Central Gulf of Alaska	1976 to 1981
46004	Eastern Gulf of Alaska	1976 to 1982
46005	North Western U.S. waters	1976 to 1982

in addition to the Langara West (211), McInnes Island (214), Hecate Strait (215) and Queen Charlotte Sound (216) measurements (Fig. 1.1). For each data set the cumulative relative frequency was determined in 0.5 m (NDBO) or 0.25 m (this study) intervals for all measurements. These distributions, which approximate expected annual conditions, were then plotted on Weibull probability paper to examine trends as a function of wave height. Sampling intervals for the data varied as follows:

	τ hours
all NDBO buoys	3
Langara West (211)	1
McInnes Is. (214), Hecate St. (215) Queen Charlotte Sd. (216)	3

The cumulative distributions were fitted with the 3-parameter analytic function

$$Q(Hm_o) = \exp\left\{ -\left[\frac{Hm_o - A}{B}\right]^C \right\} \qquad (4.1)$$

where $Q(Hm_o)$ = the probability that a significant wave height will exceed the value of Hm_o,

A, B, C = fitting parameters

Once the fitting parameters are determined (4.1) can be inverted to solve for the expected wave height at any given exceedance level. If it is assumed that all wave height samples are uncorrelated and obey the same distribution

$$Q(Hm_o) = \tau (T_R M)^{-1} \qquad (4.2)$$

where T_R = return period in years

M = number of hours in one year (thus τ/M = sampling interval in years).

Thus, from (4.1)

$$\ln \ln Q^{-1} = C \ln(Hm_o - A) - C \ln B \qquad (4.3)$$

Letting

$$y = \ln \ln Q^{-1}$$
$$m = C$$
$$b = -C \ln B$$

we obtain

$$Hm_o = A + \exp\left(\frac{y - b}{m}\right) \qquad (4.4)$$

for the wave height prediction equation.

b) Results

The cumulative distributions for the 3 offshore sites are shown in Fig. 4.2. As expected buoy 46003 measured the most severe conditions, including some very large (Hm_o> 19 m), but very rare wave heights. The departure of the upper tail of this curve from a straight line through the middle region indicates that the Weibull distribution function is not a good model for the extreme right-hand tail. The two remaining curves, representing locations increasingly further away from the principal winter storm track (46004 and then 46005) show slightly less severe sea states.

By way of examples, the following table lists the wave heights exceeded by 50%, 80% and 95% of measurements:

Percentage Exceedance		NDBO Station Numbers 46003	46004	46005
50	$Hm_o >$	2.55	2.35	2.10
80	$Hm_o >$	3.95	3.65	3.35
95	$Hm_o >$	5.60	5.20	4.90

The distributions at 46004 and 46005 are also more clearly fitted with a Weibull distribution over the full range of observed sea states above one or two metres.

The cumulative frequency curves for the four coastal stations are shown in Fig. 4.3; here a much less uniform picture emerges and one must look to the influence of landforms on sheltering certain locations to explain the distributions. Comparing Langara West with Queen Charlotte Sound we find that for Hm_o < 2.5 m the wave climate is about equally severe. This is reasonable since each location is about equally exposed to swell. One might argue that Queen Charlotte Sound, being more open to the south, will be slightly more incluenced by swell generated by southerly storms and this is borne out by the data.

At low wave heights both the Hecate Strait and McInnes Island curves lie will below the exposed sites. This is consistent with their more sheltered locations - Hecate Strait from westerly swell and McInnes Island from south-southwesterly wave energy. Moreover, as the refraction analysis has shown, the WAVEC at McInnes Island was located in an area of weak divergence produced by refraction on Queen Charlotte Bank. This would also contribute to the fact that it has the least severe low-wave climate of these four sites.

For sea states with Hm_o > 3 m, the distributions for all but Queen Charlotte Sound converge on each other, although they separate again for Hm_o > 6 m. The Queen Charlotte Sound location is obviously the most exposed, particularly to storms characterized by intense, persistent southerly along-coast flows (see the discussion of storms in Seaconsult, March, 1983a), and this exceedance curve lies furthest to the right. As expected, the Hecate Strait location, also well exposed to southerly winds, has a large-wave climate only slightly less severe than Queen Charlotte Sound.

Although Langara West faces the open ocean to its west, it is somewhat protected by the Queen Charlotte Islands especially from southerly storm winds. Consequently its large wave climate differs from the other two outer sites and this is reflected in its Hm_o-distribution curve. The steeper slope of this curve, as plotted in Fig. 4.3, will lower the wave height extremes from those calculated at Hecate Strait and Queen Charlotte Sound.

McInnes Island, which lies very close to the inner coast has the least severe large-wave climate of the four sites. It is not, however, significantly different from the Hecate Strait site except at the upper end. This is attributed to the manner in which storms affect Queen Charlotte Sound, and the fact that for southerly winds McInnes Island is only slightly less exposed than Station 215.

A comparison of cumulative distributions - Queen Charlotte Sound and Hecate Strait versus Stations 46003 and 46004 - is presented in Fig. 4.4. Somewhat surprisingly Queen Charlotte Sound was found to have a slightly more severe climate than further out in the Gulf (at 46004). This may be due to intensification of storm systems as they move coastward from 46004, or from the limitations of the short data sample at Queen Charlotte Sound (i.e. 1982 - 1984 were more stormy that the long-term trend, although this is, of course only approximately known from 7 years of data at 46004). It could also be that both factors contribute.

The slope of these distributions does indicate, however, a wave climate governed by the same factors; i.e. generated by the same sequences of storms, with differences in intensity related to the position relative to trajectory and deepening rate of the weather systems. Differences at the low end of the curves are most likely related to differing exposures to swell. As noted above, Hecate Strait differs in character from the others by the sheltering afforded by Graham Island.

One important consequence of the changes in slope of the coastal distributions (Fig. 4.3) is that all measured waves heights are <u>not</u> identically distributed. Physically this may result from the relative importance of swell arriving at each location, which is not related to local storms that give rise to the larger waves in each sample. Since we expect the largest waves, and the design wave itself, to be generated in local storms, then estimates of these conditions derived from the cumulative distributions must be based on the distribution of large waves where the contribution of background swell is removed. Only in this way can one have confidence in extrapolating into the right-hand tail of the large wave distribution.

One approximation to this is given by (4.1) with the distribution limited below by A. For the data in Fig. 4.2 and 4.3 the following fitting parameters have been obtained:

Station	No	A	B	C	R^2
Langara West	211	2.0	0.973	1.027	0.981
McInnes Island	214	1.5	1.014	0.9099	0.878
Hecate Strait	215	1.5	1.095	0.9778	0.982
Queen Charlotte Sound	216	2.0	1.224	1.013	0.975
NDBO	46003	2.0	1.125	0.954	0.998
NDBO	46004	2.0	1.062	1.047	0.985

The A-values were selected by inspection of the plotted distributions and confirmed by plotting the limited distributions; samples are shown in Fig. 4.5. The B and C parameters were calculated using a least squares regression of $\ell n\ \ell n\ Q^{-1}$ on $\ell n(Hm_o - A)$. The correlation coefficient (R^2) values are given above for each site, and the following functions for $Hm_o(T_R)$ were obtained:

Langara West -

$$Hm_o = 2.0 + \exp\left(\frac{y-0.0277}{1.0272}\right)$$

$$y = \ell n\ \ell n(8760T_R)$$

Hecate Strait -

$$Hm_o = 1.5 + \exp\left(\frac{y+0.0884}{0.9778}\right)$$

$$y = \ell n\ \ell n(2920T_R)$$

Queen Charlotte Sound -

$$Hm_o = 2.0 + \exp\left(\frac{y+0.2051}{1.0126}\right)$$

$$y = \ell n\ \ell n(2920T_R)$$

Buoy 46003 -

$$Hm_o = 2.0 + \exp\left(\frac{y+0.1126}{0.9535}\right)$$

$$y = \ell n\ \ell n(2920T_R)$$

Buoy 46004 -

$$Hm_o = 2.0 + \exp\left(\frac{y+0.0627}{1.0468}\right)$$

$$y = \ell n\ \ell n(2920T_R)$$

Normal and extreme significant wave heights by return period are given in Table 4.1. As expected from the cumulative distributions, Station 46003, lying in the primary winter storm track has the largest extremes. Large waves at Queen Charlotte Sound and Station 46004 do not differ enough to be statistically significant, which is reasonable given their exposure to storms hitting the B.C. coast. Langara West extremes are, as expected, lower due to the sheltering influence the Queen Charlotte Islands have on Dixon Entrance. Extreme waves decrease in Queen Charlotte Sound as sheltering becomes more important.

The analytic distribution for Station 46003 indicates that Hm_o = 19 m has a return period of about 208 years. Values of Hm_o above 12 m have been observed 6 times in March. It is impossible to tell from the data summarized in National Climate Data Centre (1983) whether the high value all derive from one storm (seems likely) or from several unconnected events. If they do come from one storm the return period function given above for Hm_o would be reasonable.

An extreme value analysis of significant wave height was carried out on the SOWM hindcast data. Eight maxima, one in each of 8 winter seasons from 1974 to 1982, were extracted from the long-term time series at the nearest point offshore of the study area. The data were fitted with the FT-I asymptotic function.

$$P(Hm_o) = \exp\left[-\exp\left(-\left[\frac{Hm_o - A}{B}\right]\right)\right] \tag{4.5}$$

using the plotting position formula

$$P(Hm_o) = 1 - \left[\frac{i - 0.44}{N + 0.12}\right] \tag{4.6}$$

The linear regression gives the following prediction equation

$$Hm_o(T_R) = 1.11(-\ell n(-\ell n P(Hm_o)) + 12.1 \tag{4.7}$$

with

$$P(Hm_o) = 1 - \frac{1}{T_R} \tag{4.8}$$

where T_R is the return period in years. The predictions from (4.7) give the following values for $Hm_o(T_R)$, in relation to the Weibull analyses of the 46004 buoy data and the Station 216 measurements:

	T_R Years		
	10	50	100
SOWM data	14.6	16.4	17.2
Buoy 46004	11.8	13.3	13.9
Station 216 Queen Charlotte Sd.	14.2	16.1	16.9

The SOWM predictions are in close agreement with the new measurements in Queen Charlotte Sound, but diverge markedly from the buoy data further offshore. The reasons for this difference are not well understood.

c) Limitations

As shown by the R^2 value (0.878) for McInnes Island, the 3-parameter Weibull procedure fails to yield a useful distribution function there. Other choices for A (e.g. A=4 m, attempting to isolate the large-wave population) did not improve the results. Although untested for the moment, one can hypothesize that very large waves arriving along the Queen Charlotte Sound coastline would result from westerly storm winds. Only these have sufficient fetch to generate extremes. However, the directional frequency analysis for wind speed at McKenney Rock (Fig. 4.6) shows that westerly storm winds are much less frequent than southerly - south-easterly storm winds. Thus it appears that because of the rarity of long-fetch extreme wind conditions, a longer time series of directional measurements than now available would be needed, and that the above type of Weibull analysis should be based on wave height distributions stratified by direction.

Given this type of difficulty at McInnes Island, and the variability in the quality of Weibull distribution fitting of wave height time series at the other locations, it would appear that extreme wave hindcasting is warranted. This procedure would focus directly on events producing large waves over the whole study area. Good spatial coverage would be obtained, and the problems of specifying the right-hand tail of a distribution function from low to intermediate wave heights would be avoided. Hindcasting the inner waters accurately would, however, require consideration of a number of factors. These are reviewed in subsequent sections, leading to recommendations on model selection and application.

4.2 Wave Hindcasting

a) Factors Affecting the Accuracy of Results

Six factors are important in determining the accuracy of hindcast wave spectra in the coastal waters of Queen Charlotte Sound, Hecate Strait and Dixon Entrance. These include the character of severe storms hitting the coast, the effects of bathymetry, topographic sheltering, open ocean swell, over-water wind prediction and the theory incorporated into the model. Each of these factors is discussed more fully below, including both severe event hindcasting and lower level swell-wind sea prediction as considerations.

Character of Storms

The winter wave climate is dominated by storm winds generated in transient low-pressure systems. Two such systems, each observed within this study, appear characteristic of expected severe events; these are discussed and illustrated in Seaconsult (1983a, pp. 15-17). The first type, occurring for example on Dec. 14-15, 1982, is typically a large-scale, very deep low pressure system moving slowly eastward over the Gulf of Alaska at a latitude of about 50°N. Cyclonic circulations over scales of 1000 km or more are typical. These weather systems, with central low pressures as deep as 940 to 950 mb, create strong, southerly to south-southeasterly winds along the coast. Tightening of isobars is observed between the coastal mountains and open ocean waters to the west; this gives high wind speeds across Queen Charlotte Sound and up Hecate Strait (Fig. 4.7). If these systems tend to stall over the central Gulf of Alaska, then the coastal winds will persist at strength. From the hindcasting point of view, correctly modelling the surface pressure pattern, and hence the wind field suitably reduced to some reference elevation, is the key requirement. The major complication arises from orographic flow modification by the surrounding mountains.

The second type of storm, exemplified by the December 24-25, 1982 storm (Seaconsult, 1983a, pp. 16-17), is by contrast smaller in scale than the above type. These begin over the Gulf of Alaska, often as a wave in the cyclonic circulation about the Aleutian Low, deepening rapidly as they approach the coast. The sequence of three surface pressure analyses shown in Fig. 4.8 illustrates this type of event: speeds of approach range up to 35 to 40 knots, and the tight circulation, with scales of the order of 400 to 500 km, produces very intense winds within coastal seas the size of Queen Charlotte Sound-Hecate Strait. The most severe winds, and largest waves, generally occur behind frontal features embedded in these weather systems. Inspection of Fig. 4.8c shows that winds observed at the coastal stations exceeded 55 knots, with westerly fetches, and are in good qualitative agreement with the pressure analysis for direction. Because these storms move rapidly, near the group velocity for large deep-water waves, there is the possibility of a fairly continuous of exchange of momentum from the wind to the wave field, as the storm, and the waves generated offshore, move toward the coast in concert. This overcomes the lack of long fetch resulting from the large curvature of the isobaric patterns. It appears that this type of storm may, in fact, give the most severe wave conditions in coastal waters; it was this kind of weather system discussed by James (1969) for October 22-23, 1968 with $H_s \simeq 19$ m in Queen Charlotte Sound.

Resolution of wind field variations in these storms will require spatial grids with increments of 10 to 20 km over an area of about 600 km on a side. Because of the coupling between wave generation and storm movement, the hindcast will have to begin with the formation of the storm or its entry into the Gulf of Alaska, perhaps as far west as 170°W. This suggests that a translating, fine scale grid linked to the central low pressure point of the storm, embedded in a coarser scale grid covering the Gulf of Alaska would yield an accurate, while at the same time an efficient, hindcasting approach.

It is presently unclear what problems will have to be resolved in generating accurate overwater wind fields in these types of storms. The qualitative agreement between isobaric patterns and coastal wind observations indicates that the pressure charts are, as in conventional hindcasts, the most appropriate starting point. Nevertheless, one anticipates that gradient winds will require adjustment for speed and direction in ways dependent on local effects produced mainly the the surrounding mountains. The most accurate data for either effecting the adjustment, or for verifying empirical models, would be the coastal measurements, with due regard for siting characteristics (see e.g. Phillips, 1977). As a preliminary step, the relationship of Cape St. James winds to those measured at McKenney Rock in this study, have been examined statistically in terms of directional shifts and speed ratios. The purpose is to establish a predictive relation for overwater winds in Queen Charlotte Sound using the Cape St. James data as input. This is discussed in Section (b) below. Similar relations for the other coastal stations are required, and once in place, can be used to edit pressure-field derived winds for frontal effects and landform modifications.

Boundary layer models of the general type published by Danard (1977) and Jensen and Danard (1975) could, in principle, be used to incorporate orographic and frictional effects. These are driven by free atmospheric parameters derived from upper air measurements or from geostrophic wind analyses. Because these models make a number of important simplifying assumptions, it is yet unproven that they can achieve better accuracy than a more hand-done editing procedure using observations, at similar levels of effort. Given the complexity of the coastal topography, and the need to carefully verify model-derived winds using measurements, it appears that a man-machine procedure based on pressure field analyses and boundary layer theory, with wind field editing to incorporate surface wind data (met stations and transient ships giving a partial or full kinematic analysis) is the preferable approach for extreme event hindcasting. A more objective, machine-based model should be reconsidered if a continuous, multi-year hindcast of wind and wave conditions is required.

Bathymetric Refraction

The importance of refraction on the coastal wave climate has been established in Section 3.1 using theoretical models. It was shown there that shallow-water effects can account for some of the observed variations in wave heights in Dixon Entrance, northern Hecate Strait and the eastern side of Queen Charlotte Sound. Thus, a wave hindcast model for the coastal waters must incorporate shallow water transformation processes. Given the depths over most of the area (> 20 m), bathymetric refraction is the dominant process. In particular areas - Rose Spit and the banks to the east of Graham Island - depth-dependent saturation spectra, or other non-linear parameterizations may need to be considered, although these may be best handled by a second stage localized calculation designed to meet specific user requirements. Refraction by current shear was shown to be negligible over most of the area (except the above mentioned shallow regions) and so may be ignored in an extreme event hindcast model.

Topographic Sheltering

Variations in wave climate in the coastal waters are readily linked to the exposure of each site to waves propagating in from the open ocean and to storm winds. Thus the hindcast model must properly account for the effects of surrounding landforms on wave generation, and of water depth variations producing refraction of propagating wave energy. Landform influences are automatically incorporated into spatially-gridded models (e.g. discrete spectral models) provided they have sufficient resolution. The question of model boundaries and grid resolution are discussed in more detail in Section d) below.

Swell

Swell characteristics of the wave climate along the outer coast have been discussed by Seaconsult (1983a, pp. 5-7). In this case, "swell" was linked to generation in very-distant storms (≃ 3000 to 4000 km distant), and not to longer period ($T_p > 13$ s) large waves accompanying storms as they impringe on the coast. With this definition, swell heights averaged 2.5 to 3.4 m in a range up to 4 m and were frequent in winter months, generated by severe weather systems around the Western Pacific Rim. Some even originated in the southern hemisphere.

From a coastal engineering perspective, swells of this amplitude (≈ 1 to 2 m) with periods exceeding 16 to 18 s may play an important role in the design of breakwaters and harbours. Thus the design of a hindcast study must consider how best to incorporate swell. Alternatives include:

i) active generation and propagation - implying ocean-wide wind and wave models;

ii) a hybrid model where swell is "introduced" at the boundaries - but this requires knowledge of swell characteristics in mid-ocean and a suitable probabilistic model for combining swell and local generation events into realistic scenarios for design.

Simultaneous swell-wind sea modelling also requires compromise in spectral resolution to model both accurately; some notions on resolution are sketched out in Section c).

Overwater Wind Prediction

The accuracy of predicted wave conditions is governed mainly by the quality of overwater winds, given at either 19.5 m or 10 m reference elevations, or as the friction velocity u_*. The principal difficulty in the coastal area will be to model the influence of the mountains on the isobaric pattern, and in turn, on the boundary layer reduction of the wind to a surface field. As noted earlier, the most severe wave events may prove to be associated with rapidly moving, smaller scale storms. These storms are characterized by closed circulations largely bounded by the confines of the coastal sea contained between the Queen Charlotte Islands, Vancouver Island, and the B.C. mainland, at the time the storms have their greatest impact. Given the sensitivity of wave spectra to changes in wind direction, as well as to speed, it will be necessary to resolve these highly variable winds in space and time. Since most hindcast models have propagation schemes governed by a Courant number of one, temporal resolution will not be a problem in principle (integration time steps of 10 to 20 minutes), but may prove to be in practice since pressure data will be available only on 3-hour or 6-hour time bases. There is little basis in data to interpolate meaningfully from 3-hourly weather charts down to 1/4-hourly wind fields. This type of interpolation will have an effect, yet to be determined, on wave prediction accuracy.

Model Theory

As remarked above, the wave hindcasting model adopted must:

i) accomodate rapidly varying wind and wave fields, in time and space,

ii) incorporate shallow water effects,

iii) allow for sheltering by land masses, and

iv) handle swell and local wave generation simultaneously.

The simplest parametric wave height/period models (Sverdrup-Munk-Bretschneider, Wilson Equations) based on steady over-water winds are distinctly unsuitable in view of the above requirements. Parametric spectral models (e.g. Hasselmann et al., 1976; Donelan, 1978) solve the problem of 2-dimensional spatial resolution, but are based on a theory for deep-water fetch-limited wave growth that is not appropriate for the storm characteristics found on this coast. Moreover, a hybrid calculation would be required for swell.

The best suited modelling approach is a discrete spectral model (e.g. Resio, 1981); Cardone et al., 1975; Golding, 1983) incorporating shallow water transformations. These models meet all of the above criteria; the primary requirements for accuracy are resolution of landmasses, bottom features and wave components given appropriate wind information.

b) Wind Correlations in Queen Charlotte Sound

Cape St. James wind observations represent one of the longest, consistently high quality records for the coastal area. For hindcasting wave conditions in Queen Charlotte Sound it is useful, then, to inquire as to whether or not empirical relations can be established to transform Cape St. James winds to overwater 10 m elevation winds applicable to the central area of Hecate Strait. This question has been addressed here by examining the correlation of winds at Cape St. James with those measured simultaneously at McKenney Rock in this study.

A U2A anemometer was in place at Cape St. James at an elevation of 100.3 m above MSL. A one-minute mean wind observation (speed and direction) has beed assumed. The McKenney Rock station anemometer was located 29.2 m above MSL. A one-minute mean wind was recorded here also.

Nearly-synchronous wind data pairs (within ± 15 minutes) were selected from each time series for comparison. This yielded 3916 data pairs. First the statistics (mean and standard deviation) of differences in direction

$$d_{ij} = D_{ij}(CSJ) - D_{ij}(MR) \qquad (4.9)$$

where D = direction
CSJ = Cape St. James
MR = McKenney Rock

were tabulated in five speed classes (i) and 8 direction classes (j) for the CSJ winds. These were computed in two ways: for the measured time series and for the time series reduced to 10 m above MSL. The reduction formula used was

$$U_{10} = U_Z \left(\frac{10}{h_Z}\right)^{\alpha} \qquad (4.10)$$

where U = wind speed (m/s)
h_Z = anemometer elevation (m)
α = 0.15

These yield reduction coefficients of 0.71 and 0.85 at CSJ and MR respectively. Atmospheric stability considerations were neglected, and any gust effects from the cliffs around Cape St. James on the anemometer readings were ignored.

The directional differences d_{ij} are given in Tables 4.2 and 4.3 for U_i, $i=1,\ldots,5$ in 5 m/s increments, and D_j, $j=1,\ldots,8$ in 45 degree increments. The mean wind shifts follow expected trends: highest winds are from the SE and show reasonably small counterclockwise shifts; greater rotations averaging about 50 to 60 degree counterclockwise appear in S to W winds, in keeping with flow modification by the Coastal Range mountains; N, NE winds rarely attain high speeds, presumably due to blocking by the Queen Charlotte Islands, and may be unrepresentative of McKenney Rock winds for this reason.

For reduced winds there are too few values above 15 m/s to give a reliable statistical measure. Between 5 and 15 m/s (Table 4.3) the standard deviation ranges from about one-half to two times the mean shift. Such large variability, commonly seen in wind statistics, makes the d_{ij} coefficients difficult to use in a deterministic sense, and they would only be appropriate for converting a long time series of CSJ winds to over-water MR winds for subsequent statistical analysis.

Finally, the ratios of wind speed

$$r_{ij} = U_{ij}(MR)/U_{ij}(CSJ) \qquad (4.11)$$

were computed in three ways: (i) without any corrections for direction and height, (ii) correcting for direction using the d_{ij} coefficients, and (iii) correcting for direction and anemometer height with (4.10). The results are given in Tables 4.4 to 4.6. We find that, generally, both mean ratios and standard deviations decrease with increasing wind speed. It is surprising to find, however, that for well exposed directions (SE, S, SW) some r-values exceed one giving higher wind speeds at MR that at CSJ. It is to be noted, however, that in most of these cases the standard deviation tends to be rather large.

As shown in Table 4.4, 1748 data pairs or some 44.6% of the sample failed to lie within 30 degrees of each other and so were not included in the calculation of r_{ij}. Applying the d_{ij} coefficients reduced the rejection total to 1140; relaxing the directional coincidence criteria to 45 degrees reduced the total yet further to 776, or 19.8% of the sample (Tables 4.5 and 4.6).

Based on the coefficients in Tables 4.3 and 4.6, overwater wind speed U and direction D near McKenney Rock can be estimated from measured winds at Cape St. James using

$$\left.\begin{aligned} U &= 0.71\ r_{ij} U(CSJ) \\ D &= d_{ij} + D(CSJ) \end{aligned}\right\} \qquad (4.12)$$

where $U(CSJ)$ = anemometer wind speed at Cape St. James

r_{ij} = speed transfer coefficient in the i-th speed class based on 0.71 U(CSJ) and the j-th direction sector (Table 4.6)

$D(CSJ)$ = wind direction at the Cape St. James anemometer

d_{ij} = directional shift parameter in the i-th speed class based on 0.71 U(CSJ) and the j-th direction sector (Table 4.3)

Relation (4.12) applies only in a statistical sense, i.e. averaged over many realizations and should not be used to convert individual storm time series in a strictly deterministic manner. The variance to be expected for converted speed and direction is contained in the tables for r_{ij} and d_{ij}; simulated wind time series reflecting this variability could be derived from the Cape St. James records assuming the values of r and d are normally distributed about their means, and that U and D show some degree of auto-correlation.

The large variances noted above indicate a less than satisfactory correlation. Certainly one consequence of this is the implied difficulty in deriving vector wind fields over the inner waters with only the coastal wind observations for supplemental input to the isobaric analyses. One suspects that often these wind observations will fail to be representative of the overwater surface wind, especially in small scale weather systems characterized by large wind shear. It follows, therefore, that the coastal data stations are not adequate for prescribing winds over Queen Charlotte Sound - Hecate Strait for hindcasting, and that an automatic weather station (or several) at exposed sites like McKenney Rock are needed in the future. This hypothesis requires further testing by hindcasting wind fields during the 1982-84 study periods for comparison with the McKenney Rock measurements.

c) Spectral Resolution

For some engineering applications, concerned principally with freely-floating or tethered-floating operations and breakwater-harbour design, swell information is needed. If these data are hindcasted, then the spectral parameterization must resolve swell and distinguish it from locally generated wind waves. Generally, swell will appear distinctly separate from wind sea only at low energy sea states. Two examples of bi-modal spectra are shown in Fig. 4.9. As noted above, the sea state is comparatively low; Hm_o equals 3.5 m and 1.7 m respectively.

In order to model this type of combined sea response, one must choose the type of frequency discretization most suitable for the type of information needed, without compromising how physical processes, e.g. wave-wave interactions, are modelled in the generation stage. There are really only two choices: one where equal frequency increments are used (very convenient for model coding) and one where sequential frequencies are in a constant ratio. These can be represented by:

(1) $$f_{i+1} - f_i = \Delta f = \text{constant}$$

(2) $$\frac{f_{i+1}}{f_i} = \text{constant}$$

A comparison of these choices is shown in Fig. 4.9 for f_i = 0.04 Hz, Δf = 0.0121 Hz and f_{i+1}/f_i = 1.13. The first method gives the best resolution at the high-frequency end of the spectrum, but poorest over the swell portion. Method (2), conversely, resolves swell best but has increasingly poor resolution at higher frequencies. It is clear that both methods would work (the choice for Δf and the ratio are quite arbitrary here) but that method (2) gives the better frequency discrimination of sea and swell. A second illustration of approach (2) is shown in Fig. 4.10.

The period discrimination for each method, corresponding to the frequencies illustrated above, is as follows for the swell portion of the spectrum:

	Central Period (s)						
Approach (1)	35.8	25.0	19.2	15.6	13.1 . . .		
Approach (2)	28.3	25.0	22.1	19.6	17.3	15.3	13.6

This shows how the equal-ratio approach provides a much more even resolution of swell with periods above 13 s. The choice of method will depend upon the hindcasting strategy, i.e. the importance of accurately modelled swell, and the effect of diminished resolution in the high-frequency tail. This latter aspect may not be too important since the tail is usually saturated above 0.17 Hz under most moderate wind conditions.

d) Spatial Coverage and Resolution

Model Boundaries and Grid Scales

If a commitment is made to hindcasting distant swell and local wave generation, then model boundaries are prescribed by surrounding landmasses on the Pacific Rim. As noted earlier hemispheric (or global) wind modelling would then be required in order to simulate storms properly over the whole ocean basin.

In a more modest approach it would be possible to place mid-ocean boundaries so as to capture characteristic West Coast storms, and introduce swell data, if it is known, at these boundaries explicitly. Consideration of large scale storms and wind flow patterns indicates that a model area bounded by 127°W - 160°W and 37°N - 60°N would be appropriate for the Gulf of Alaska. Coarse grid resolution, suitable to model winds and waves from large scale weather systems, and to give a rough resolution of the coastal seas so that wave fields can be spun-up there to reasonable initial values, should be approximately 60 km. This would yield about 700 water points.

It is clear, however, that the smaller scale storms require finer resolution to model the wind field variations; a spacing to 10 to 20 km was suggested earlier, or about 3 to 6 times finer than the coarse grid. These scales are based on wind field curvatures inferred from isobaric patterns and some coastal measurements, and should be sufficiently small to model the effect of rapid changes in wind orientation and speed on local wind wave generation.

Topographic and Bathymetric Resolution

Landforms must be resolved sufficiently well to provide realistic sheltering effects on locations in the coastal waters, and bottom features must be parameterized at fine enough scales to give accurate refraction calculations. Our refraction studies (Section 3.1) have shown that in Queen Charlotte Sound and Hecate Strait these can be achieved with grid dimensions of 10 to 15 km. Two problems arise however: 1) resolution of the multitude of small islands and shoals along the inner coast is then too coarse and an "effective land boundary" must be placed just seaward of these islands, and 2) resolution of Learmonth Bank in the mouth of Dixon Entrance, shown previously to be important in modifying long-period waves, is insufficient for accurate refraction calculations.

The first problem is not serious in that a normal regional hindcast would not be expected to apply around the small islands and inlets. Diffraction effects, not incorporated into wind-wave hindcast models, would be expected, and a second level of engineering calculation treating combined refraction-diffraction, sheltering, and reflection, on very fine grid scales, would normally be made drawing boundary conditions from the hindcast spectra.

The second problem, concerning Learmonth Banks, is more serious; resolution on scales of 2 to 5 km is required. This demands a grid 3 to 5 times smaller than prescribed above for wind and bathymetry. Since this feature may be expected to alter hindcast spectra inside Dixon Entrance it must be modelled; the most practical solution is a special grid, nested into the coarser grids, upon which pure refraction or combined refraction-spectral growth can be calculated in a manner that transfers spectral wave information across the Bank. Since at its shallowest, water depths are about 45 m, wave periods shorter than about 9 s will be unaffected, and for all practical purposes only waves with periods greater than about 11 s need be considered. This gives a high-frequency cutoff of about 0.091 Hz for the Learmonth Bank refraction modifications. Since most hindcast models have only 5 to 7 frequency bands below this value, this may not be an onerous calculation and should be seriously considered.

e) Hindcasting Strategy

From the above discussion it appears that two types of storm systems must be examined in a hindcast study to determine extreme wave conditions. In terms of selecting and applying a model, the small-scale, rapidly moving storms are the more difficult of the two since fine grid resolution of winds, and of the wave action density fields, will be required along the storm trajectory, not just within coastal waters.

Model Implementation

The only class of model capable of meeting the requirements for accurate wave growth under rapidly varying wind conditions, allowing for sheltering and refraction, and providing 2-dimensional wave field output is the discrete spectral type with a depth-dependent propagation scheme. The most advanced of these - the Resio (1981) model in its latest version ADWAVE, the latest version of the Cardone et al. (1976) ODGP model and the System 21 model of the Danish Hydraulic Institute - all incorporate frequency-dependent relaxation procedures for wave growth under winds with rapidly changing directions, and procedures to simulate nonlinear wave-wave interactions. It is not clear how well any of these models reproduce exchanges of energy between wind sea under active generation and swell propagating through an area from remote sources. This exchange is not the process being modelled by wave-wave interactions, which takes place at higher frequencies within the spectrum being generated by local wind. In fact, energy exchanges between sea and swell are not well understood, and it is not clear if this will prove to be an important source of error for present state-of-the-art models applied in the study area.

The spectral, wind field and topographical resolution requirements may be summarized as follows:

Parameter Name	Symbol	Suggested Resolution	
energy density	$S(f,\theta)$	$1.12 < \frac{f_{i+1}}{f_i} < 1.15$, $i=1,2,\ldots,13$	
	(224 D.O.F.)	$f_1 = 0.174$ Hz	
		$\theta_{j+1}=\theta_j+\Delta\theta$,	$j=1,2,\ldots,15$
		$\theta_1 = 0°T$, $\Delta\theta = 22.5°$	
wind fields	$\underset{\sim}{U}(\underset{\sim}{x})$	$\Delta s \sim 60$ km $\Delta s \sim 10$ to 20 km	large systems small systems
land forms		$\Delta s \sim 10$ to 15 km	
bathymetry	$d(\underset{\sim}{x})$	$\Delta s \sim 10$ to 15 km, except $\Delta s \sim 2$ to 5 km	 on Learmonth Bank

Grid sizes for the coastal waters are particularly onerous for hindcasting the deep ocean conditions. Although a translating fine scale grid was suggested earlier for the small scale storms, this would lead to a very complicated code. A better compromise might be a set of three nested grids at multiples of 2 with the following properties (Δs = grid spacing, equal in both directions):

region	grid size
inner waters of Queen Charlotte Sound, Hecate Strait Dixon Entrance	Δs = 15 km except over Learmonth Bank where Δs=3 km used only where required
normal to coast, extending out along small scale storm trajectory $\pm$ 400 km to either side	Δs = 30 km matched to inner grid along outer coast
Gulf of Alaska	Δs = 60 km matched to mid-size grid

This approach is illustrated in Fig. 4.11, incorporating the earlier recommended mid-ocean boundaries. In this way, increasing emphasis is placed on wind field accuracy where it matters most, while preserving necessary resolution near the coast.

Decisions on Swell

The intent of hindcasting as described above is to predict storm generated waves accurately within the coastal waters. For strong persistent winds, and for storms that move roughly with the speed of the waves they generate, we may expect peak spectral wave periods of 12 to 15 s or more at maximum conditions. However, swell from distant sources, having up to 22 s periods as measured in this study, would not be predicted by the models. Two alternatives for introducing swell are then possible, based on empirical swell spectra derived from measurements in the North Pacific and elsewhere.

The first alternative would be to introduce the swell spectra with assumed directional properties along either the coarse, or fine grid ocean boundaries, independently of local wind conditions. The objective would be to compute wind sea and swell propagation, growth and dissipation simultaneously over most or part of the model domain, to give combined spectra at some inshore site of interest. One problem to be addressed would be the timing of such "introduced" swell so that it combines properly at the inshore site with maximum sea conditions. This approach is attractive for spectral models that compute energy exchanges between sea and swell, or that include wind-induced dissipation on swell (a weak process). If such processes can be correctly modelled then, in principle, the inshore spectra will be the most representative for combined conditions.

The other alternative would be to treat swell independently of the hindcast model and solve for it in a separate calculation. Then the sea and swell spectra at any inshore site could be added to give the final result. Because the primary factors affecting swell as it propagates into the coastal area are refraction, sheltering and, to a lesser extent, bottom frictional dissipation simpler models based on back-tracing wave rays from the site of interest could be used. Fig. 3.11 illustrates one such ray diagram for the McInnes Island buoy location. Swell energy propagates inward along each ray, with energy dissipation due to friction, and growth due to local wind (again, a weak process at the periods being considered). Typically 8 to 12 such ray diagrams will be used to transfer energy shoreward from the offshore swell spectrum, and in this way a complete directional swell spectrum $S(f,\theta)$ is computed at the inshore location.

In approaching the hindcasting problem this way one must, however, deal with the fact that the probability of the combined wave height, or design condition, is then conditional on the swell occurrence. The assessment of risk is thus governed by two independent probabilities, one for sea and one for swell. The present study has shown that swell is often observed in winter on the outer coast, but the precise nature of swell spectra, and their frequency of occurrence as a function of energy content, are not yet documented. The data collected in this study form a starting point although are of too short a duration to give reliable statistics. They could be supplemented by the NDBO buoy data further offshore, the Canadian buoy data at Tofino, and by the SOWM hindcast data (Lazanoff and Stevenson, 1978).

Thus to consider the effects of swell with a hindcast model defined on mid-ocean boundaries, four steps are required:

1) derive swell characteristics - spectral shape, energy content and directional distribution,
2) decide on where to introduce swell,
3) decide on computational procedure,
4) derive the probability model appropriate for combined design conditions for the problem being considered.

Interannual Variability

As shown above, application of a spectral model is closely tied to resolution of small scale storms and coastal features. The most efficient design in terms of how far out into the Pacific Ocean one must extend the intermediate grid will be linked to the size and trajectory, or sets of trajectories, for these weather systems. Our knowledge of these storms is presently too imprecise to finalize the model design; thus, a more complete documentation of the storm climatology (small and large-scale weather systems) is required for the northeastern Gulf of Alaska.

A preliminary examination of interannual variability (Seaconsult, 1983a; 1983b) has indicated reasonably large year-to-year changes in such parameters as maximum wave height, percentage occurrence of storm winds, and numbers of explosively deepening cyclones (ses also Murty et al. (undated), Danielson et al., 1957) at given offshore locations. These appear to be linked to variations in storm intensity and trajectory, as well as to the actual number of storms forming in any one year. The data are not always consistent, however, and it is believed that a better storm climatology, discriminating the storm types noted above in terms of wave generating potential, is warranted. In view of the apparently large variability from year-to-year, such a climatology should extend back as far in time as reliable weather data are available. In addition to optimizing the model application, it is a necessary step to calculating reliable return periods for the hindcast wave heights.

4.3 Conclusions

Conclusions following from the above analysis and discussion are:

1) Measured time series of wave height are too short to evaluate reliable extremes, particularly near the coast. Directional wave data are also required to discriminate large-wave populations for statistical analysis. Storm-based hindcasting is presently warranted for extreme wave estimates because of the limitations on measured data.

2) Different classes of weather systems are linked to severe sea states in the coastal waters. The worst appears to be small-scale, rapidly translating storms, moving onshore at about the group velocity of long wind waves. Present knowledge of these storms is not adequate to carry out wave hindcasting. An assessment of historical storm data concentrating on storm classification in relation to wave generation potential, frequency of occurrence, characteristics, and trajectory mapping are needed.

3) Given adequate wind field input, wave hindcast accuracy will depend on correctly reproducing the effects of bathymetric refraction, topographic sheltering and swell in addition to local generation and dissipation mechanisms. For small scale storms and coastal landforms, a grid resolution of 15 km would be sufficiently

accurate except over Learmonth Bank in Dixon Entrance where spacings of 3 km are required. The discrete spectral class of hindcast model appears most suitable for the coastal waters, operating with a minimum of 195 degrees of freedom made up of 13 frequencies in constant sequential ratio and 15 directions. The model must incorporate shallow water effects. Complete boundary and grid specifications are given in the text.

4) The correlation of Cape St. James winds with measurements at McKenney Rock demonstrates that prediction of overwater winds using the long-term Cape St. James observations is inaccurate in a deterministic sense. This result likely holds for the other shore stations in the area. Thus it appears that the shore station data are not adequate for verifying, or for incorporating directly into overwater wind fields. One or more automatic weather stations on exposed locations such as McKenney Rock are recommended. Further correlation studies between McKenney Rock measurements and other shore stations, together with wind field hindcasting of storm winds in Queen Charlotte Sound, are, however, required to strengthen the above conclusion and to yield useful hindcasting procedures.

5) Hindcasting of design sea states based on combined swell-wind sea conditions will require careful hindcast design. Where mid-ocean or coastal boundaries are used in the wave model, swell data are required for input. This demands information on:

- swell spectral shape
- swell direction
- frequency of occurrence

that is not now available. Studies of historical data are needed to quantify these parameters.

REFERENCES

Borgman, L.E., 1969. "Directional Spectra Models for Design Use." Proc. Offshore Tech. Cong., Paper No. OTC 1069, 721-746.

Cardone, V.J., W.J. Pierson and E.G. Ward, 1975. "Hindcasting the Directional Spectra of Hurricane-Generated Waves." Proc. Offshore Tech. Conf., Paper OTC 2332.

Cardone, V.J., H. Carlson, J.A. Ewing, K. Hasselmann, S. Lazanoff, W. McLeish and D. Ross, 1981. "The Surface Wave Environment in the GATE B/C Scale - Phase III." J. Phys. Oceanog., 11, 1280-1293.

Danard, M., 1977. "Computing Winds in Barrow Strait, NWT and Vicinity." Dept. of National Defence, Victoria B.C.

Danielson, E.F., W.V. Burt and M. Rattray, Jr.,1957. "Intensity and Frequency of Severe Storms in the Gulf of Alaska." Trans. Am. Geophys. Union, Vol. 38, No. 1, 44-49.

Donelan, M.A., 1978a. "A Simple Numerical Model for Wave and Wind Stress Prediction." Unpublished Manuscript, Environment Canada, CCIW, Burlington, 11 pp. + Tables and Figures.

Funke, E.R. and E.P.D. Mansard, 1979. "On the Synthesis of Realistic Sea-States in a Laboratory Flume." Nat. Res. Council, Canada, Hydraulic Laboratory Report LTR-HY-66.

Golding, B., 1983. "A Wave Prediction System for Real-Time Sea-State Forecasting." Journal Quart. JR Met Soc., Vol. 109, 393-416.

Hafer, R.A., 1970. "Wave Measurements from the Drilling Rig Sedco 135F off the Coast of British Columbia." Defence Res. Establ. Pacific, Report No. 70-3, 111 pp.

Hasselman, D.E., M. Dunckel, J.A. Ewing, 1980. "Directional Wave Spectra Observed During JONSWAP 1973." J. Phys. Oceanog., 10, (8), 1264-1280.

Hasselman, K., D.B. Ross, P. Muller and W. Sell, 1976. "A Parametric Wave Prediction Model." J. Phys. Oceanog., 6, 200-228.

Hodgins, D.O., 1983. "Ocean Waves: New Data Requirements for the East Coast." East Coast Offshore, 27-31

Holthuizen, 1983. "Observations of the Directional Distribution of Ocean-Wave Energy in Fetch-Limited Conditions." J. Phys. Oceanog., 13(2), 191-207.

Huang, N.E. and S.R. Long, 1981. "On the Importance of the Significant Slope in Empirical Wind-Wave Studies." J. Phys. Oceanog., 11, 569-573.

Huang, N.E., S.R. Long, C.C. Tung, Y. Yuen and L.F. Bliven, 1981. A Unified Two-Parameter Wave Spectral Model for a General Sea State." J. Fluid Mech., 112, 203-224

Huang, N.E., P.A. Hwang, H. Want, S.R. Long and L.F. Bliven, 1983. "A Study of the Spectral Models for Waves In Finite Water Depths." J. Geophys. Res., 88, C14, 9579-9587

Huang, N.E., S.R. Long, L.F. Bliven and C.C. Tung, 1984. "The Non-Gaussian Joint Probability Density Function of Slope and Elevation for a Nonlinear Gravity Wave Field." J. Geophys. Res., 89, C2, 1961-1972.

James, R.W., 1969. "Abnormal Changes in Wave Heights." Mariner's Weather Log, 13(6), 252-255.

Jensen, J.V., and M.B. Danard, 1975. "A Numerical Model for Surface Winds in Juan de Fuca, Haro and Georgia Straits." Prepared for AES, Meteorological Services Research Branch, Downsview, Ontario.

Lawson, L.M. and R.B. Long, 1983. "Multi-model Properties of the Surface-Wave Field Observed with Pitch-Roll Buoys During GATE." J. Phys. Oceanog., 13, 474-486.

Lazanoff, S.M. and N.M. Stevenson, 1975. "An Evaluation of a Hemispherical Operational Spectral Wave Model." Fleet Numerical Weather Central Tech. Report No. 75-3, 102 pp.

LeBlond, P.M. and L.A. Mysak, 1978. Waves in the Ocean. Ebevier, Amsterdam, 602 pp.

Long, R.B., 1980. "The Statistical Evaluation of Directional Spectrum Estimates from Pitch-Roll Buoy Data." J. Phys. Oceanog., 10, 944-952.

Long, R.B. and K. Hasselmann, 1979. "A Variational Technique For Extracting Directional Spectra from Multicomponent Wave Data." J. Phys. Oceanog., 9, 373-381.

Longuet-Higgins, M.S., D.F. Cartwright and N.D. Smith, 1961. Observations of the Directional Spectrum of Sea Waves Using the Motions of a Floating Buoy." Ocean Waves Spectra, Prentice-Hall, Englewood Cliffs, 111-132.

Mitsuyasu, H., F. Tasui, T. Suhara, S. Mizuno, M. Ohkusa, T. Honda and K. Rikiishi, 1975. "Observations of the Directional Spectrum of Ocean Waves Using a Cloverleaf Buoy." J. Phys. Oceanog., 5, 750-760.

Munk, W.H. and R.S. Arthur, 1952. "Wave Intensity Along a Refracted Ray." Proc. Nat. Bureau Standards Semicentennial Symposium on Gravity Waves, Wash., D.C. Nat. Bur. Standards, Circular 521, 95-108.

Murty, T.S., G.A. McBean, B. McKay, (undated). "Explosive Cyclogenesis Over the Northeast Pacific Ocean." Inst. of Ocean Sciences, Sidney, B.C.

National Climate Data Centre, 1983. Climate Summaries for NOAA Data Buoys. NOAA, U.S. Department of Commerce.

Neu, H.J.A., 1982. "11-Year Deep-Water Wave Climate of Canadian Atlantic Waters." Can. Tech. Dept. Hydrog. and Ocean Sci., No. 13.

Nue, H.J.A., 1984. "Interannual Variations and Longer-Term Changes in the Sea-State of the North Atlantic from 1970 to 1982." J. Geophys. Res., 89(C4), 6397-6402.

Ottesen Hansen, N., 1978. "Long Period Waves in Natural Wave Trains." Inst. Hydrodyn. and Hydraulic Eng., Tech. Univ. Denmark, Prog. Rep. 46, 13-24.

Phillips, D.W., 1977. "A Marine Climatology of Two Approaches To Kitimat, British Columbia." Atm. Envir. Service, Dowsview, Ontario, 74 pp.

Resio, D.T., 1981. "The Estimation of Wind-Wave Generation in a Discrete Spectra Model." J. Phys. Oceanog., 11, 510-525.

Sand, S.E., 1983. "Wave Grouping Described by Bounded Long Waves." Ocean Engineering, 9(6), 567-580.

Seaconsult Marine Research Ltd., 1983a. "Data Assessment, Analysis and Interpretation." Progress Report No. 1, Fisheries and Oceans, Canada.

Seaconsult Marine Research Ltd., 1983b. "Data Assessment, Analysis and Interpretation". Progress Report No. 2, Fisheries and Oceans, Canada.

Watts, J.S. Jr. and R.E. Faulkner, 1968. "Designing a Drilling Rig for Severe Seas." Ocean Industry, Vol. 3, No. 11, 28-27.

Worthington, H.W. and J.B. Herbich, 1971. Computer Predictions of Wave Heights in Coastal Areas." Proc. Offshore Technology Conf., Houston, Texas, Vol. II, 142-156.

TABLES

Table 2.1

Comparison of measured significant wave height exceedances with equivalent visual wave height exceedances (SSMO) for Stations 213 (Bonilla Island) and 215 (Hecate Strait).

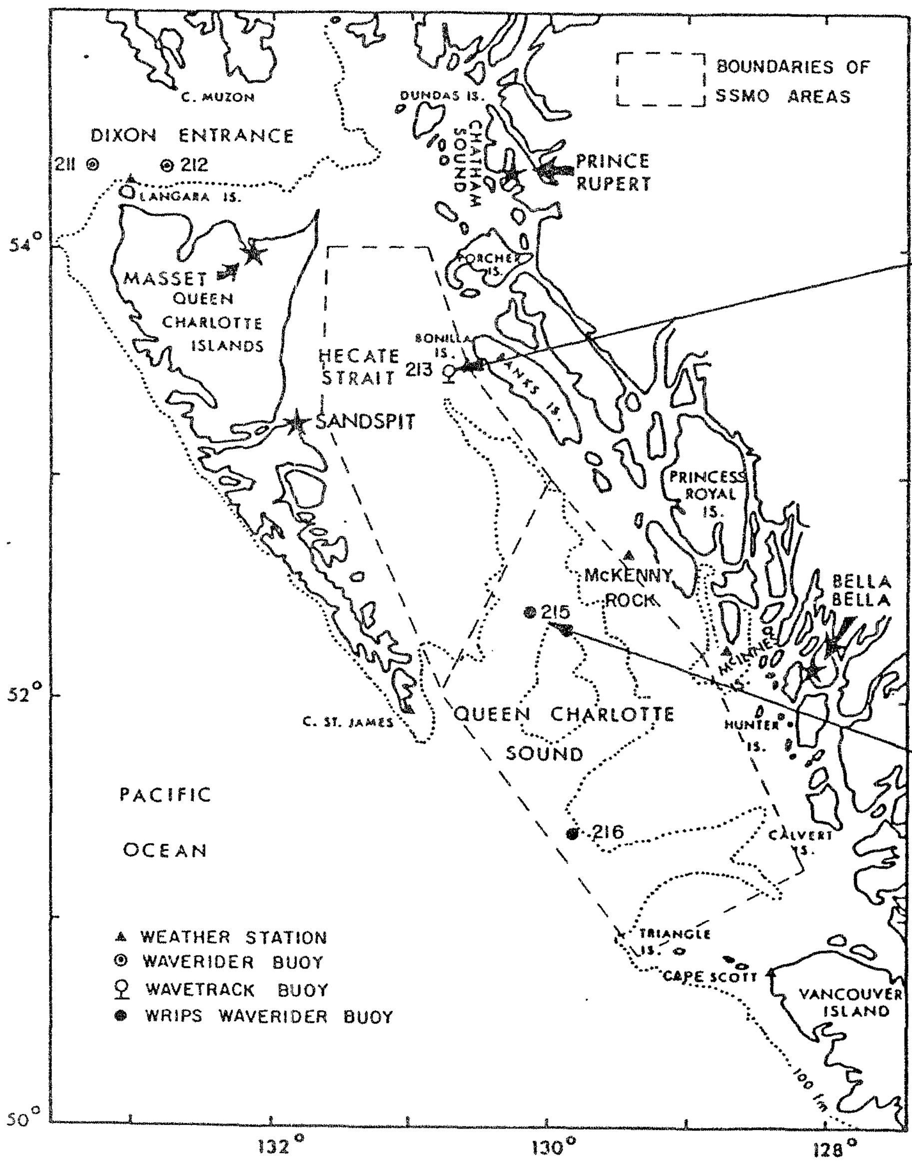

MONTH	% Exceedance of 2 m		% Exceedance of 4 m		% Exceedance of 6 m	
	SSMO	MEAS	SSMO	MEAS	SSMO	MEAS
November	39.0	20.9	5.1	3.1	0.0	0.5
December	39.7	34.5	4.8	2.9	0.0	0.5

MONTH	% Exceedance of 2 m		% Exceedance of 4 m		% Exceedance of 6 m	
	SSMO	MEAS	SSMO	MEAS	SSMO	MEAS
October	50.0	30.9	9.0	8.1	2.1	1.2
November	37.3	31.6	3.8	7.2	0.0	2.1
December	60.2	56.1	19.4	16.7	5.8	3.7

Table 2.2

Operational Wave Criteria

Location	Season: Fall	Winter	Spring	Summer	Annual
Langara West	1.75/9.5	n.a.	1.75/9.5	1.25/8.5	1.75/9.5
Langara East	1.75/9.5	3.25/14.5	2.25/12.5	0.75/8.5	1.25/9.5
Bonilla Island	1.25/4.5	1.25/9.5	1.25/4.5	n.a.	1.25/4.5
McInnes Island	0.75/8.5	3.25/8.5 (1)	1.25/9.5	0.75/16.5	0.75/14.5
Hecate Strait	0.75/14.5	2.25/10.5	1.75/9.5	0.75/15.5	0.75/15.5
Queen Charlotte Sound	1.75/9.5	n.a.	1.75/9.5	1.75/9.5	1.75/9.5

(1) very tentative due to few data

Table 2.3

Mean and Maximum Significant Wave Heights (m) on an Annual and Seasonal Basis

Season		Langara West	Langara East	Bonilla Island	McInnes Island	Hecate Strait	Queen Charlotte Sound
Fall	Mean	2.6	2.2	1.7	1.7	1.9	2.9
	Max	9.0	6.7	8.2	6.7	9.2	10.4
Winter	Mean	3.2	2.9	1.7	3.9	3.0	4.0
	Max	8.8	7.3	6.8	6.8	10.6	11.4
Spring	Mean	2.4	2.1	1.2	2.4	2.2	2.7
	Max	7.8	6.9	5.6	7.3	8.8	9.5
Summer	Mean	1.5	1.2	-	1.1	1.1	1.7
	Max	4.2	3.5	-	3.8	3.7	4.1
1983	Mean	2.3	2.1	1.5	1.4	2.1	2.7
	Max	9.0	7.3	8.2	6.7	9.2	10.8

Table 2.4

Mean and Maximum Peak Periods (s)
on an Annual and Seasonal Basis

Season		Langara West	Langara East	Bonilla Island	McInnes Island	Hecate Strait	Queen Charlotte Sound
Fall	Mean	10.7	10.7	8.4	9.7	10.7	11.1
	Max	18.3	18.3	25.6	20.0	19.7	19.7
Winter	Mean	11.6	12.1	8.6	11.5	10.7	12.3
	Max	25.6	21.3	16.0	18.2	23.3	23.3
Spring	Mean	11.2	11.4	8.1	11.0	10.9	11.5
	Max	21.3	21.3	21.3	22.2	21.3	21.3
Summer	Mean	9.5	8.2	-	11.2	12.5	10.8
	Max	21.3	14.2	-	22.2	19.7	19.7
1983	Mean	10.5	10.7	8.5	10.3	11.4	11.3
	Max	25.6	21.3	25.6	22.2	23.3	23.3

Table 2.5

Extreme Significant Wave Heights (m)
Estimated from Various Datasets

Location (analysis)	Return Period T_R (years) 10	50	100
NEDN (Gumbel) 49.9°N 132.1°W	14.6	16.4	17.2
NDBO (Weibull) Station 46004	11.8	13.3	13.9
Station 216 (Weibull)	14.2	16.1	16.9
Station 215 (Weibull)	13.4	14.5	16.1
Station 211 (Weibull)	12.4	13.8	14.4

Notes: The Gumbel analysis is based on 8 annual maxima extracted from the SOWM hindcast.

The NDBO data span seven years.

The coastal data at Stations 211, 215 and 216 span less than 2 years.

Table 2.6

Extreme Significant Wave Heights
in Northern B.C. Coastal Waters

Area	Return Period (years)		
	10	50	100
Outer coast, mouth of Queen Charlotte Sound	14.5	16.3	17.3
Inner coast of Queen Charlotte Sound (Station 214)	9.3	10.4	11.1
Southern Hecate Strait (Station 215)	13.8	15.5	16.4
Northern Hecate Strait (Station 213)	11.2	12.6	13.3
Mouth of Dixon Entrance (Station 211)	12.3	13.9	14.7

N.B. Values shown in this table are approximate and limited in reliability by the length of data base from which they were derived.

Table 4.1

Expected Normal and Extreme Significant Wave Heights in the Gulf of Alaska and B.C. Coastal Waters

	Return Period T_R (years)					
Location	1	2	5	10	50	100
Station 46003	11.9	12.8	14.0	15.0	17.1	18.0
Station 46004	9.7	10.4	11.2	11.8	13.3	13.9
Langara West	10.3	11.0	11.8	12.4	13.8	14.4
Queen Charlotte Sd.	11.5	12.3	13.4	14.2	16.1	16.9
Hecate Strait	10.7	11.5	12.5	13.4	14.5	16.1

Wave heights are in metres

Table 4.2

Directional Differences Between Cape St. James Winds and McKenney Rock Winds - As Measured

CSJ Wind Speed (m/s)	N	NE	E	SE	S	SW	W	NW
0 ≤ U < 5	3 46 108	- 2 63 167	-21 74 44	-16 50 129	-32 37 161	-63 54 118	-45 77 152	15 63 245
5 ≤ U < 10	- 4 36 46	-17 40 158	-21 46 58	-15 34 222	-32 25 283	-55 30 154	-57 56 196	-10 55 289
10 ≤ U < 15	0 0 1	-11 44 54	-24 40 26	-14 27 149	-28 24 117	-48 22 56	-54 43 68	-15 55 75
15 ≤ U < 20	- - 0	23 23 2	8 31 6	-10 20 63	-35 23 22	-51 22 15	-69 34 15	-26 47 9
U ≥ 20	- - 0	- - 0	0 - 4	-10 24 37	-45 0 5	-23 23 2	-60 34 6	-90 64 3
All	1 43 155	- 9 53 381	-20 55 138	-14 35 600	-32 28 588	-56 39 345	-53 62 437	- 2 59 621

Legend:
3 = mean value
46 = standard deviation
108 = number of obs.

d_{ij} = clockwise rotation (positive) transferring from CSJ to MR

Table 4.3

Directional Differences d_{ij} Between Cape St. James Winds and McKenney Rock Winds - Reduced to 10 m Above MSL

CSJ Wind Speed (m/s)	N	NE	E	SE	S	SW	W	NW
$0 < U < 5$	1 44 143	-8 58 246	-24 65 67	-16 43 222	-33 32 291	-63 46 196	-51 72 248	9 59 382
$5 \leq U < 10$	-4 29 12	-14 40 128	-20 44 61	-14 32 256	-29 24 261	-48 26 123	-54 48 161	-19 55 214
$10 \leq U < 15$	- - -	19 33 7	6 27 8	-10 22 97	-34 22 33	-47 20 24	-62 41 26	-9 65 23
$15 \leq U < 20$	- - -	- - -	0 0 2	-9 23 19	-45 0 3	-45 0 1	-90 0 1	-113 68 2
$U > 20$	- - -	- - -	- - -	-8 17 6	- - -	0 0 1	-45 0 1	- - -

Legend:
1 = mean value
44 = standard deviation
143 = number of obs.

d_{ij} = clockwise rotation (positive) transferring from CSJ to MR

Table 4.4

Wind Speed Ratios for Anemometer Winds
McKenney Rock to Cape St. James

Coefficients derived for: MEASURED WINDS

Total number of records in analysis: 3916
Number of records with missing data: 584
Number of records with zero wind speed at one or both sites: 67

Number of records with difference in direction between sites exceeding 30. deg.: 1748

DIRECTION		[WIND SPEED (m/s)					]
		0-5	5-10	10-15	15-20	20+	ALL
NORTH	μ	2.32	1.37	0.96	0.0	0.0	1.98
	σ	1.43	0.43	0.0	0.0	0.0	1.18
	N	66	35	1	0	0	102
NORTHEAST	μ	1.63	0.97	0.69	0.41	0.0	1.12
	σ	0.81	0.41	0.27	0.0	0.0	0.55
	N	56	88	36	1	0	181
EAST	μ	3.12	0.80	0.56	0.51	0.45	1.07
	σ	2.05	0.32	0.20	0.09	0.08	0.86
	N	9	24	13	5	4	55
SOUTHEAST	μ	2.18	1.39	1.05	0.88	0.74	1.33
	σ	1.55	0.60	0.39	0.28	0.19	0.78
	N	76	162	120	51	31	440
SOUTH	μ	2.11	1.45	1.25	1.01	1.15	1.53
	σ	1.05	1.26	0.37	0.09	0.09	1.03
	N	61	138	68	9	2	278
SOUTHWEST	μ	1.65	1.07	0.97	0.89	0.41	1.20
	σ	1.06	0.31	0.18	0.13	0.0	0.61
	N	15	28	7	2	1	53
WEST	μ	1.16	0.74	0.70	0.66	0.84	0.84
	σ	0.65	0.29	0.26	0.09	0.0	0.41
	N	17	26	14	4	1	62
NORTHWEST	μ	2.46	1.11	0.72	0.89	0.0	1.52
	σ	1.63	0.50	0.33	0.09	0.0	1.03
	N	118	179	45	4	0	346

μ = average
σ = standard deviation
N = number of observations

Table 4.5

Wind Speed Ratios for Anemometer Winds McKenney Rock to Cape St. James Incorporating Directional Shift

Coefficients derived for: MEASURED WINDS

Total number of records in analysis: 3916
Number of records with missing data: 584
Number of records with zero wind speed at one or both sites: 67

Number of records with difference in direction between sites (accounting for directional transfer matrix) exceeding 45. deg.: 776

DIRECTION		WIND SPEED (m/s) 0-5	5-10	10-15	15-20	20+	ALL
NORTH	μ	2.73	1.33	0.96	0.0	0.0	2.25
	σ	2.60	0.45	0.0	0.0	0.0	2.12
	N	84	43	1	0	0	128
NORTHEAST	μ	1.73	0.97	0.70	0.41	0.0	1.17
	σ	1.00	0.40	0.26	0.0	0.0	0.65
	N	82	123	43	1	0	249
EAST	μ	1.91	0.71	0.56	0.50	0.45	0.88
	σ	1.32	0.30	0.15	0.10	0.08	0.62
	N	17	41	22	4	4	88
SOUTHEAST	μ	2.28	1.31	0.99	0.82	0.71	1.30
	σ	2.23	0.59	0.39	0.29	0.20	1.03
	N	93	201	142	62	35	533
SOUTH	μ	2.38	1.67	1.36	1.08	1.12	1.75
	σ	1.19	0.68	0.40	0.18	0.07	0.78
	N	135	273	115	22	5	550
SOUTHWEST	μ	2.57	1.56	1.21	0.91	0.72	1.73
	σ	2.02	0.69	0.46	0.14	0.0	1.17
	N	77	140	55	15	1	288
WEST	μ	1.28	1.06	0.87	0.76	0.75	1.05
	σ	0.70	0.40	0.39	0.20	0.09	0.47
	N	54	127	52	12	6	251
NORTHWEST	μ	2.33	1.07	0.70	0.74	0.68	1.46
	σ	1.57	0.50	0.33	0.23	0.07	1.01
	N	141	205	48	6	2	402

μ = average
σ = standard deviation
N = number of observations

Table 4.6

Wind Speed Ratios r_{ij} for 10 m Winds
McKenney Rock to Cape St. James
Incorporating Directional Shift

Coefficients derived for: WINDS AT 10 m ABOVE MSL

Total number of records in analysis: 3916
Number of records with missing data: 584
Number of records with zero wind speed at one or both sites: 67

Number of records with difference in direction between sites
(accounting for directional transfer matrix)
exceeding 45. deg.: 776

DIRECTION		[		WIND SPEED (m/s)			]
		0-5	5-10	10-15	15-20	20+	ALL
NORTH	μ	2.82	1.48	0.0	0.0	0.0	2.69
	σ	2.78	0.35	0.0	0.0	0.0	2.65
	N	116	12	0	0	0	128
NORTHEAST	μ	1.74	0.99	0.65	0.0	0.0	1.40
	σ	1.05	0.41	0.36	0.0	0.0	0.83
	N	140	104	5	0	0	249
EAST	μ	1.63	0.75	0.60	0.48	0.0	1.06
	σ	1.36	0.27	0.11	0.02	0.0	0.86
	N	33	47	6	2	0	88
SOUTHEAST	μ	2.23	1.35	0.97	0.81	0.73	1.55
	σ	2.06	0.59	0.33	0.26	0.10	1.27
	N	180	234	95	18	6	533
SOUTH	μ	2.54	1.74	1.37	1.28	0.0	2.10
	σ	1.26	0.57	0.30	0.03	0.0	0.95
	N	260	254	33	3	0	550
SOUTHWEST	μ	2.63	1.55	1.20	0.86	0.0	2.07
	σ	1.93	0.56	0.27	0.0	0.0	1.43
	N	147	116	24	1	0	288
WEST	μ	1.45	1.12	0.89	1.00	0.76	1.25
	σ	0.68	0.45	0.25	0.0	0.0	0.56
	N	116	112	21	1	1	251
NORTHWEST	μ	2.22	1.02	0.94	0.89	0.0	1.75
	σ	1.64	0.47	0.30	0.0	0.0	1.31
	N	245	142	14	1	0	402

μ = average
σ = standard deviation
N = number of observations

FIGURES

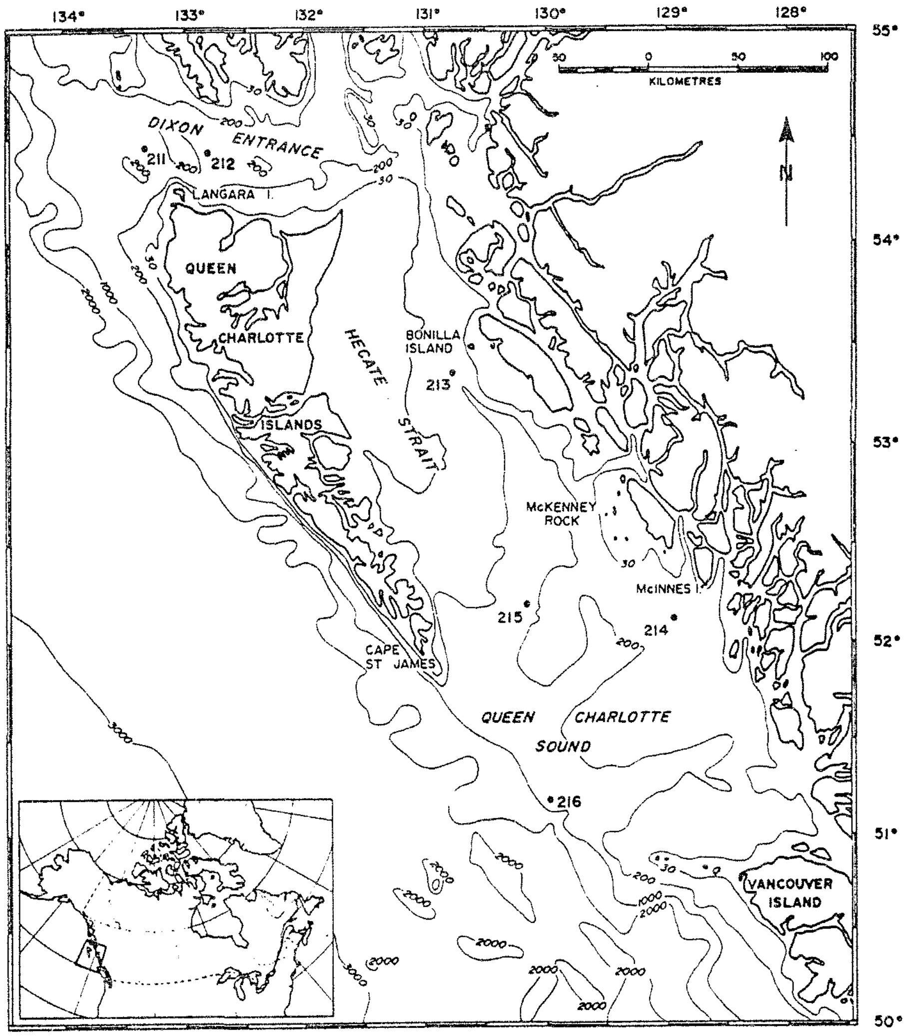

Legend

Station	Name	Instrument Type
211	Langara West	Waverider Buoy
212	Langara East	Waverider Buoy
213	Bonilla Island	Endeco Wave Track
214	McInnes Island	WAVEC Buoy
215	Hecate Strait	WRIPS Buoy
216	Queen Charlotte Sd.	WRIPS Buoy
-	McKenney Rock	Weather Station

Fig. 1.1 Instrument disposition in the 1982-84 wave measurement program.

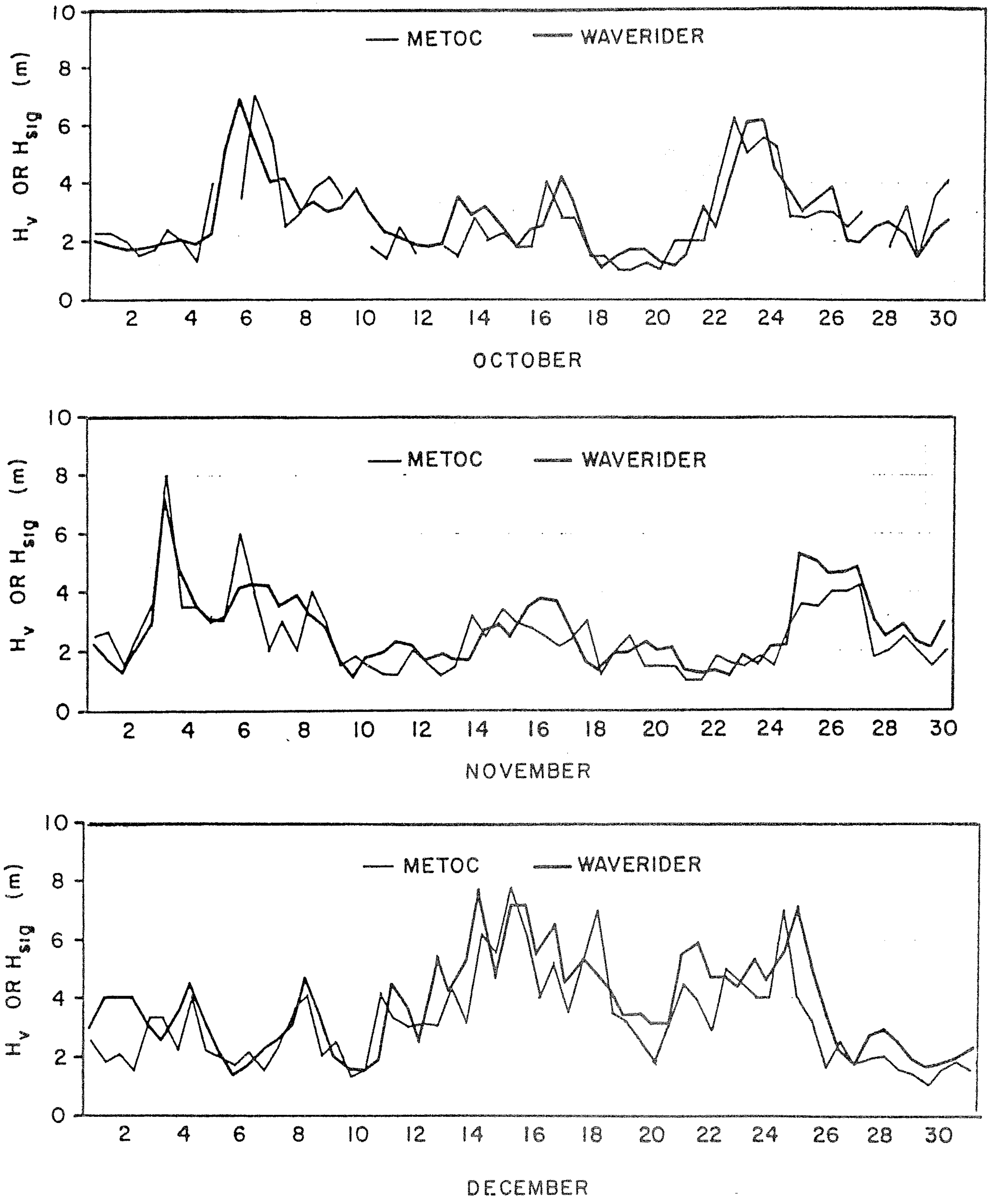

Fig. 2.1 Comparison of METOC wave heights with Waverider measurements at Station 216.

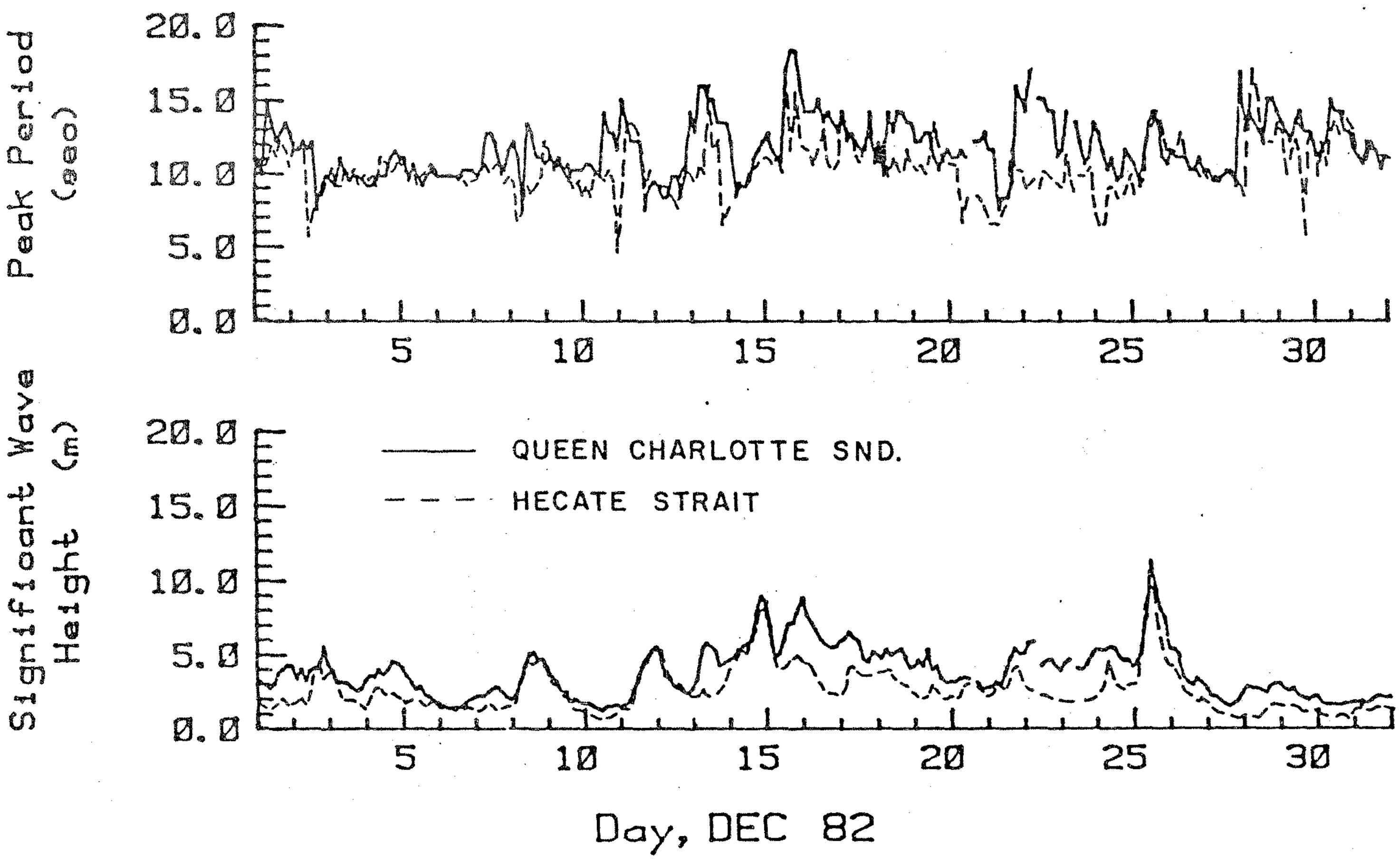

Fig. 2.2a Comparison of wave measurements at Station 216 and 215.

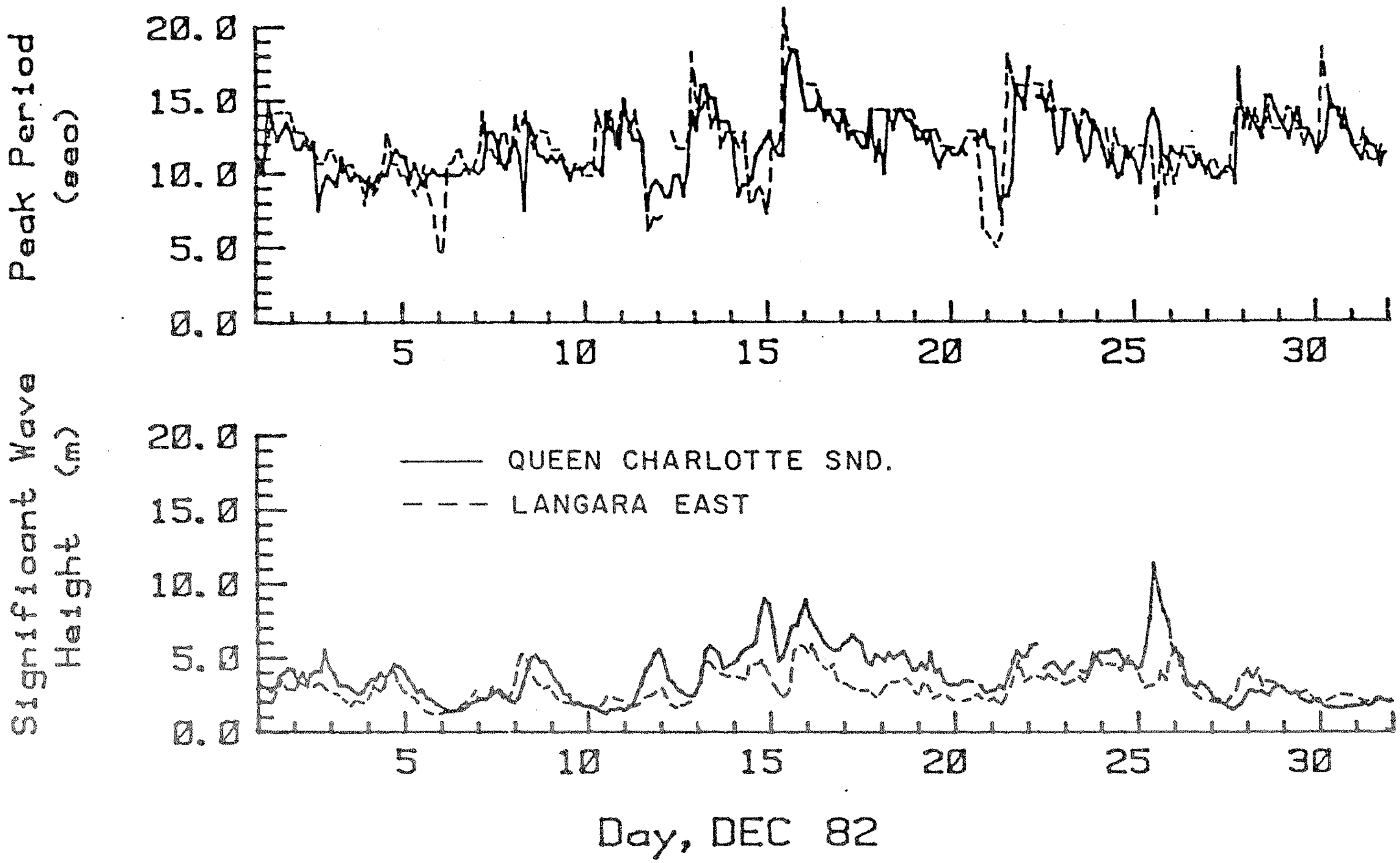

Fig. 2.2b Comparison of wave measurements at Stations 216 and 212.

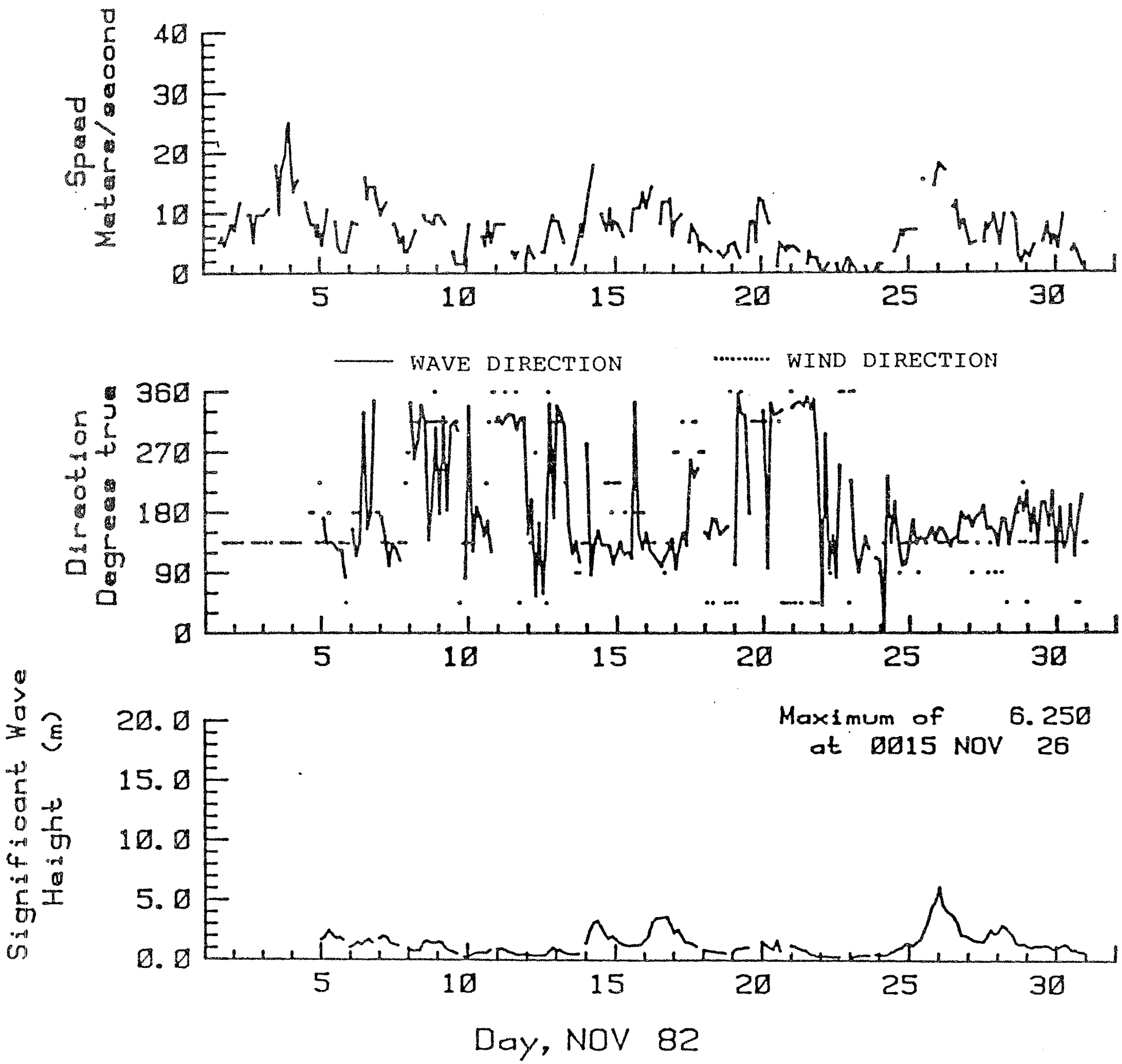

Fig. 2.3 Time series comparison of wind and directional wave properties at Station 213 for November, 1982.

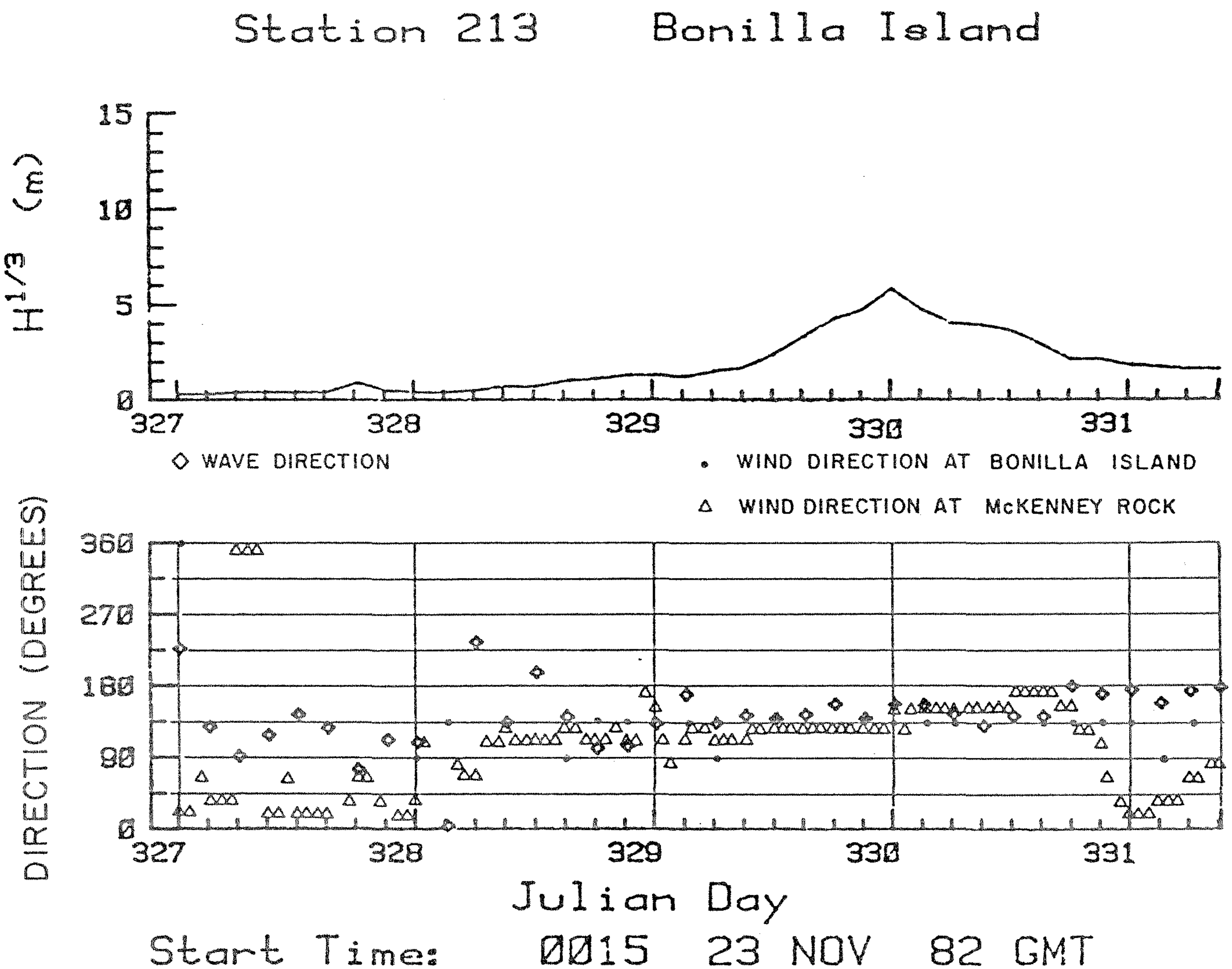

Fig. 2.4 Comparison of wind and wave direction at Bonilla Island during the storm of November 26, 1982.

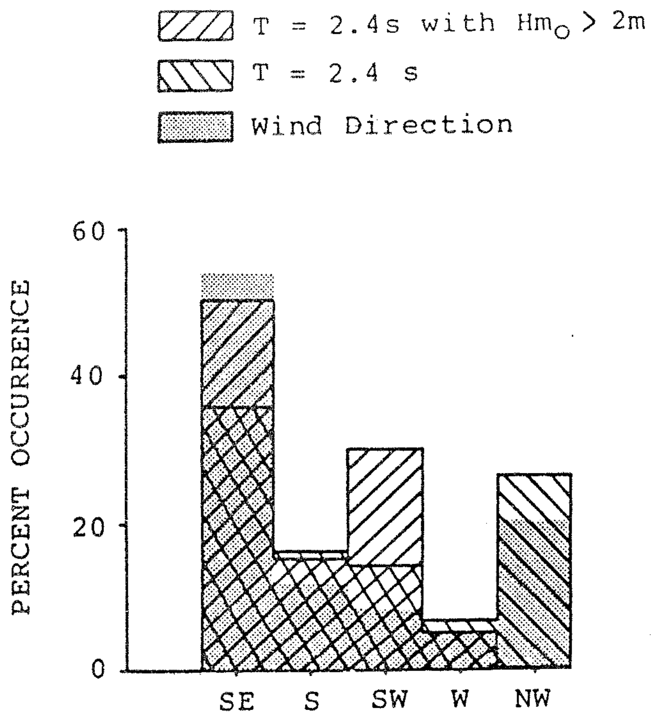

Fig. 2.5 Distribution of wind and wave directions at Station 213 for November, 1982.

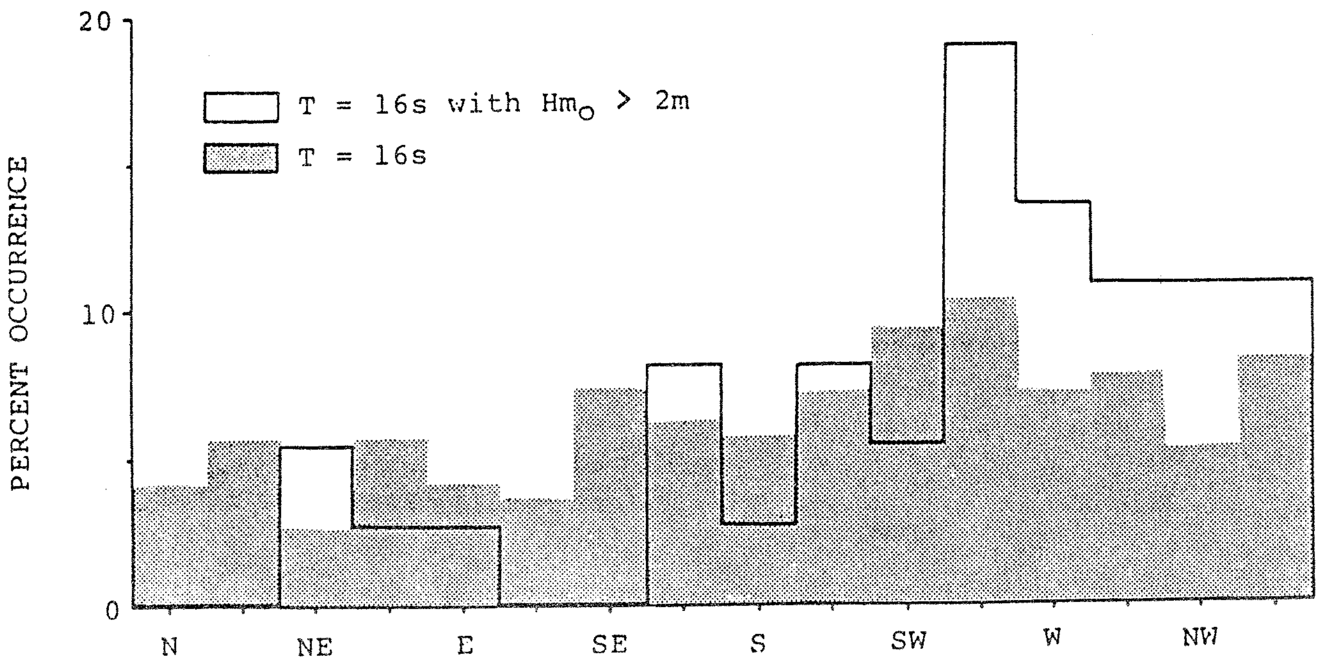

Fig.2.6 Distribution of low frequency (T = 16s) wave directions at Station 213 for November, 1982.

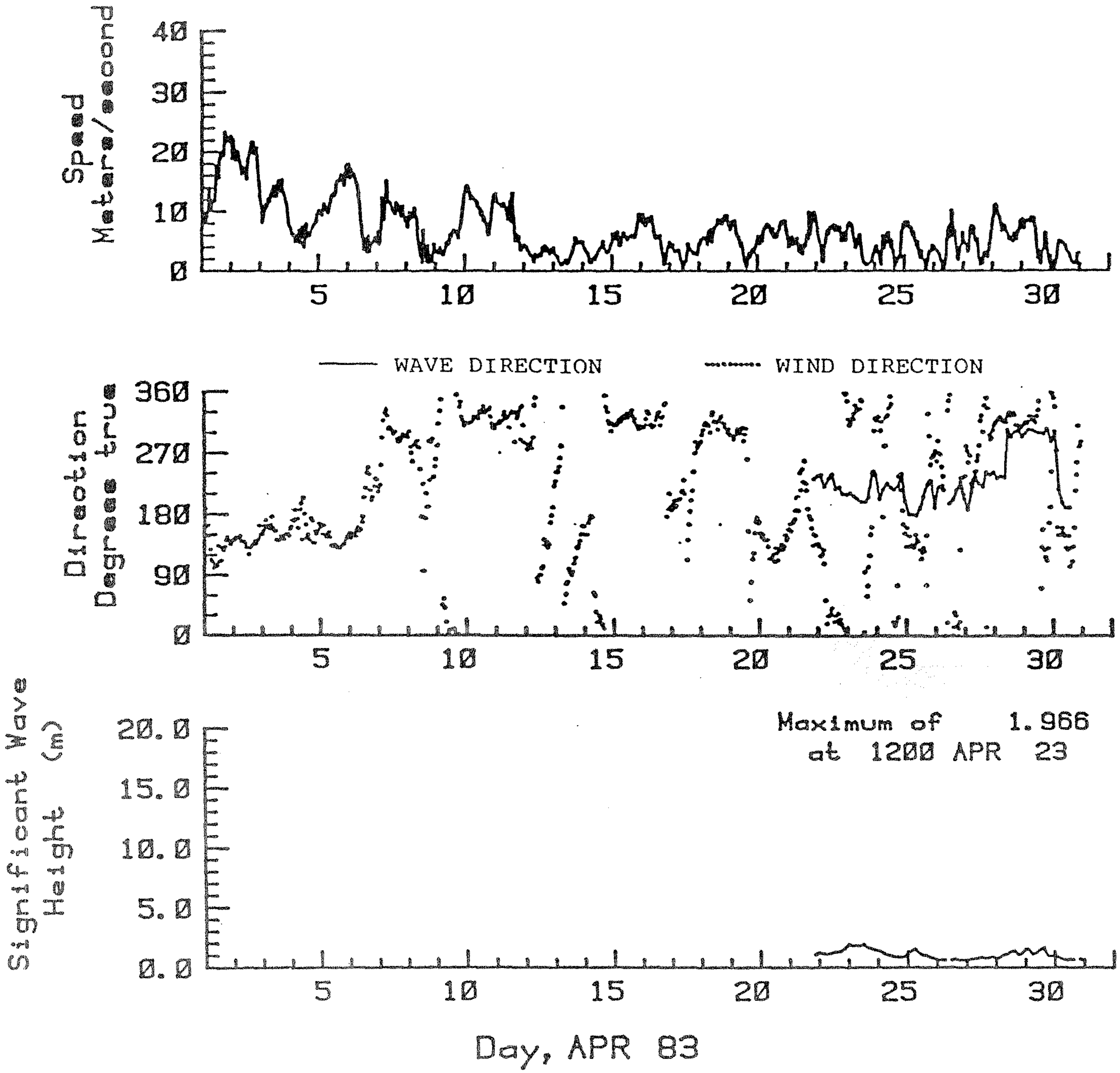

Fig. 2.7a Time series comparison of wind and directional wave parameters at Station 214 for April, 1983.

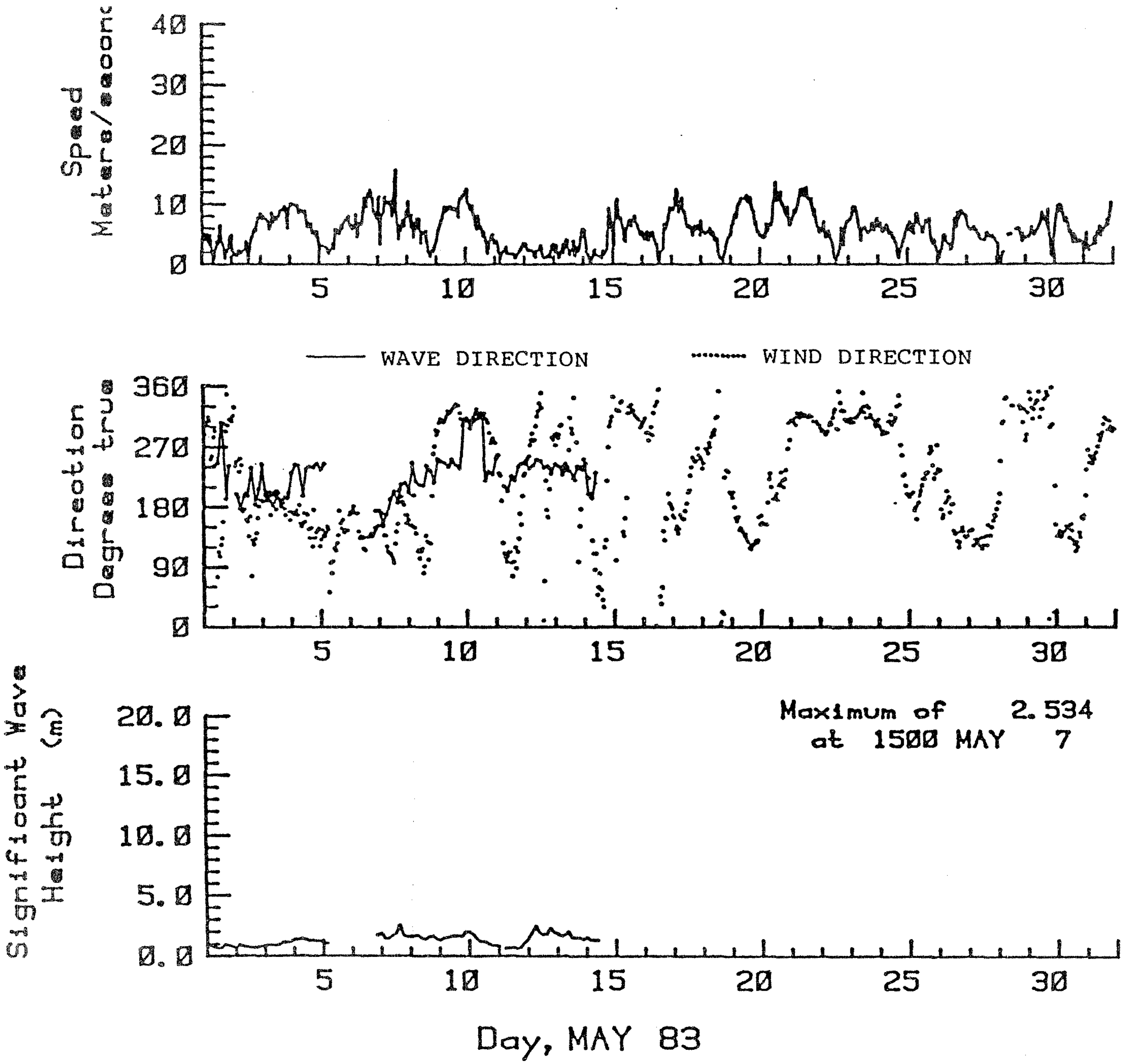

Fig. 2.7b Time series comparison of wind and directional wave parameters at Station 214 for May, 1983.

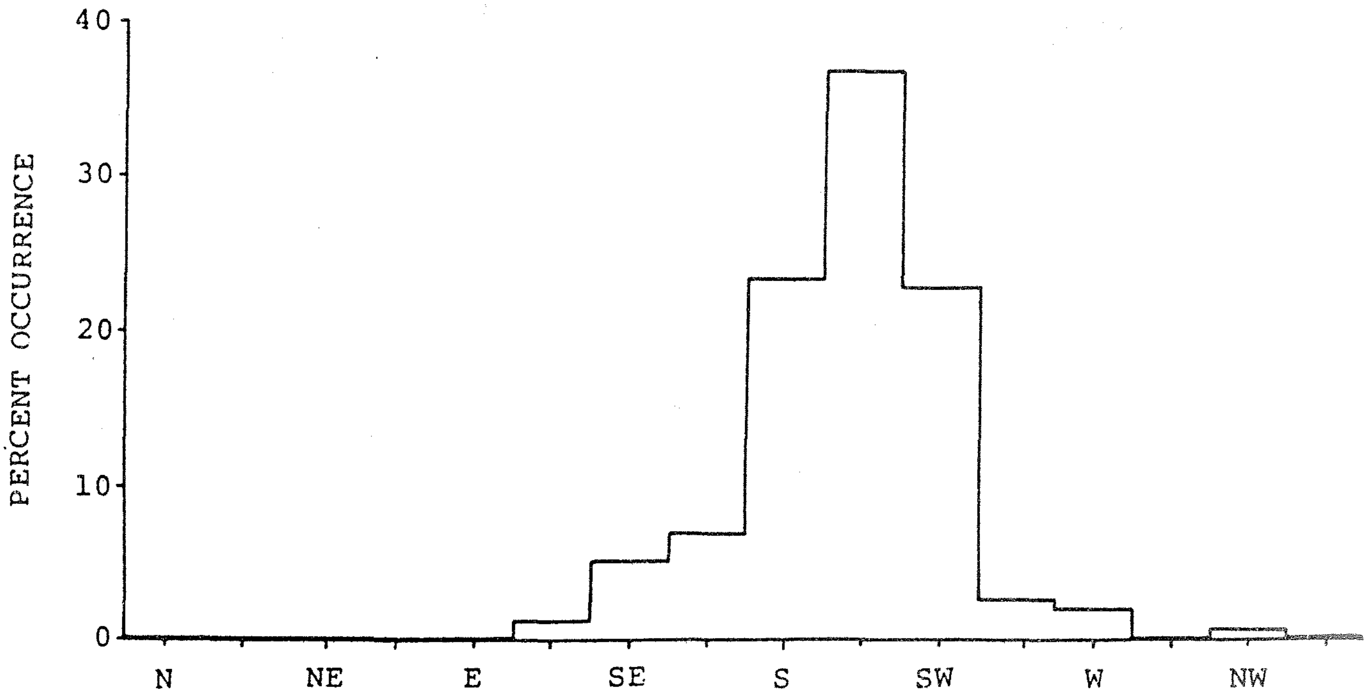

Fig. 2.8 Distribution of low frequency (T = 16s) wave directions at Station 214 for April and May, 1983.

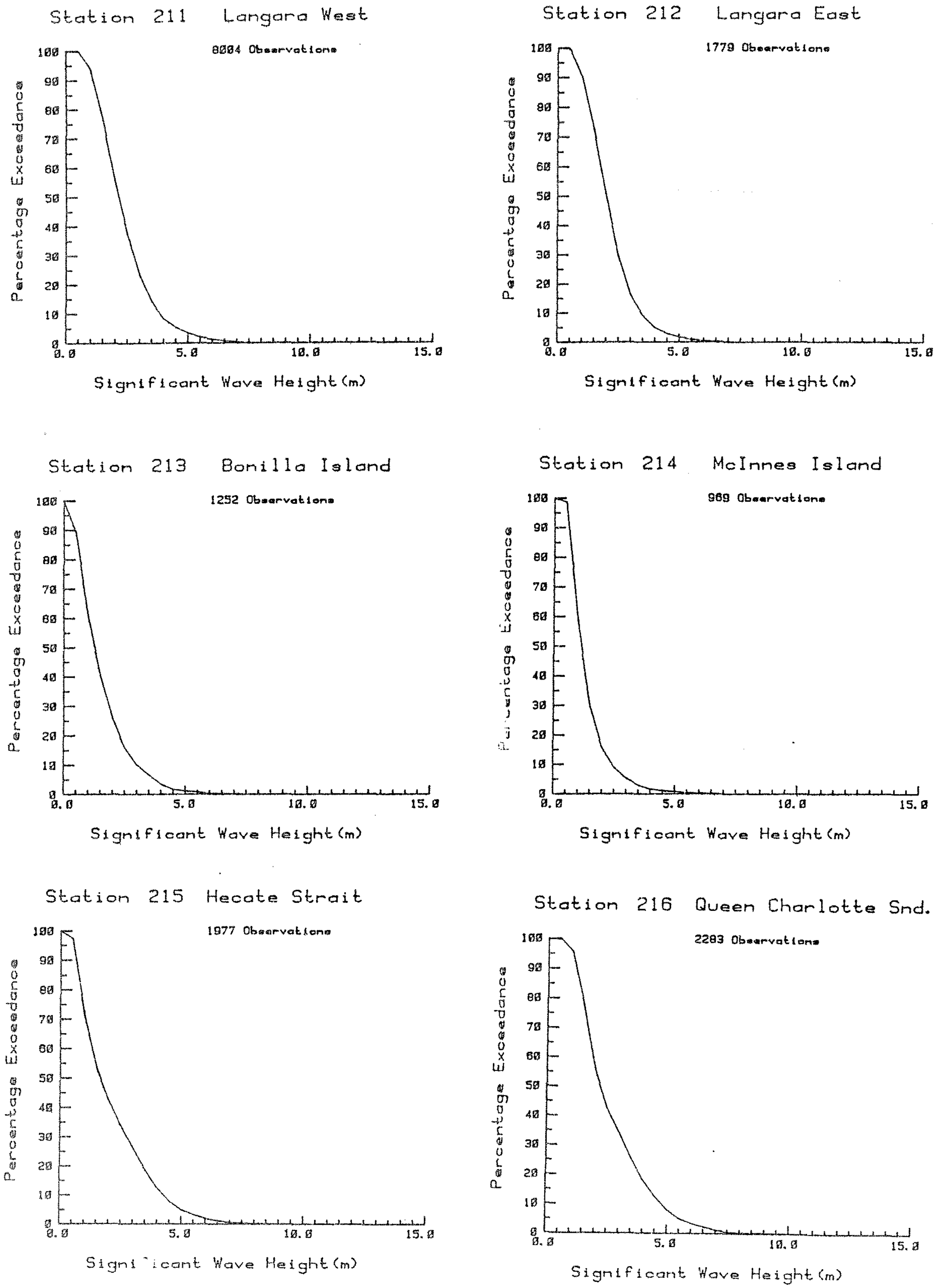

Fig. 2.9 Annual significant wave height exceedance diagrams.

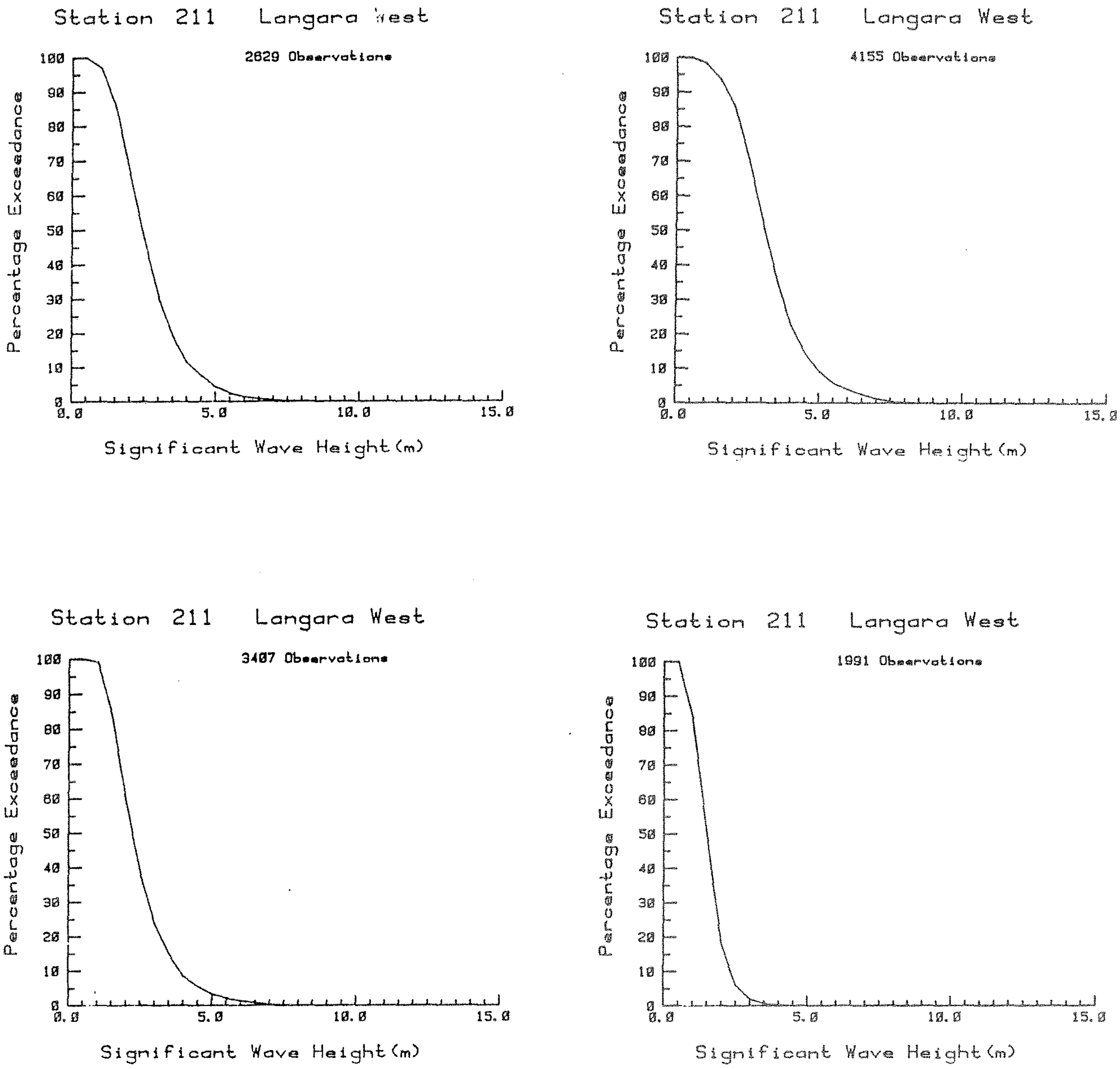

Fig. 2.10 Seasonal significant wave height exceedance diagrams. The diagrams are ordered fall, winter, summer and spring proceeding clockwise around the page starting from the upper left corner.

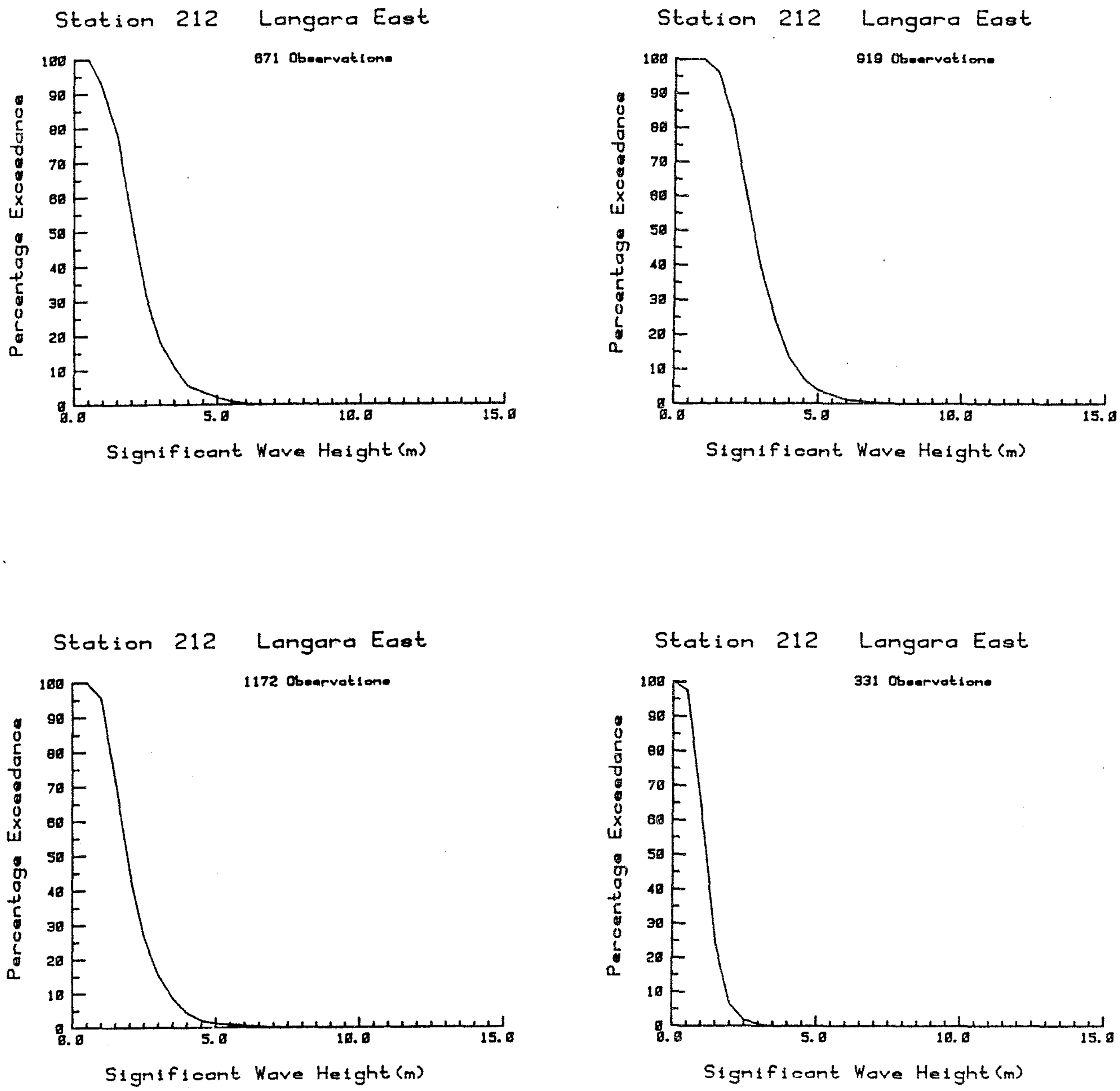

Fig. 2.10 continued

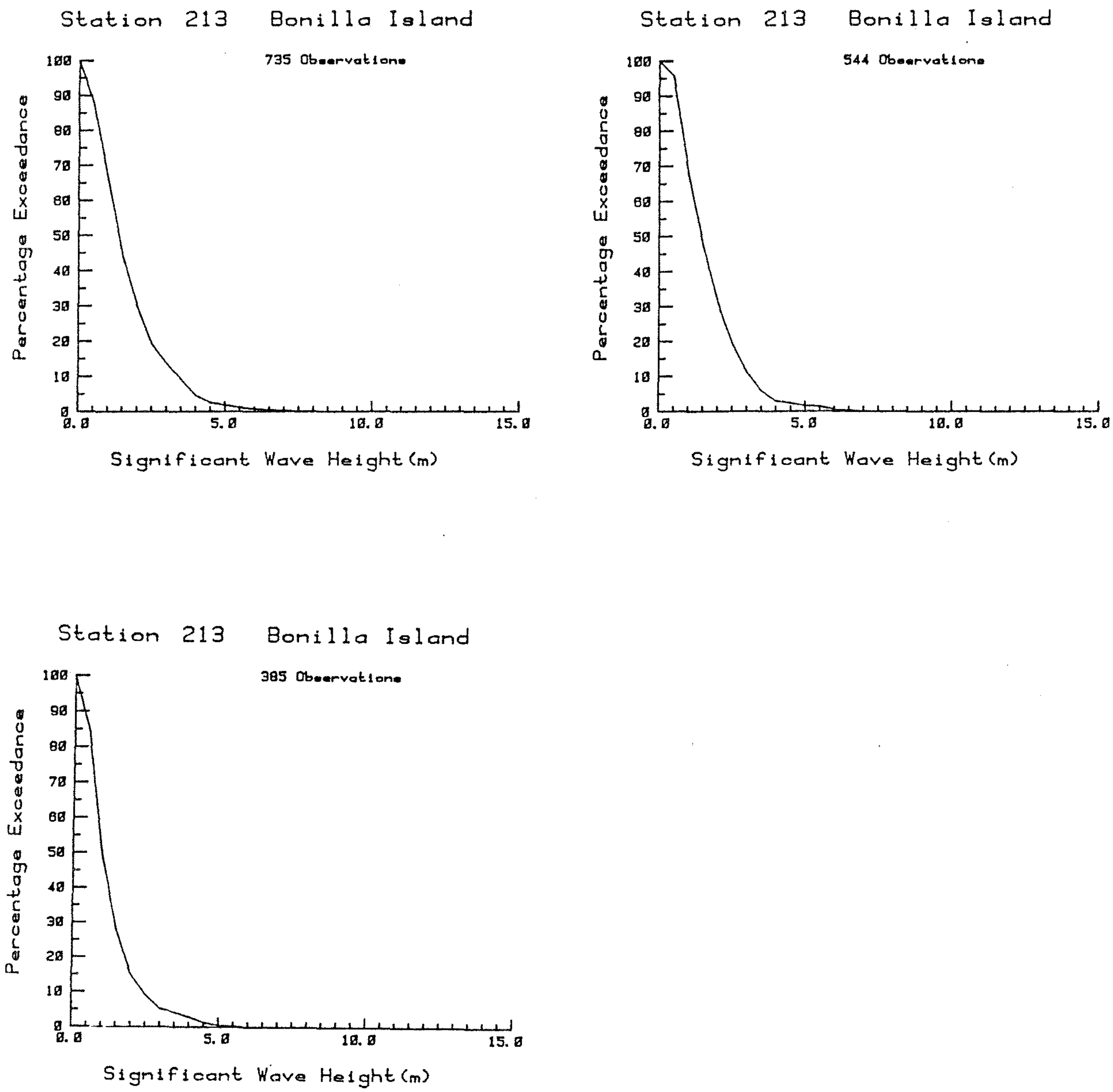

Fig. 2.10 continued

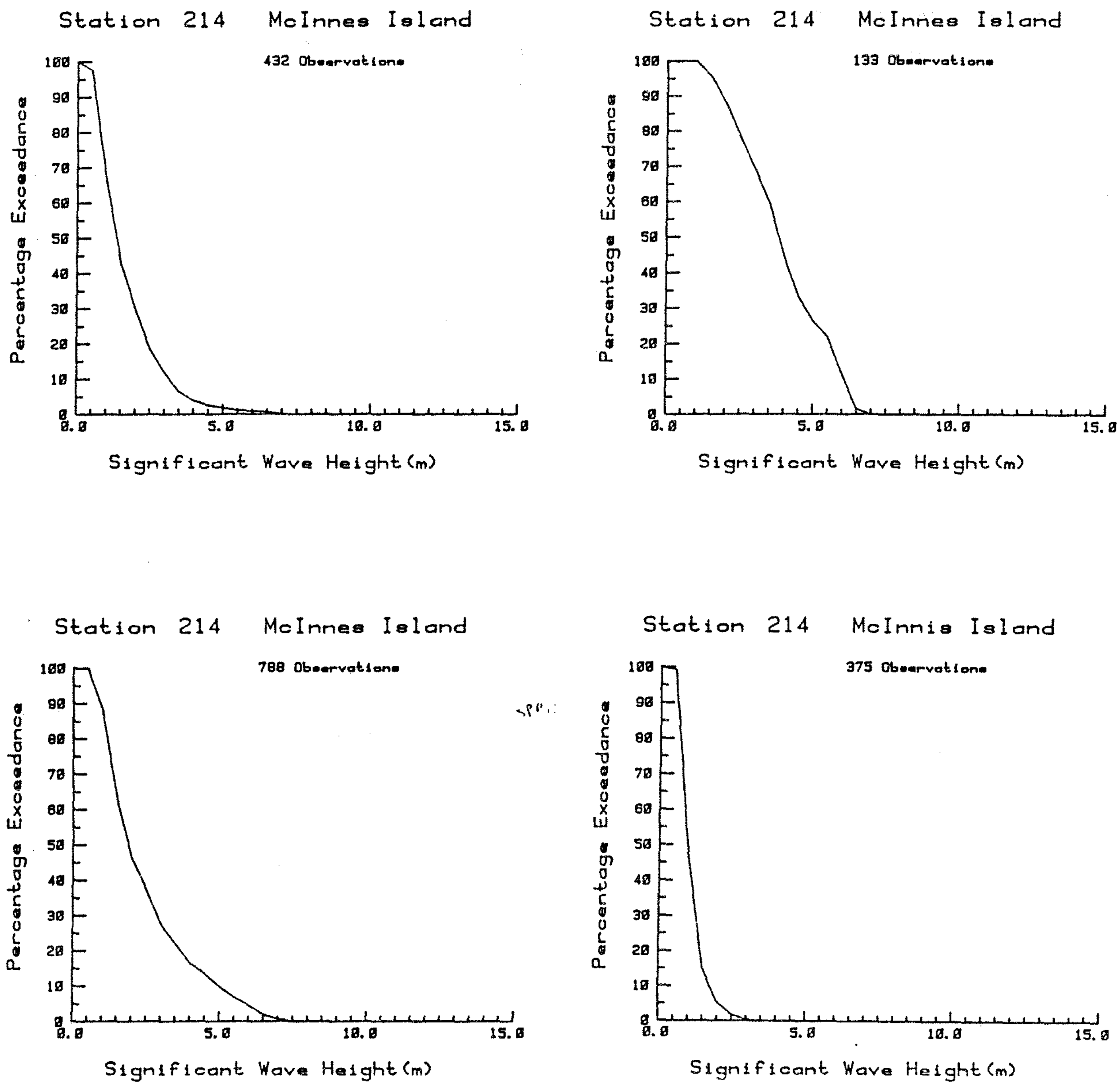

Fig. 2.10 continued

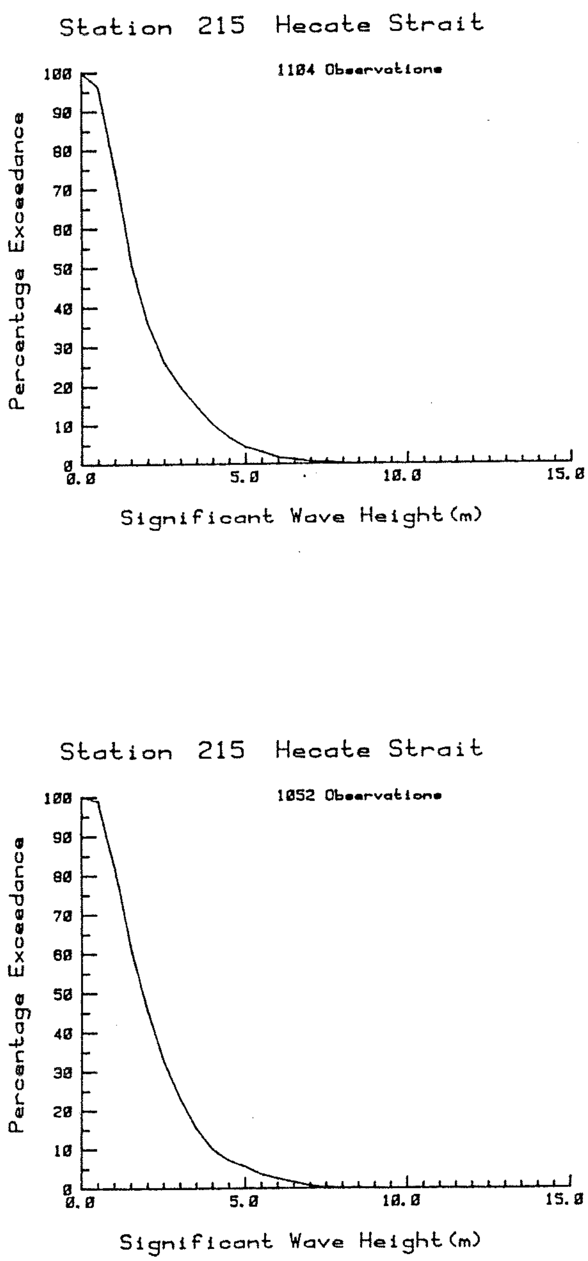

Fig. 2.10 continued

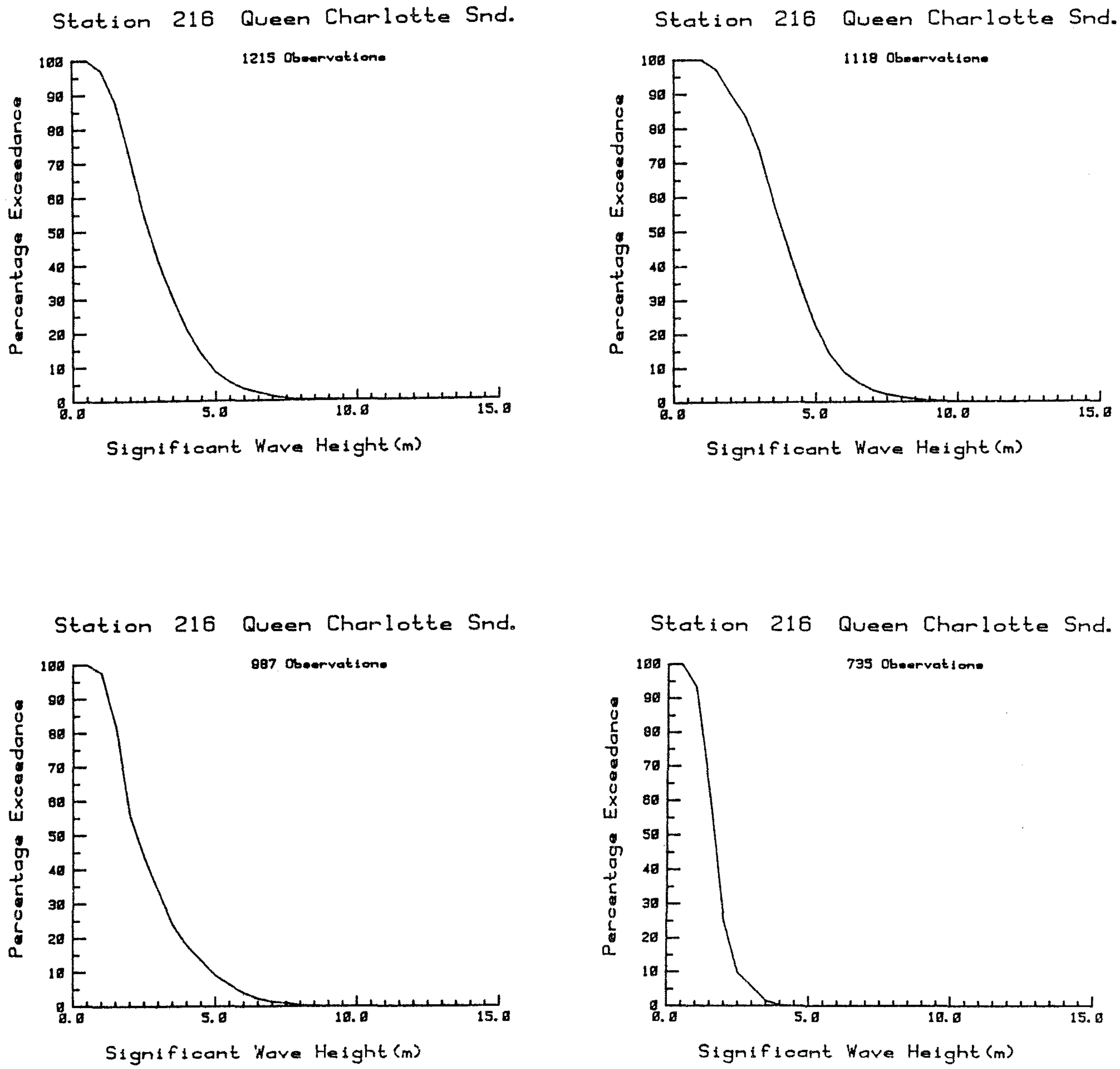

Fig. 2.10 continued

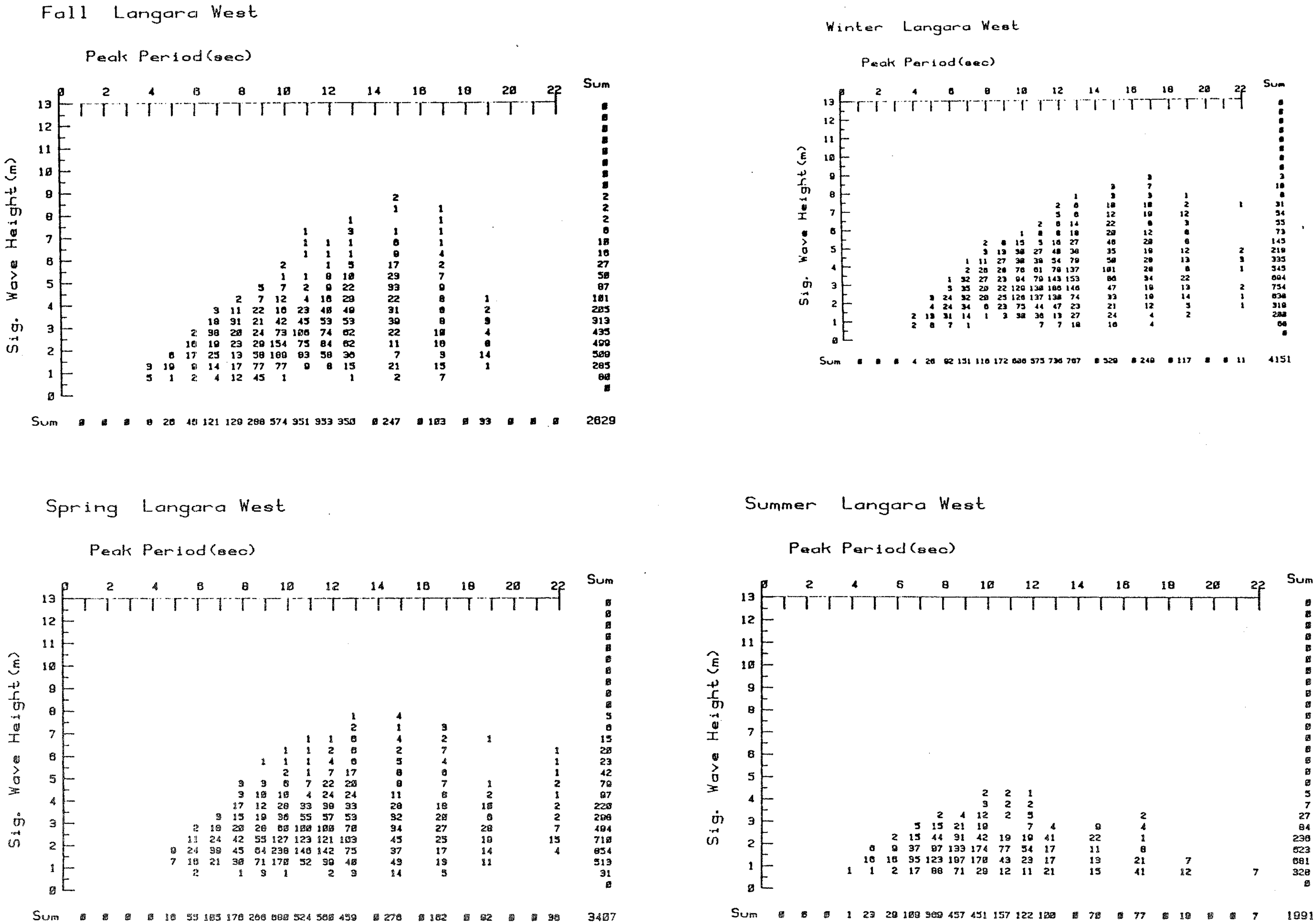

Fig. 2.11 Seasonal bivariate histograms of H_s vs T_p.

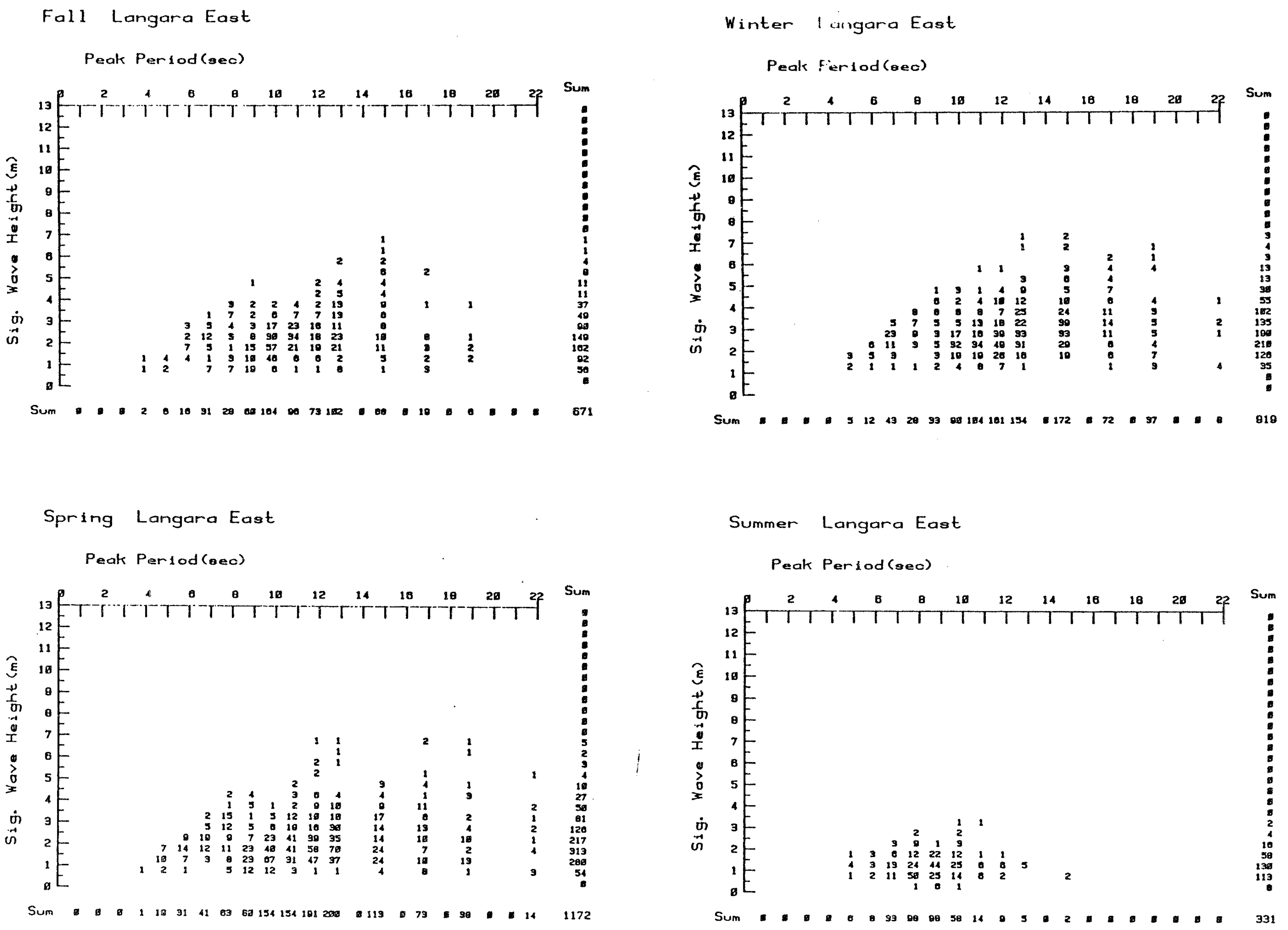

Fig. 2.11 Continued

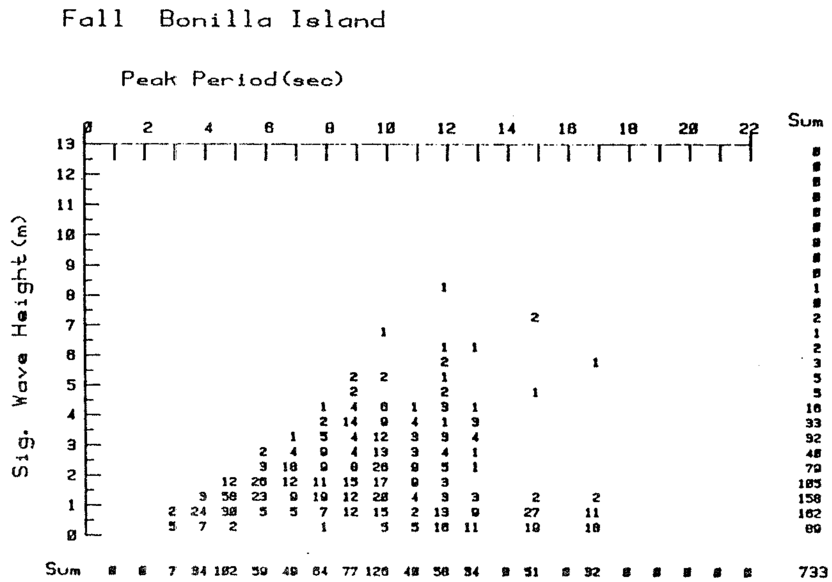

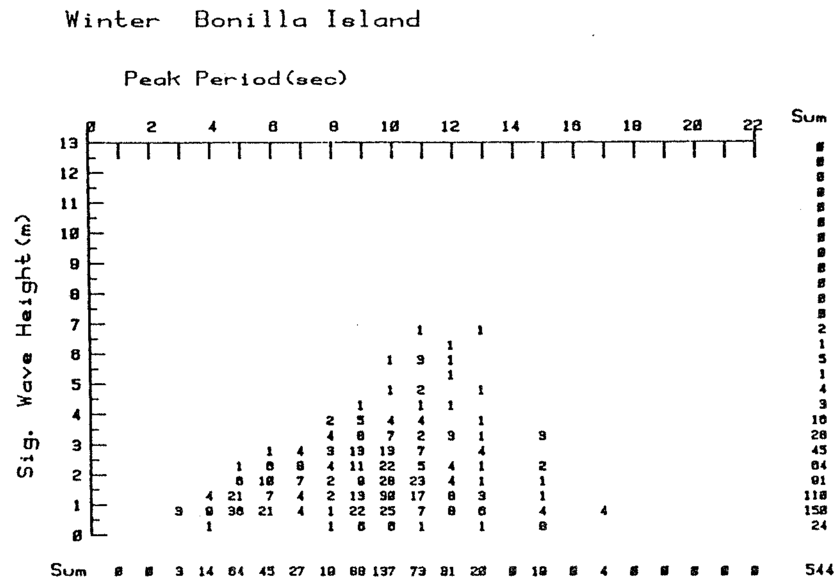

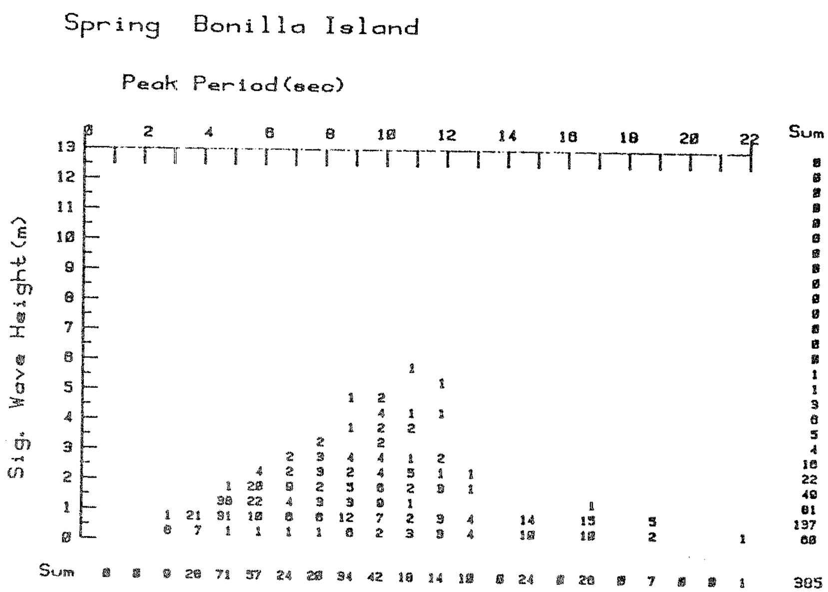

N/A

Fig. 2.11 Continued

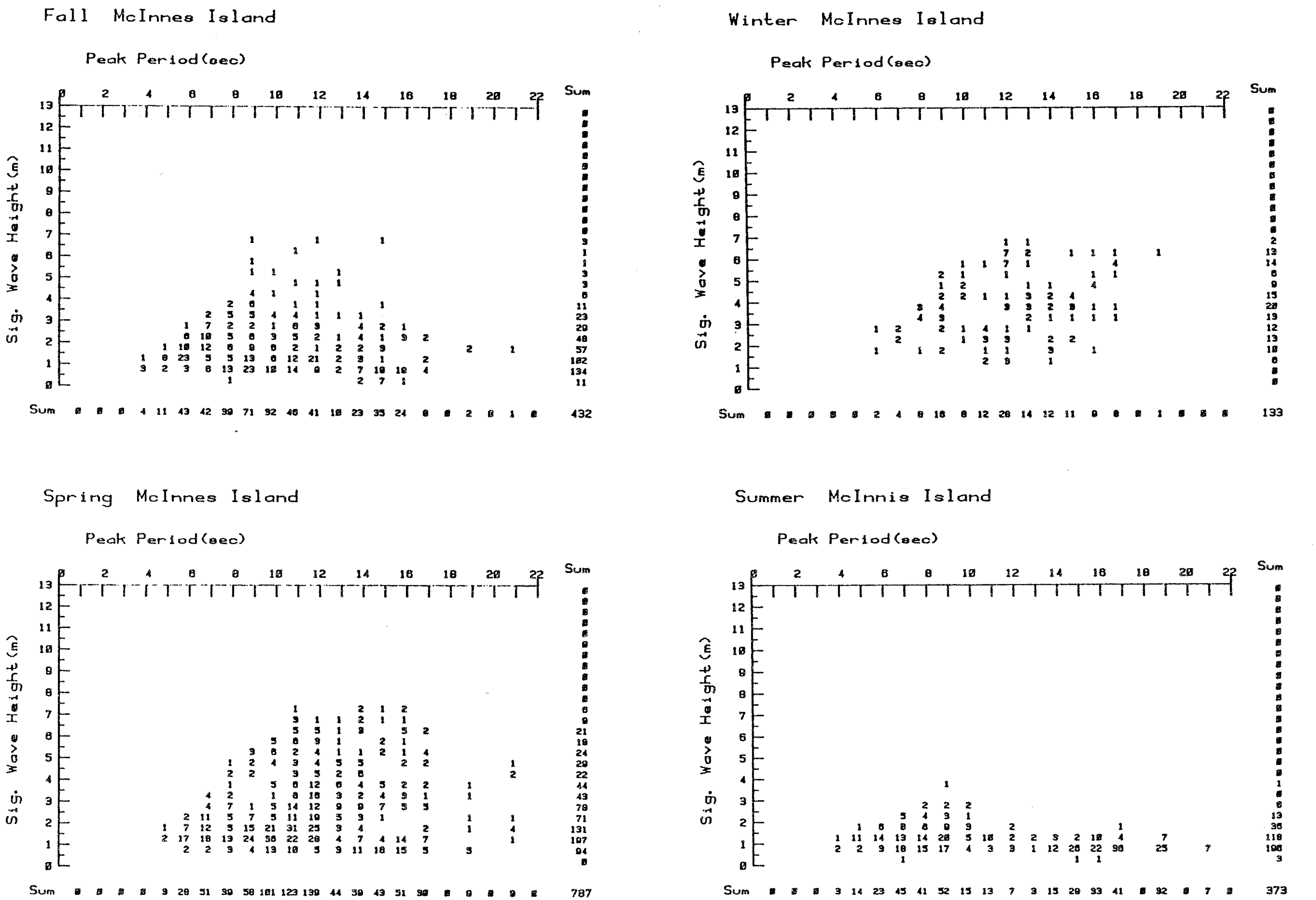

Fig. 2.11 Continued

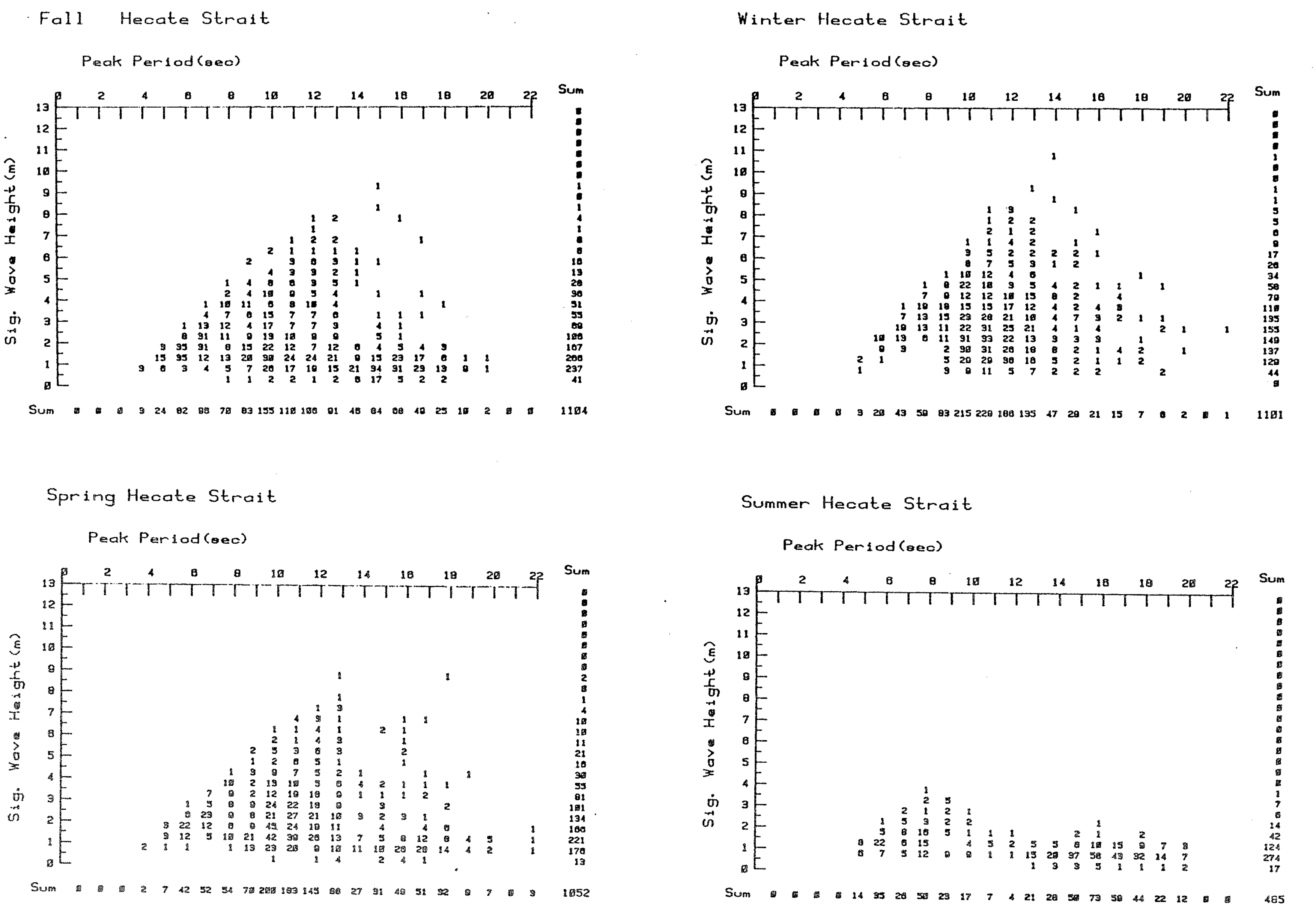

Fig. 2.11 Continued

Fall Queen Charlotte Snd.

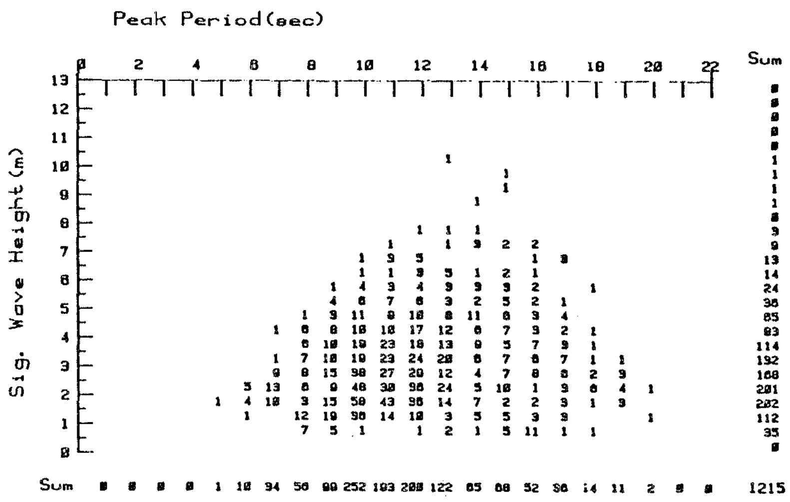

Winter Queen Charlotte Snd.

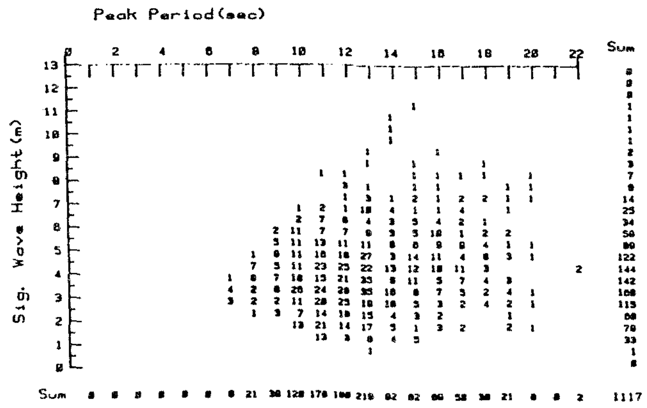

Spring Queen Charlotte Snd.

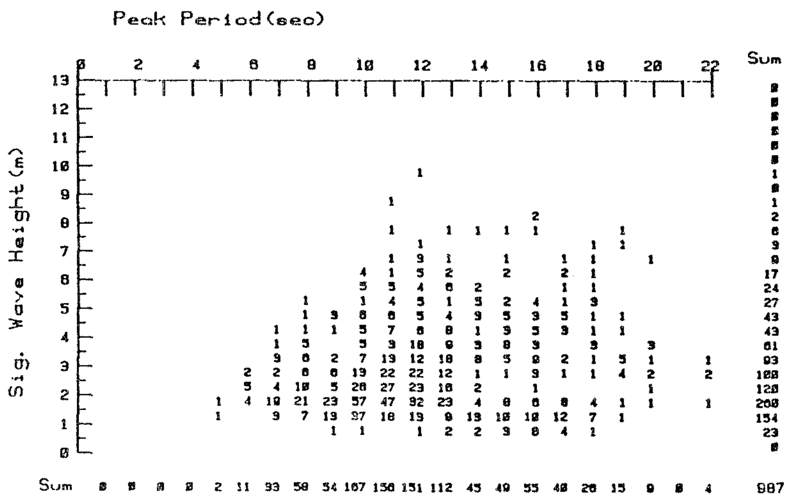

Summer Queen Charlotte Snd.

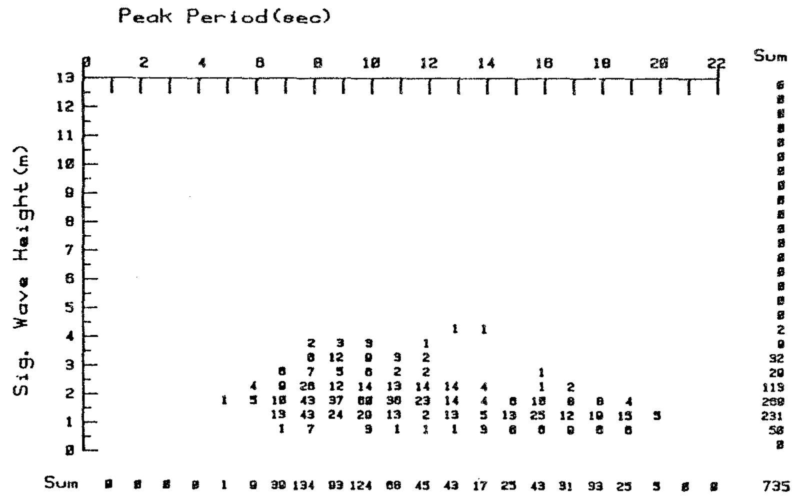

Fig. 2.11 Continued

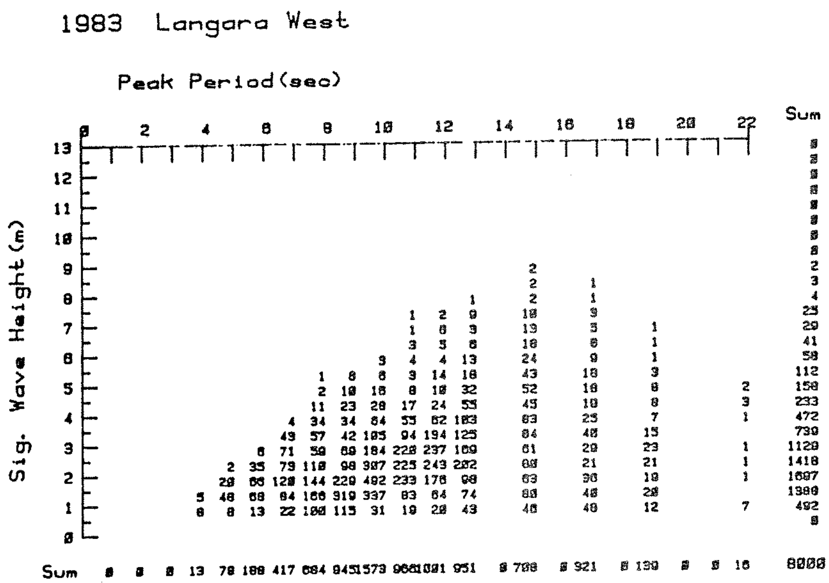

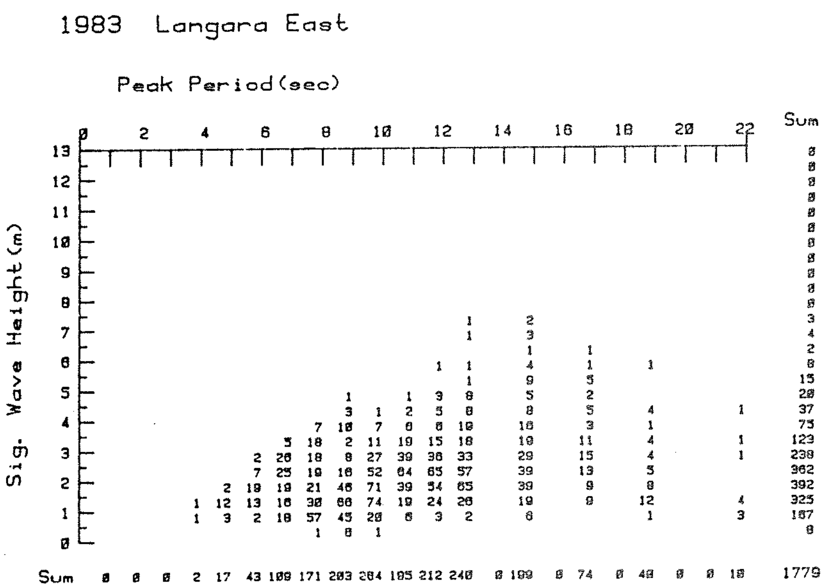

Fig. 2.12 Annual bivariate histograms of H_s vs T_p.

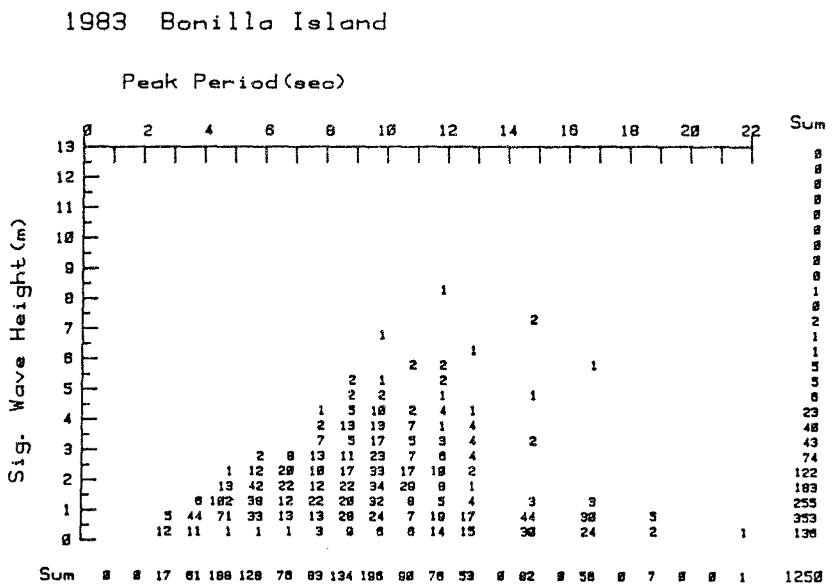

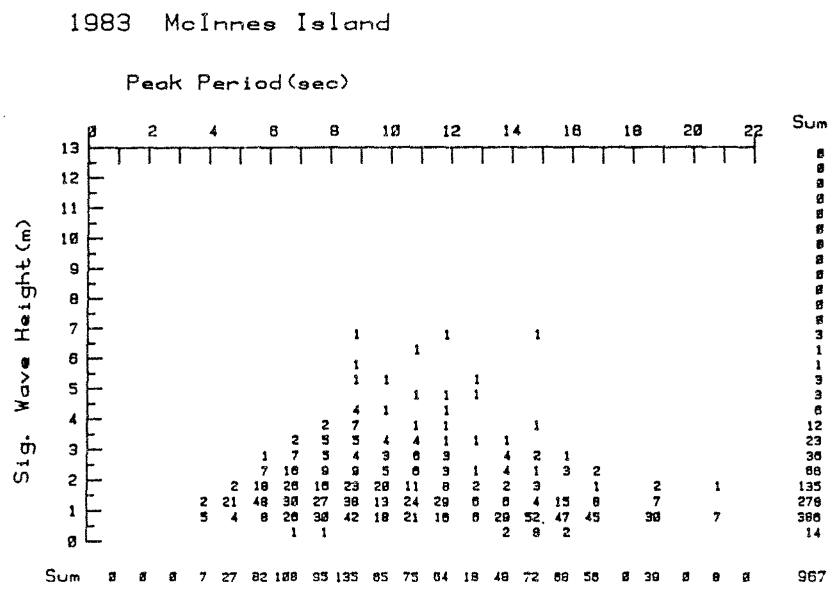

Fig. 2.12 continued

1983 Hecate Strait

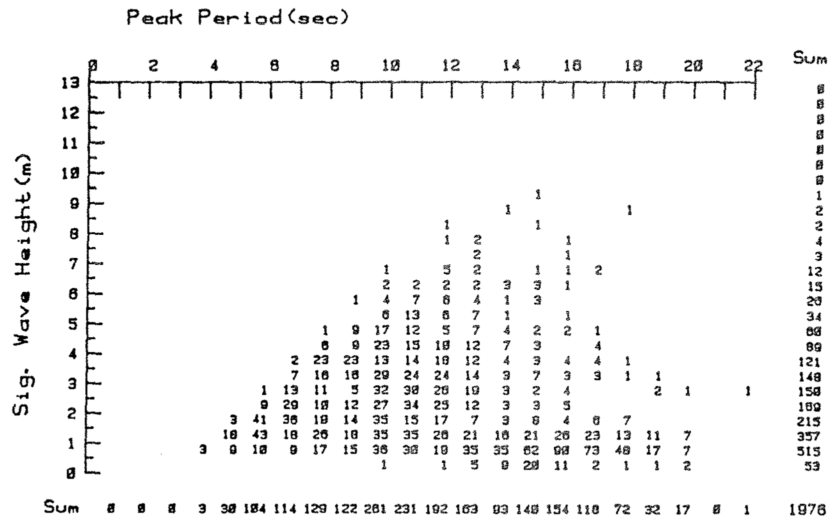

1983 Queen Charlotte Snd.

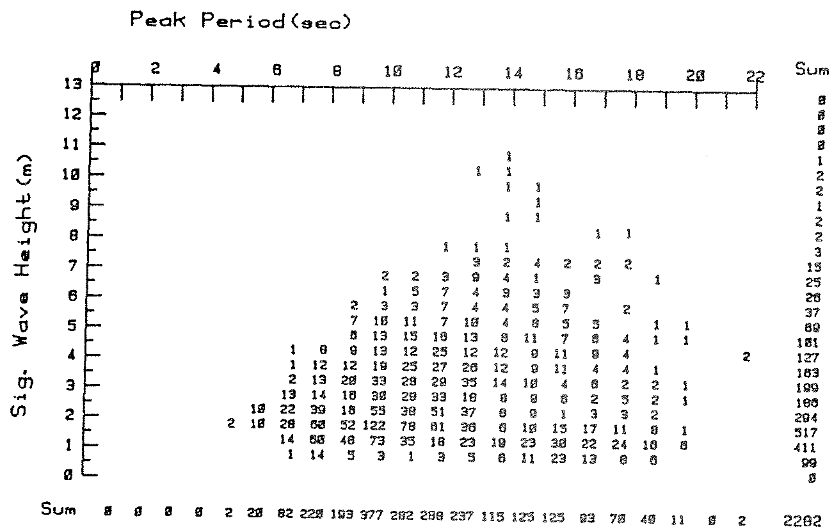

Fig. 2.12 continued

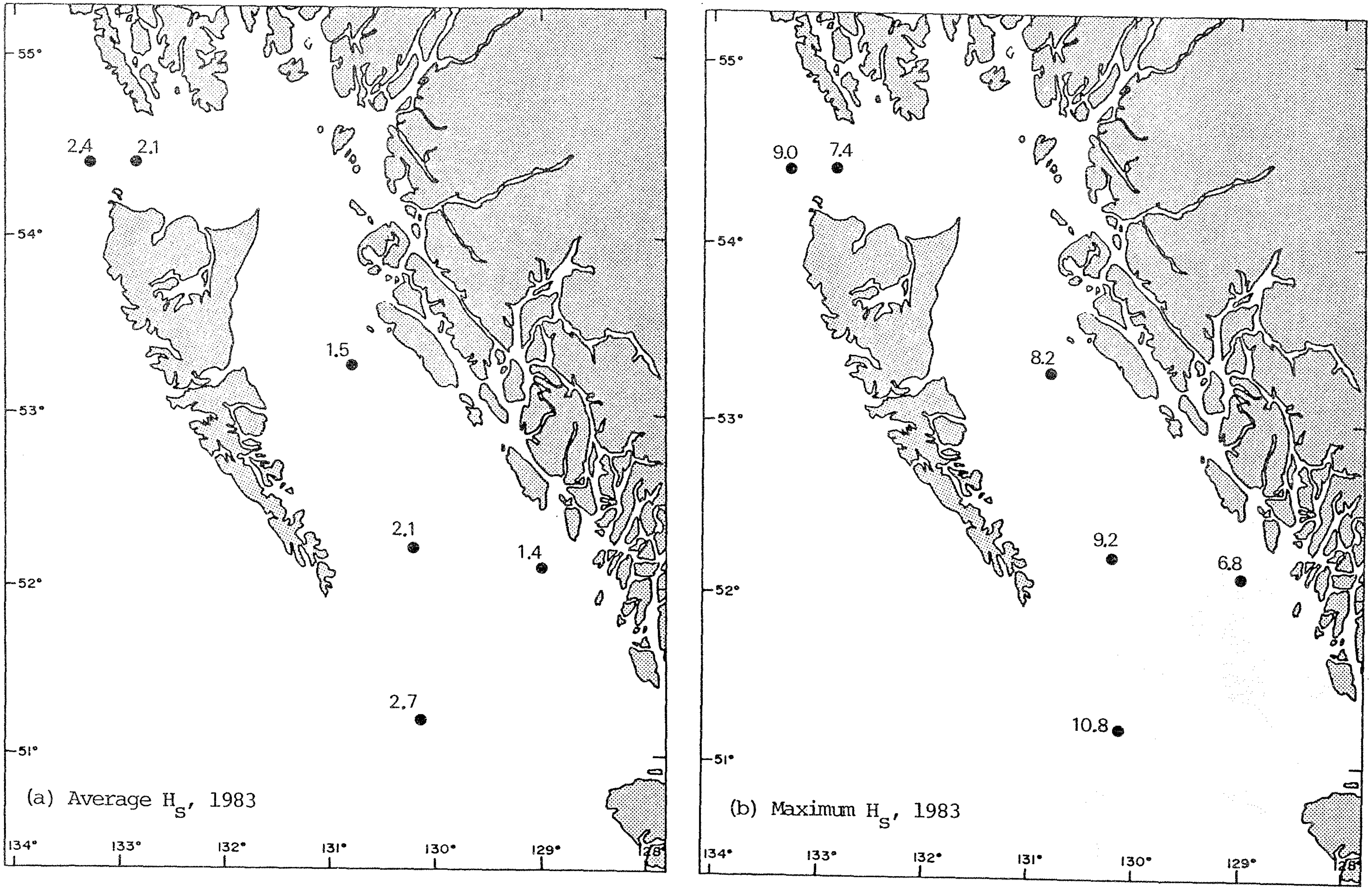

Fig. 2.13 Average value of H_s, 1983 (a). Maximum value of H_s, 1983 (b).
Average value of T_p, 1983 (c). Maximum value of T_p, 1983 (d).

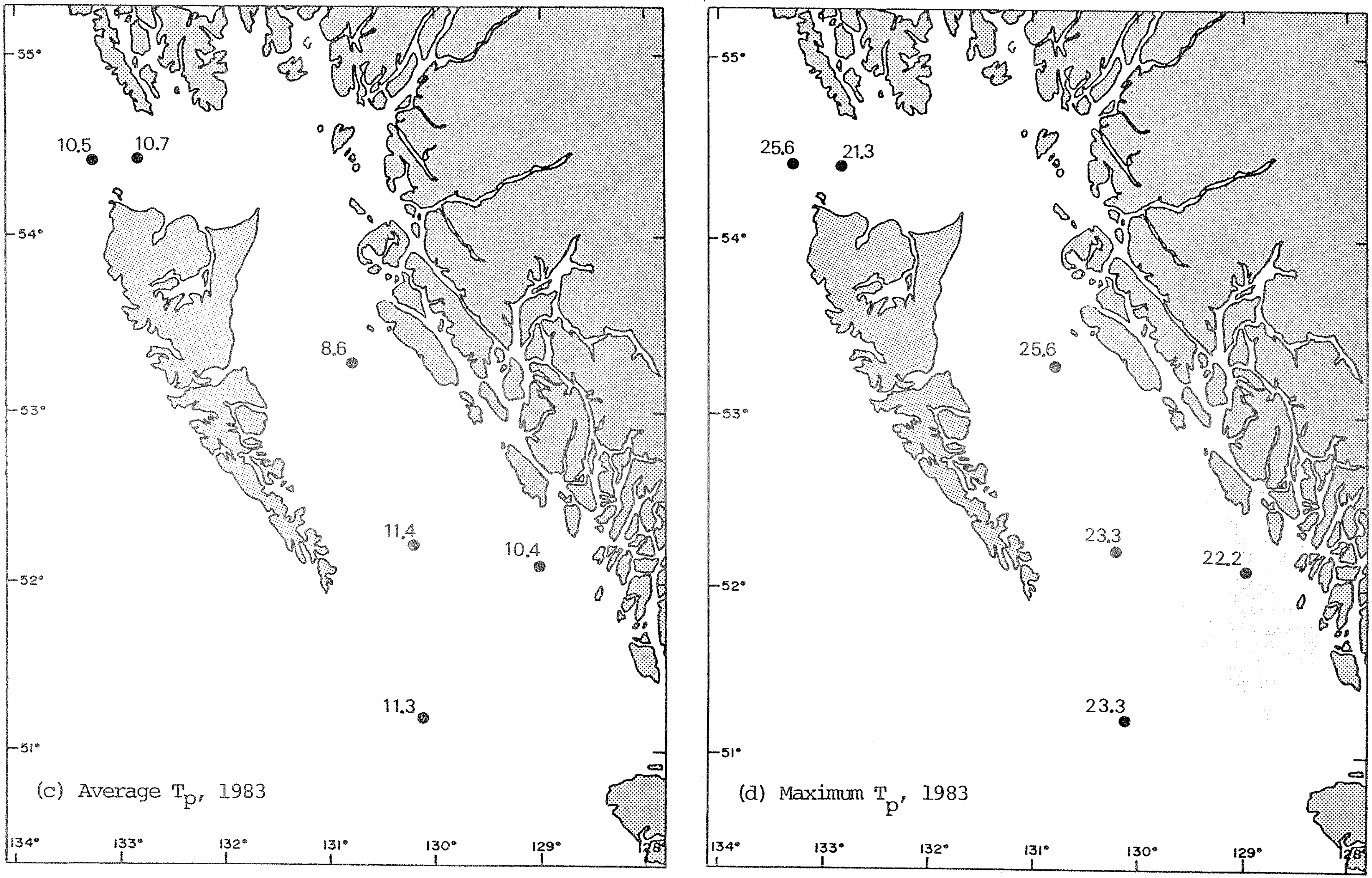

Fig. 2.13 continued

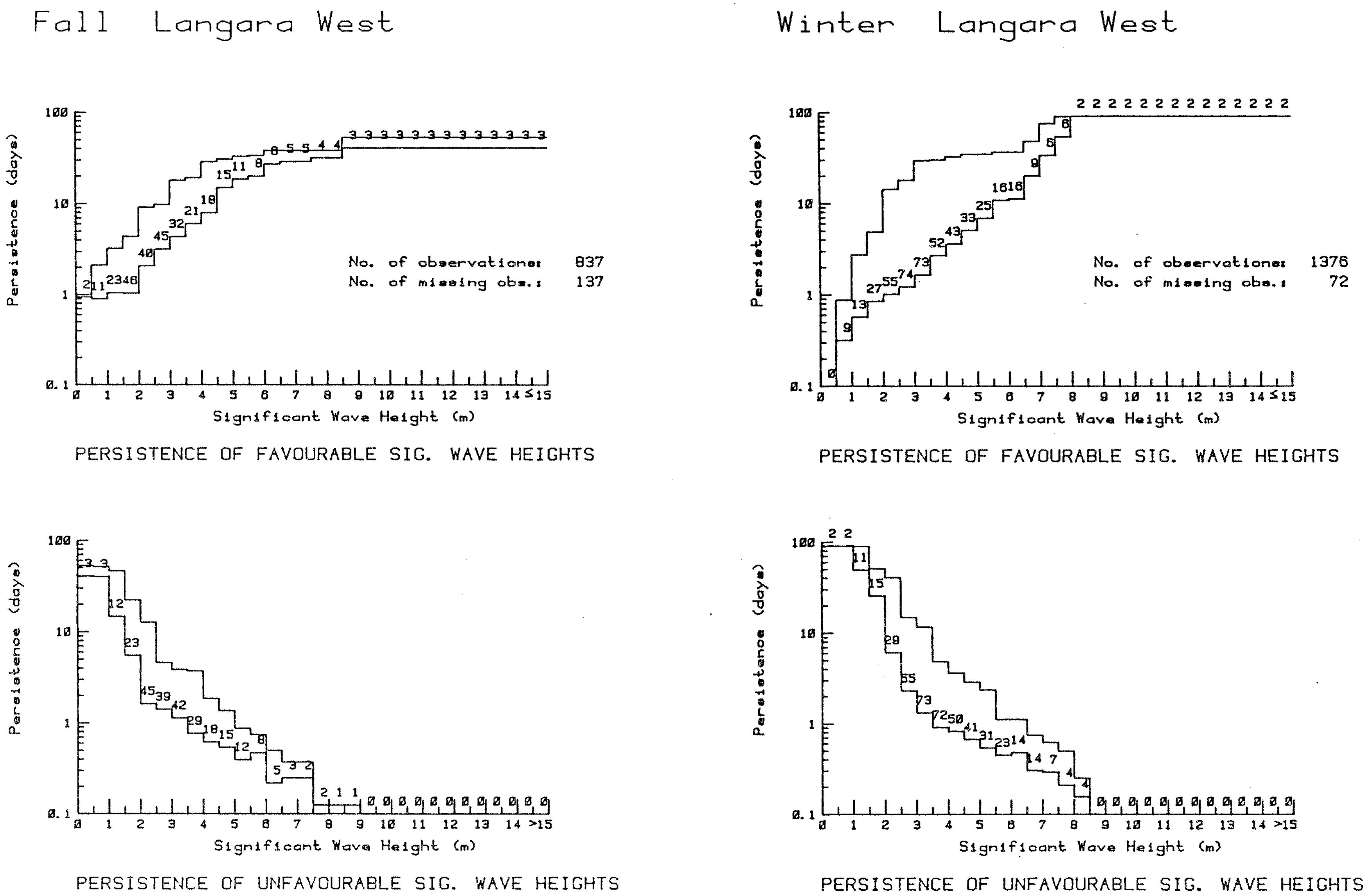

Fig. 2.14 Persistence statistics of wave heights on a seasonal basis. Upper panels show the maximum (upper curve) and average (lower curve) number of days over which significant wave heights were less than the plotted value. The lower panel gives maximum and average persistences of waves into heights greater than the plotted value. Numbers along the average curve indicate the number of occurences over which the average is calculated.

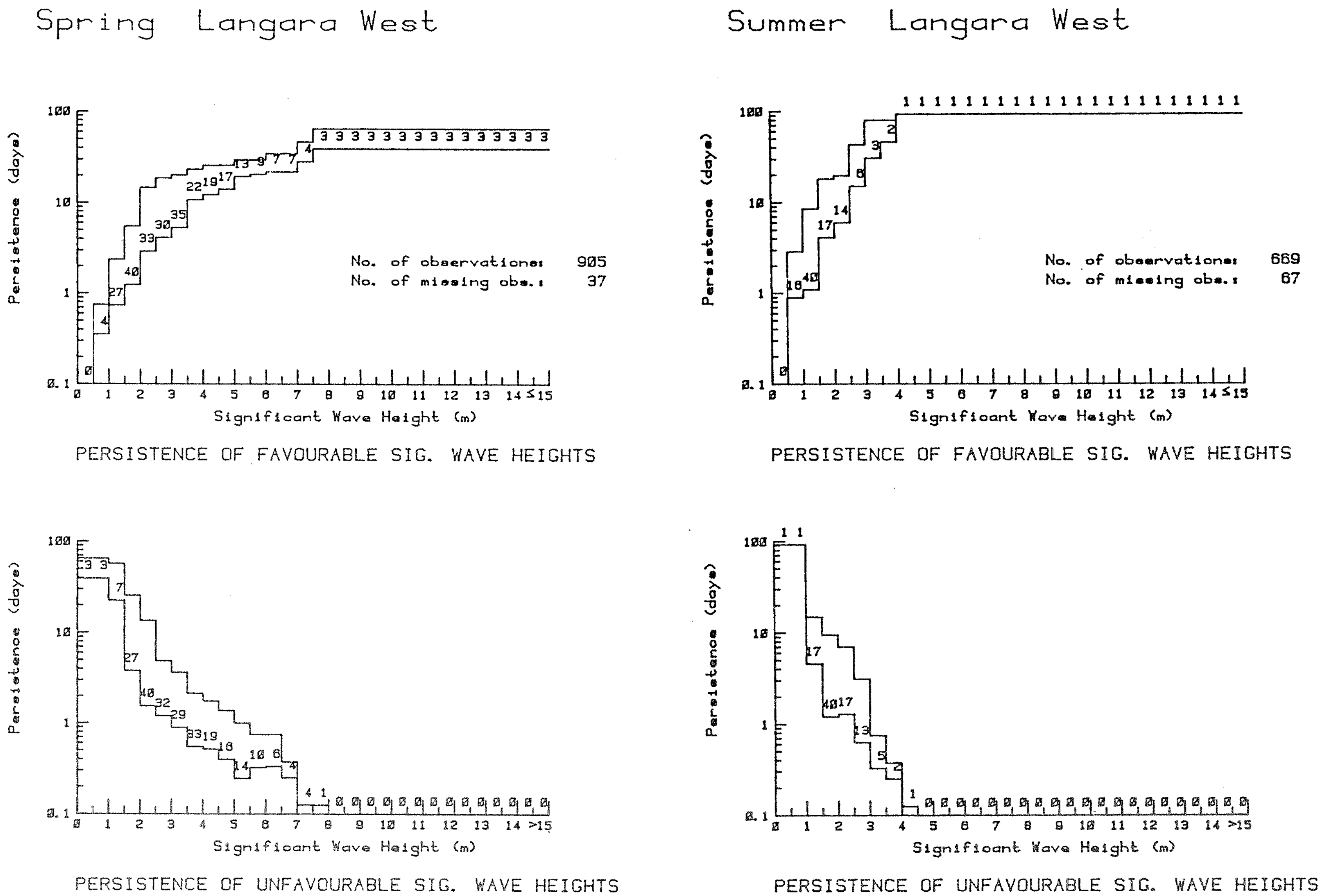

Fig. 2.14 continued

Spring Langara East

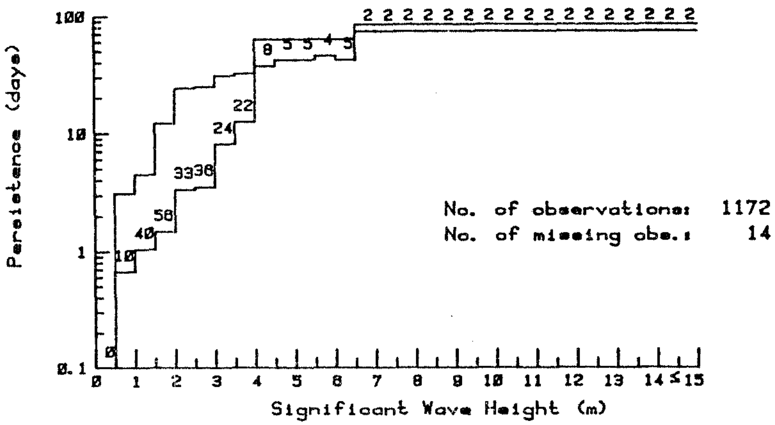

PERSISTENCE OF FAVOURABLE SIG. WAVE HEIGHTS

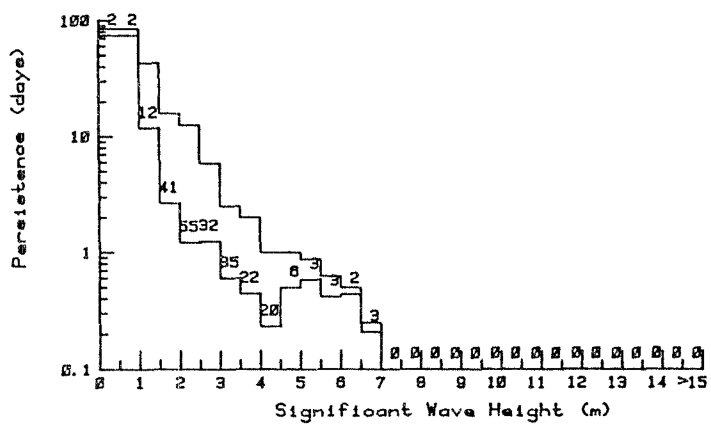

PERSISTENCE OF UNFAVOURABLE SIG. WAVE HEIGHTS

Summer Langara East

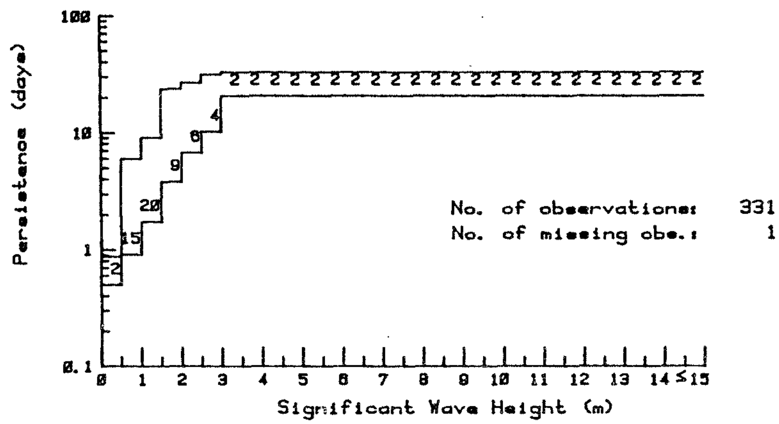

PERSISTENCE OF FAVOURABLE SIG. WAVE HEIGHTS

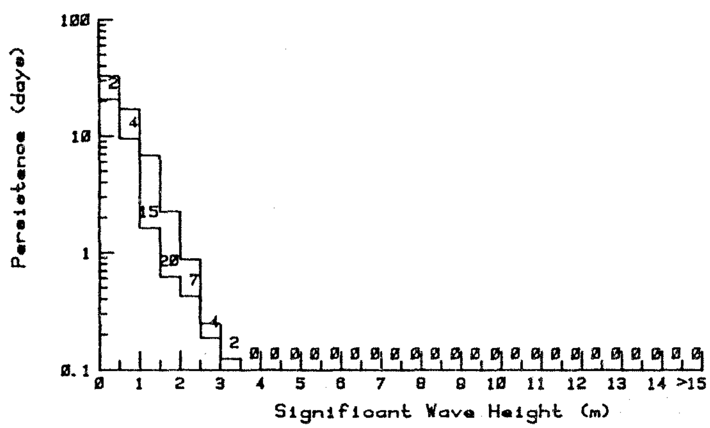

PERSISTENCE OF UNFAVOURABLE SIG. WAVE HEIGHTS

Fig. 2.14 continued

Winter Langara East

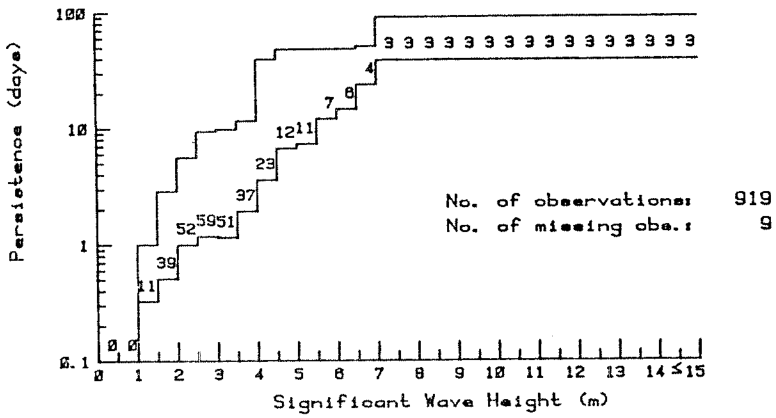

PERSISTENCE OF FAVOURABLE SIG. WAVE HEIGHTS

Fall Langara East

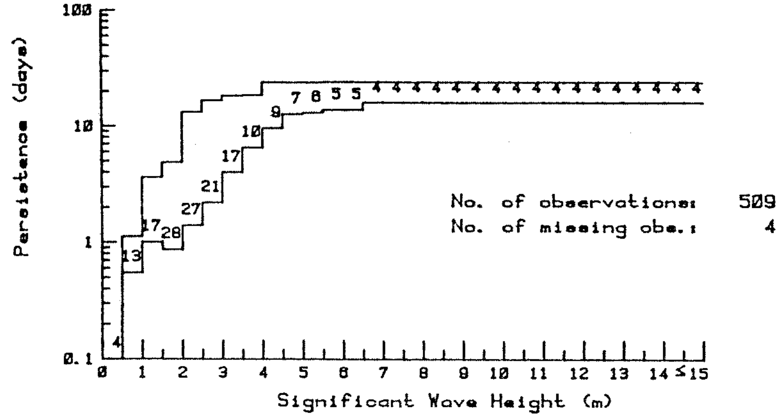

PERSISTENCE OF FAVOURABLE SIG. WAVE HEIGHTS

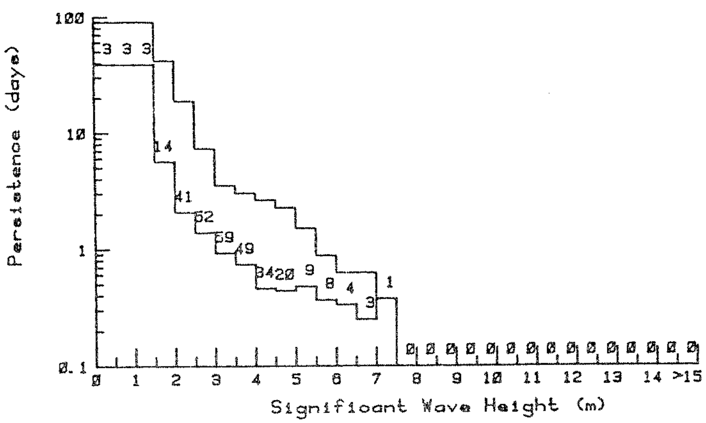

PERSISTENCE OF UNFAVOURABLE SIG. WAVE HEIGHTS

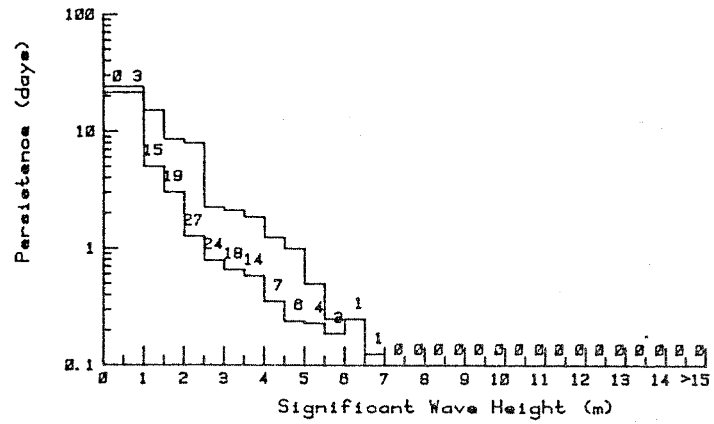

PERSISTENCE OF UNFAVOURABLE SIG. WAVE HEIGHTS

Fig. 2.14 continued

Spring Bonilla Island

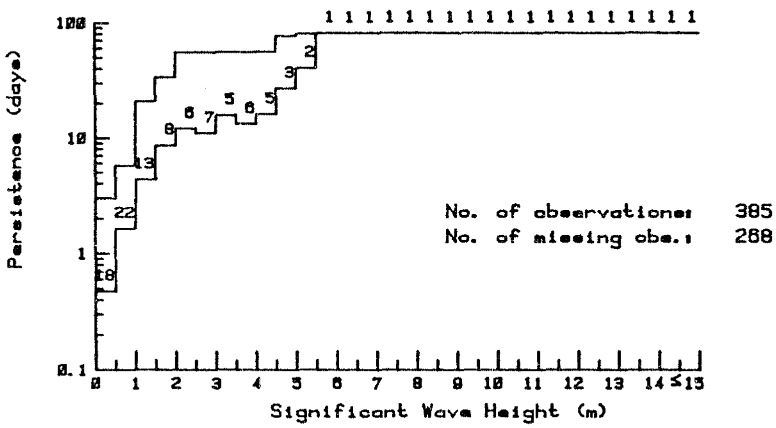

PERSISTENCE OF FAVOURABLE SIG. WAVE HEIGHTS

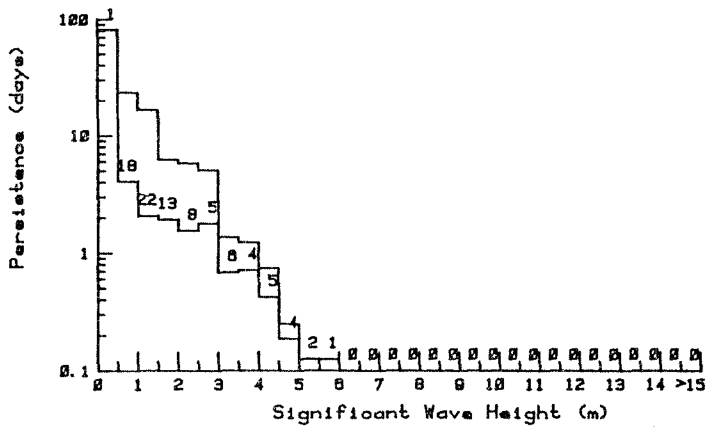

PERSISTENCE OF UNFAVOURABLE SIG. WAVE HEIGHTS

Fig. 2.14 continued

Fall Bonilla Island

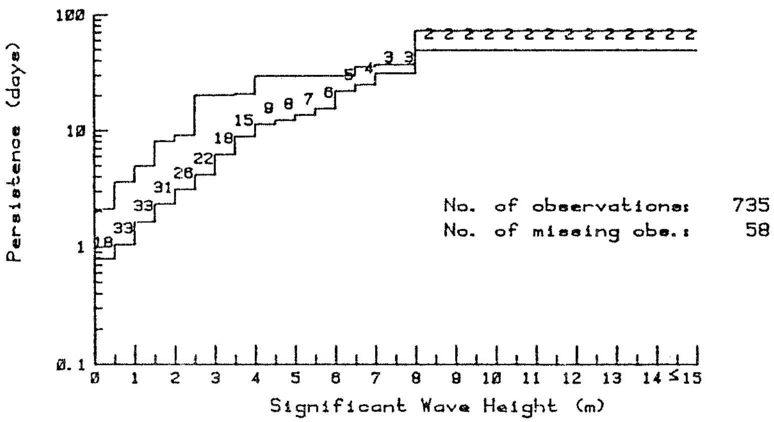

PERSISTENCE OF FAVOURABLE SIG. WAVE HEIGHTS

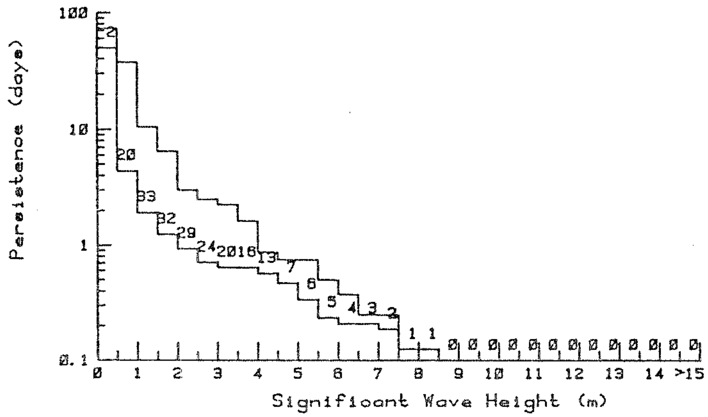

PERSISTENCE OF UNFAVOURABLE SIG. WAVE HEIGHTS

Winter Bonilla Island

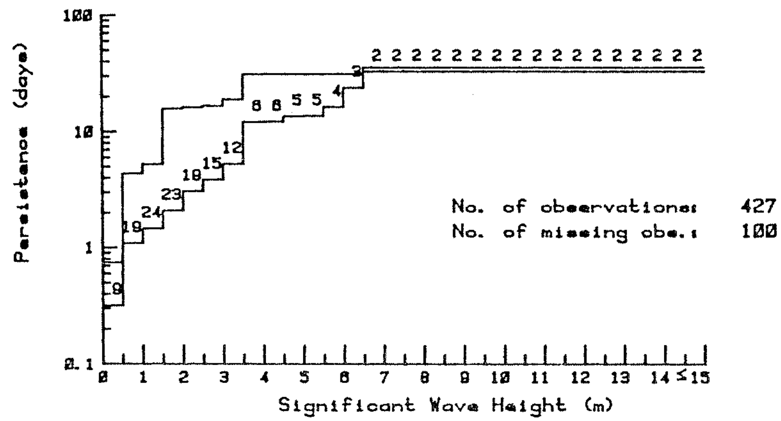

PERSISTENCE OF FAVOURABLE SIG. WAVE HEIGHTS

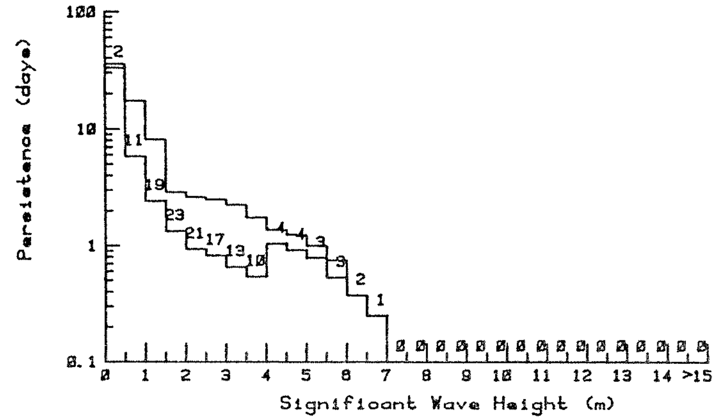

PERSISTENCE OF UNFAVOURABLE SIG. WAVE HEIGHTS

Fig. 2.14 continued

Fall McInnes Island

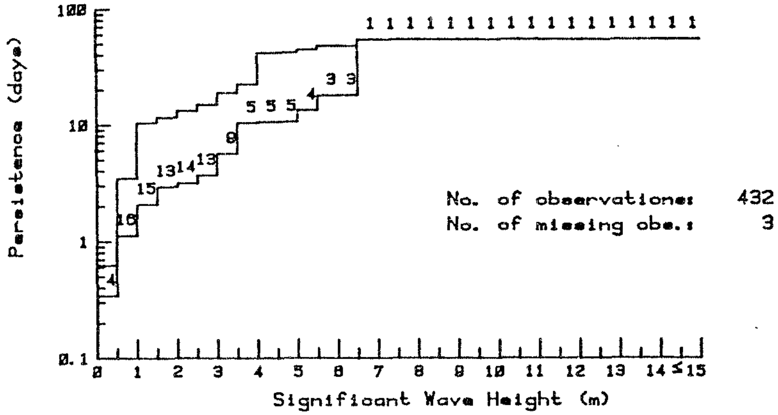

PERSISTENCE OF FAVOURABLE SIG. WAVE HEIGHTS

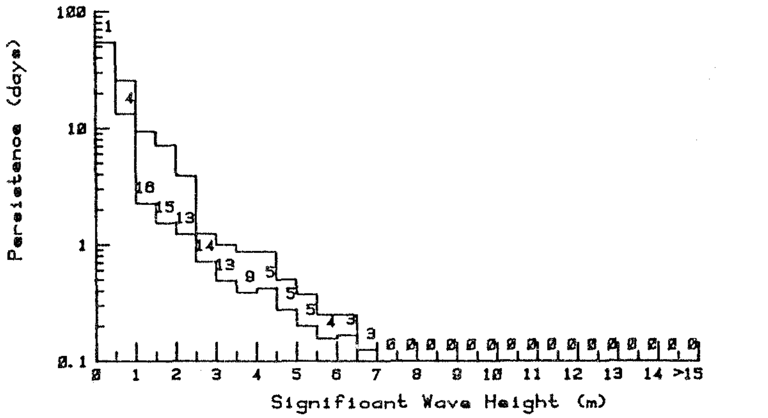

PERSISTENCE OF UNFAVOURABLE SIG. WAVE HEIGHTS

Winter McInnes Island

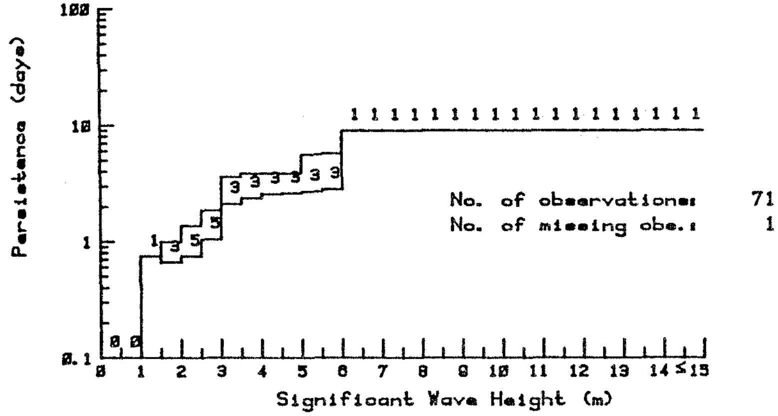

PERSISTENCE OF FAVOURABLE SIG. WAVE HEIGHTS

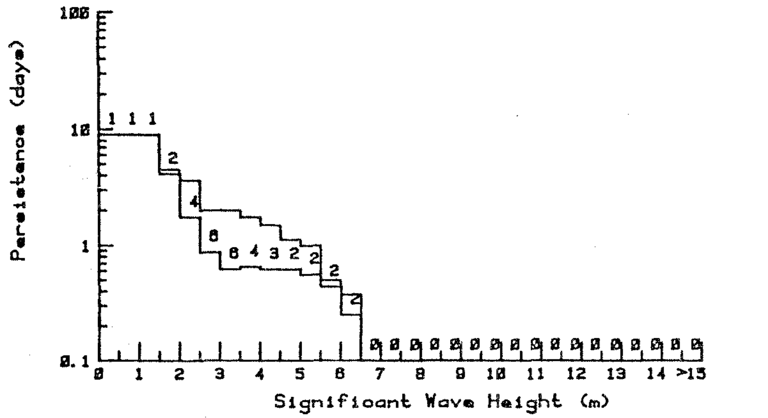

PERSISTENCE OF UNFAVOURABLE SIG. WAVE HEIGHTS

Fig. 2.14 continued

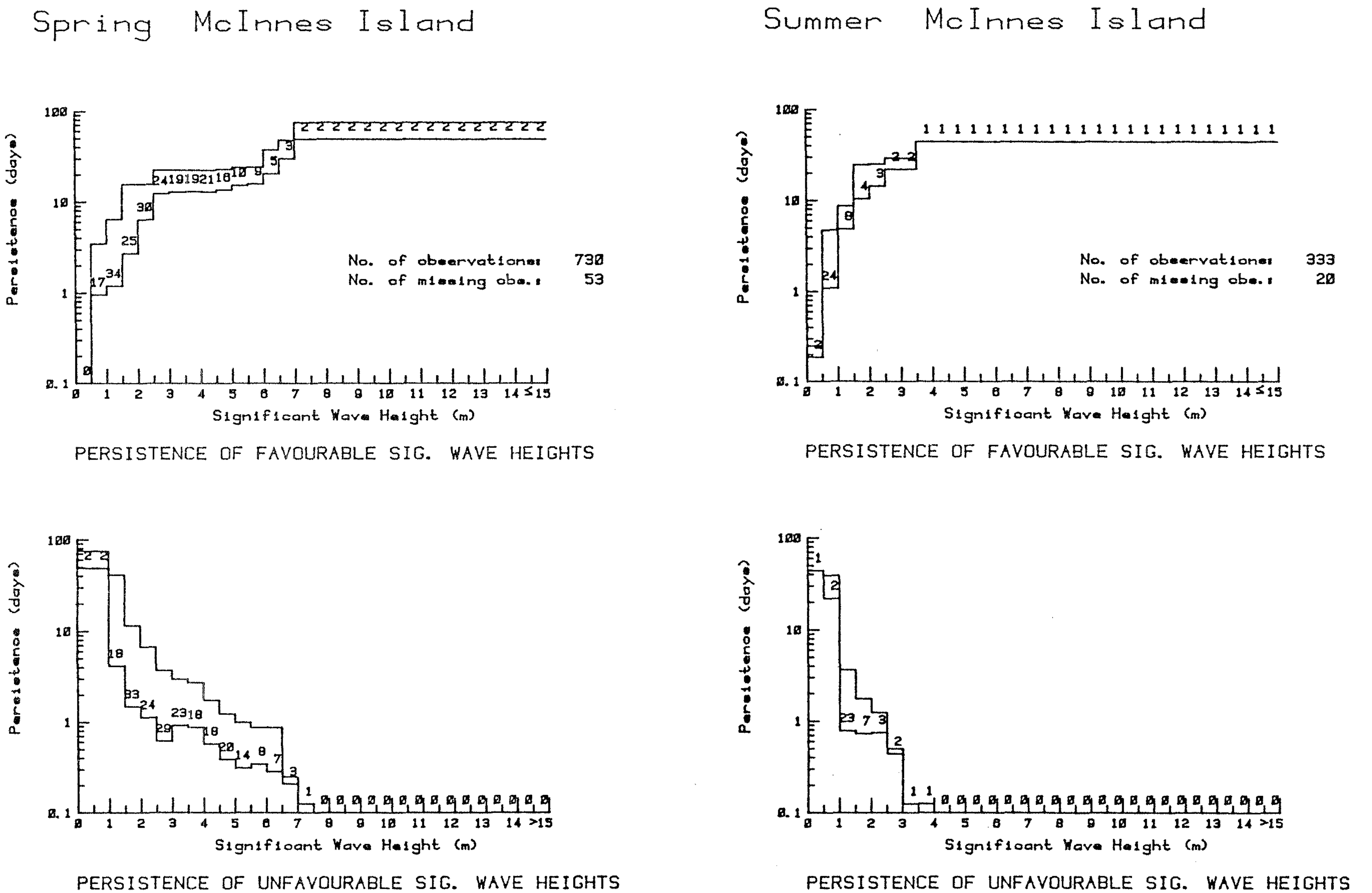

Fig. 2.14 continued

Fall Hecate Strait

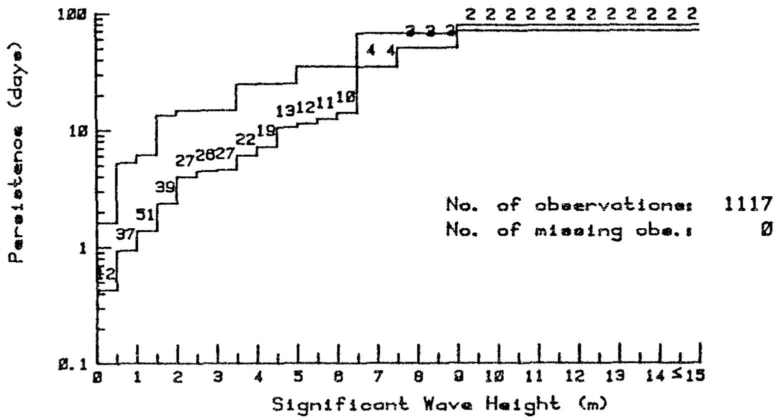

PERSISTENCE OF FAVOURABLE SIG. WAVE HEIGHTS

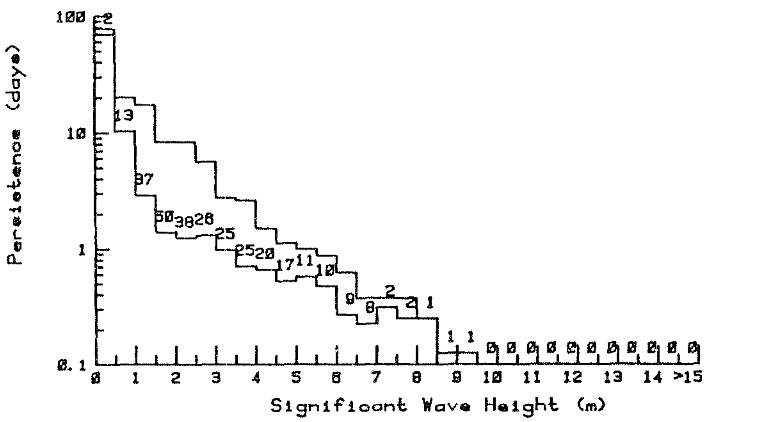

PERSISTENCE OF UNFAVOURABLE SIG. WAVE HEIGHTS

Winter Hecate Strait

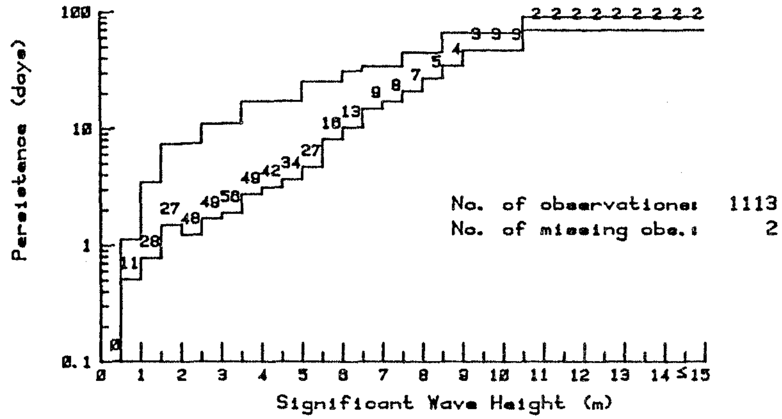

PERSISTENCE OF FAVOURABLE SIG. WAVE HEIGHTS

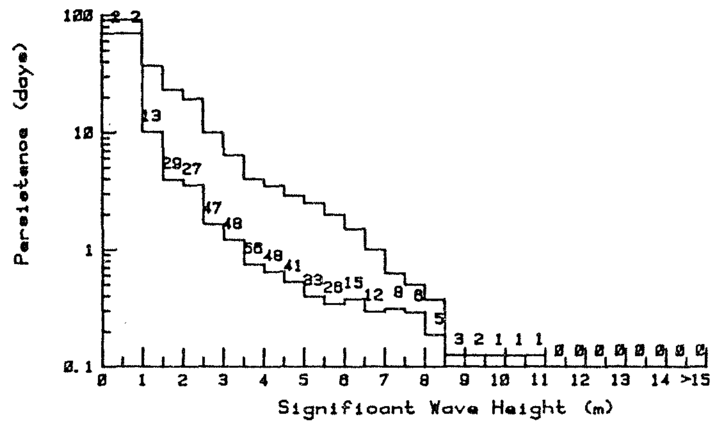

PERSISTENCE OF UNFAVOURABLE SIG. WAVE HEIGHTS

Fig. 2.14 continued

Spring Hecate Strait

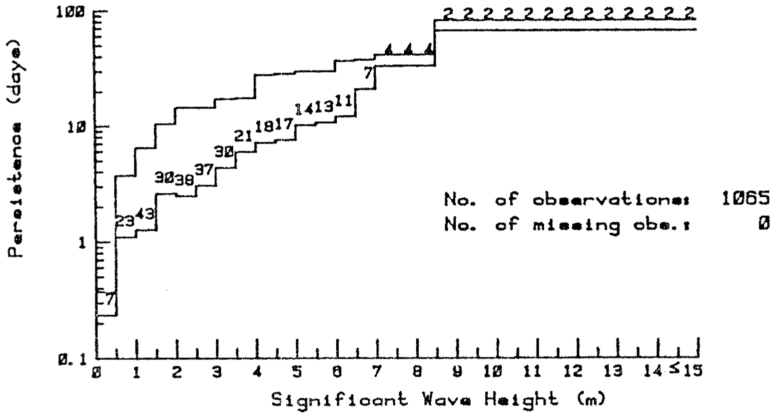

PERSISTENCE OF FAVOURABLE SIG. WAVE HEIGHTS

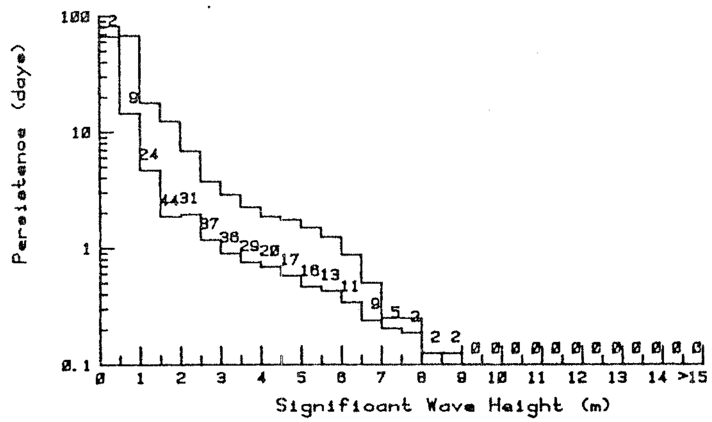

PERSISTENCE OF UNFAVOURABLE SIG. WAVE HEIGHTS

Summer Hecate Strait

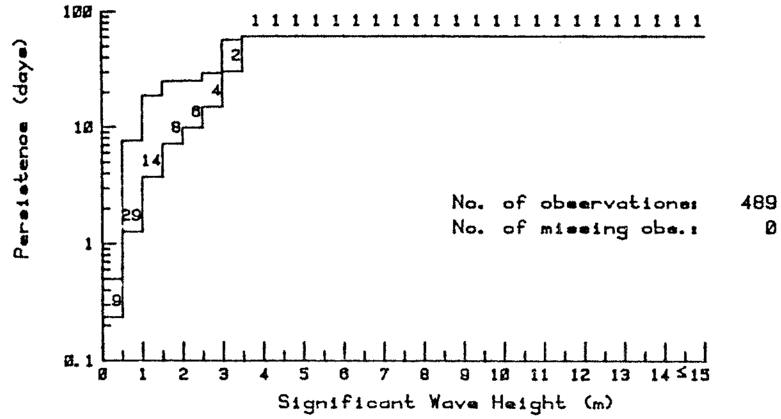

PERSISTENCE OF FAVOURABLE SIG. WAVE HEIGHTS

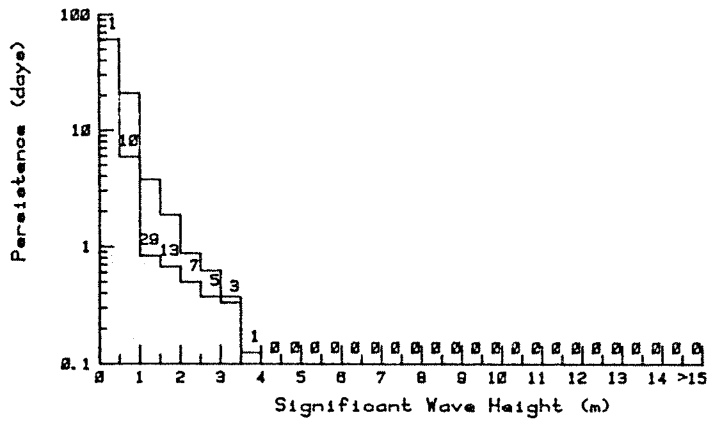

PERSISTENCE OF UNFAVOURABLE SIG. WAVE HEIGHTS

Fig. 2.14 continued

Fall Queen Charlotte Snd.

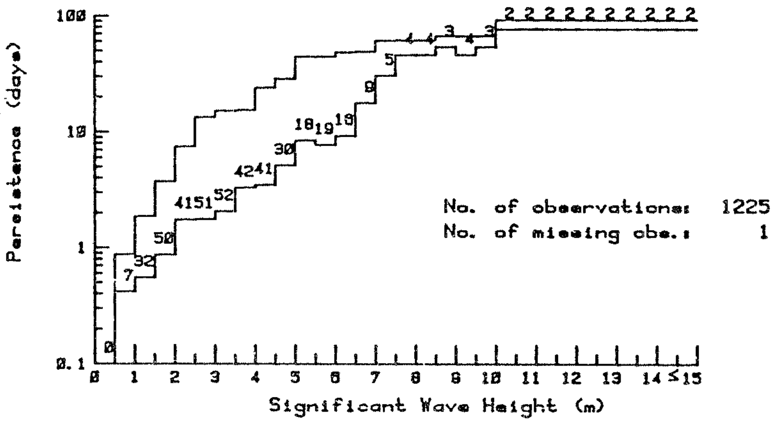

PERSISTENCE OF FAVOURABLE SIG. WAVE HEIGHTS

Winter Queen Charlotte Snd.

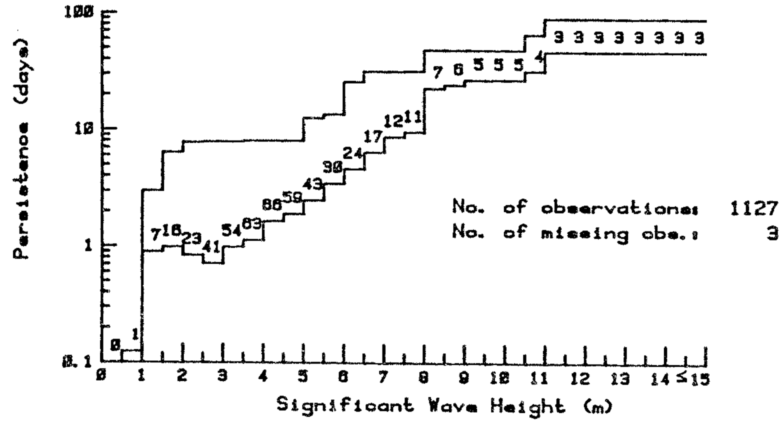

PERSISTENCE OF FAVOURABLE SIG. WAVE HEIGHTS

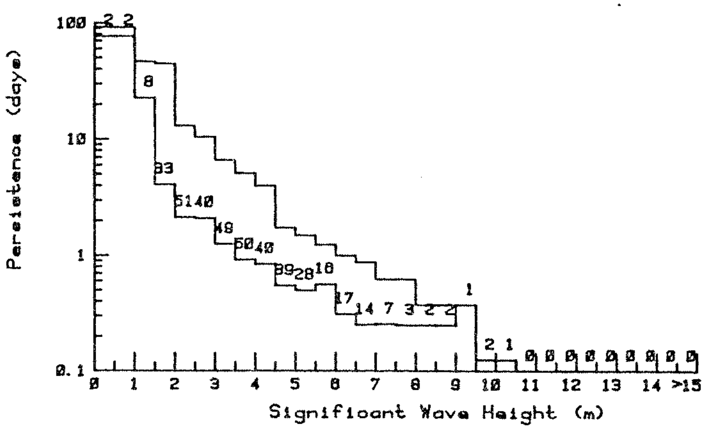

PERSISTENCE OF UNFAVOURABLE SIG. WAVE HEIGHTS

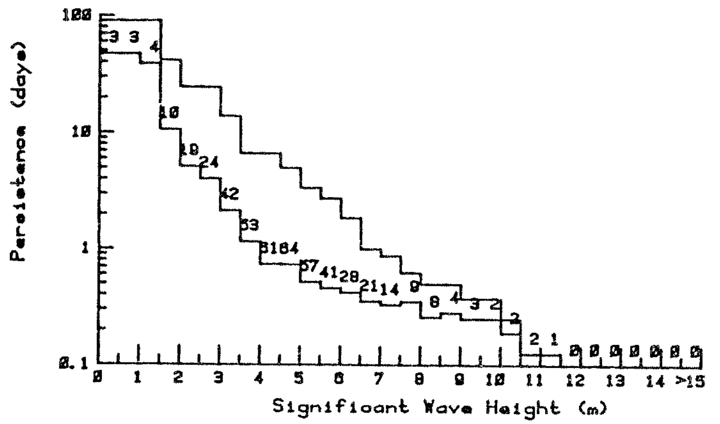

PERSISTENCE OF UNFAVOURABLE SIG. WAVE HEIGHTS

Fig. 2.14 continued

Spring Queen Charlotte Snd.

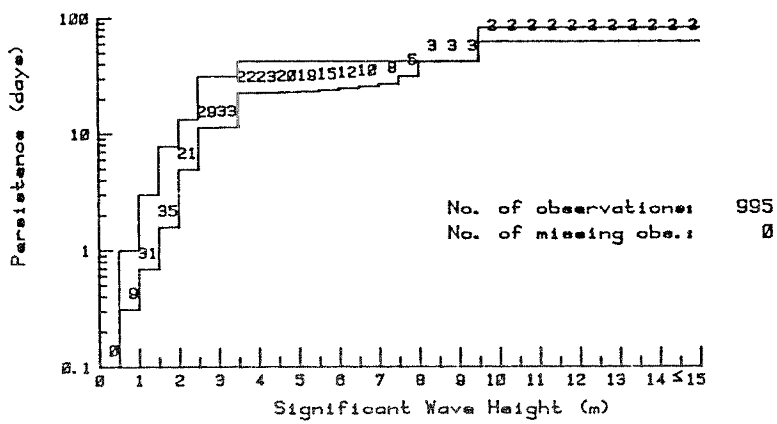

PERSISTENCE OF FAVOURABLE SIG. WAVE HEIGHTS

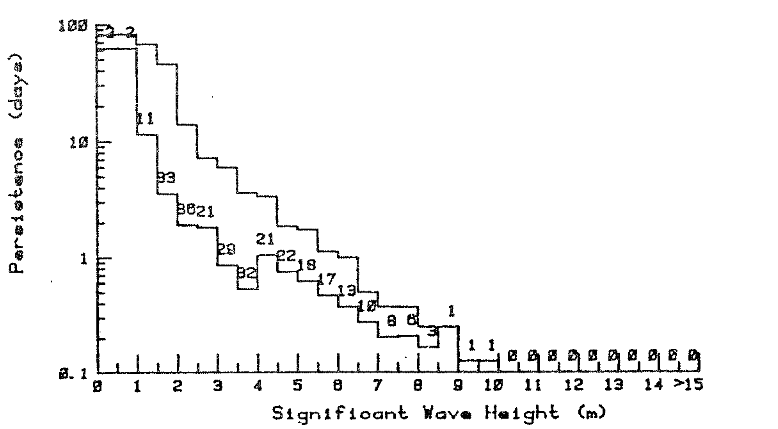

PERSISTENCE OF UNFAVOURABLE SIG. WAVE HEIGHTS

Summer Queen Charlotte Snd.

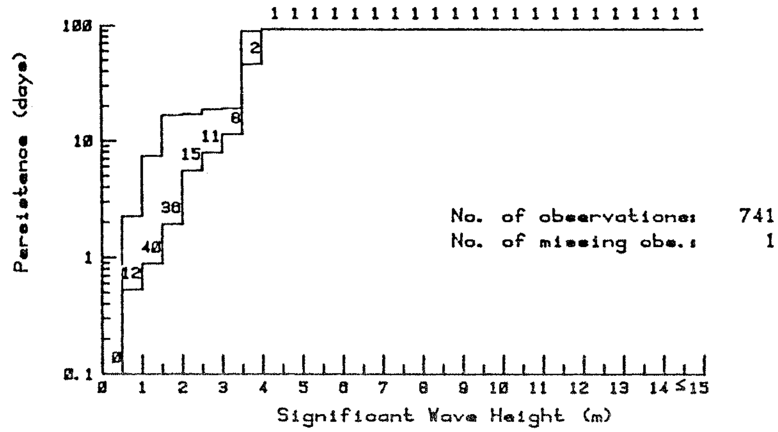

PERSISTENCE OF FAVOURABLE SIG. WAVE HEIGHTS

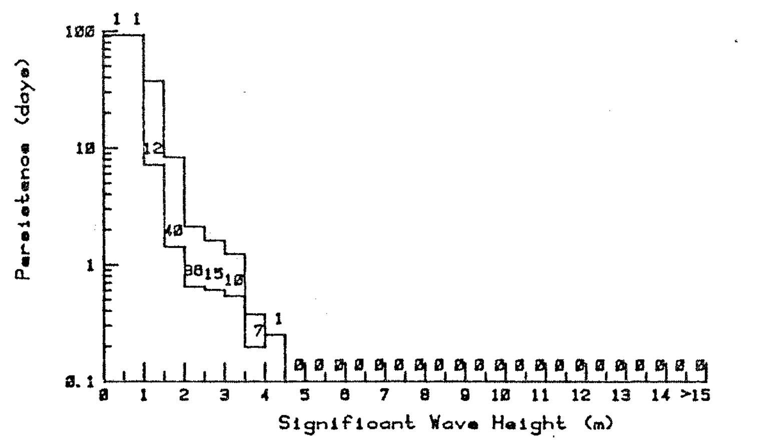

PERSISTENCE OF UNFAVOURABLE SIG. WAVE HEIGHTS

Fig. 2.14 continued

1983 Langara West

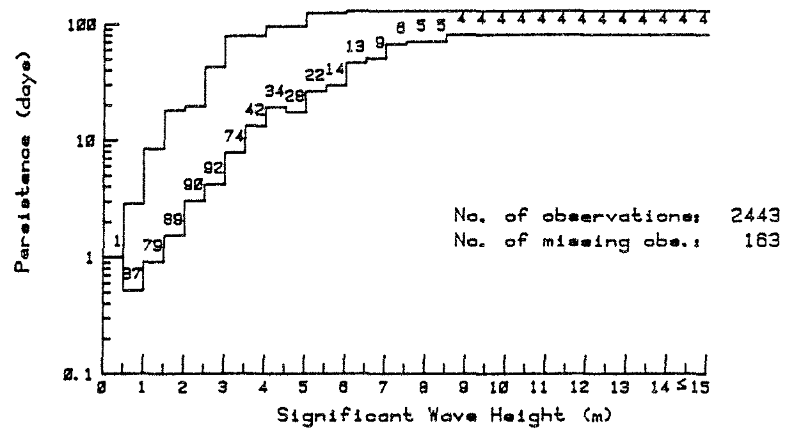

PERSISTENCE OF FAVOURABLE SIG. WAVE HEIGHTS

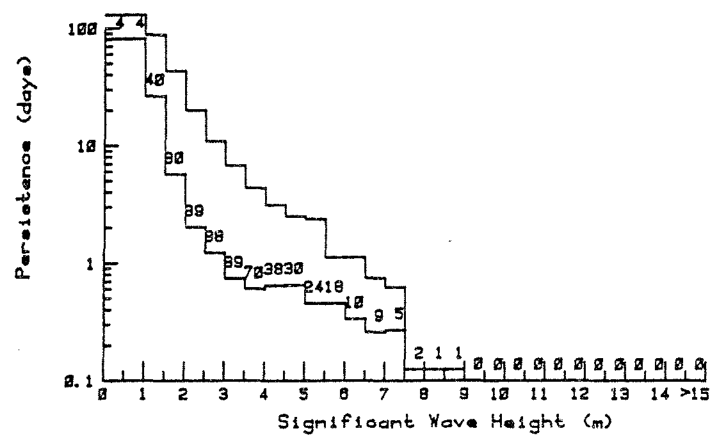

PERSISTENCE OF UNFAVOURABLE SIG. WAVE HEIGHTS

Fig. 2.15 Annual wave height persistence statistics, plotted as for Fig. 2.14.

1983 McInnes Island

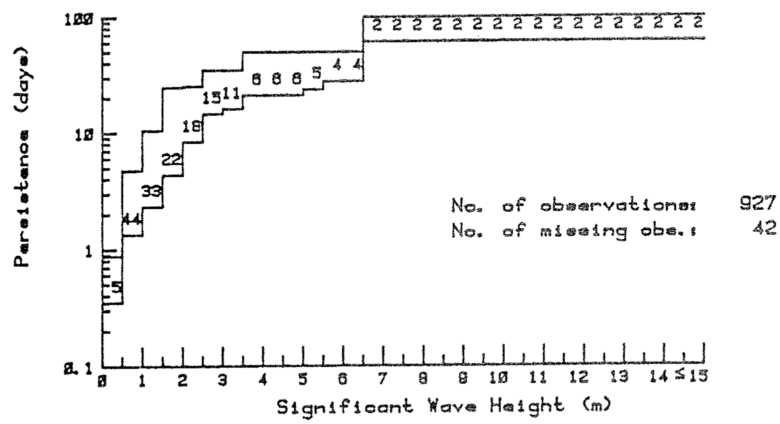

PERSISTENCE OF FAVOURABLE SIG. WAVE HEIGHTS

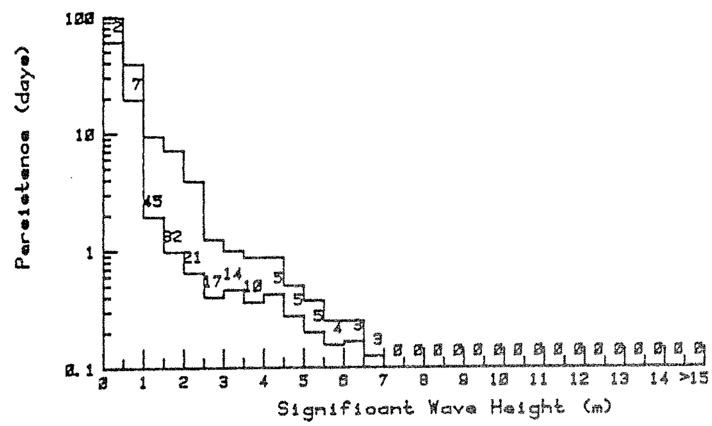

PERSISTENCE OF UNFAVOURABLE SIG. WAVE HEIGHTS

Fig. 2.15 Continued

1983 Hecate Strait

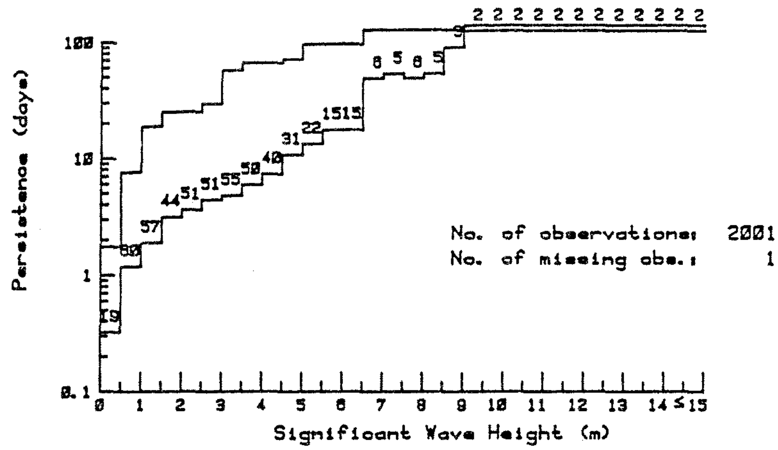

PERSISTENCE OF FAVOURABLE SIG. WAVE HEIGHTS

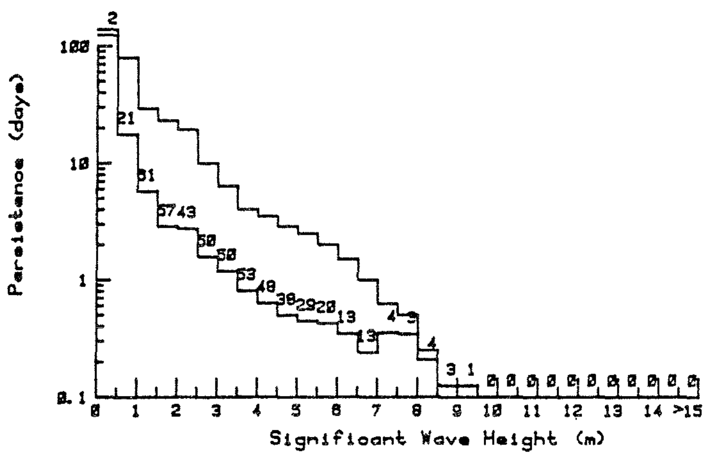

PERSISTENCE OF UNFAVOURABLE SIG. WAVE HEIGHTS

Fig. 2.15 Continued

1983 Queen Charlotte Snd.

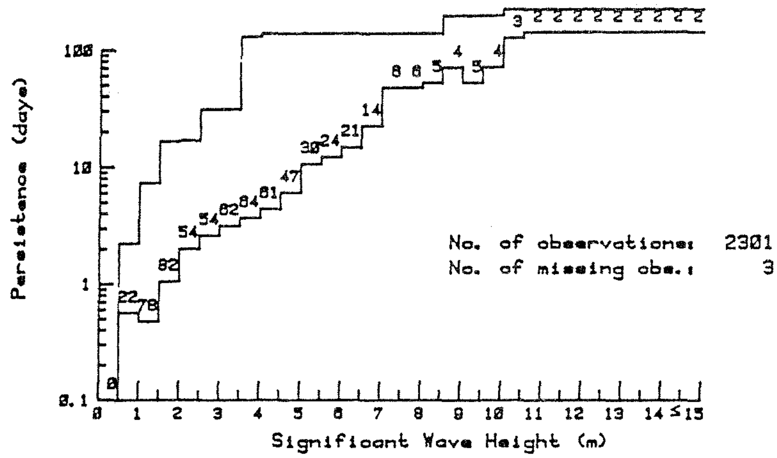

PERSISTENCE OF FAVOURABLE SIG. WAVE HEIGHTS

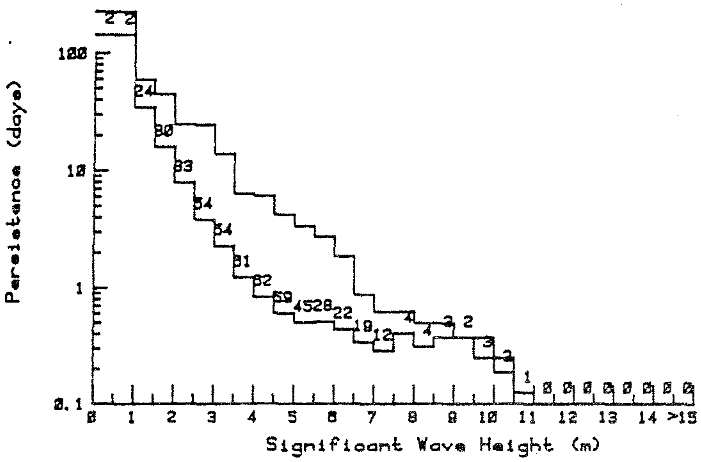

PERSISTENCE OF UNFAVOURABLE SIG. WAVE HEIGHTS

Fig. 2.15 Continued

1983 Langara East

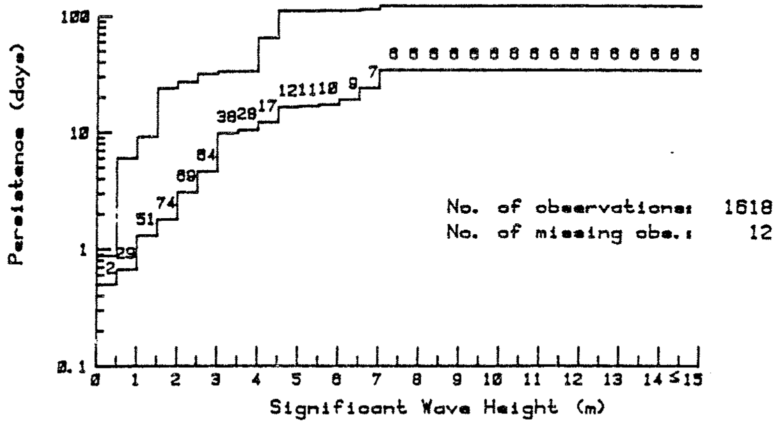

PERSISTENCE OF FAVOURABLE SIG. WAVE HEIGHTS

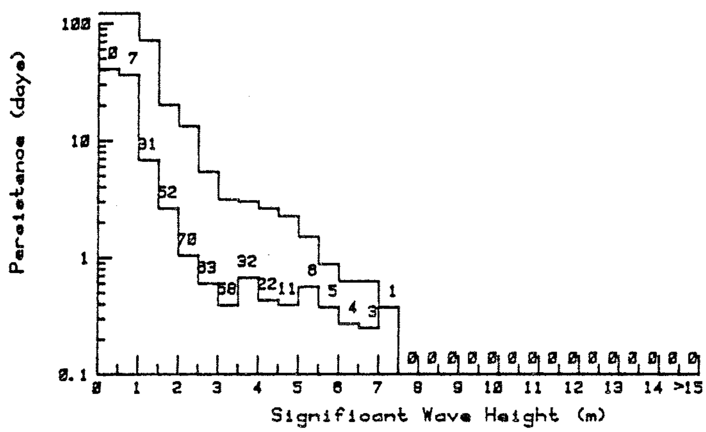

PERSISTENCE OF UNFAVOURABLE SIG. WAVE HEIGHTS

Fig. 2.15 continued

1983 Bonilla Island

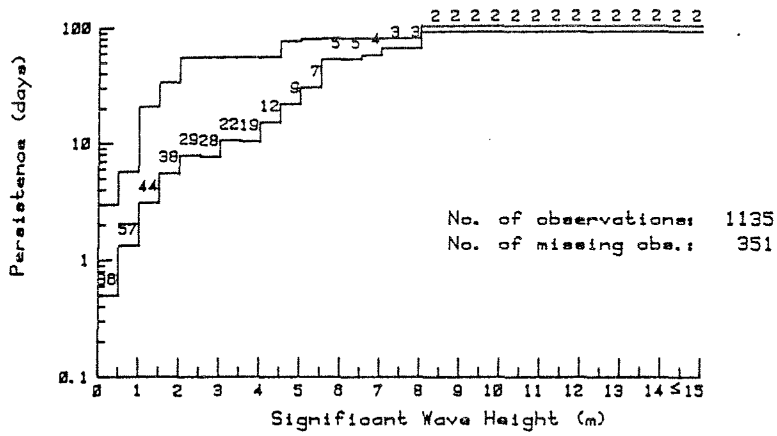

PERSISTENCE OF FAVOURABLE SIG. WAVE HEIGHTS

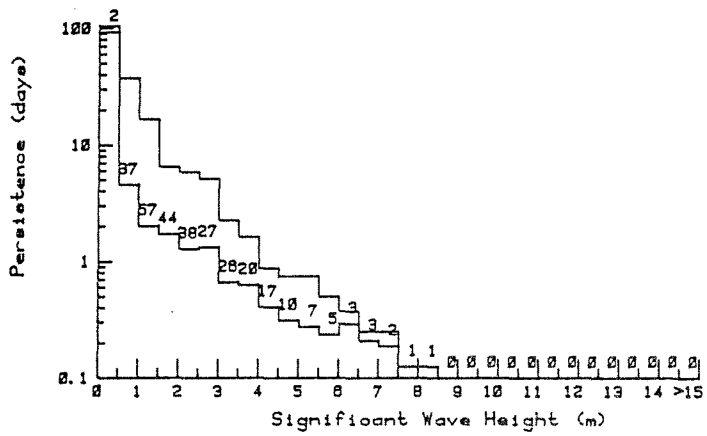

PERSISTENCE OF UNFAVOURABLE SIG. WAVE HEIGHTS

Fig. 2.15 continued

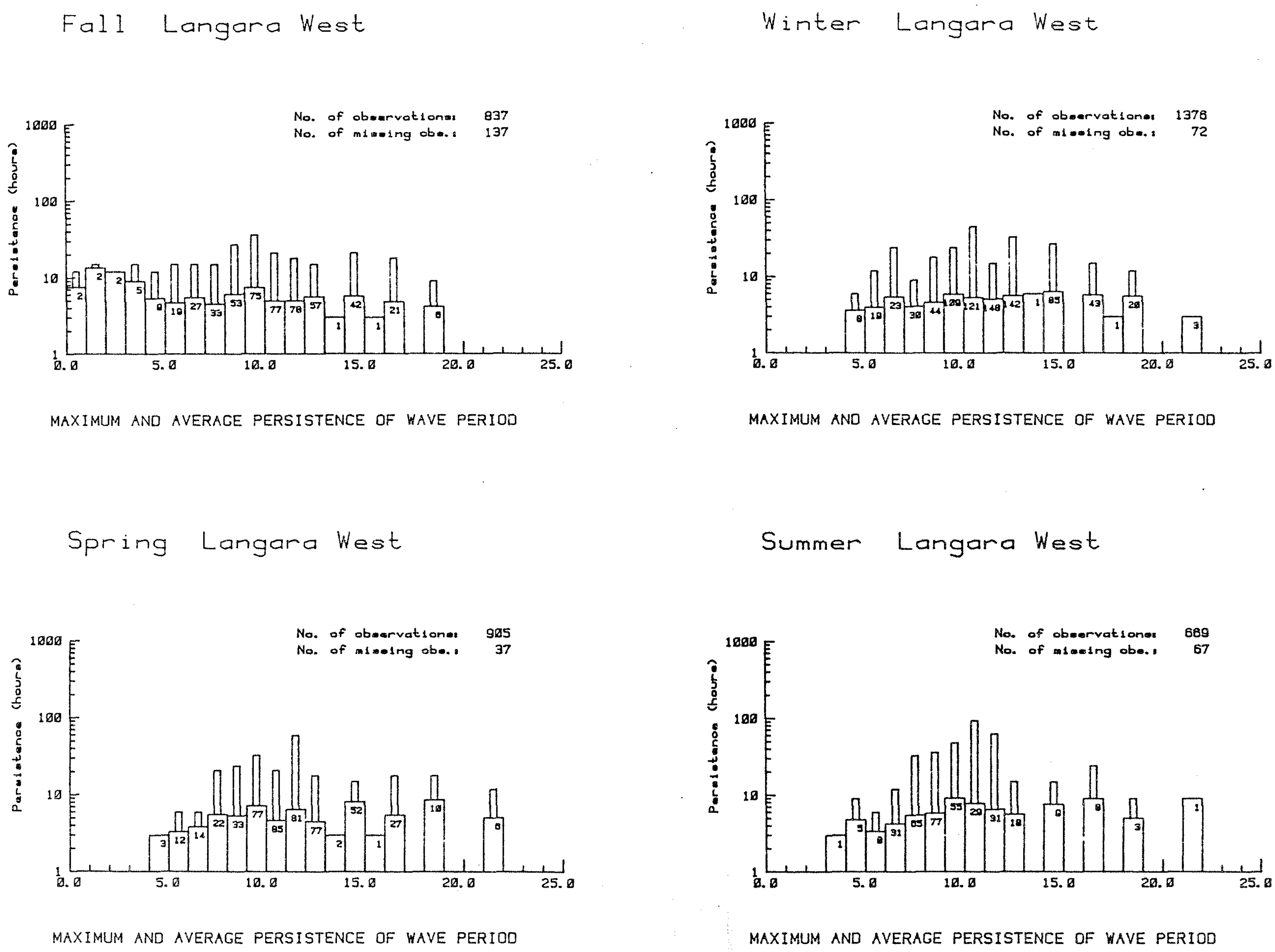

Fig. 2.16 Persistence statistics of wave periods on a seasonal basis. Full columns show the average; narrow extensions show the maximum persistence values over the number of durations indicated.

Fall Langara East

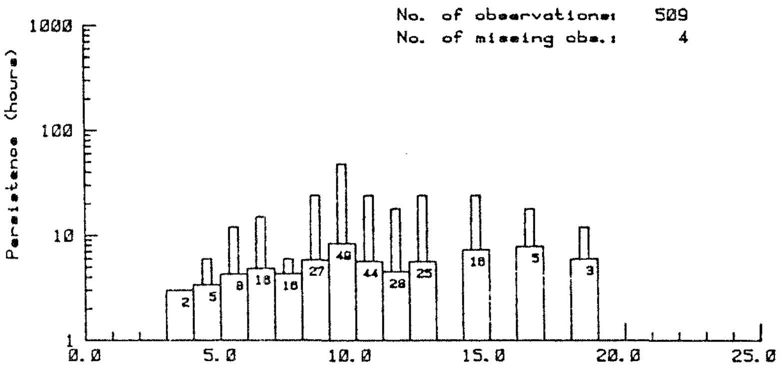

MAXIMUM AND AVERAGE PERSISTENCE OF WAVE PERIOD

Winter Langara East

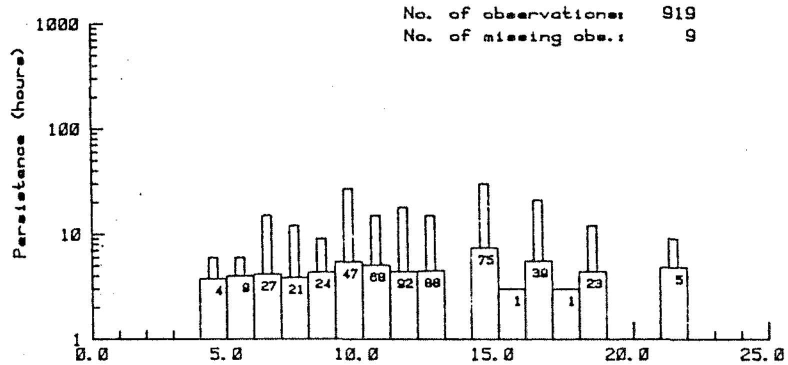

MAXIMUM AND AVERAGE PERSISTENCE OF WAVE PERIOD

Spring Langara East

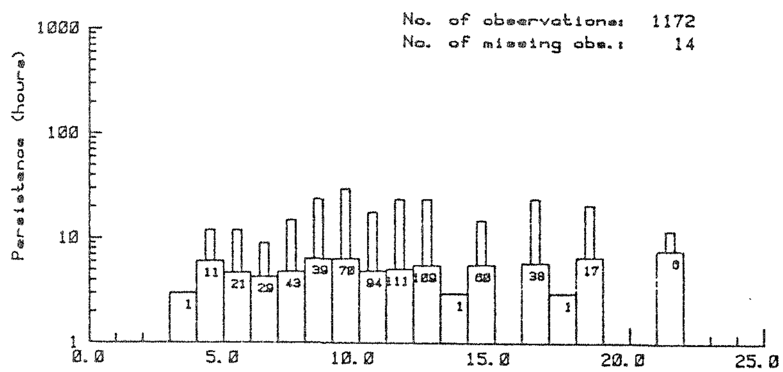

MAXIMUM AND AVERAGE PERSISTENCE OF WAVE PERIOD

Summer Langara East

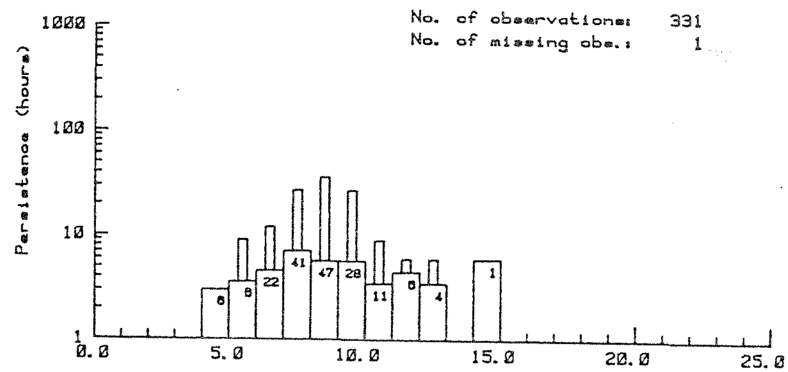

MAXIMUM AND AVERAGE PERSISTENCE OF WAVE PERIOD

Fig. 2.16 continued

Fall Bonilla Island

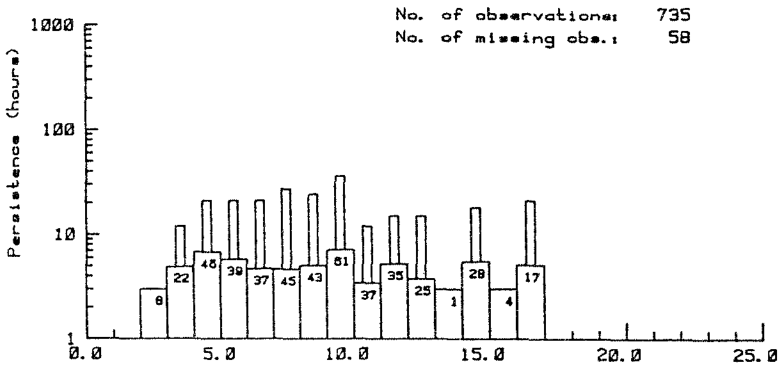

MAXIMUM AND AVERAGE PERSISTENCE OF WAVE PERIOD

Winter Bonilla Island

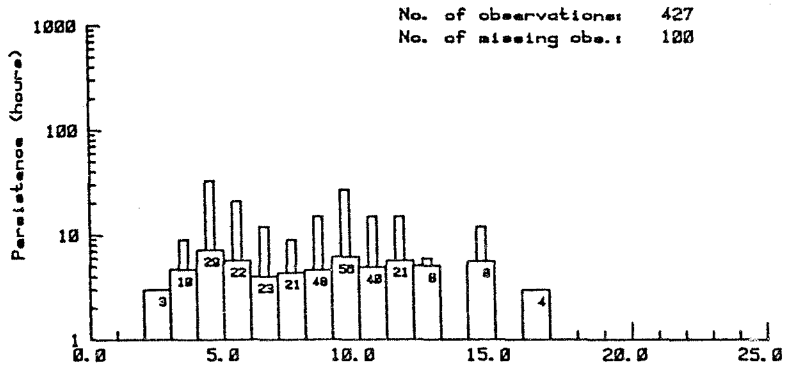

MAXIMUM AND AVERAGE PERSISTENCE OF WAVE PERIOD

Spring Bonilla Island

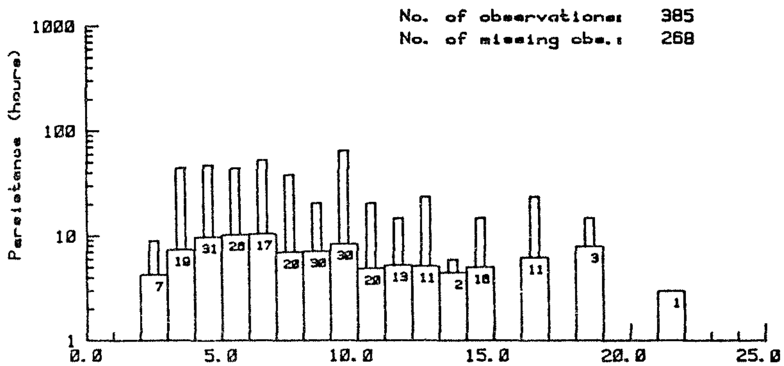

MAXIMUM AND AVERAGE PERSISTENCE OF WAVE PERIOD

Fig. 2.16 continued

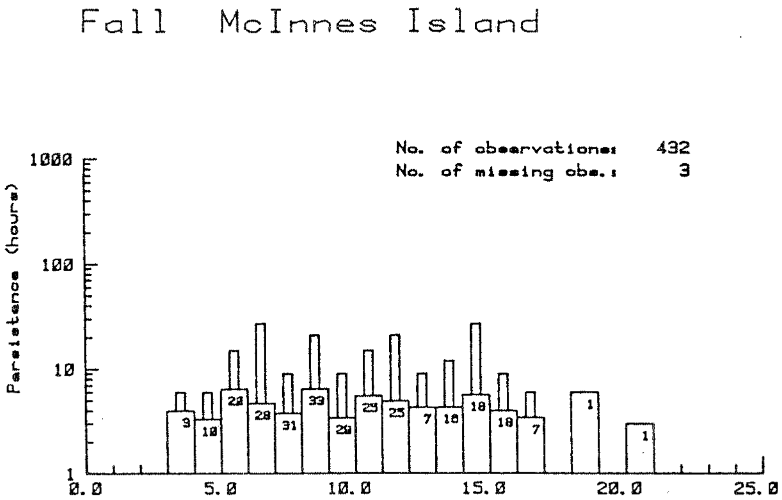

MAXIMUM AND AVERAGE PERSISTENCE OF WAVE PERIOD

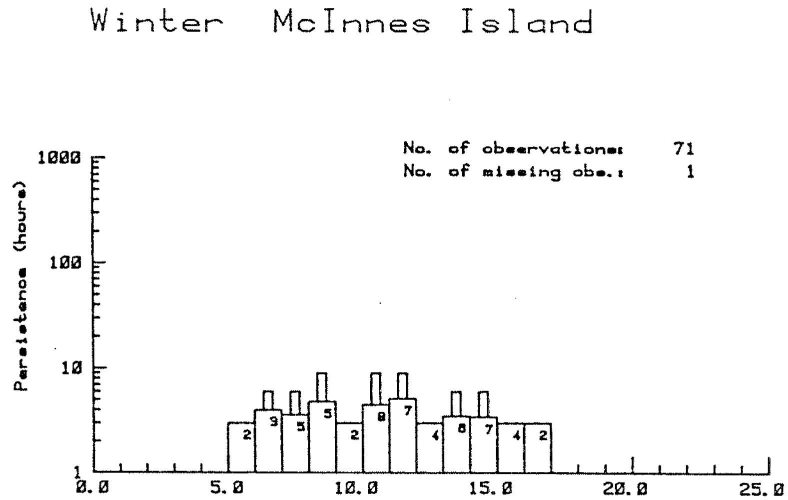

MAXIMUM AND AVERAGE PERSISTENCE OF WAVE PERIOD

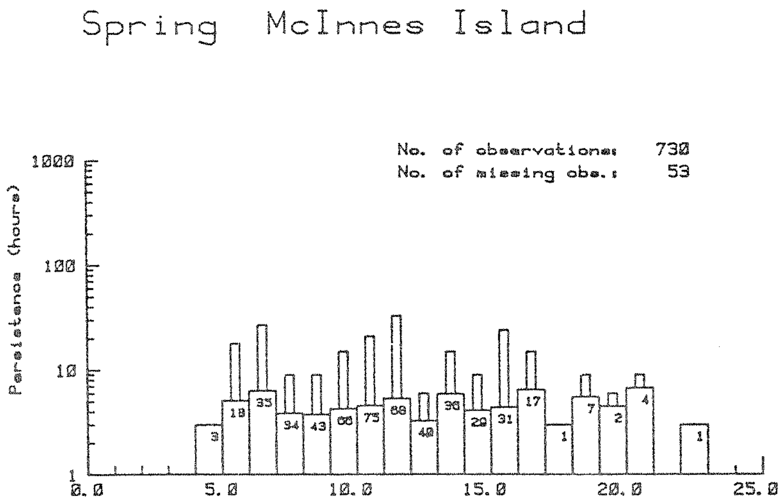

MAXIMUM AND AVERAGE PERSISTENCE OF WAVE PERIOD

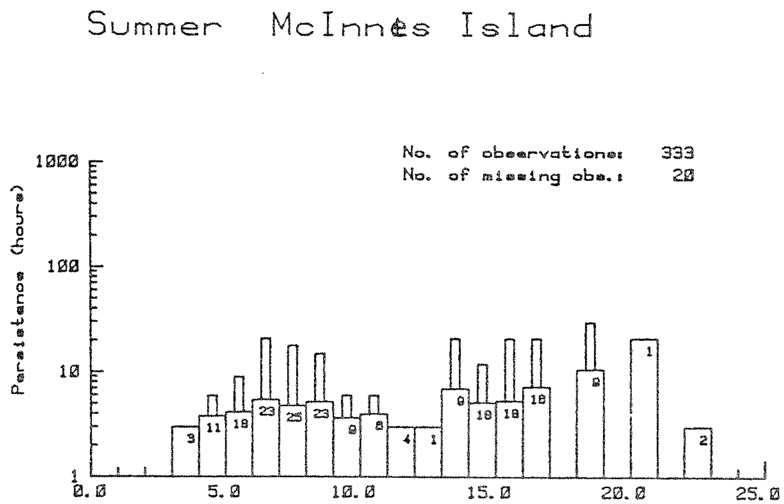

MAXIMUM AND AVERAGE PERSISTENCE OF WAVE PERIOD

Fig. 2.16 continued

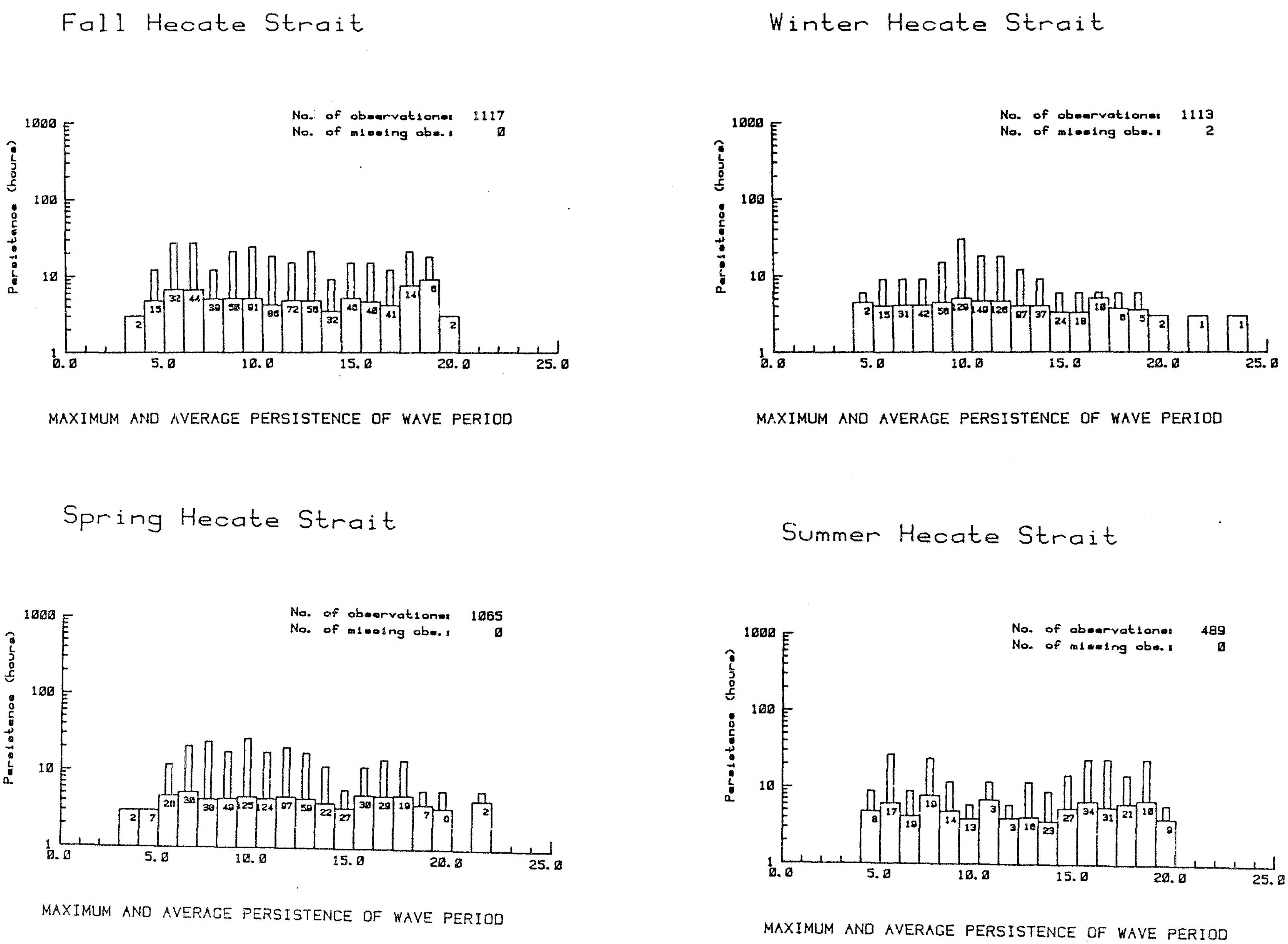

Fig. 2.16 continued

Fall Queen Charlotte Snd.

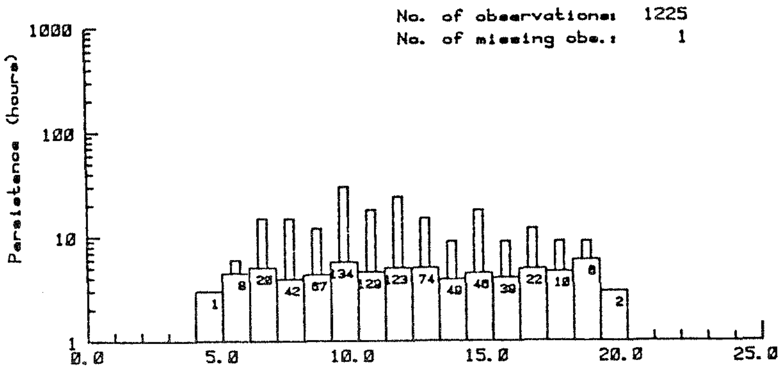

MAXIMUM AND AVERAGE PERSISTENCE OF WAVE PERIOD

Winter Queen Charlotte Snd.

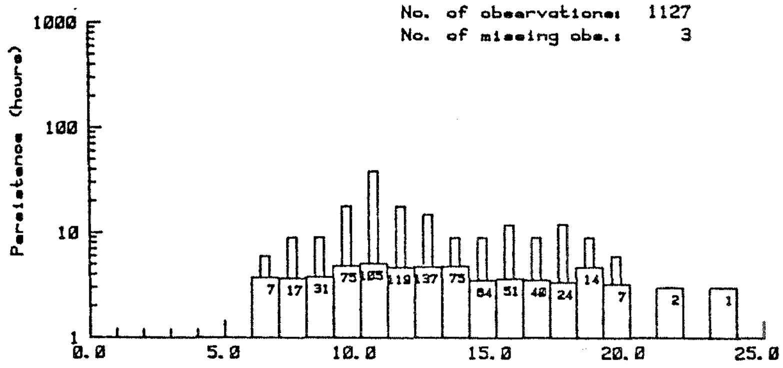

MAXIMUM AND AVERAGE PERSISTENCE OF WAVE PERIOD

Spring Queen Charlotte Snd.

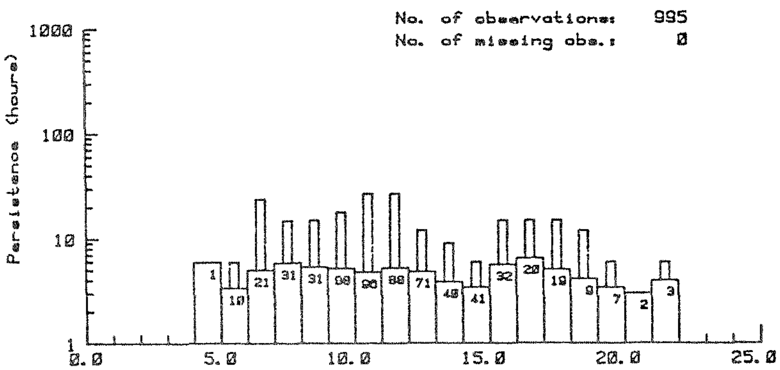

MAXIMUM AND AVERAGE PERSISTENCE OF WAVE PERIOD

Summer Queen Charlotte Snd.

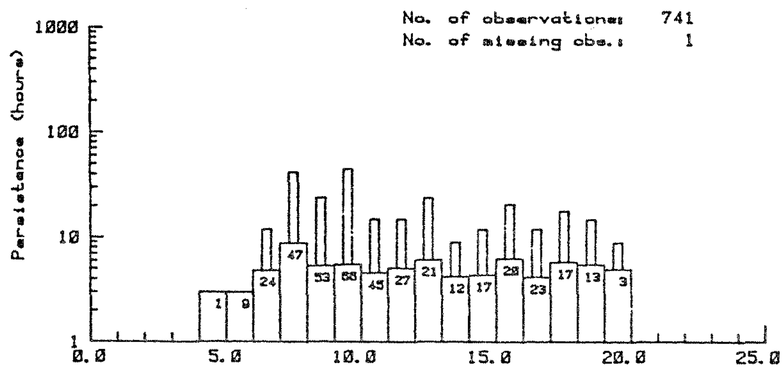

MAXIMUM AND AVERAGE PERSISTENCE OF WAVE PERIOD

Fig. 2.16 continued

1983 Langara West

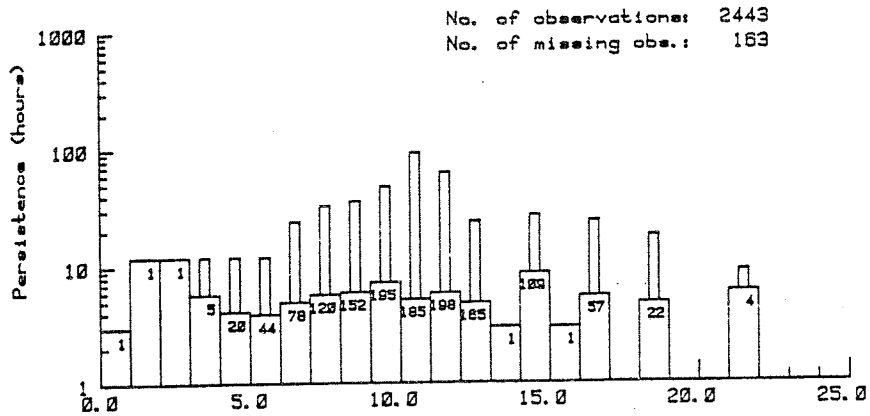

MAXIMUM AND AVERAGE PERSISTENCE OF WAVE PERIOD

1983 Langara East

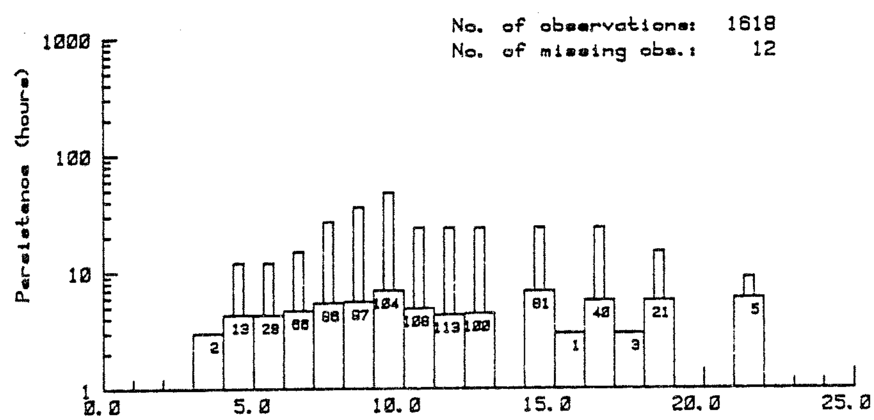

MAXIMUM AND AVERAGE PERSISTENCE OF WAVE PERIOD

Fig. 2.17 Annual persistence statistics, shown as for the seasonal statistics of Fig. 2.16.

1983 Bonilla Island

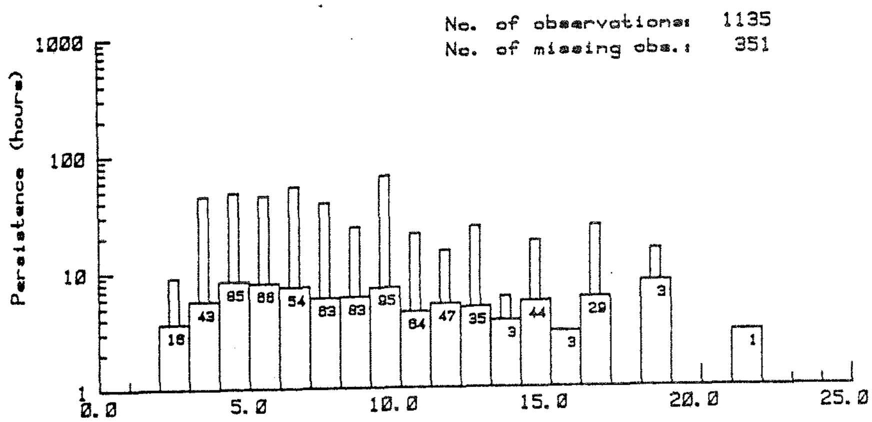

MAXIMUM AND AVERAGE PERSISTENCE OF WAVE PERIOD

1983 McInnes Island

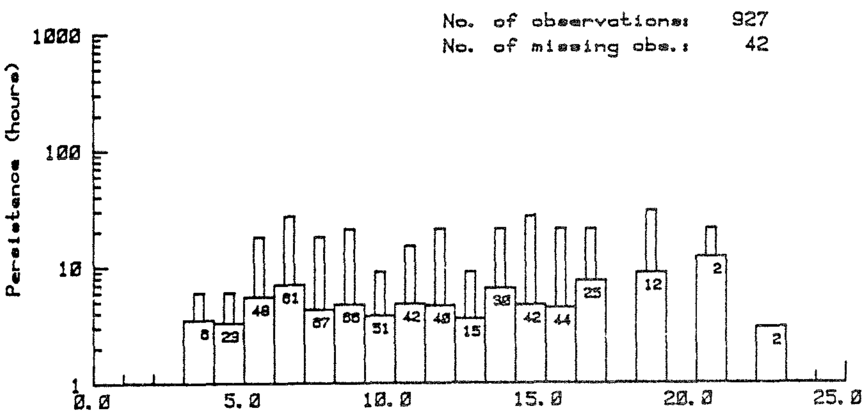

MAXIMUM AND AVERAGE PERSISTENCE OF WAVE PERIOD

Fig. 2.17 continued

1983 Hecate Strait

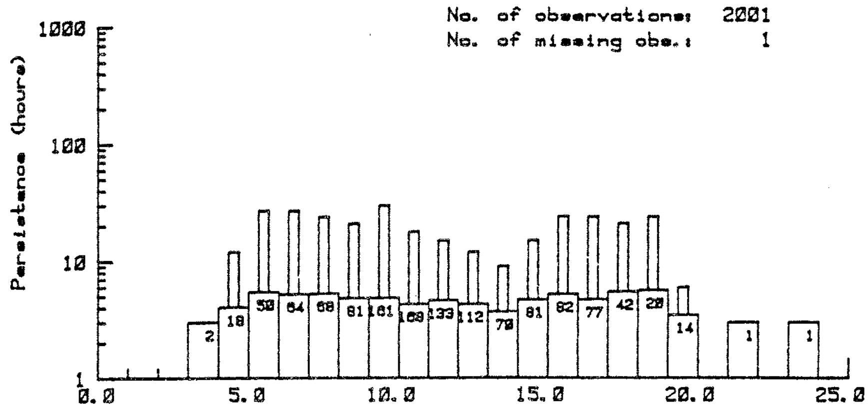

MAXIMUM AND AVERAGE PERSISTENCE OF WAVE PERIOD

1983 Queen Charlotte Snd.

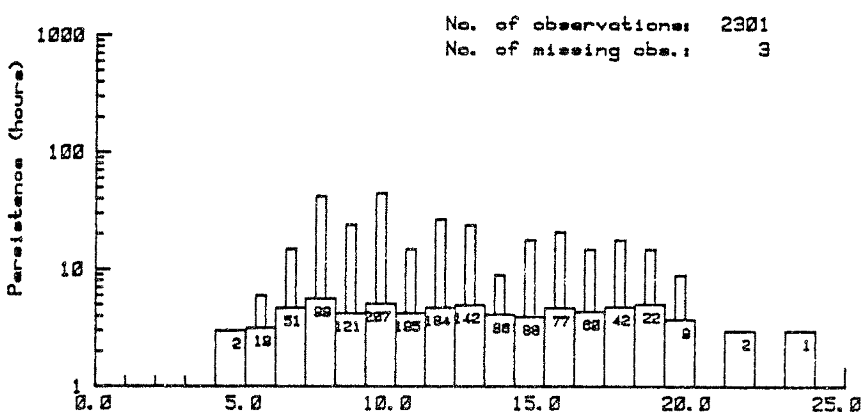

MAXIMUM AND AVERAGE PERSISTENCE OF WAVE PERIOD

Fig. 2.17 continued

Fall McInnes Island

Peak Direction

Peak Period (sec)	N	NNE	NE	ENE	E	ESE	SE	SSE	S	SSW	SW	WSW	W	WNW	NW	NNW	Sum
22																	0
21												1					1
20																	0
19												2					2
18																	0
17									3	3	1	1					8
16									2	13	4	5					24
15									7	15	4	9					35
14									1	7	7	8					23
13										1	3	6					10
12										3	13	24	1				41
11									4	5	9	28					46
10									4	2	6	20					32
9								5	7	5	25	29					71
8								3	8	2	9	15	1	1			39
7								5	8	6	7	3	1	8	4		42
6								8	9	2	1	3	7	5	8		43
5								2	2	1		1	1	2	2		11
4	1									1					2		4
3																	0
2																	0
1																	0
Sum	1	0	0	0	0	0	0	23	55	66	89	155	11	16	16	0	432

Winter McInnes Island

Peak Direction

Peak Period (sec)	N	NNE	NE	ENE	E	ESE	SE	SSE	S	SSW	SW	WSW	W	WNW	NW	NNW	Sum
22																	0
21																	0
20																	0
19											1						1
18																	0
17											4	4					8
16											3	6					9
15											6	5					11
14											7	5					12
13										4	6	4					14
12									4	12	9	3					28
11										1	9	2					12
10								2	1	3	2						8
9								6	6	1				3			16
8								3	4					1			8
7								1	2					1			4
6								2									2
5																	0
4																	0
3																	0
2																	0
1																	0
Sum	0	0	0	0	0	0	0	14	17	21	47	29	0	5	0	0	133

Fig. 2.18 Joint histograms of significant wave height H_s and peak period T_p versus mean wave direction on a seasonal basis.

Spring McInnes Island

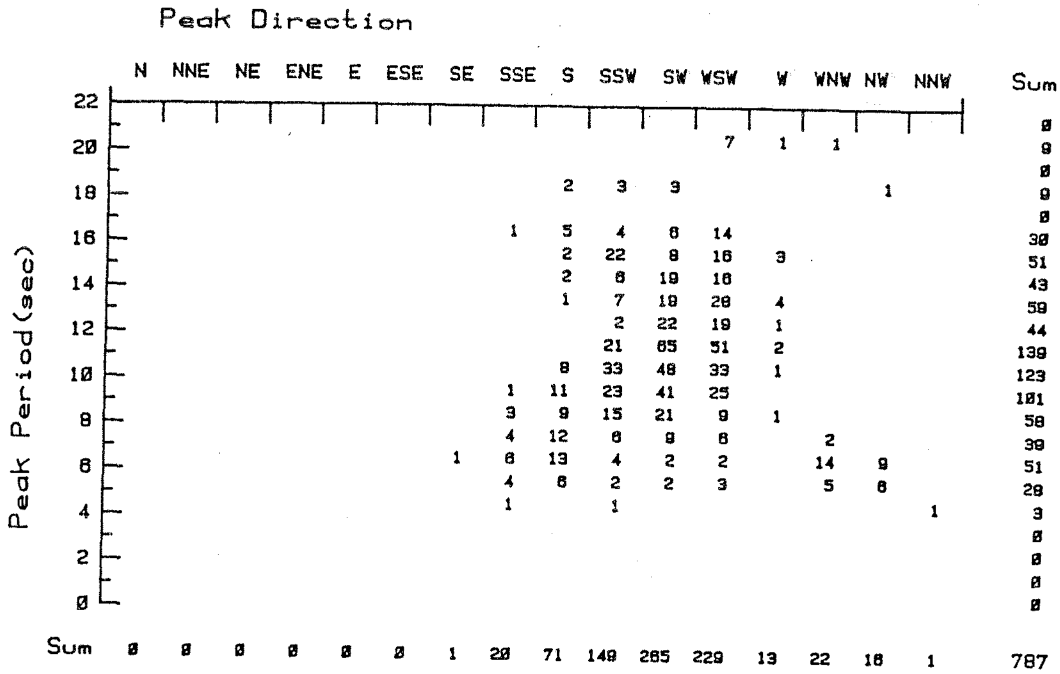

Summer McInnis Island

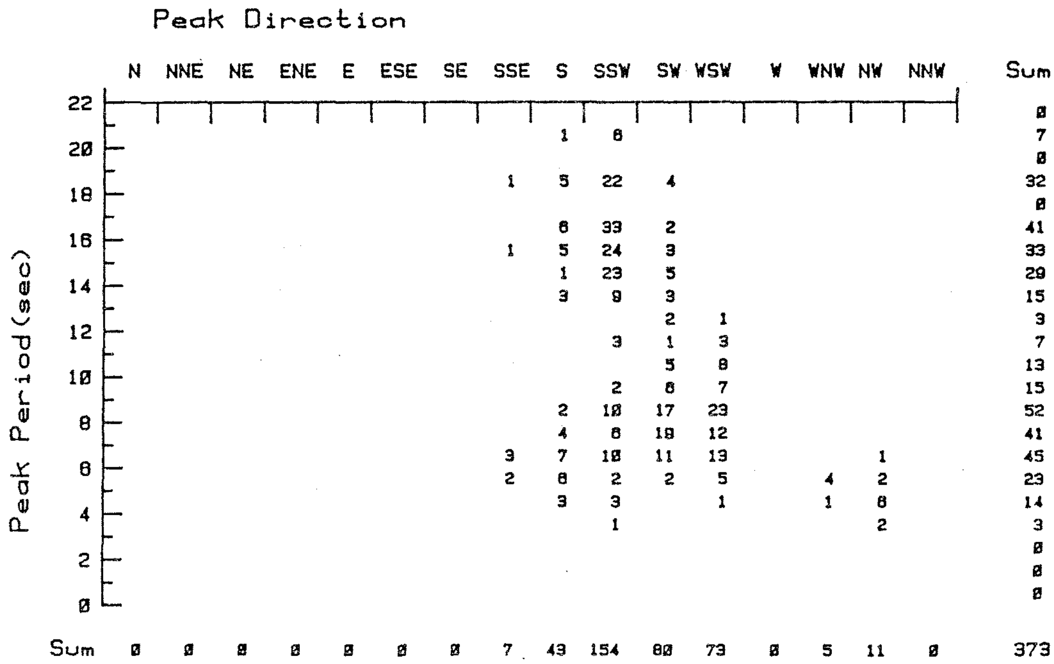

Fig. 2.18 continued

1983 McInnes Island

Peak Direction

Peak Period (sec)	N	NNE	NE	ENE	E	ESE	SE	SSE	S	SSW	SW	WSW	W	WNW	NW	NNW	Sum
22																	0
21									1	6		1					8
20																	0
19								1	7	25	4	2					39
18																	0
17									13	38	4	1					56
16								1	7	47	8	5					68
15									8	41	14	9					72
14									5	21	13	9					48
13										1	8	9					18
12										6	14	43	1				64
11									4	6	18	47					75
10									4	10	18	33					65
9								5	9	20	46	55					135
8								3	13	10	35	31	1	2			95
7								8	18	16	19	18	1	17	11		108
6								11	19	5	5	11	7	9	15		82
5								3	5	5		2	1	3	9		27
4	1									2					4		7
3																	0
2																	0
1																	0
Sum	1	0	0	0	0	0	0	32	113	259	208	276	11	31	38	0	967

1983 McInnes Island

Peak Direction

Sig. Wave Height (m)	N	NNE	NE	ENE	E	ESE	SE	SSE	S	SSW	SW	WSW	W	WNW	NW	NNW	Sum
13																	0
12.5																	0
12																	0
11.5																	0
11																	0
10.5																	0
10																	0
9.5																	0
9																	0
8.5																	0
8																	0
7.5																	0
7								1				2					3
6.5									1								1
6								1									1
5.5								1	1			1					3
5									1		1	1					3
4.5								2	2	2							6
4									7	2	1	2					12
3.5								3	7	8	3	2					23
3								1	10	10	3	12					36
2.5								10	9	7	18	14		4	4		66
2								6	17	26	26	45	3	10	2		135
1.5								6	24	44	63	99	6	15	21		278
1	1							1	34	150	90	97	2	2	11		388
0.5									1	11	1	1					14
Sum	1	0	0	0	0	0	0	32	114	260	208	276	11	31	38	0	969

Fig. 2.19 Joint histograms of significant wave height H_s and peak period T_p versus mean wave direction on an annual basis.

Fall McInnes Island

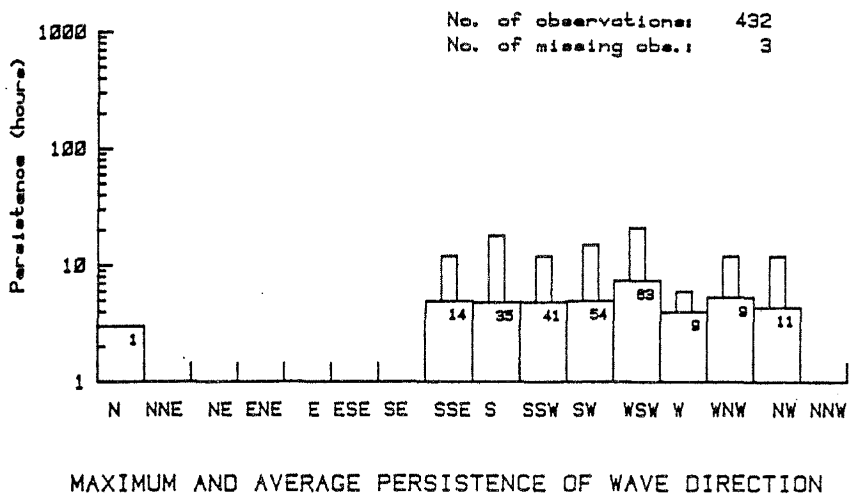

Winter McInnes Island

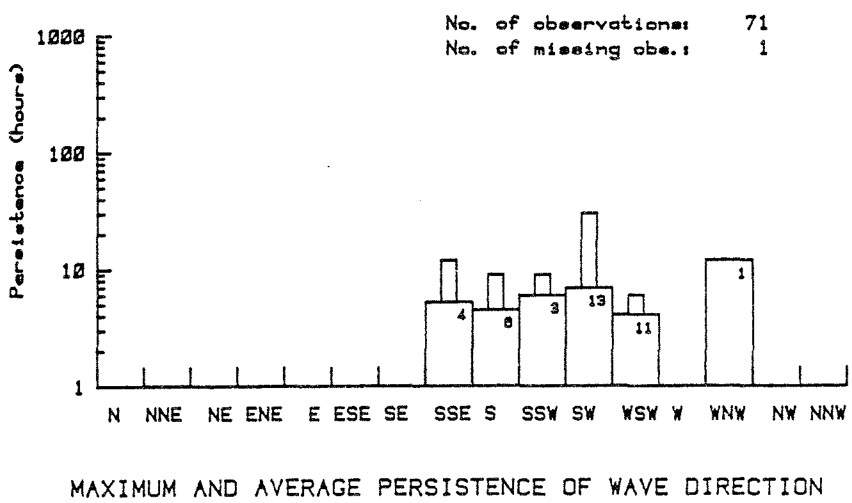

Fig. 2.20 Wave direction persistence diagrams on a seasonal basis.

Spring McInnes Island

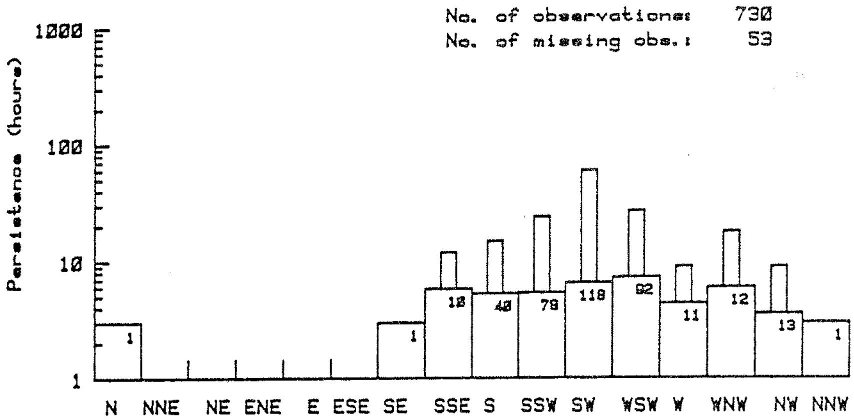

MAXIMUM AND AVERAGE PERSISTENCE OF WAVE DIRECTION

Summer McInnis Island

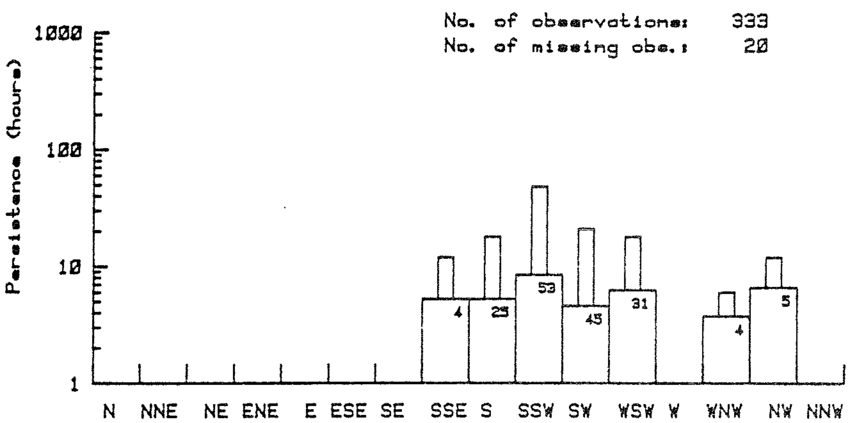

MAXIMUM AND AVERAGE PERSISTENCE OF WAVE DIRECTION

Fig. 2.20 continued

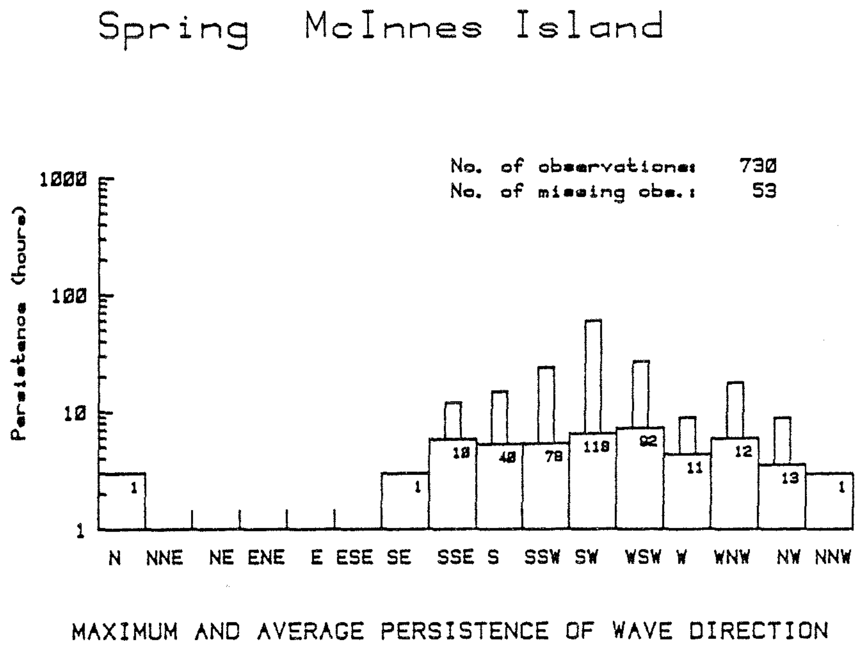

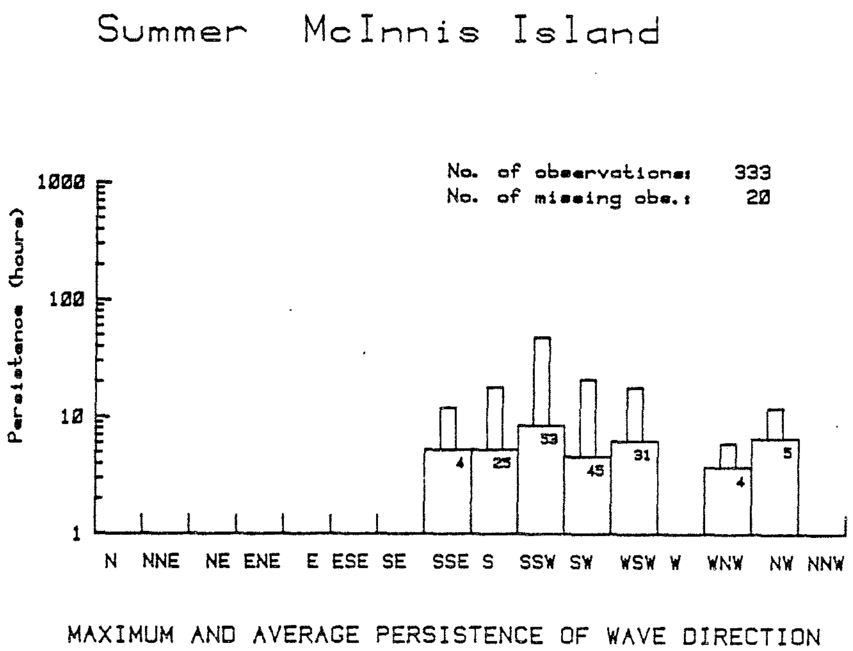

Fig. 2.20 continued

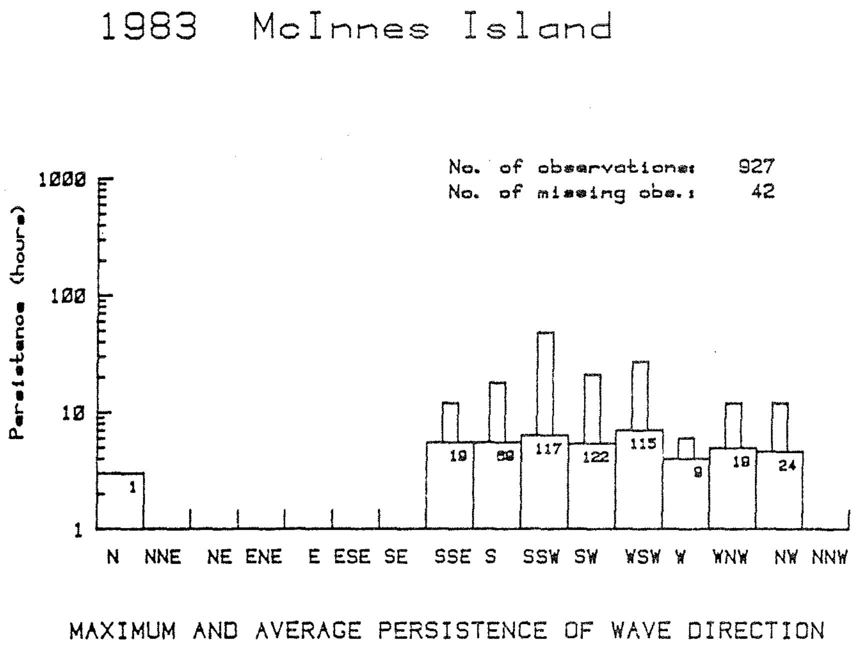

Fig. 2.21 Wave direction persistence diagram on an annual basis.

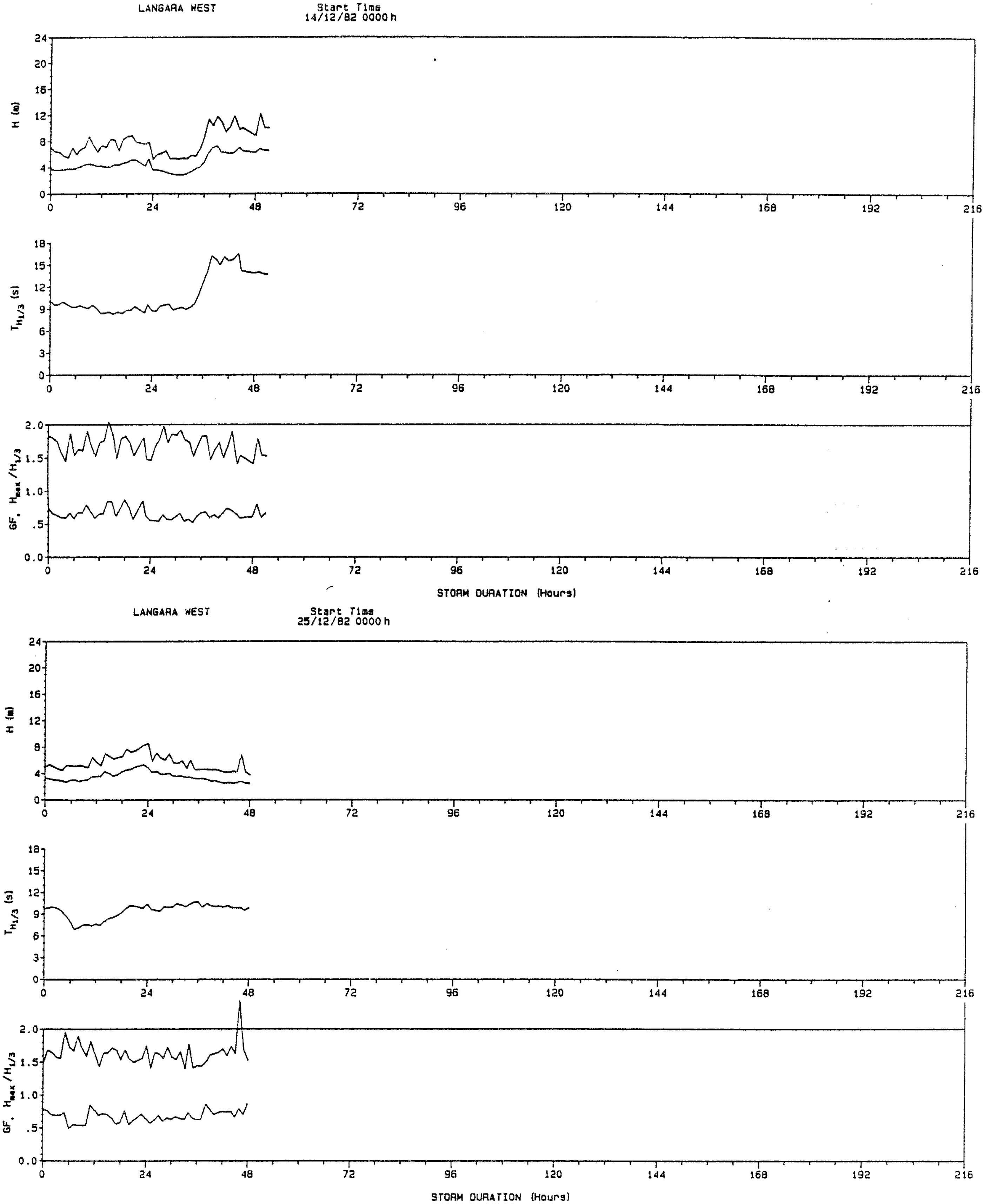

Fig. 2.22 Time series of wave height, ($H_{1/3}$, H_{max}) significant wave period, GF, and the ratio $H_{max}/H_{1/3}$ at Langara West.

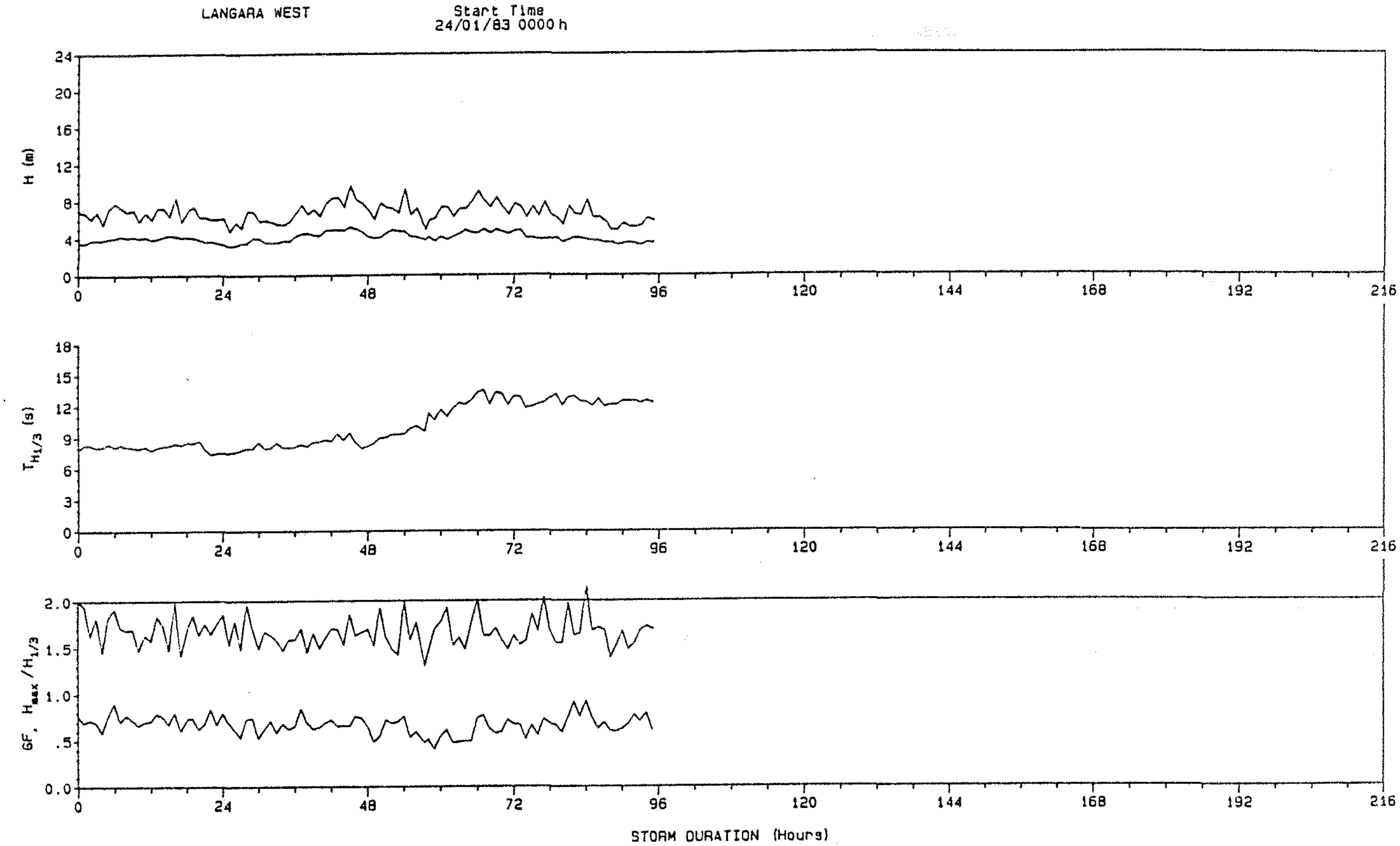

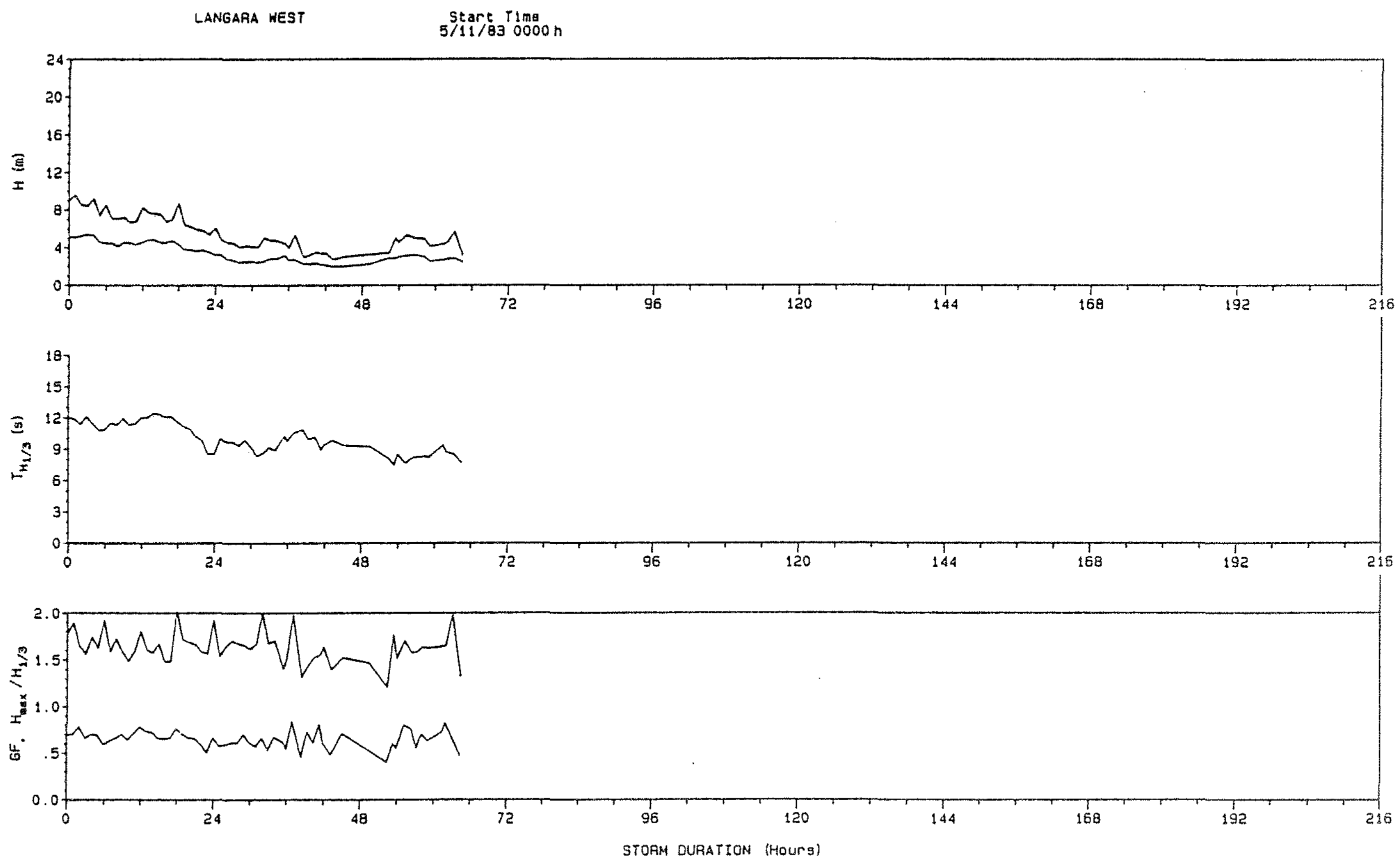

Fig. 2.22 continued

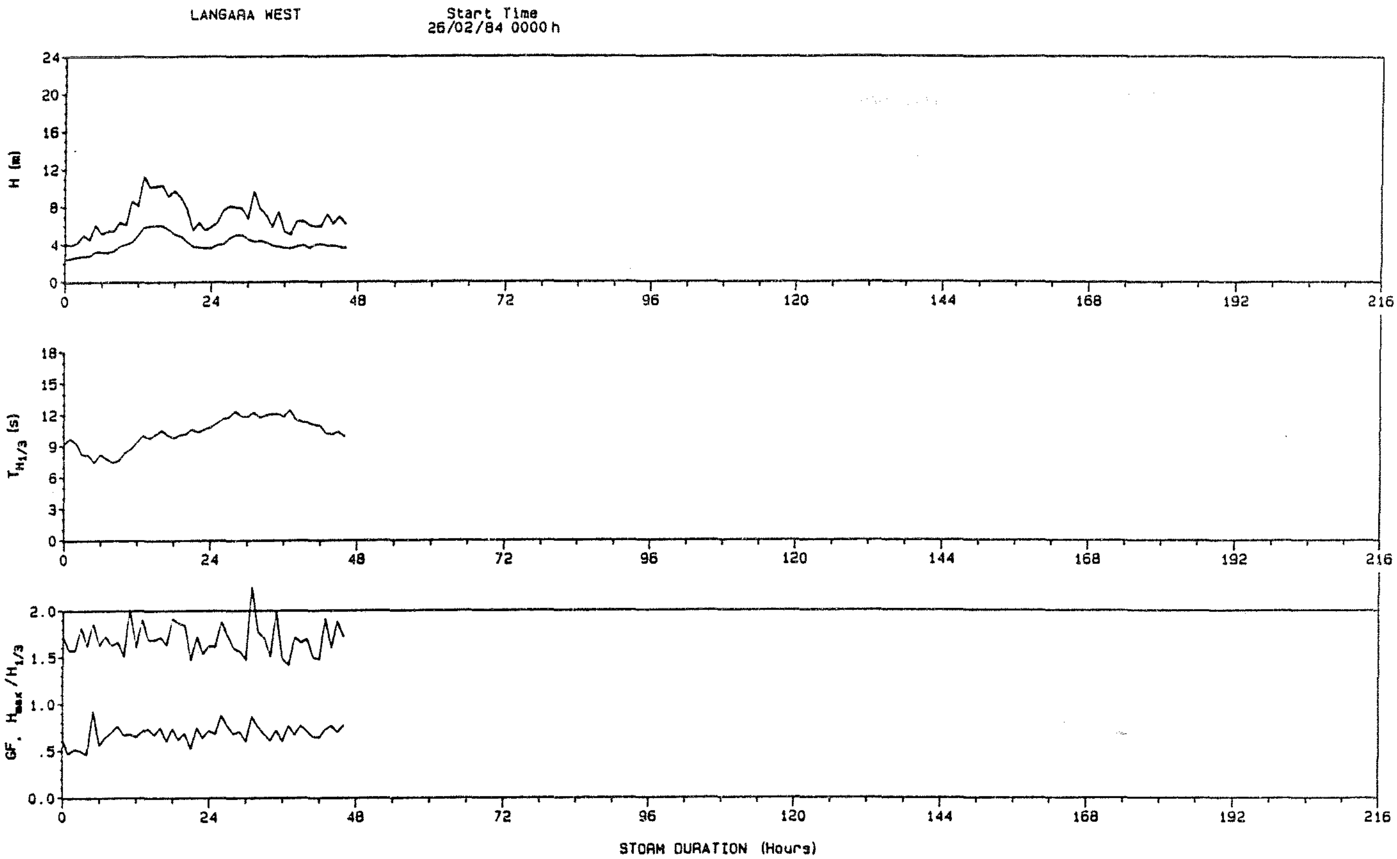

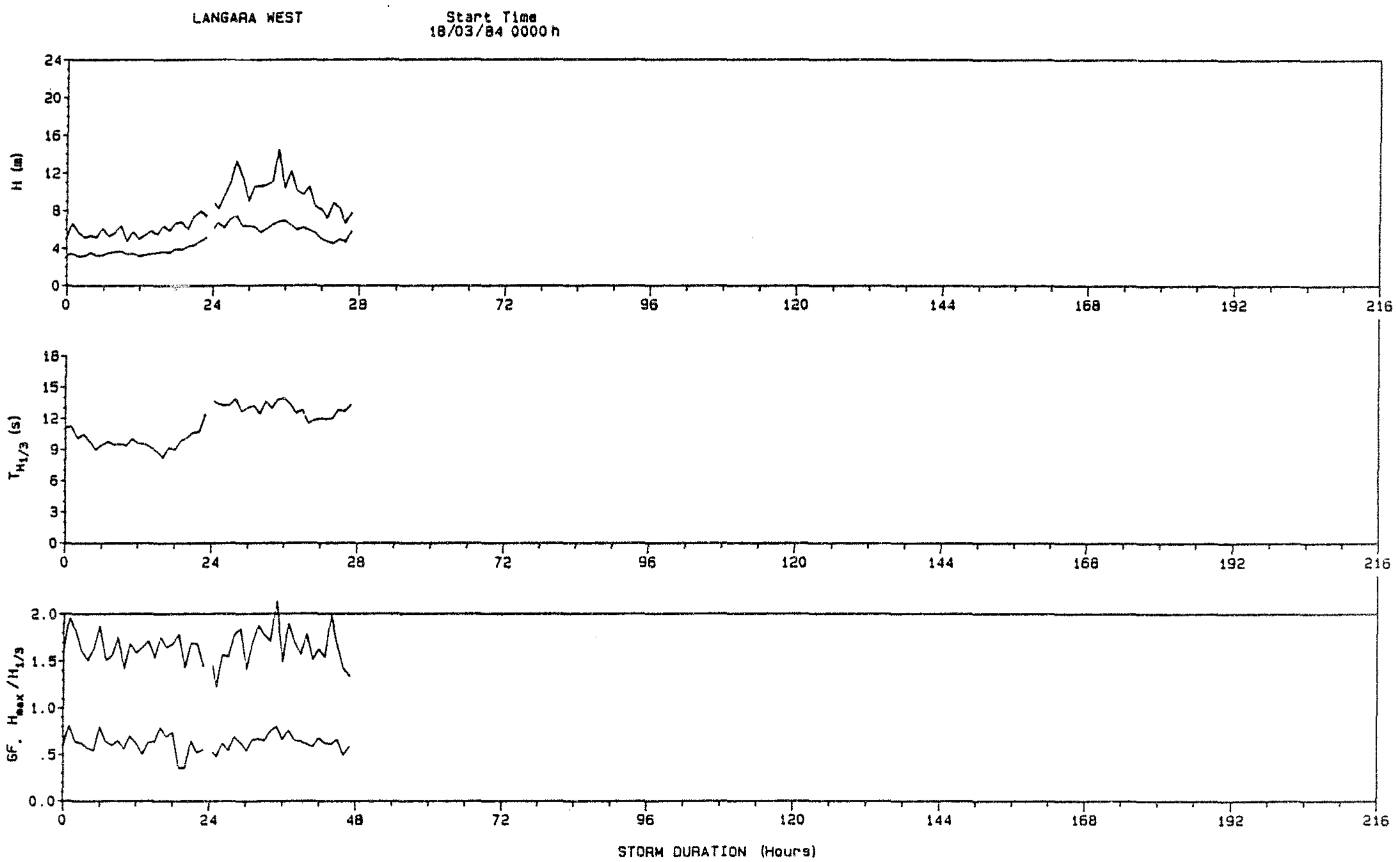

Fig. 2.22 continued

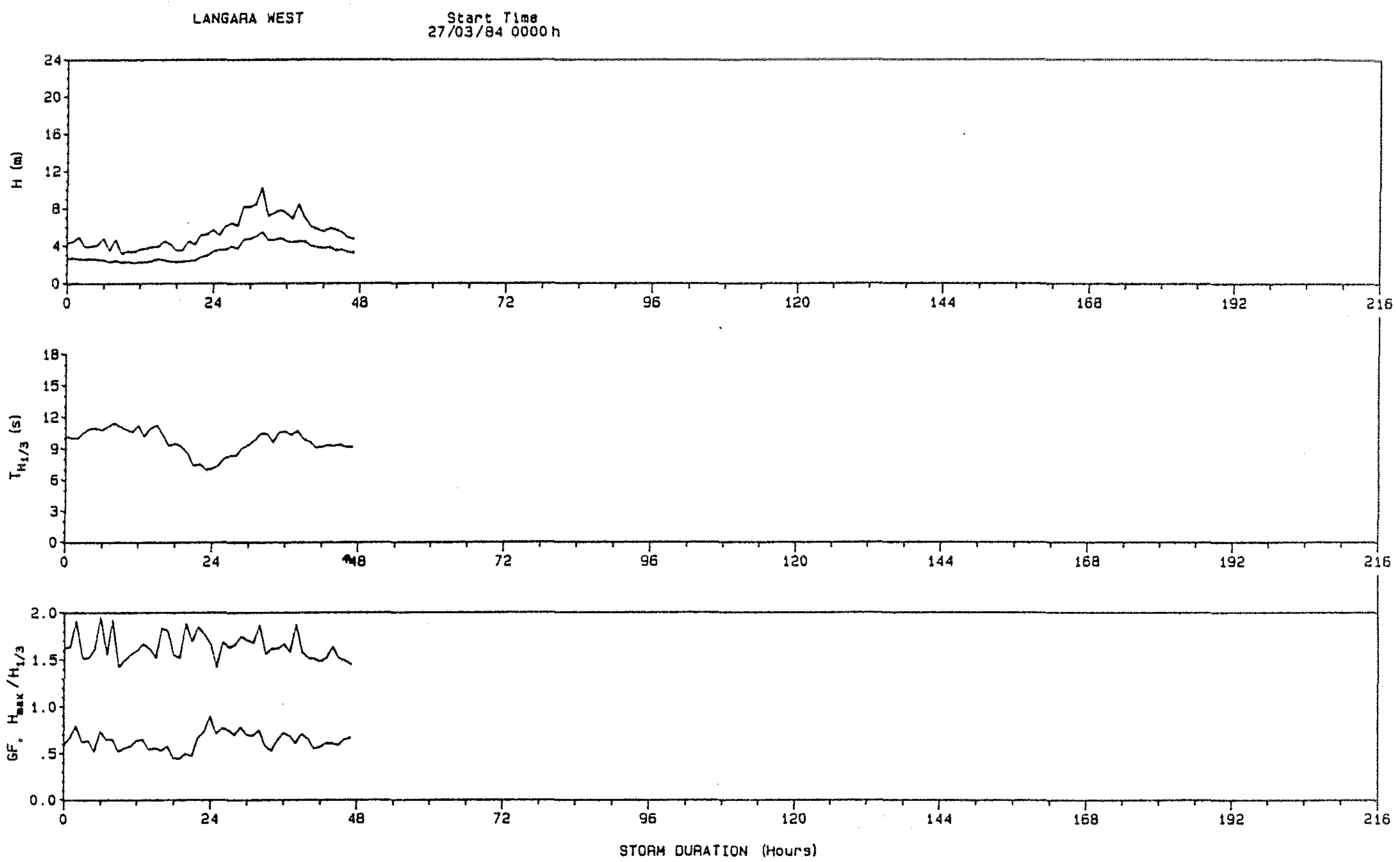

Fig. 2.22 continued

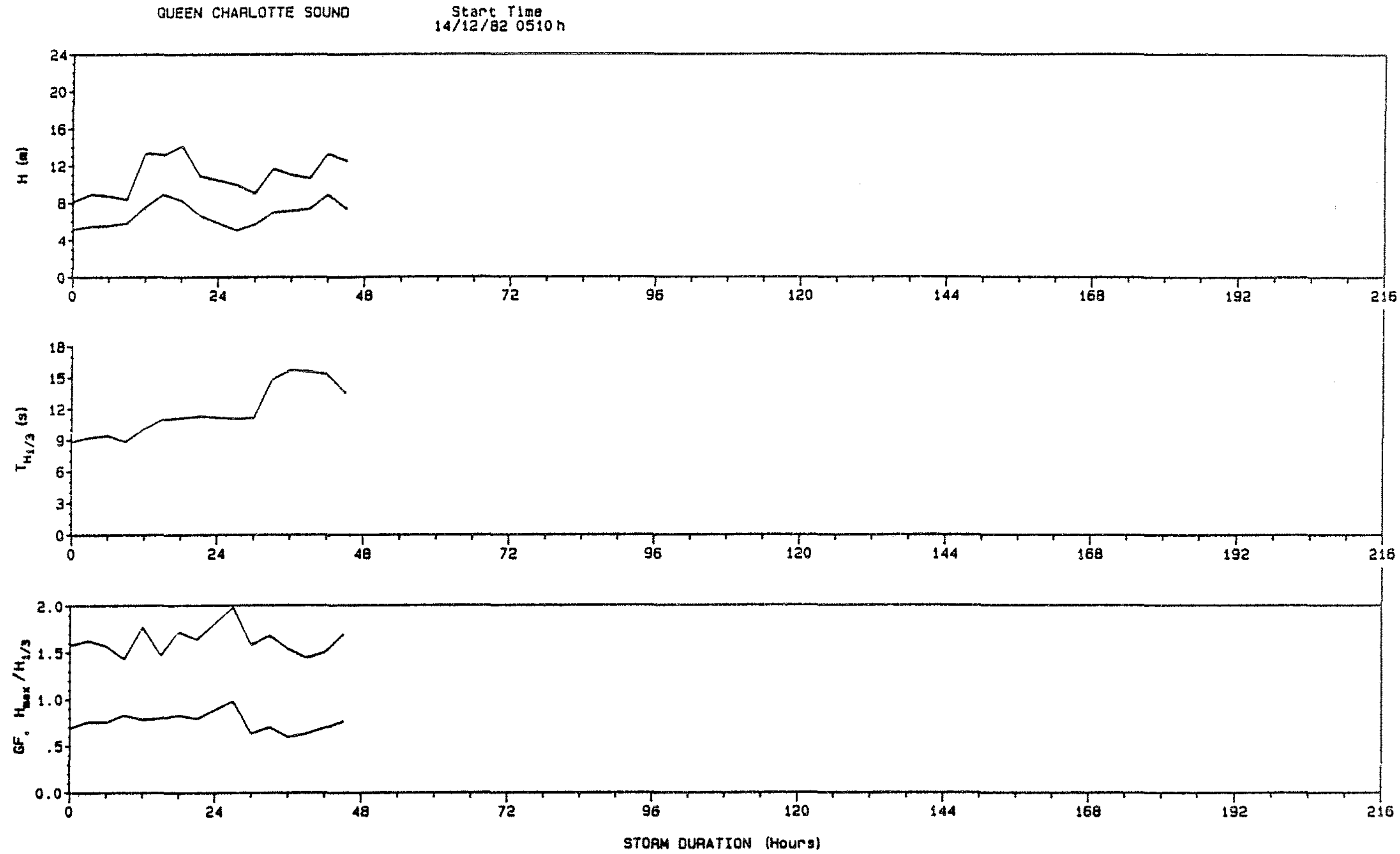

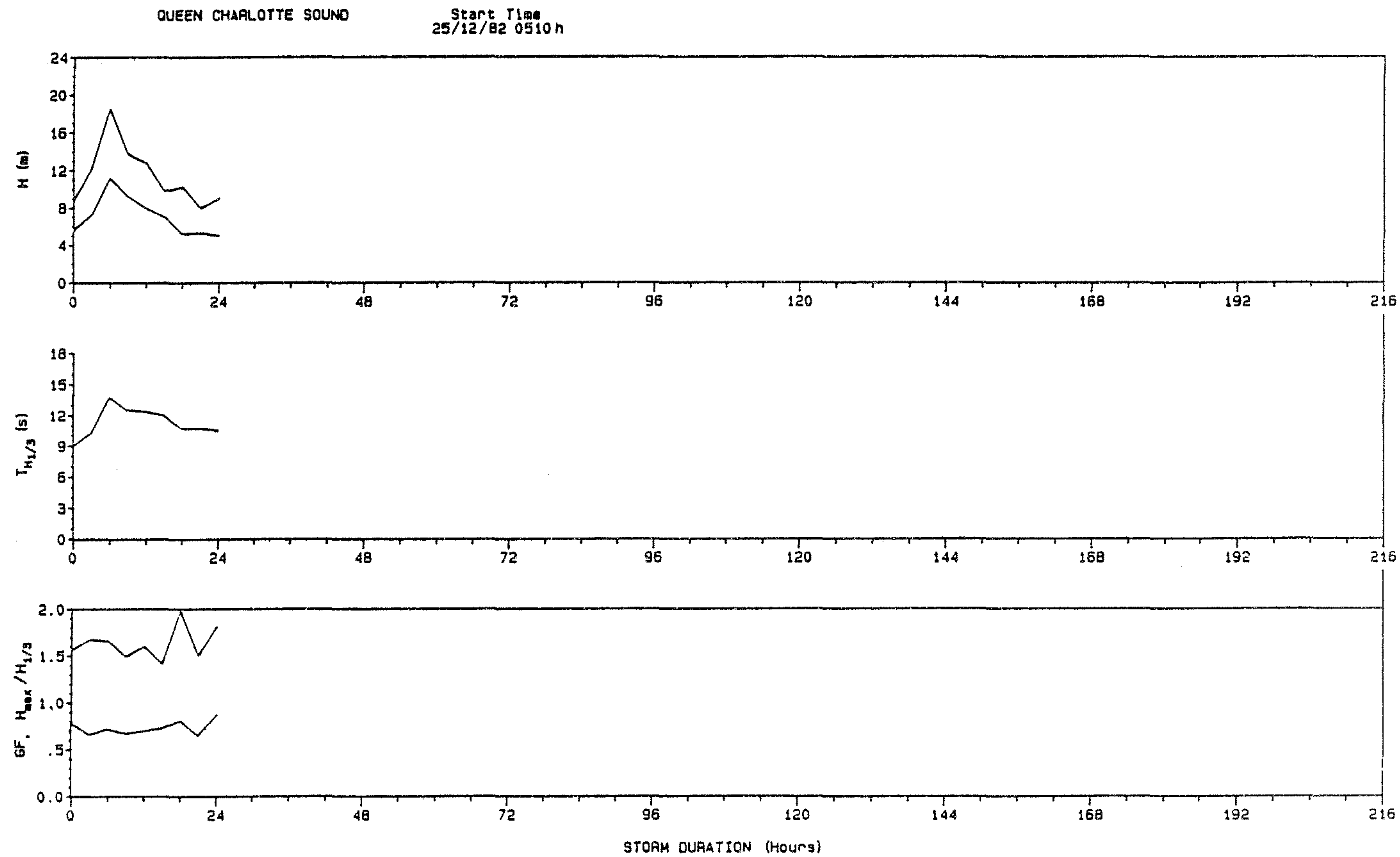

Fig. 2.23 Time series of wave height ($H_{1/3}$, H_{max}) significant wave period, GF, and the ratio $H_{max}/H_{1/3}$ at Queen Charlotte Sound.

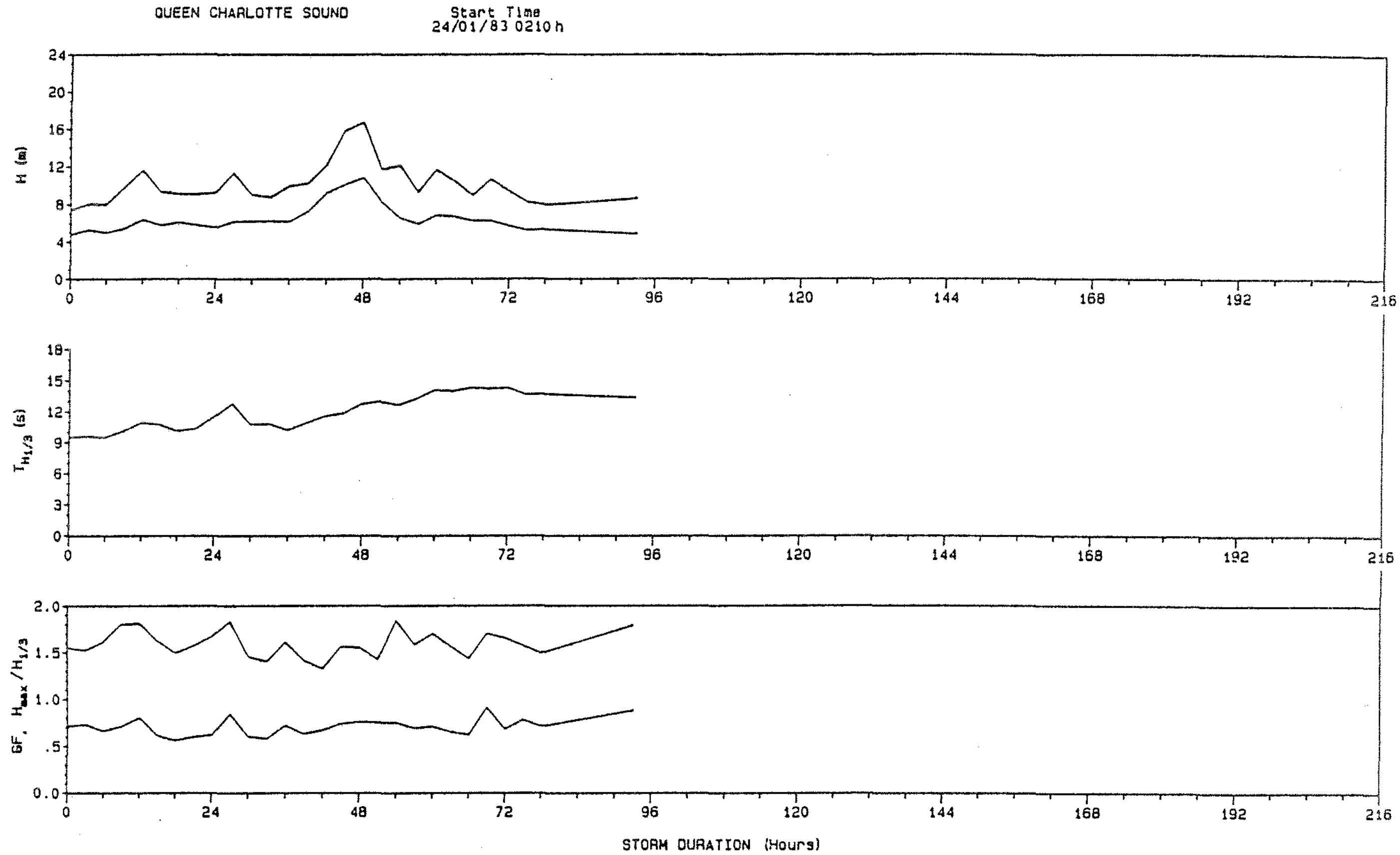

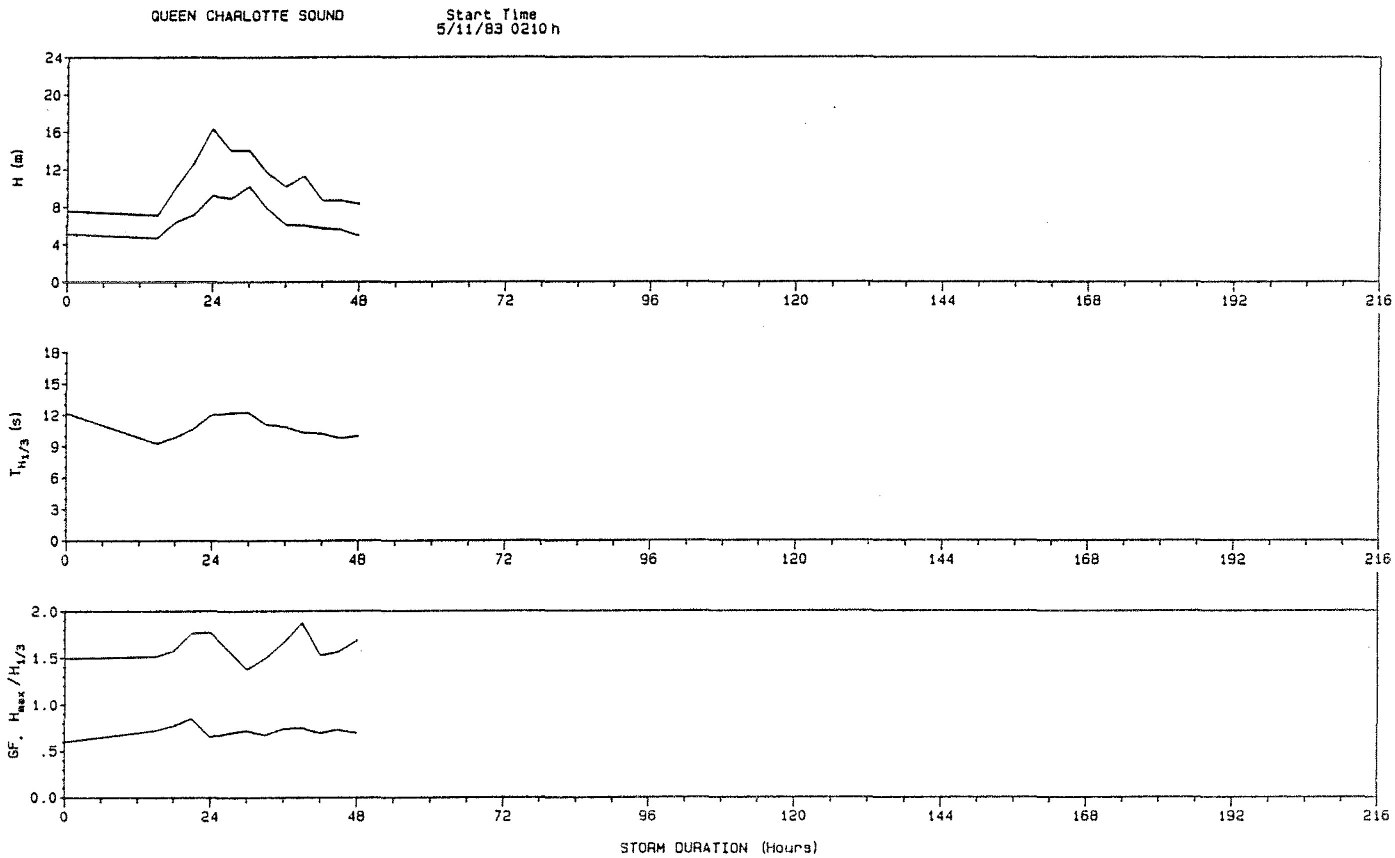

Fig. 2.23 continued

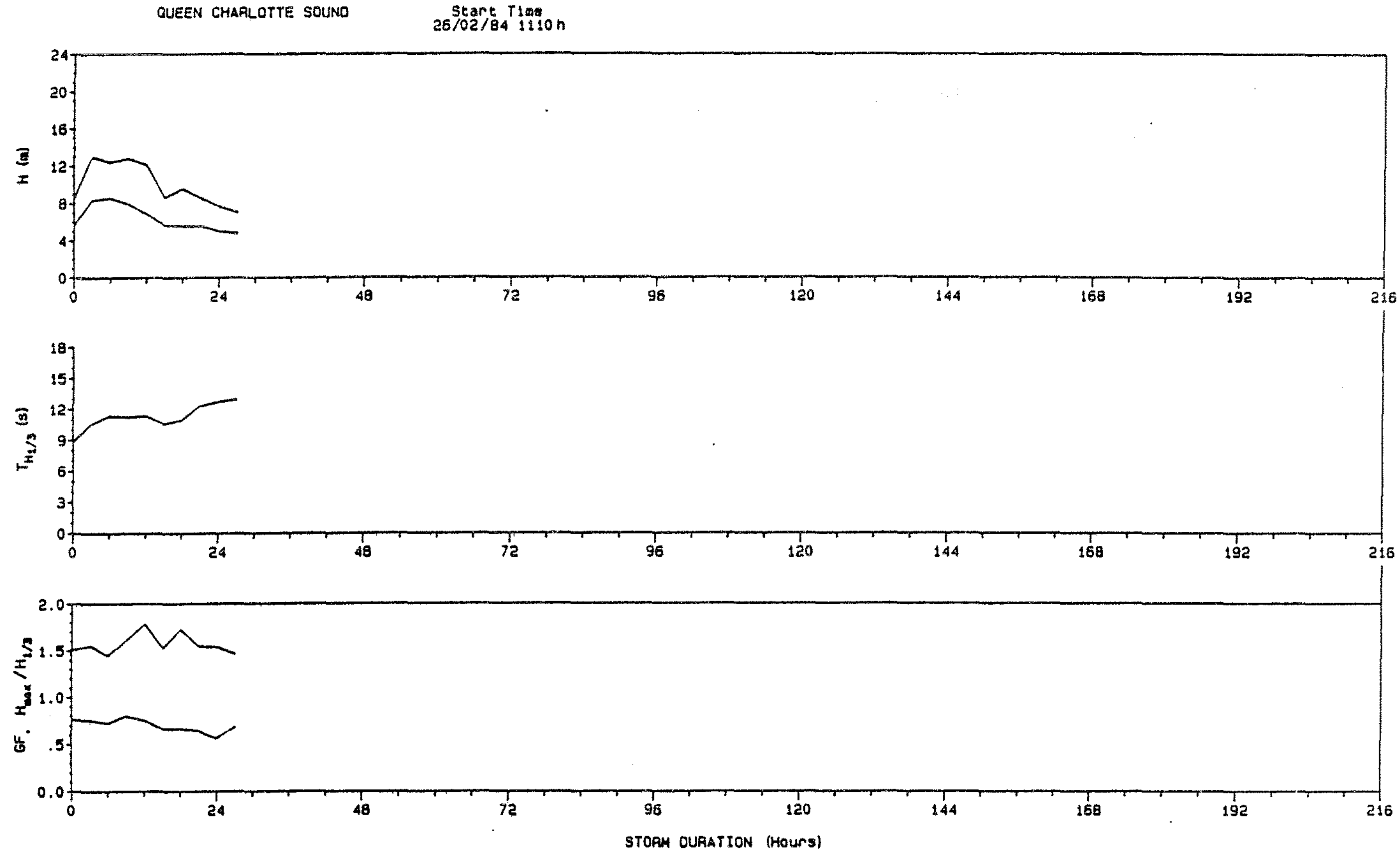

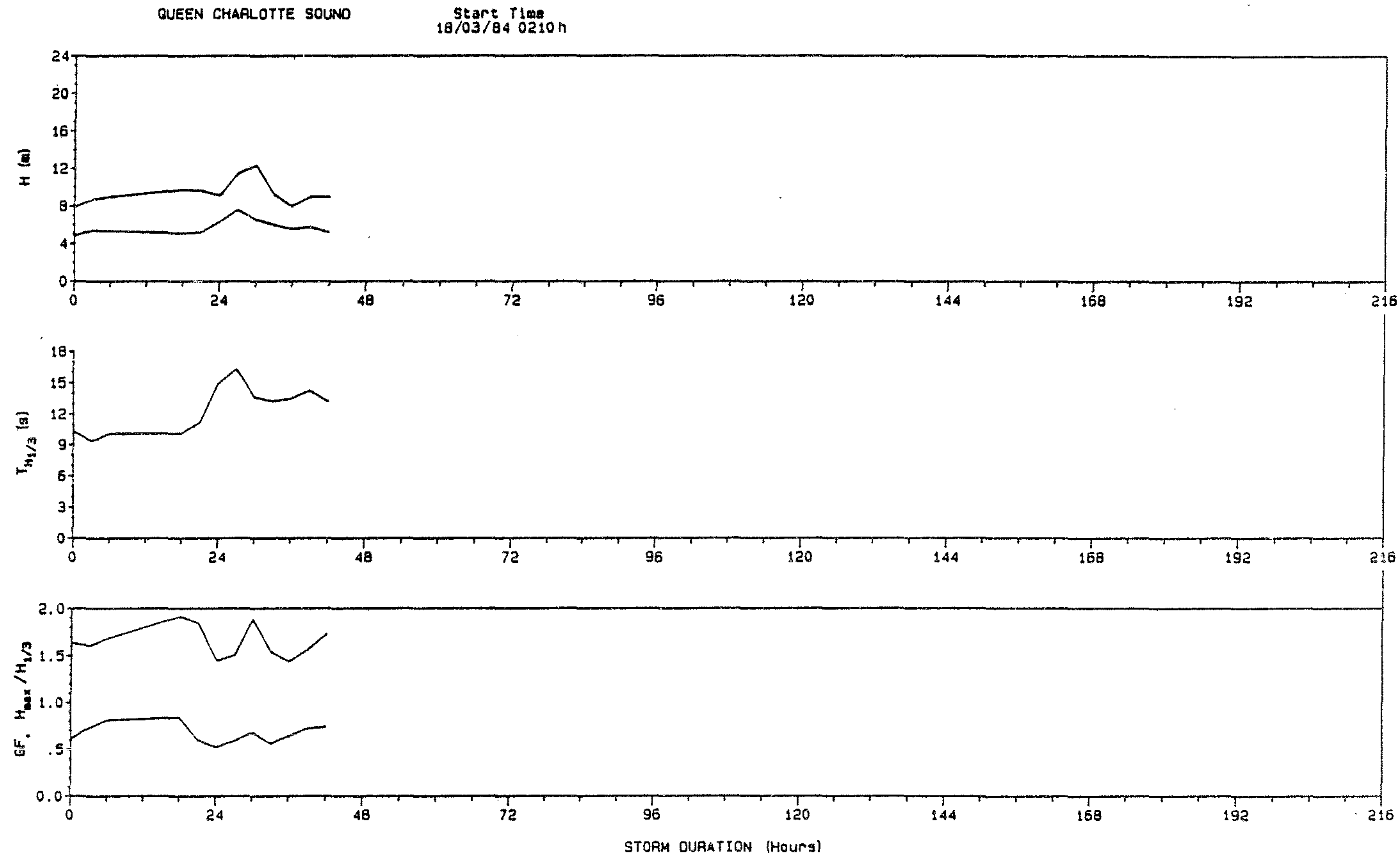

Fig. 2.23 continued

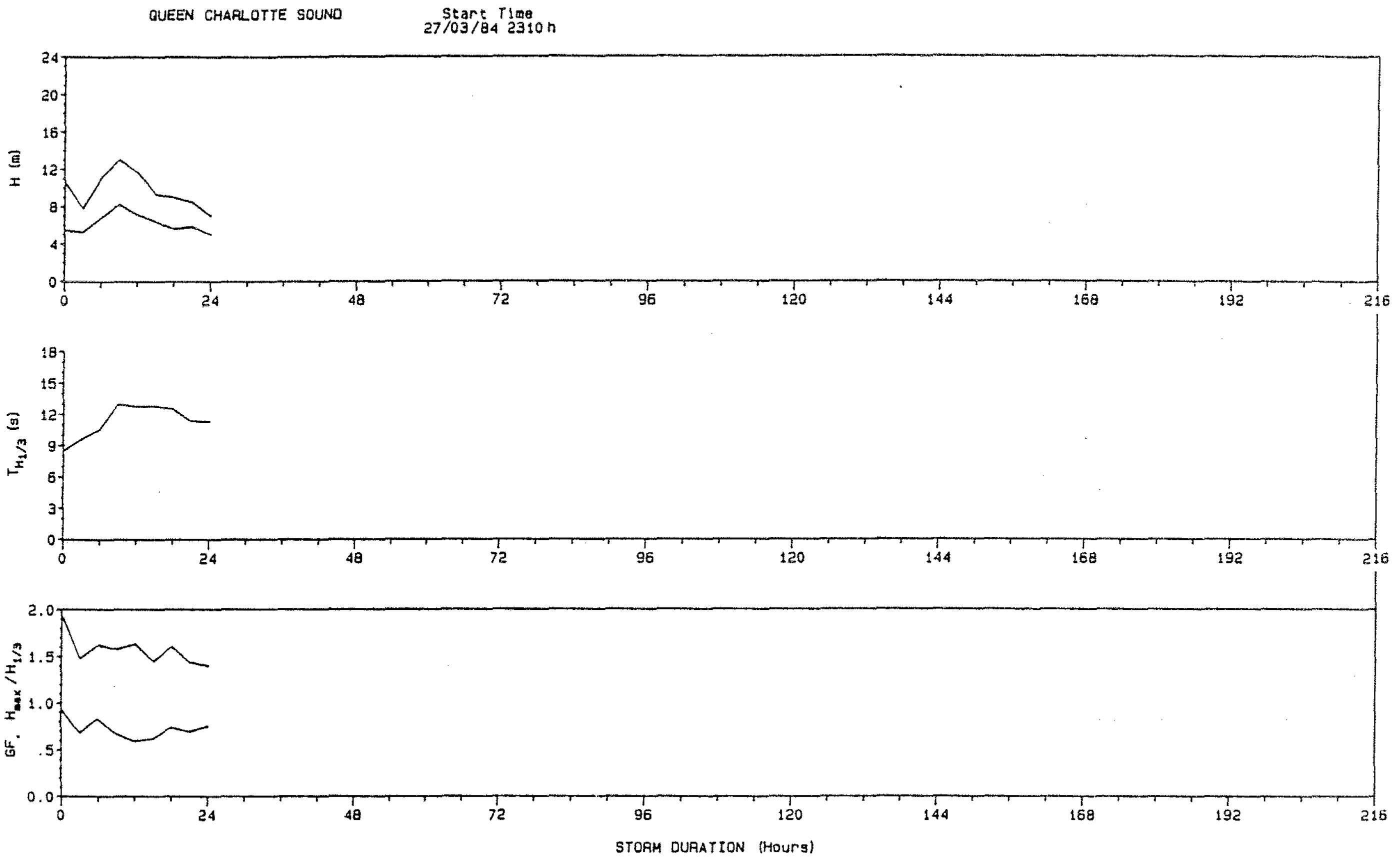

Fig. 2.23 continued

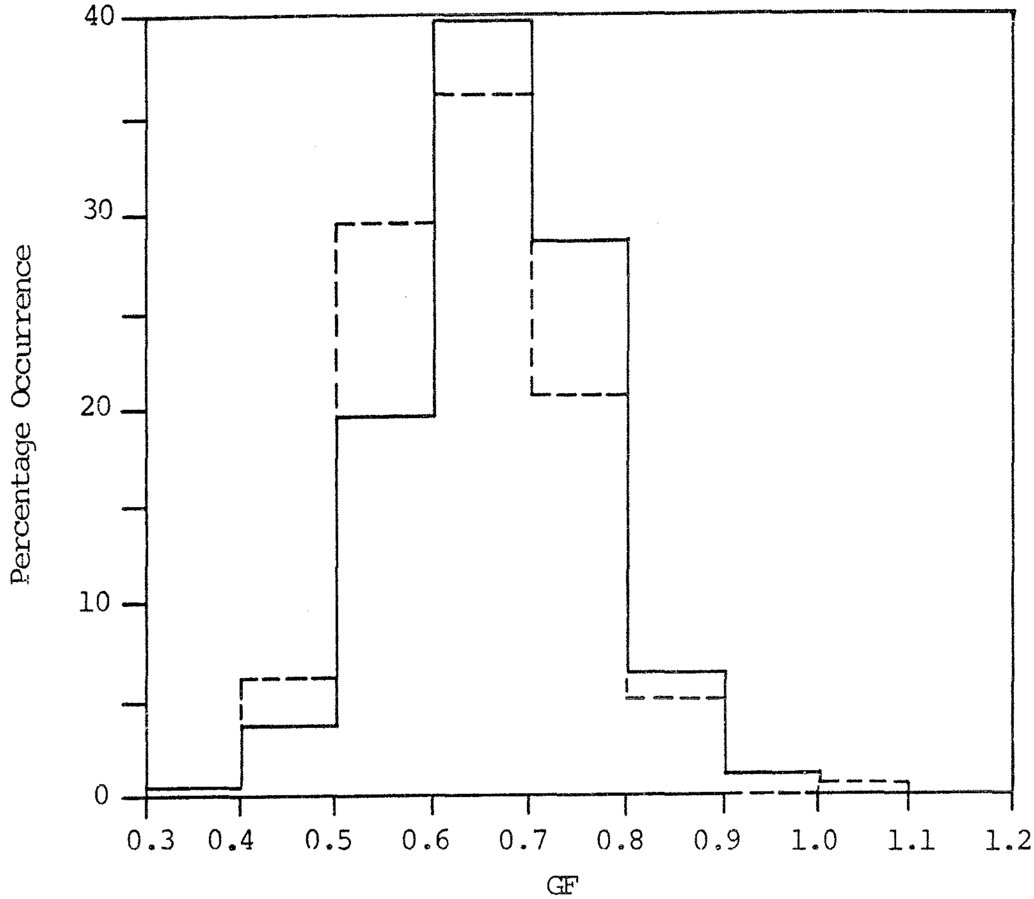

Fig. 2.24 Marginal distribution of the groupiness factor GF at Langara West, Queen Charlotte Sound and Hecate Strait (——) and at McInnes Island (---).

LANGARA WEST, HECATE STRAIT, QUEEN CHARLOTTE SOUND

SIGNIFICANT WAVE HEIGHT vs. GROUPINESS FACTOR

GF	SIGNIFICANT WAVE HEIGHT (m) 0 to 1	1 to 2	2 to 3	3 to 4	4 to 5	5 to 6	6 to 7	7 to 8	8 to 9	9 to 10	10 to 11	11 to 12	NO. OF OBS.	% TOTAL	% EXCEED
.3- .4	0	0	1	2	1	0	0	0	0	0	0	0	4	.7	99.3
.4- .5	0	1	9	4	5	0	1	0	0	0	0	0	20	3.6	95.7
.5- .6	0	1	20	38	20	15	9	5	0	0	0	0	108	19.5	76.2
.6- .7	0	0	30	65	59	28	21	11	3	4	0	0	221	39.9	36.3
.7- .8	0	1	13	38	33	30	22	8	7	1	4	1	158	28.5	7.8
.8- .9	0	0	4	5	12	6	5	1	2	0	0	0	35	6.3	1.4
.9- 1.0	0	0	0	2	1	3	1	1	0	0	0	0	8	1.4	0.0
NO. OF OBS.	0	3	77	154	131	82	59	26	12	5	4	1	554		
% TOTAL	0.0	.5	13.9	27.8	23.6	14.8	10.6	4.7	2.2	.9	.7	.2			
% EXCEED	100.0	99.5	85.6	57.8	34.1	19.3	8.7	4.0	1.8	.9	.2	0.0			

Fig. 2.25 Joint frequency histogram of GF and $H_{1/3}$ for Langara West, Queen Charlotte and Hecate Strait.

LANGARA WEST, HECATE STRAIT, QUEEN CHARLOTTE SOUND

Hmax:H1/3 vs. GROUPINESS FACTOR

GF \ Hmax:H1/3	1.0 to 1.1	1.1 to 1.2	1.2 to 1.3	1.3 to 1.4	1.4 to 1.5	1.5 to 1.6	1.6 to 1.7	1.7 to 1.8	1.8 to 1.9	1.9 to 2.0	2.0 to 2.1	2.1 to 2.2	2.2 to 2.3	2.3 to 2.4	2.4 to 2.5	NO. OF OBS.	% TOTAL	% EXCEED
.3- .4	0	0	1	0	1	0	1	1	0	0	0	0	0	0	0	4	.7	99.3
.4- .5	0	0	2	3	2	5	4	2	2	0	0	0	0	0	0	20	3.6	95.7
.5- .6	0	0	0	5	27	41	17	11	5	2	0	0	0	0	0	108	19.5	76.2
.6- .7	0	0	0	3	41	53	66	29	18	9	1	0	0	1	0	221	39.9	36.3
.7- .8	0	0	0	3	15	32	45	28	17	13	3	1	0	0	1	158	28.5	7.8
.8- .9	0	0	0	0	1	5	5	8	7	7	1	0	1	0	0	35	6.3	1.4
.9- 1.0	0	0	0	0	0	0	2	0	3	2	0	1	0	0	0	8	1.4	0.0
NO. OF OBS.	0	0	3	14	87	136	140	79	52	33	5	2	1	1	1	554		
% TOTAL	0.0	0.0	.5	2.5	15.7	24.5	25.3	14.3	9.4	6.0	.9	.4	.2	.2	.2			
% EXCEED	100.0	100.0	99.5	96.9	81.2	56.7	31.4	17.1	7.8	1.8	.9	.5	.4	.2	0.0			

Fig. 2.26 Joint frequency distribution of $H_{max}/H_{1/3}$ and GF for Langara West, Queen Charlotte and Hecate Strait.

LANGARA WEST, HECATE STRAIT, QUEEN CHARLOTTE SOUND

Hmax:H1/3 vs. SIGNIFICANT WAVE HEIGHT

H1/3 (m) \ Hmax:H1/3	1.0 to 1.1	1.1 to 1.2	1.2 to 1.3	1.3 to 1.4	1.4 to 1.5	1.5 to 1.6	1.6 to 1.7	1.7 to 1.8	1.8 to 1.9	1.9 to 2.0	2.0 to 2.1	2.1 to 2.2	2.2 to 2.3	2.3 to 2.4	2.4 to 2.5	NO. OF OBS.	% TOTAL	% EXCEED
0.0- .5	0	0	0	0	0	0	0	0	0	0	0	0	0	0	0	0	0.0	100.0
.5- 1.0	0	0	0	0	0	0	0	0	0	0	0	0	0	0	0	0	0.0	100.0
1.0- 1.5	0	0	0	0	0	0	0	0	0	0	0	0	0	0	0	0	0.0	100.0
1.5- 2.0	0	0	0	1	0	1	1	0	0	0	0	0	0	0	0	3	.5	99.5
2.0- 2.5	0	0	0	2	5	11	8	2	3	2	0	0	0	1	0	34	6.1	93.3
2.5- 3.0	0	0	1	0	0	9	16	5	5	6	0	0	0	0	1	43	7.8	85.6
3.0- 3.5	0	0	0	1	9	12	16	11	4	5	0	0	0	0	0	58	10.5	75.1
3.5- 4.0	0	0	1	1	13	25	28	13	8	5	1	1	0	0	0	96	17.3	57.8
4.0- 4.5	0	0	0	0	11	10	18	12	6	5	3	0	1	0	0	66	11.9	45.8
4.5- 5.0	0	0	0	1	11	15	19	10	5	3	1	0	0	0	0	65	11.7	34.1
5.0- 5.5	0	0	0	1	7	13	7	5	6	5	0	0	0	0	0	44	7.9	26.2
5.5- 6.0	0	0	0	2	6	16	6	5	2	1	0	0	0	0	0	38	6.9	19.3
6.0- 6.5	0	0	0	1	12	6	7	4	8	0	0	0	0	0	0	39	6.9	12.5
6.5- 7.0	0	0	1	0	3	5	5	4	2	0	0	1	0	0	0	21	3.8	8.7
7.0- 7.5	0	0	0	2	3	4	5	3	0	0	0	0	0	0	0	17	3.1	5.6
7.5- 8.0	0	0	0	0	2	2	2	2	1	0	0	0	0	0	0	9	1.6	4.0
8.0- 8.5	0	0	0	0	1	2	1	1	1	0	0	0	0	0	0	6	1.1	2.9
8.5- 9.0	0	0	0	0	3	2	0	0	0	1	0	0	0	0	0	6	1.1	1.8
9.0- 9.5	0	0	0	1	1	0	0	2	1	0	0	0	0	0	0	5	.9	.9
9.5-10.0	0	0	0	0	0	0	0	0	0	0	0	0	0	0	0	0	0 0	.9
10.0-10.5	0	0	0	1	0	1	0	0	0	0	0	0	0	0	0	2	.4	.5
10.5-11.0	0	0	0	0	0	2	0	0	0	0	0	0	0	0	0	2	.4	.2
11.0-11.5	0	0	0	0	0	0	1	0	0	0	0	0	0	0	0	1	.2	0.0
NO. OF OBS.	0	0	3	14	87	136	140	79	52	33	5	2	1	1	1	554		
% TOTAL	0.0	0.0	.5	2.5	15.7	24.5	25.3	14.3	9.4	6.0	.9	.4	.2	.2	.2			
% EXCEED	100.0	100.0	99.5	96.9	81.2	56.7	31.4	17.1	7.8	1.8	.9	.5	.4	.2	0.0			

Fig. 2.27 Joint frequency distribution of $H_{1/3}$ and $H_{max}/H_{1/3}$ for Langara West, Queen Charlotte Sound and Hecate Strait.

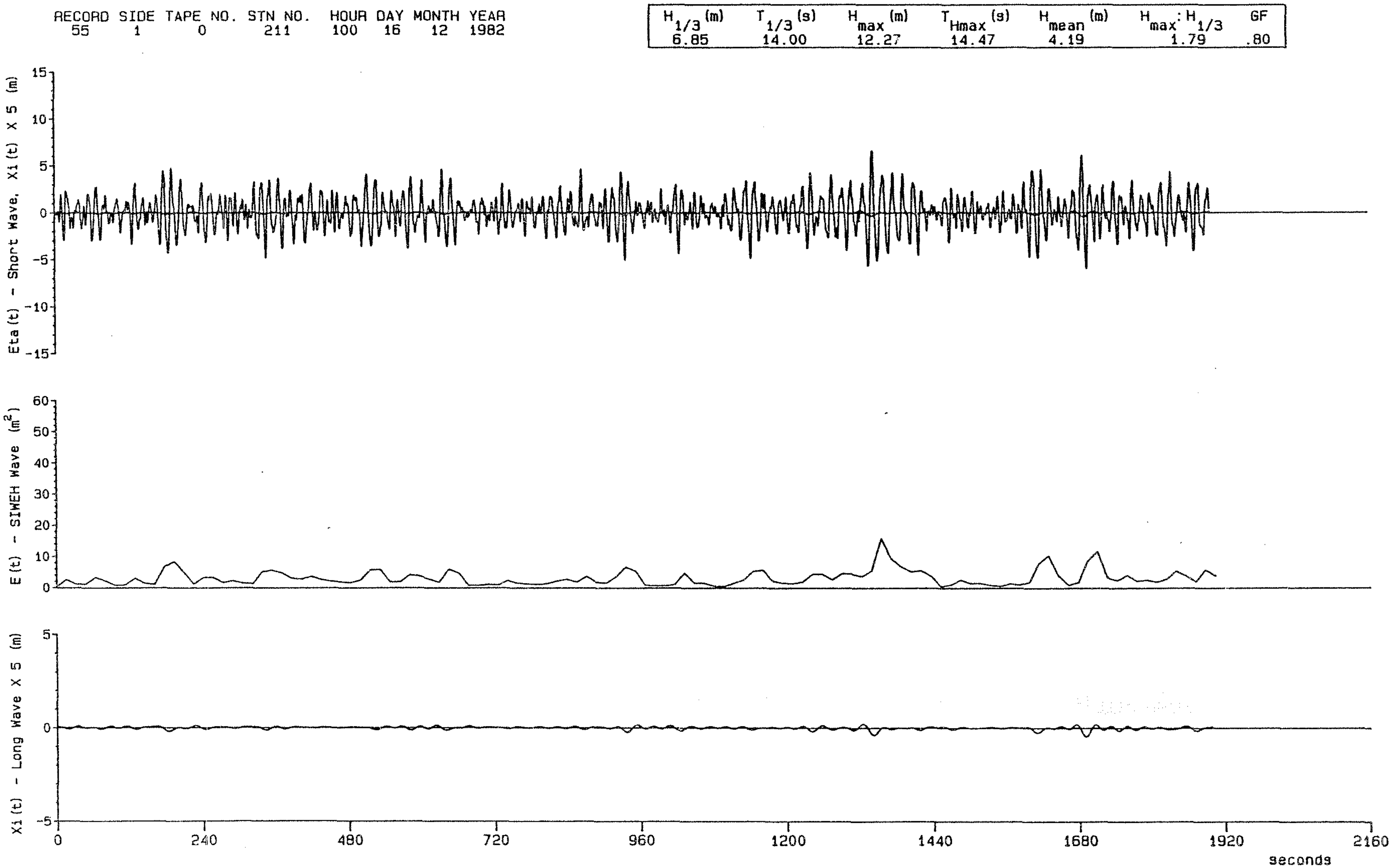

Fig. 2.28 Selected wave trace histories, showing the SIWEH and bound long wave functions.

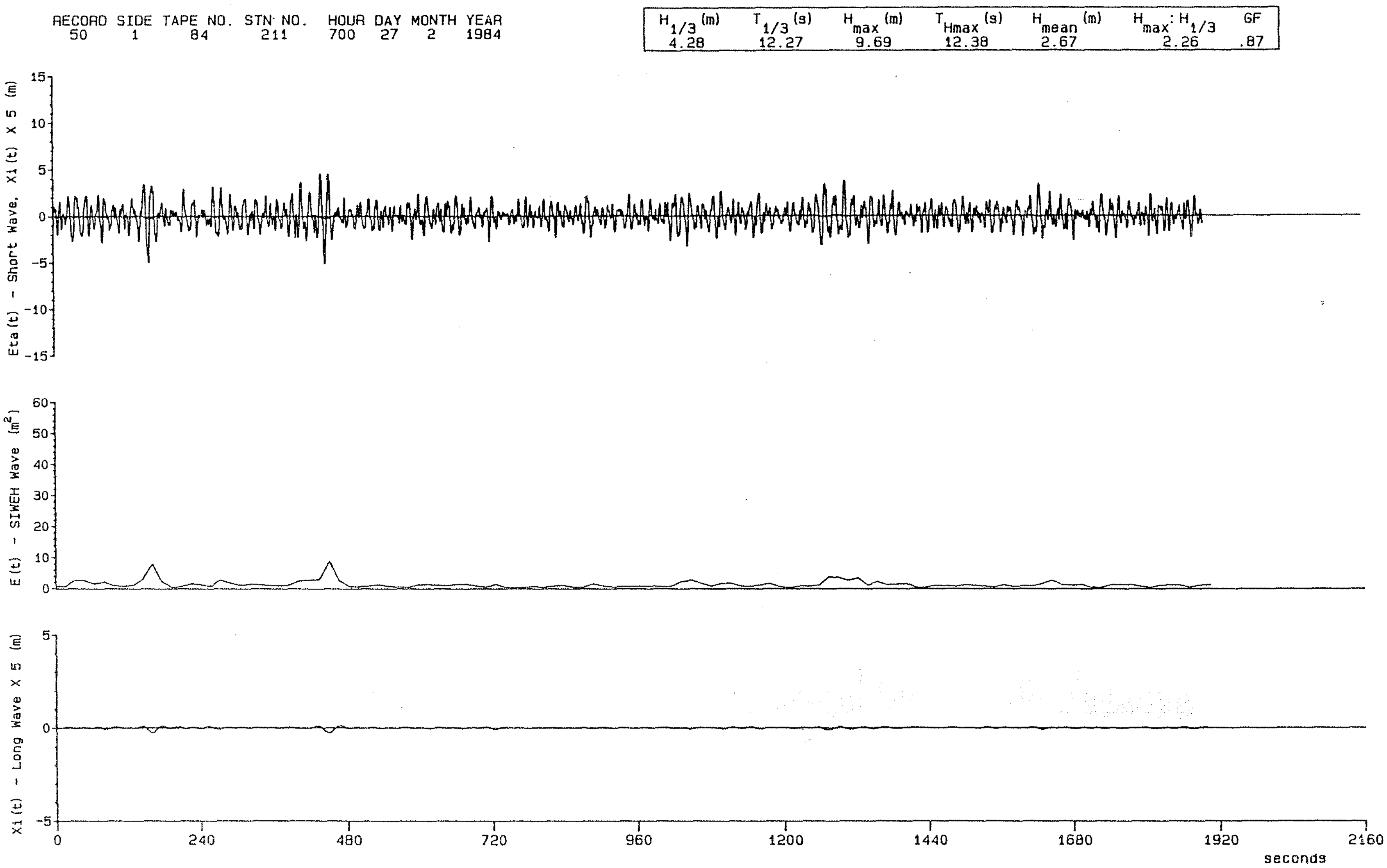

Fig. 2.28 continued

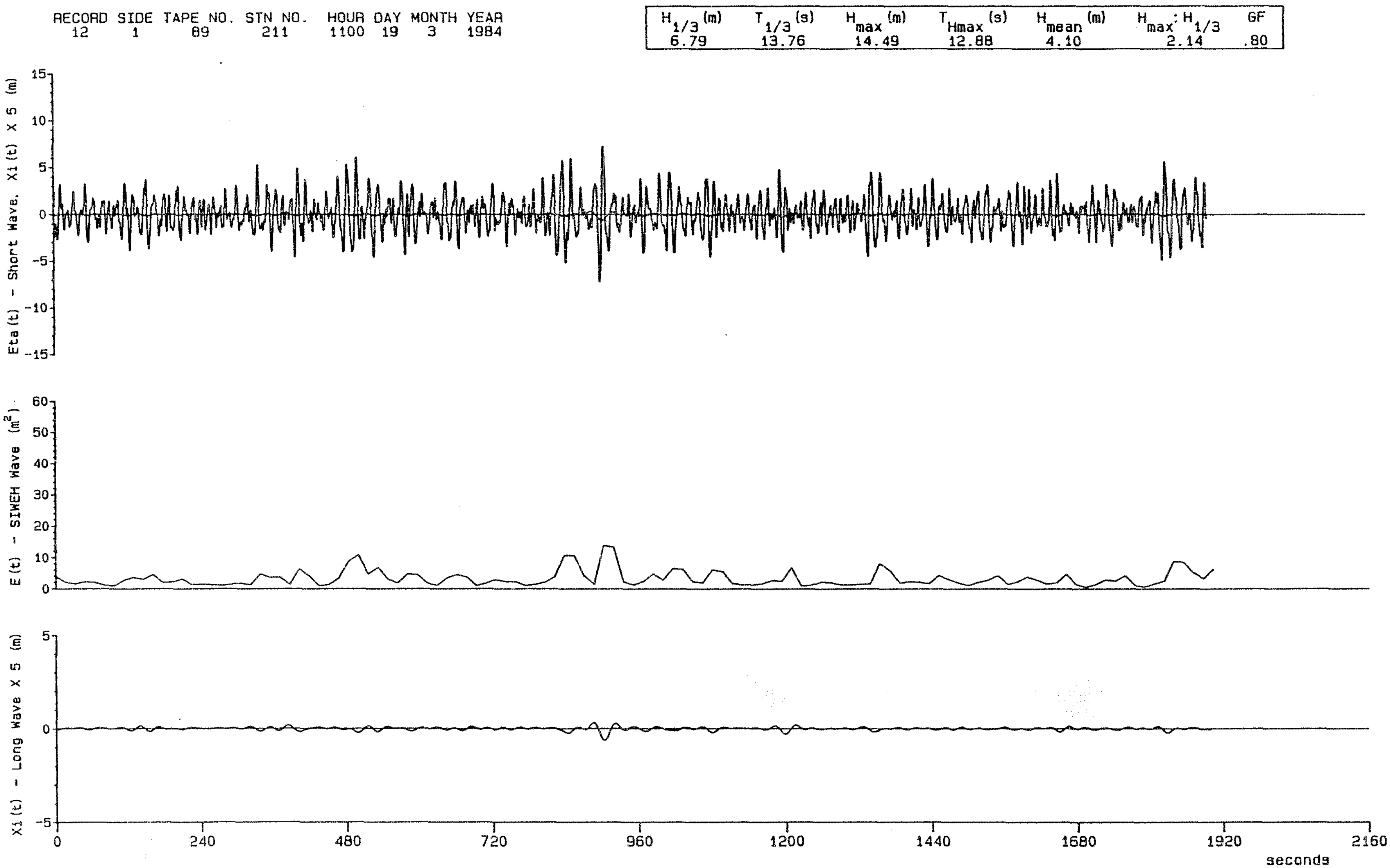

Fig. 2.28 continued

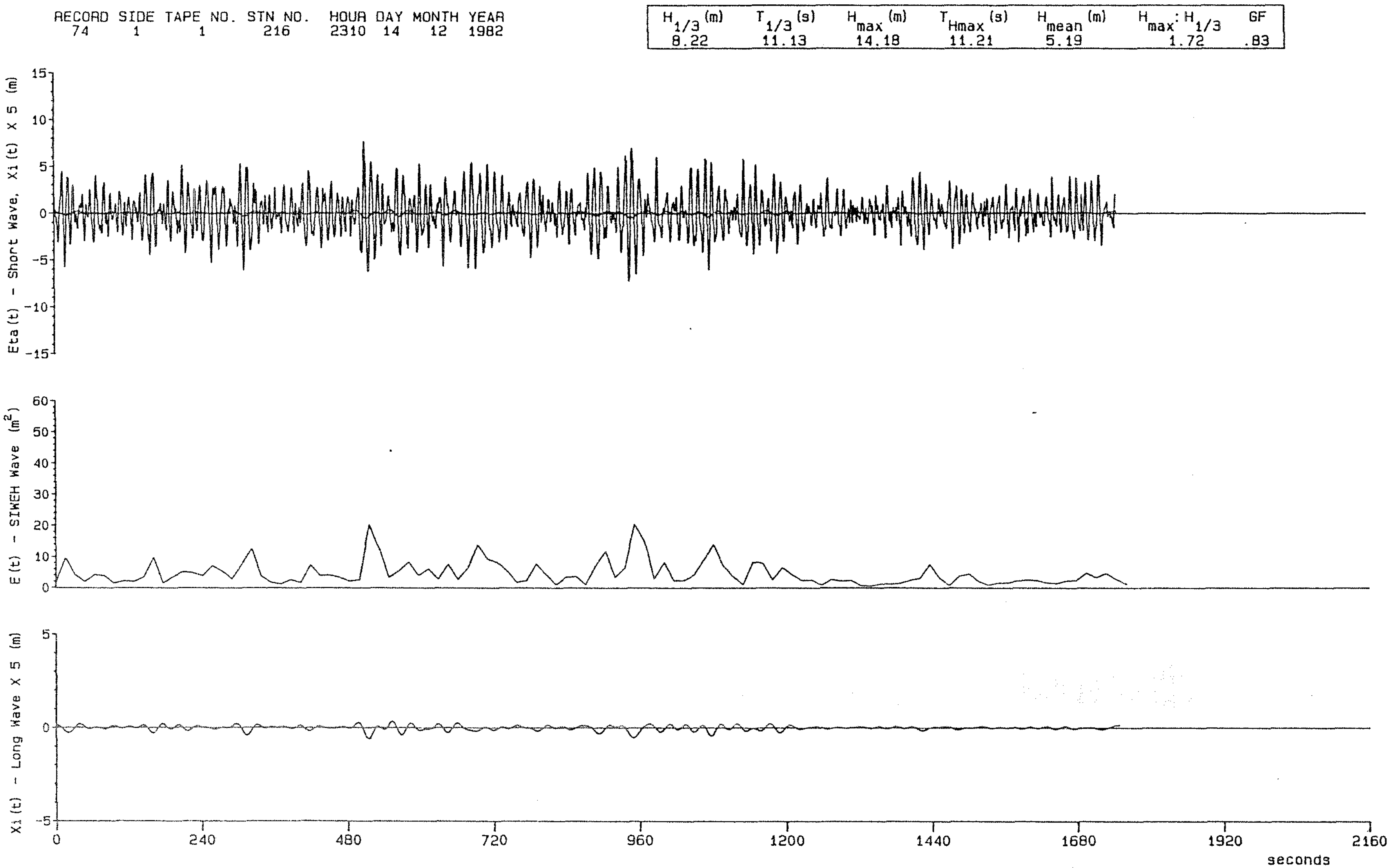

Fig. 2.28 continued

RECORD	SIDE	TAPE NO.	STN NO.	HOUR	DAY	MONTH	YEAR
76	1	1	216	810	15	12	1982

$H_{1/3}$ (m)	$T_{1/3}$ (s)	H_{max} (m)	T_{Hmax} (s)	H_{mean} (m)	$H_{max}:H_{1/3}$	GF
5.01	11.01	9.93	10.63	3.14	1.98	.98

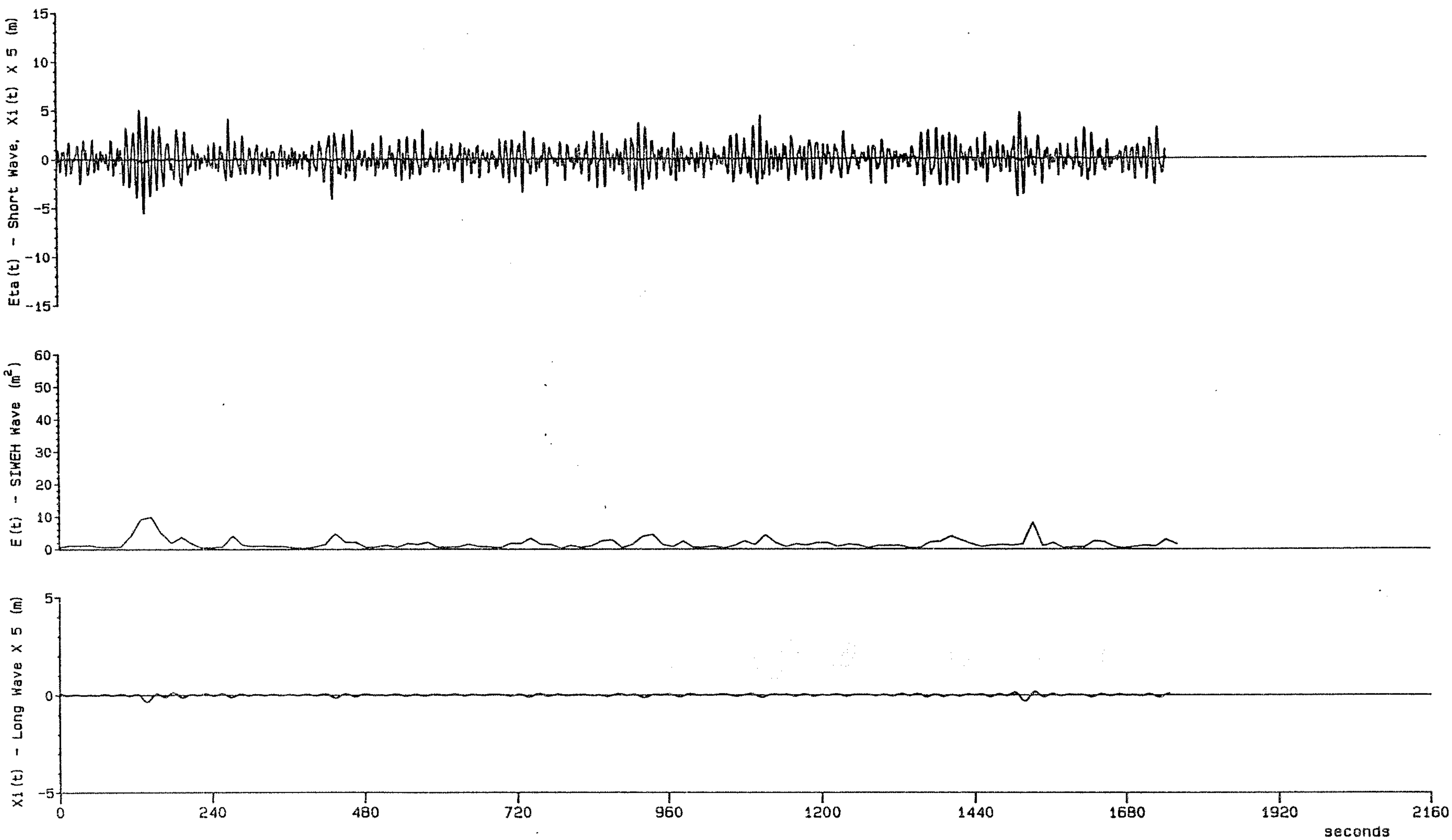

Fig. 2.28 continued

RECORD SIDE TAPE NO. STN NO. HOUR DAY MONTH YEAR
168 1 1 216 1410 24 1 1982

$H_{1/3}$ (m)	$T_{1/3}$ (s)	H_{max} (m)	T_{Hmax} (s)	H_{mean} (m)	$H_{max}:H_{1/3}$	GF
6.38	10.90	11.56	10.62	4.17	1.81	.80

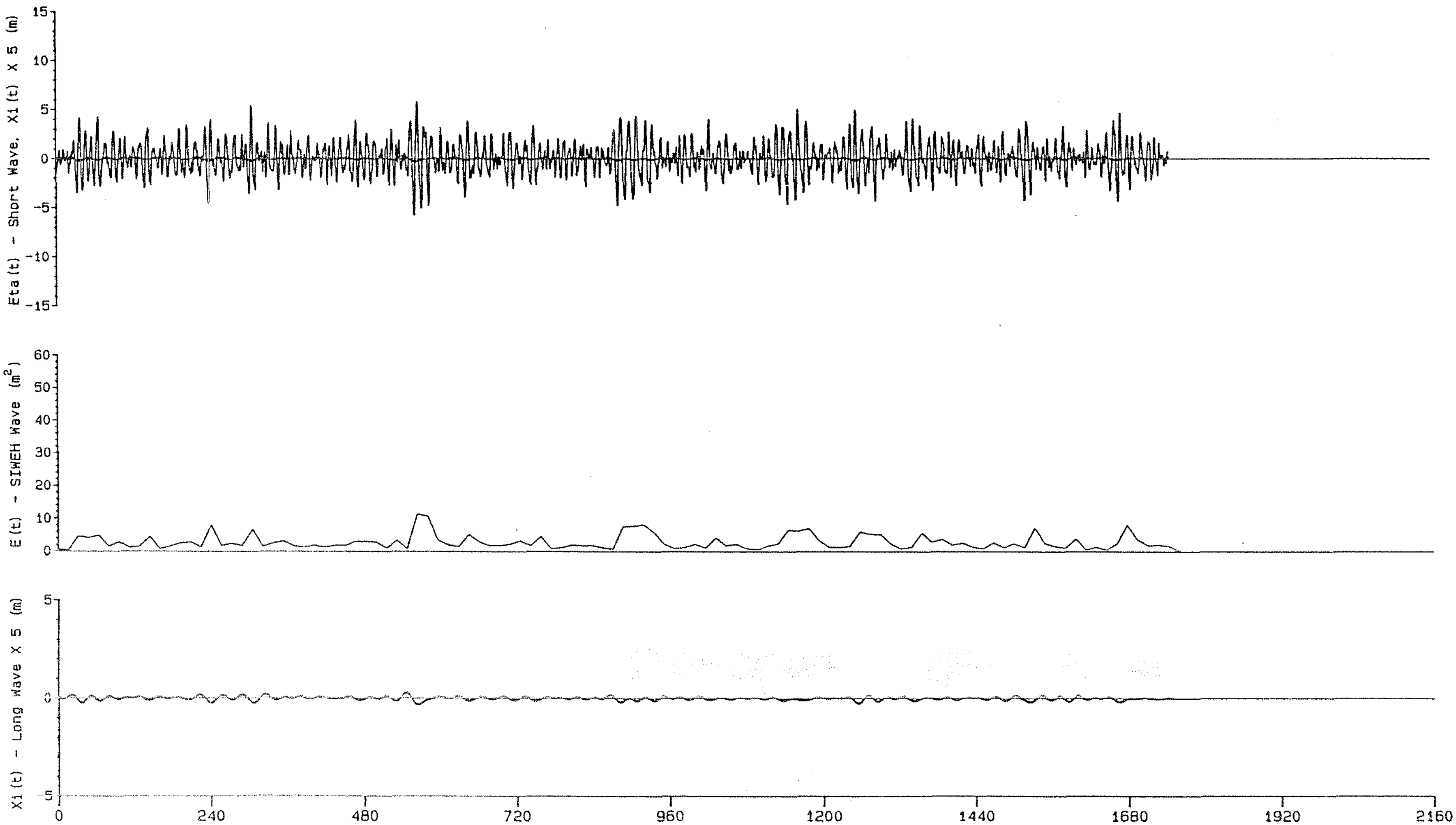

Fig. 2.28 continued

RECORD	SIDE	TAPE NO.	STN NO.	HOUR	DAY	MONTH	YEAR
173	1	1	216	510	25	1	1982

$H_{1/3}$ (m)	$T_{1/3}$ (s)	H_{max} (m)	T_{Hmax} (s)	H_{mean} (m)	$H_{max}:H_{1/3}$	GF
6.17	12.75	11.30	10.86	3.86	1.83	.84

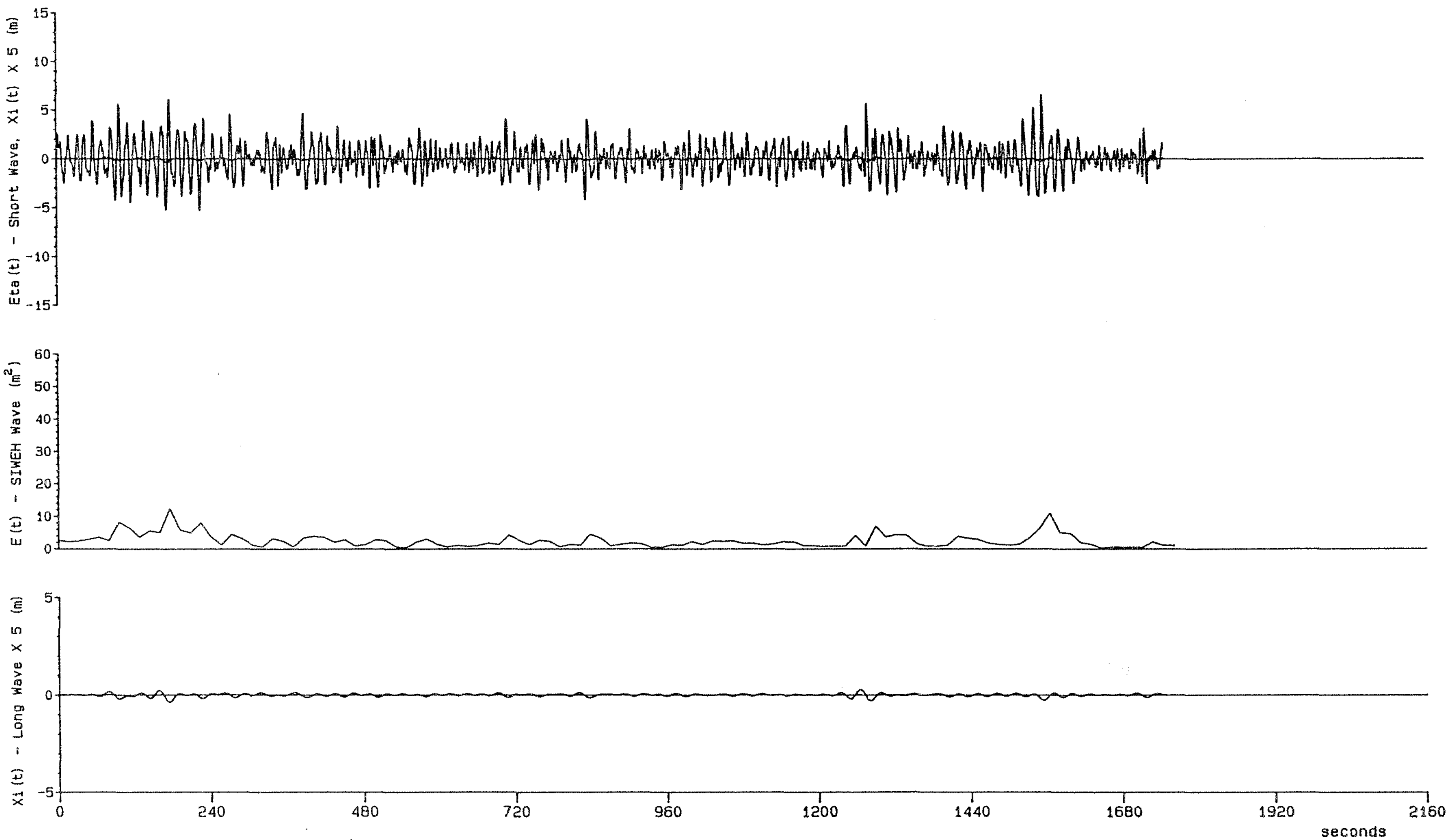

Fig. 2.28 continued

RECORD	SIDE	TAPE NO.	STN NO.	HOUR	DAY	MONTH	YEAR
77	1	3	216	2010	26	2	1984

$H_{1/3}$ (m)	$T_{1/3}$ (s)	H_{max} (m)	T_{Hmax} (s)	H_{mean} (m)	$H_{max}:H_{1/3}$	GF
7.90	11.21	12.76	10.89	5.14	1.61	.80

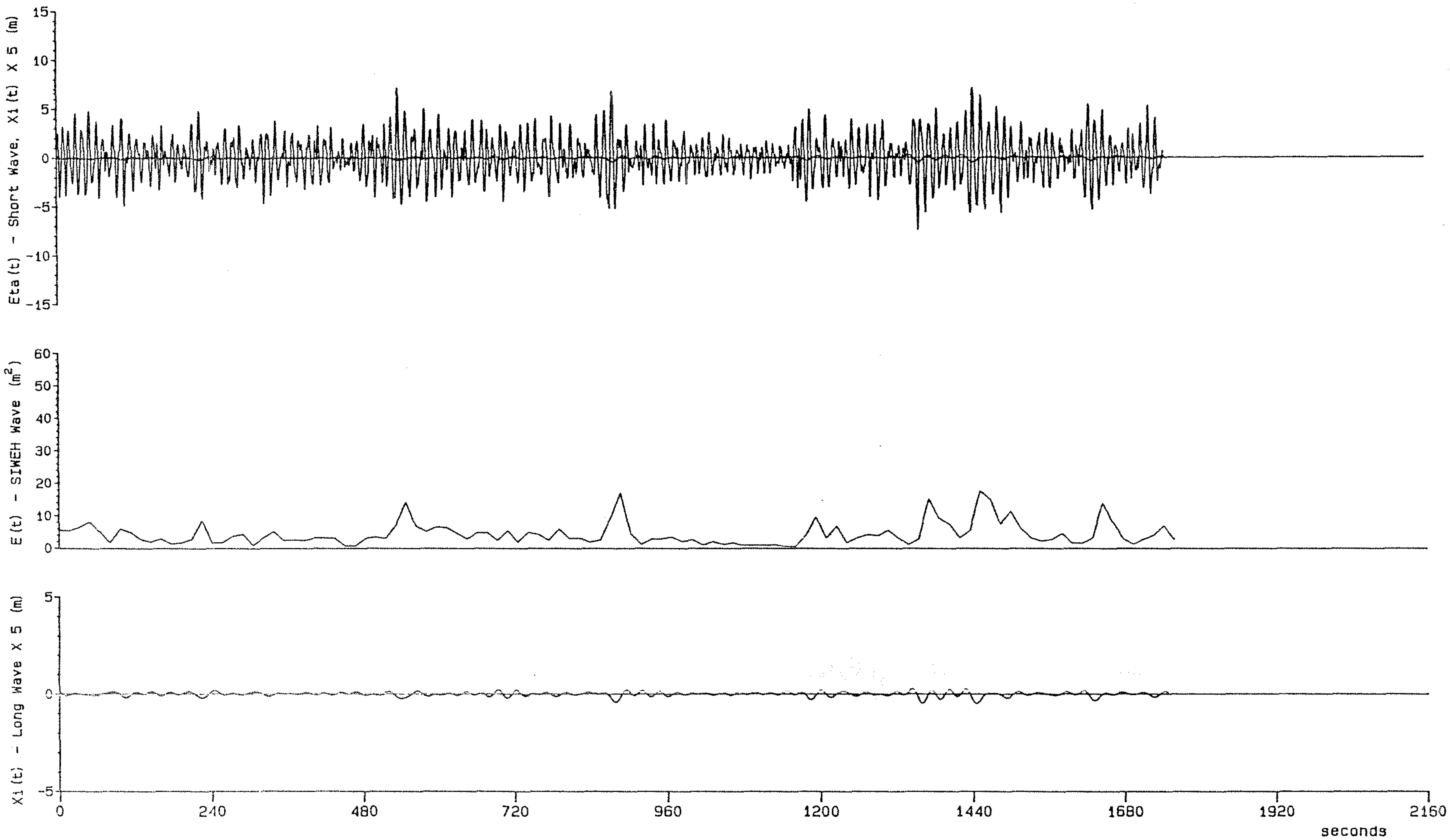

Fig. 2.28 continued

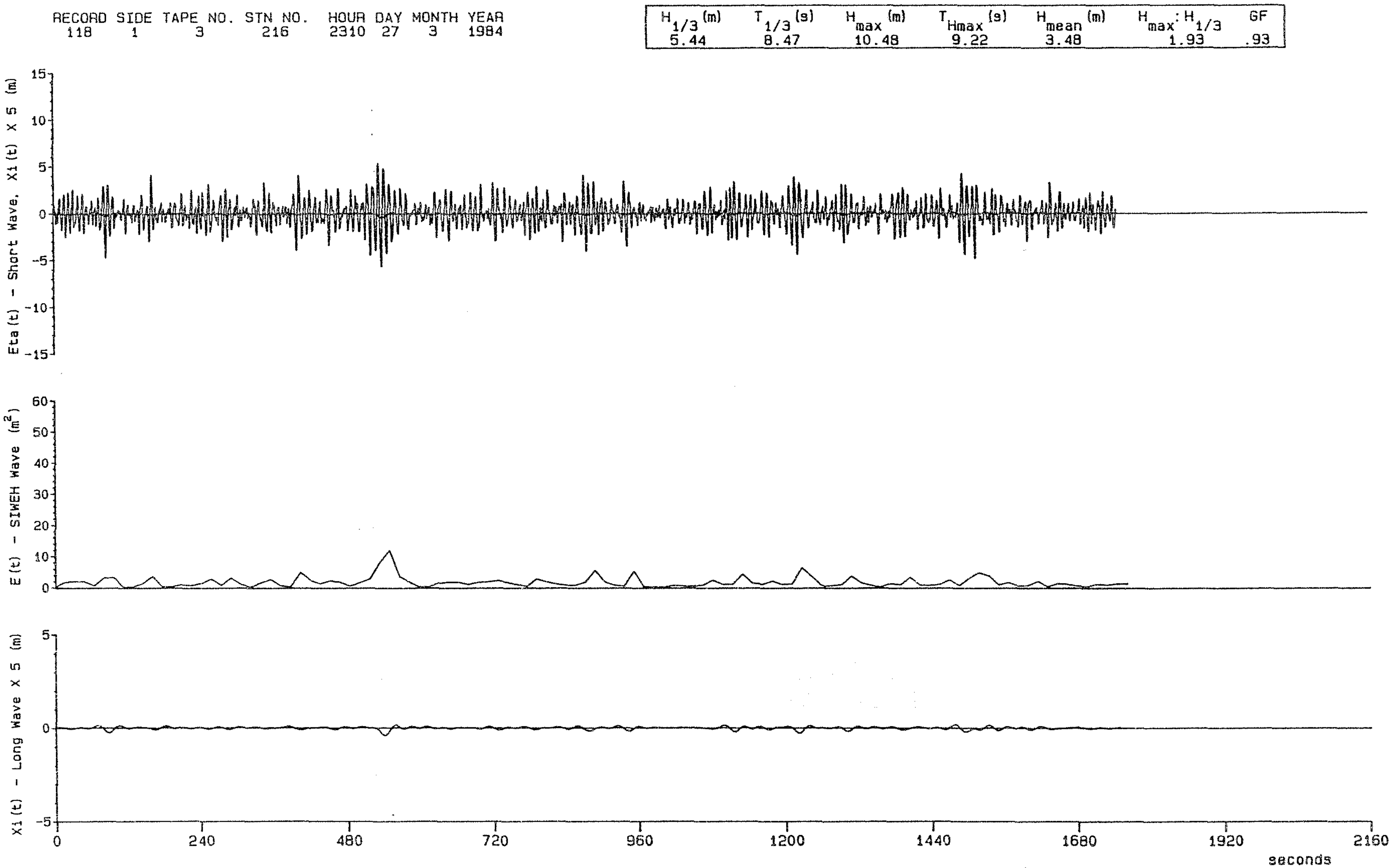

Fig. 2.28 continued

RECORD	SIDE	TAPE NO.	STN NO.	HOUR	DAY	MONTH	YEAR
115	1	1	216	1110	25	12	1982

$H_{1/3}$ (m)	$T_{1/3}$ (s)	H_{max} (m)	T_{Hmax} (s)	H_{mean} (m)	$H_{max}:H_{1/3}$	GF
11.19	13.77	18.54	12.08	6.99	1.66	.72

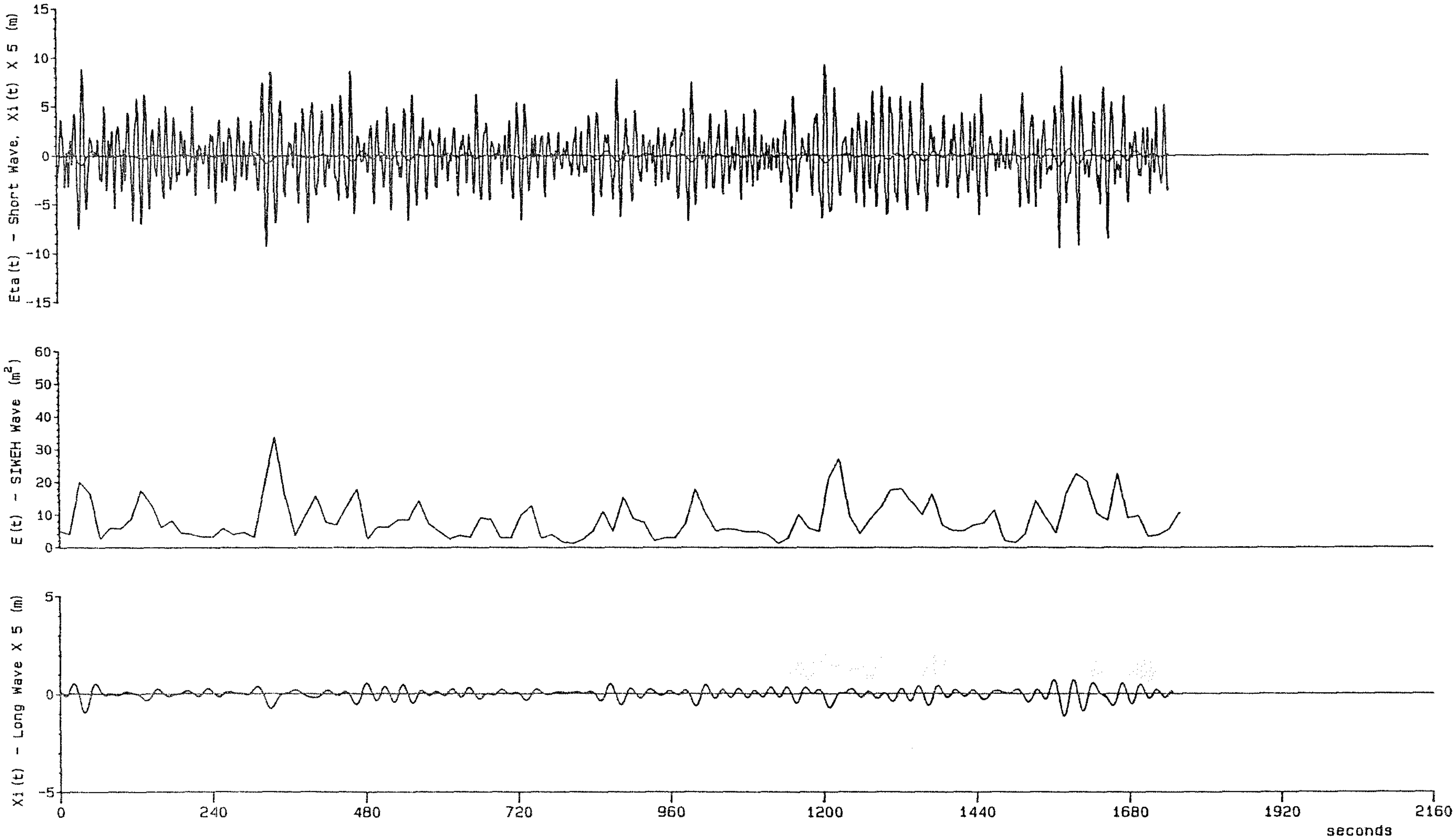

Fig. 2.28 continued

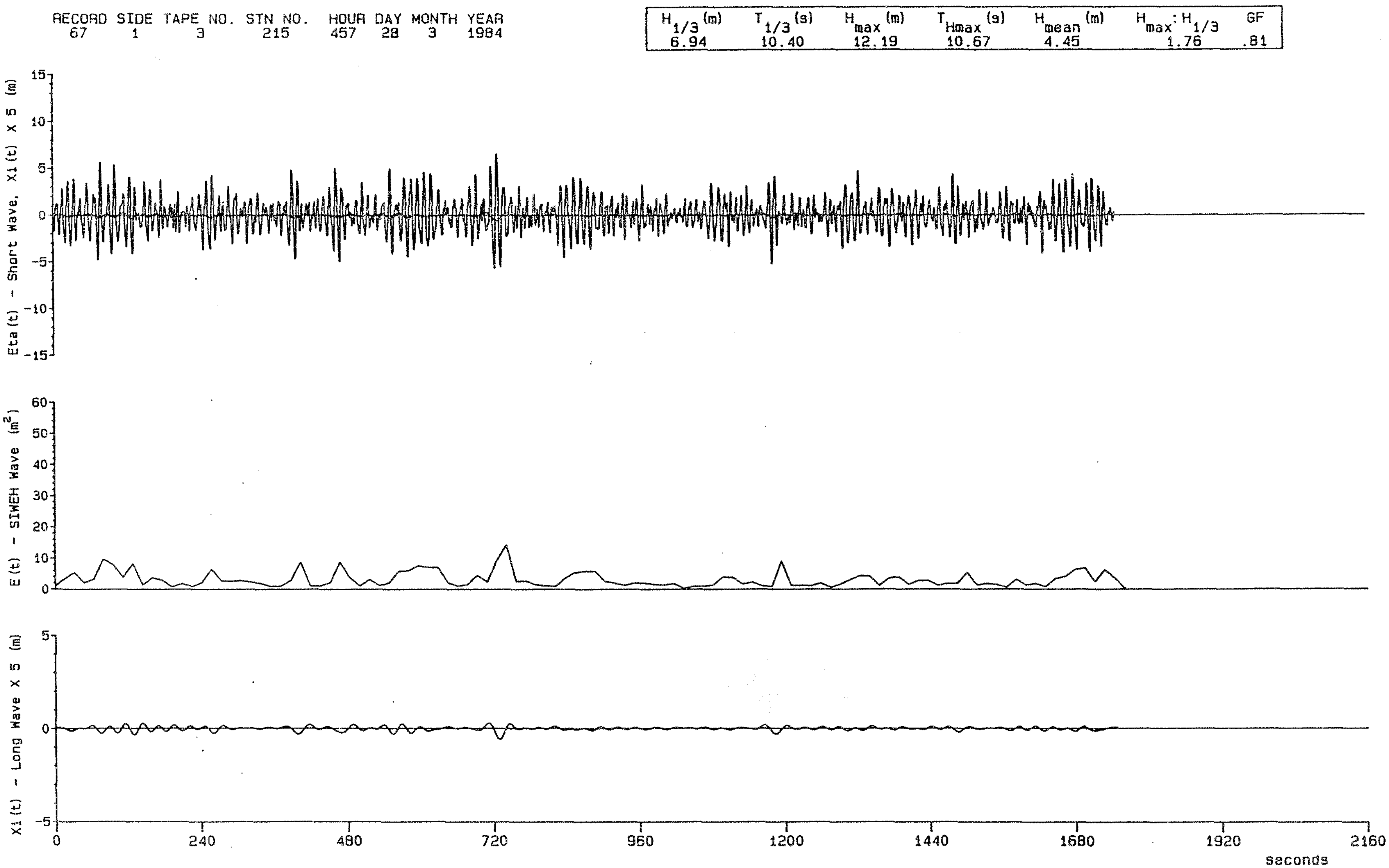

Fig. 2.28 continued

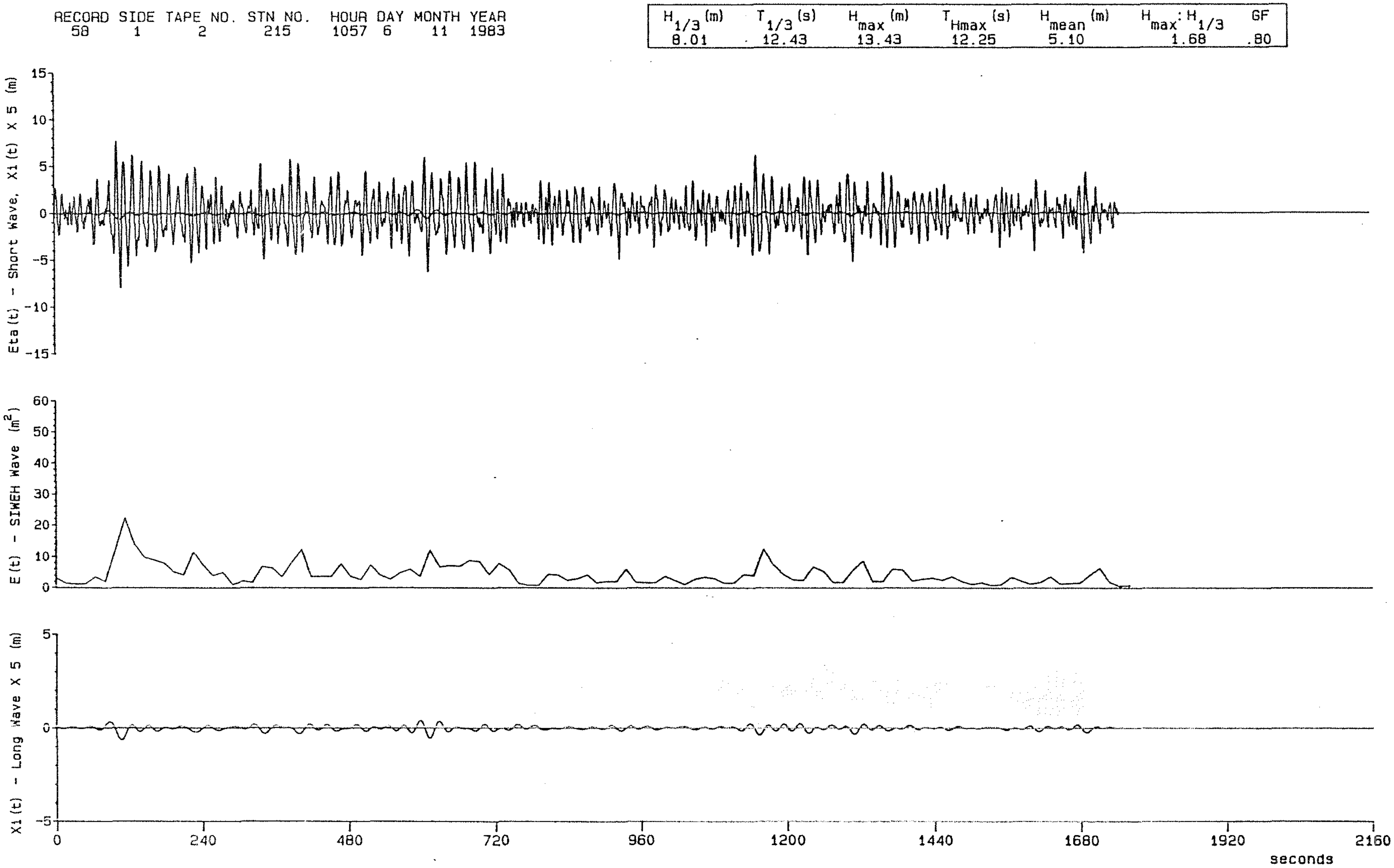

Fig. 2.28 continued

RECORD	SIDE	TAPE NO.	STN NO.	HOUR	DAY	MONTH	YEAR
21	1	17	214	1610	26	2	1984

$H_{1/3}$ (m)	$T_{1/3}$ (s)	H_{max} (m)	T_{Hmax} (s)	H_{mean} (m)	$H_{max}:H_{1/3}$	GF
5.71	10.11	10.44	9.91	3.65	1.83	1.03

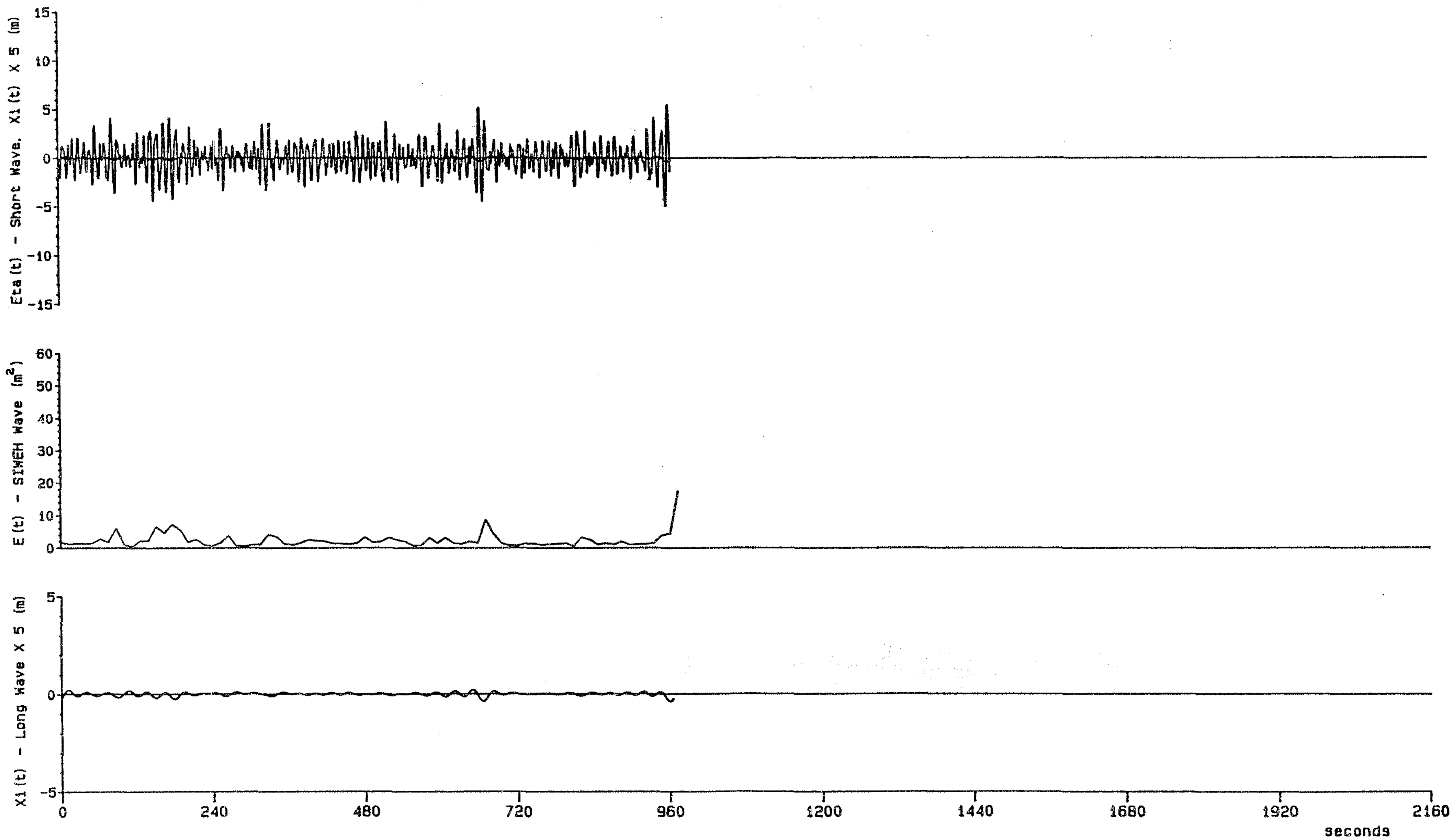

Fig. 2.28 continued

RECORD	SIDE	TAPE NO.	STN NO.	HOUR	DAY	MONTH	YEAR
25	1	17	214	1800	26	2	1984

$H_{1/3}$ (m)	$T_{1/3}$ (s)	H_{max} (m)	T_{Hmax} (s)	H_{mean} (m)	$H_{max}:H_{1/3}$	GF
6.11	10.60	12.13	10.37	3.84	1.99	.88

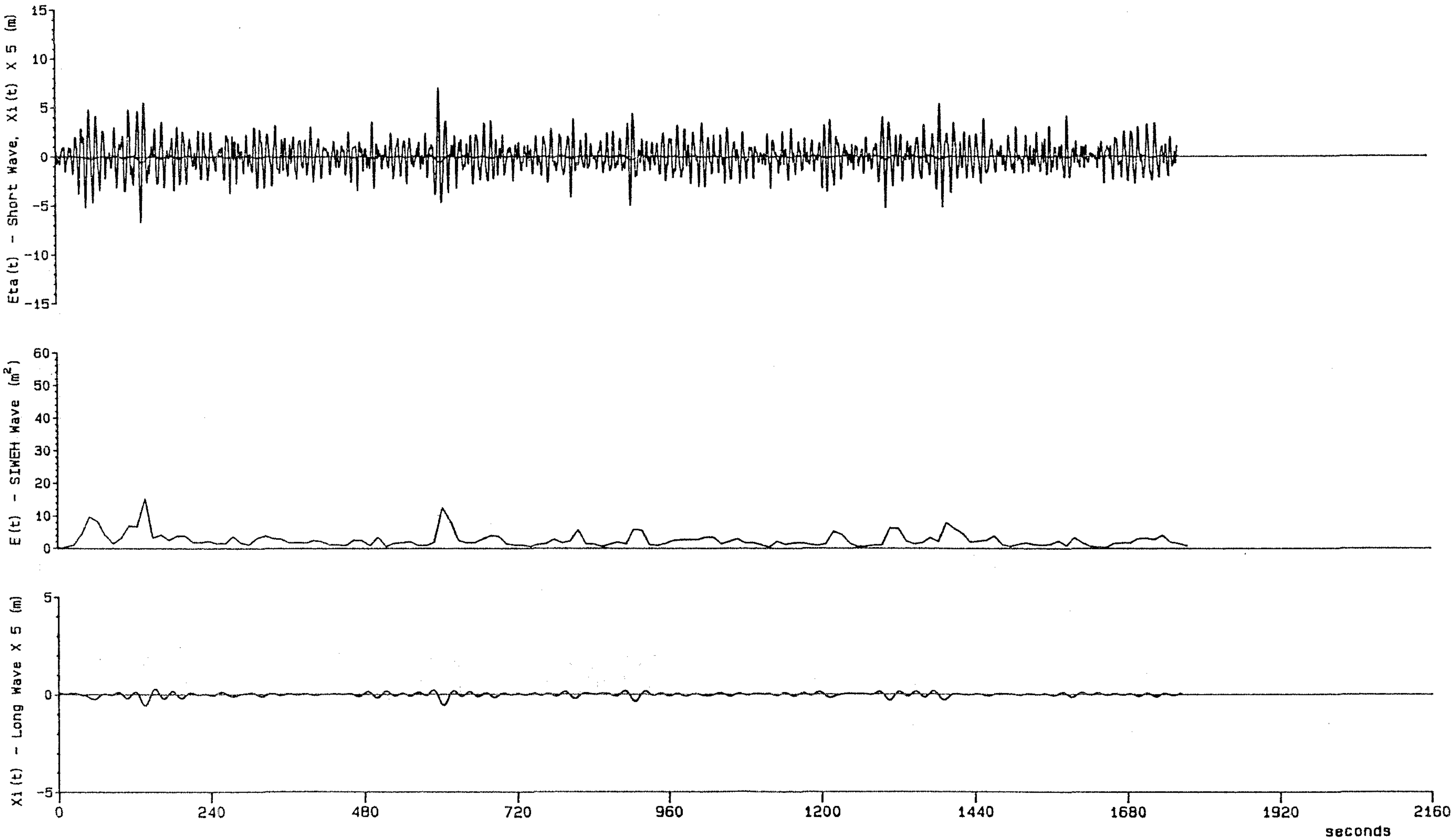

Fig. 2.28 continued

RECORD	SIDE	TAPE NO.	STN NO.	HOUR	DAY	MONTH	YEAR
27	1	20	214	601	19	3	1984

$H_{1/3}$ (m)	$T_{1/3}$ (s)	H_{max} (m)	T_{Hmax} (s)	H_{mean} (m)	$H_{max}:H_{1/3}$	GF
4.43	12.93	10.75	16.07	2.78	2.42	.76

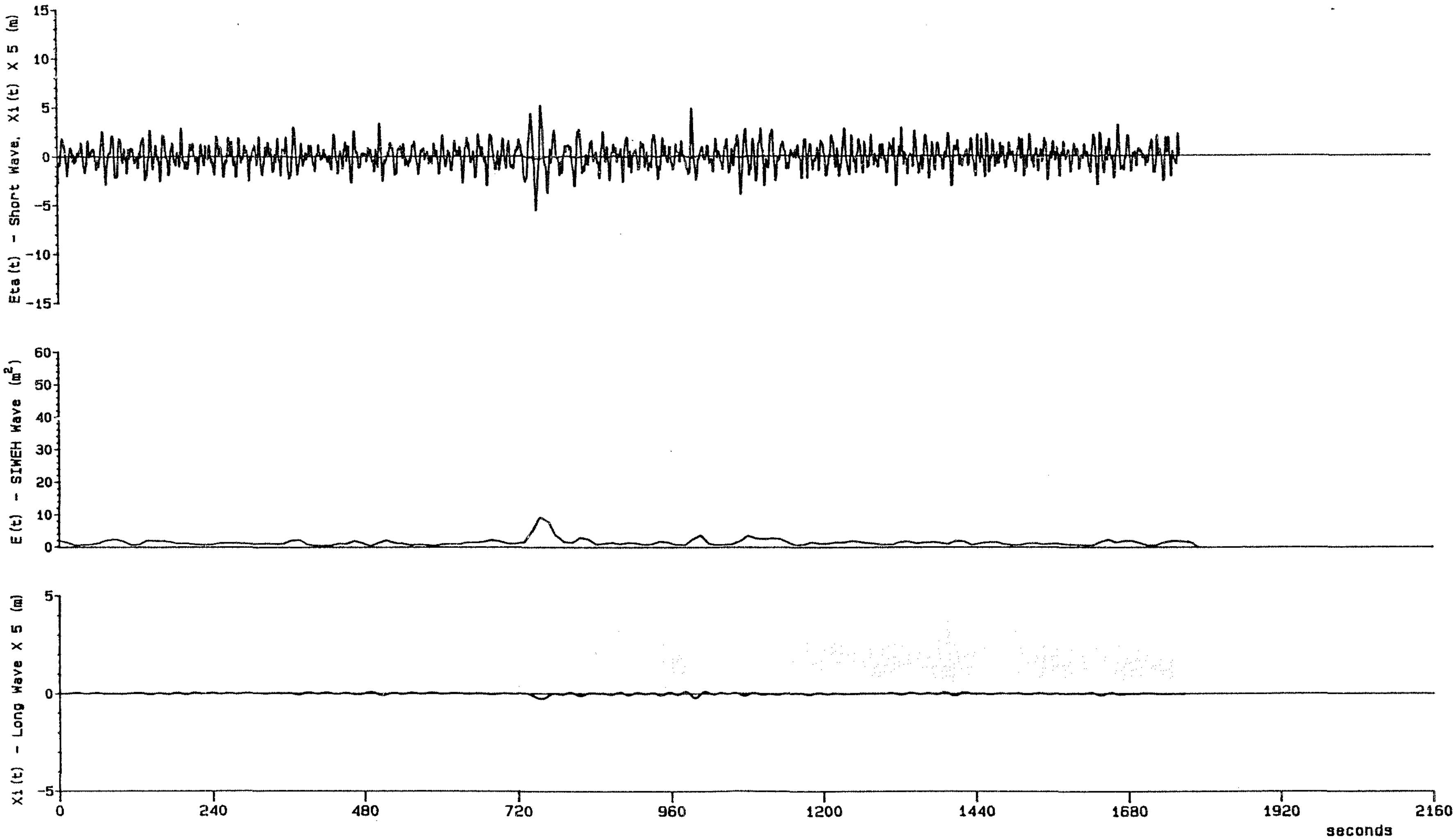

Fig. 2.28 continued

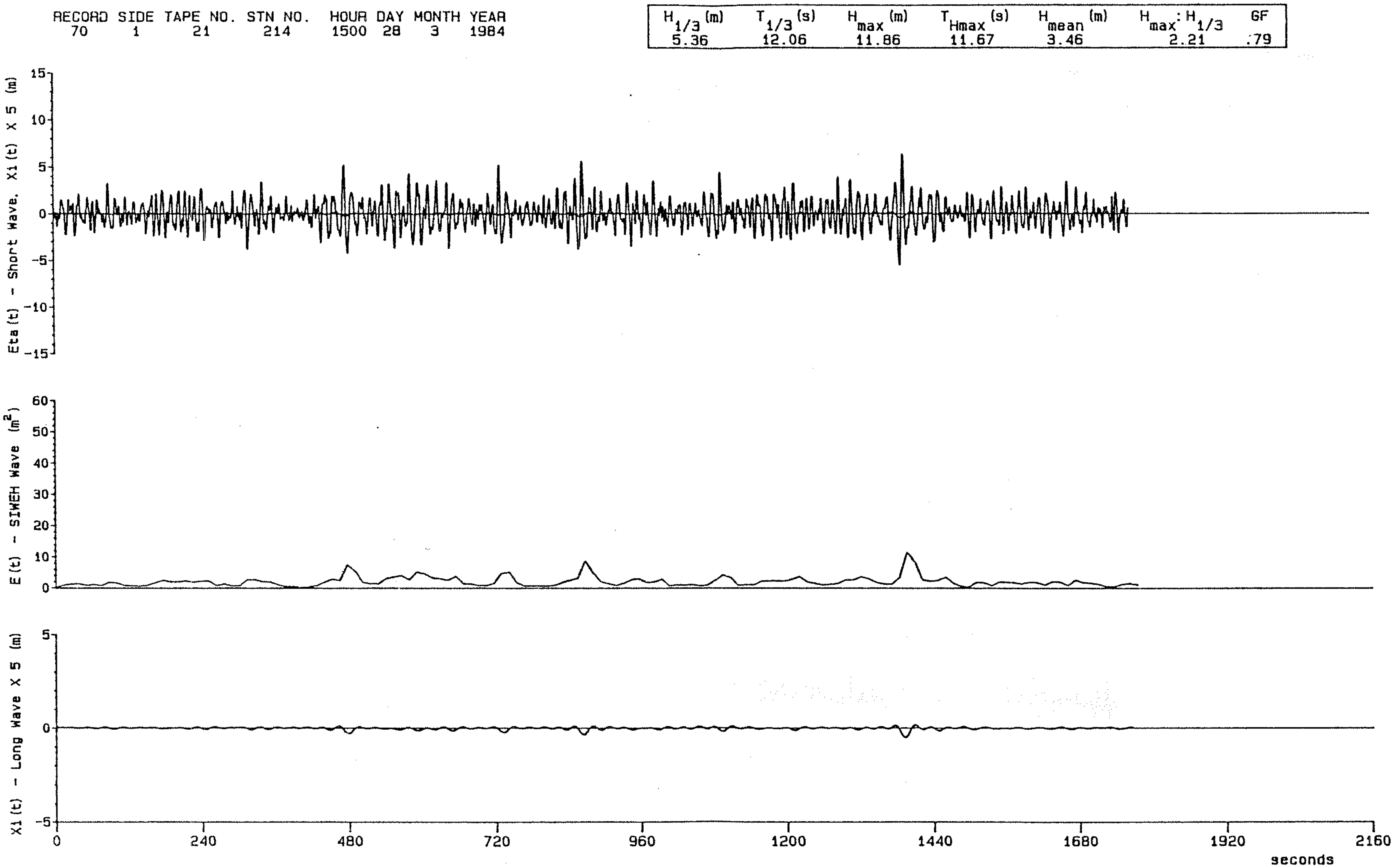

Fig. 2.28 continued

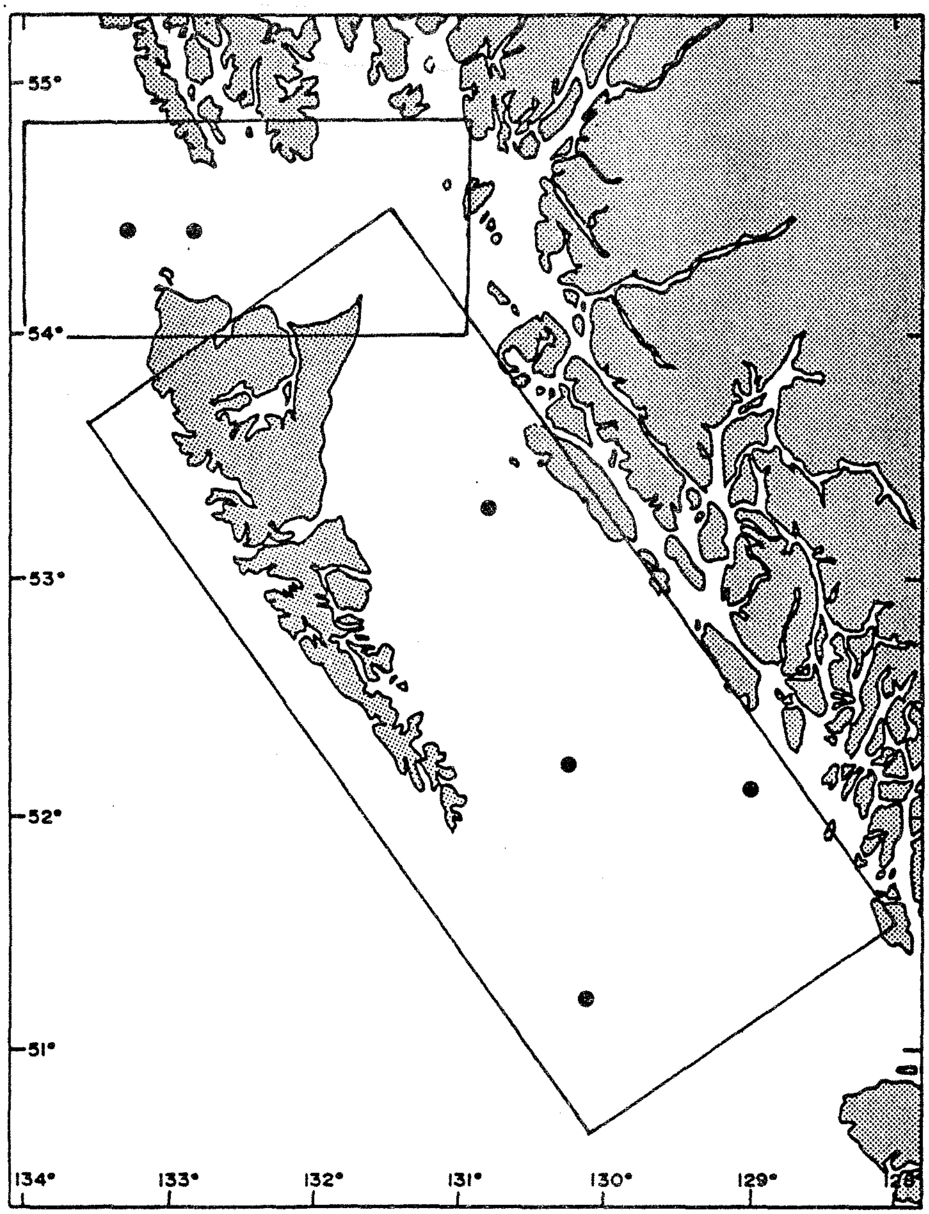

Fig. 3.1 Map of study area showing the two regions for which refraction calculations have been made.

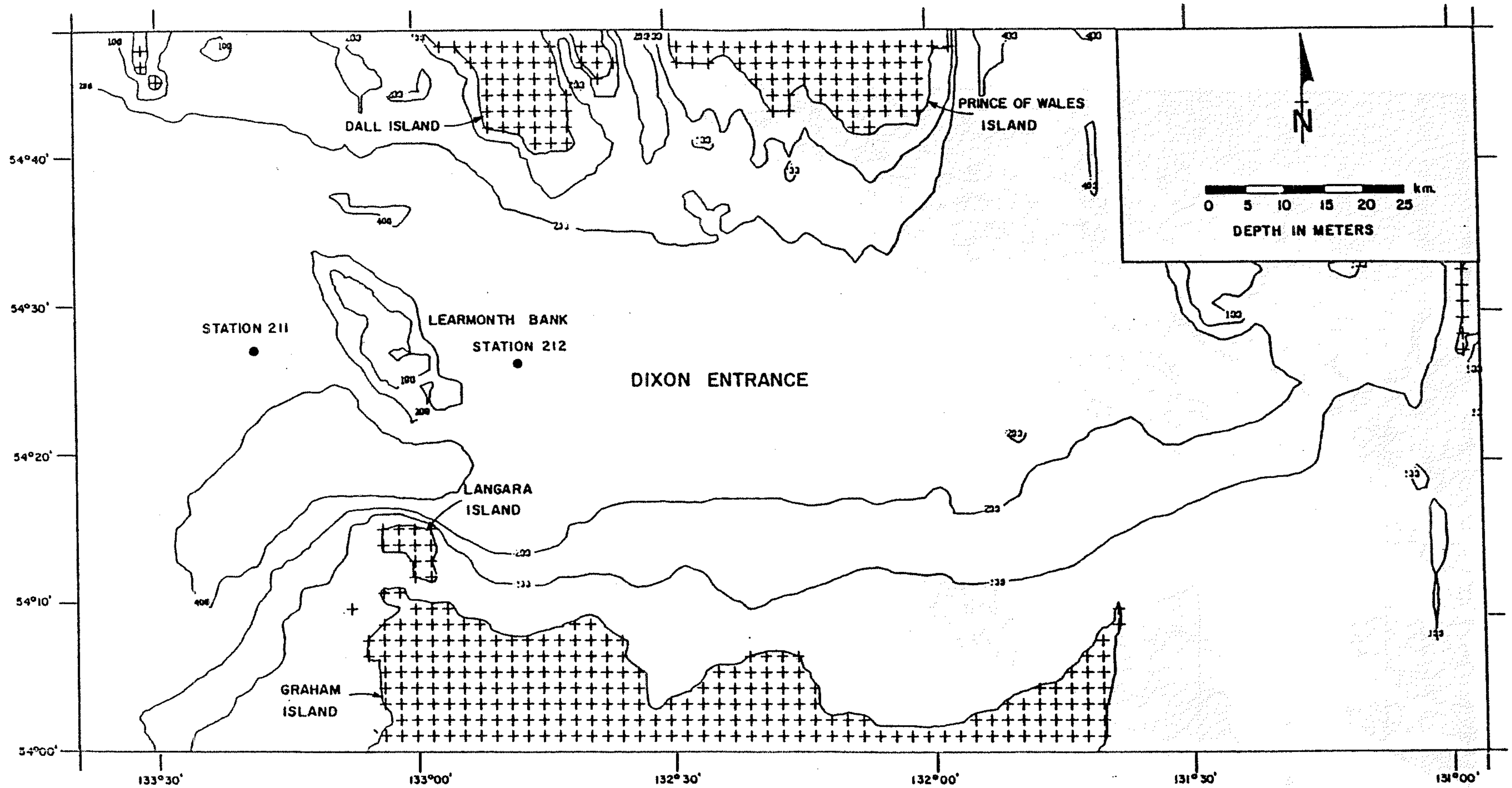

Fig 3.2a Refraction domain in Dixon Entrance showing bottom contours.

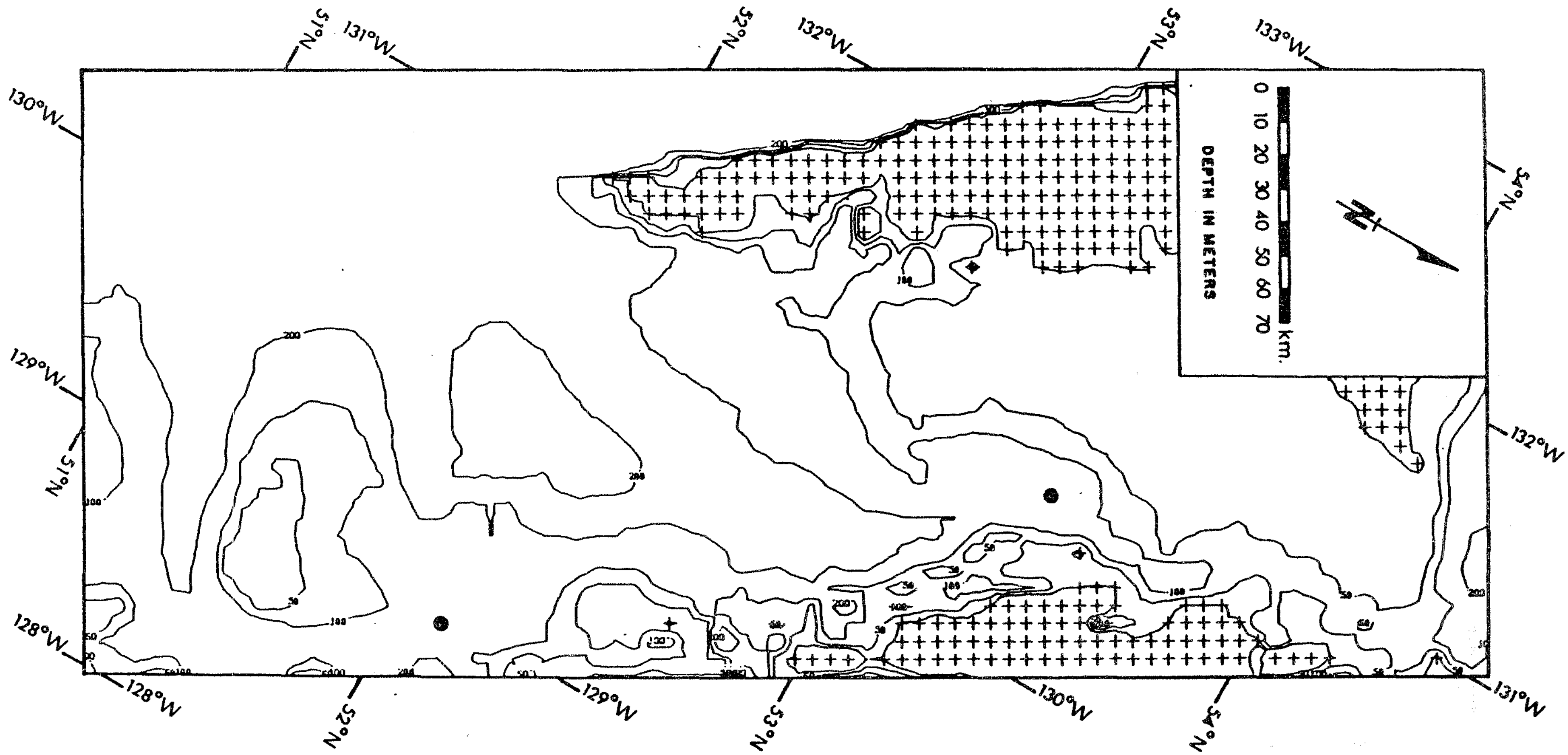

Fig. 3.2b Refraction domain in Hecate Strait-Queen Charlotte Sound showing bottom contours.

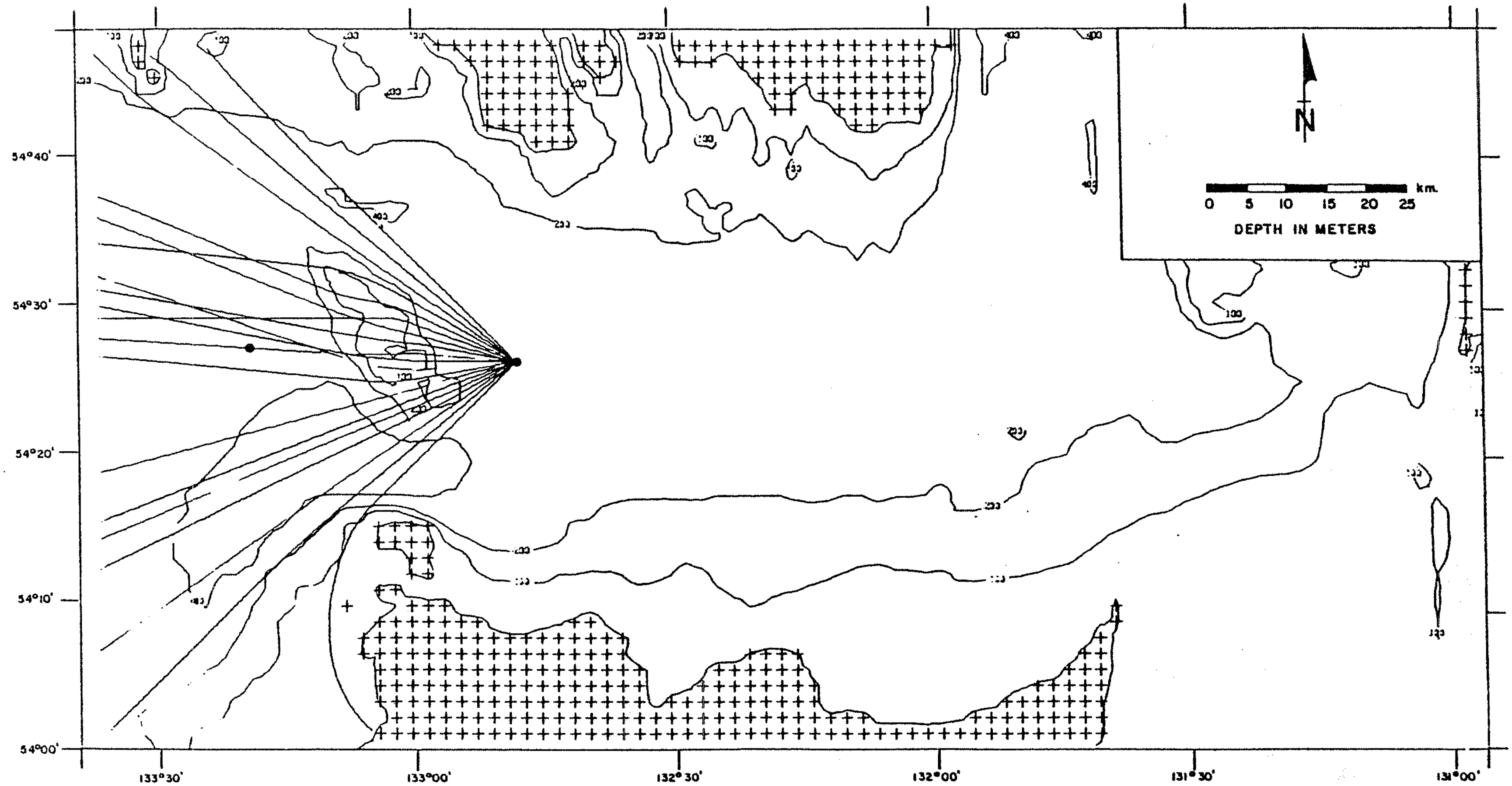

Fig. 3.3a Reverse ray patterns for Station 212 (Langara East) for a wave period of 16 s.

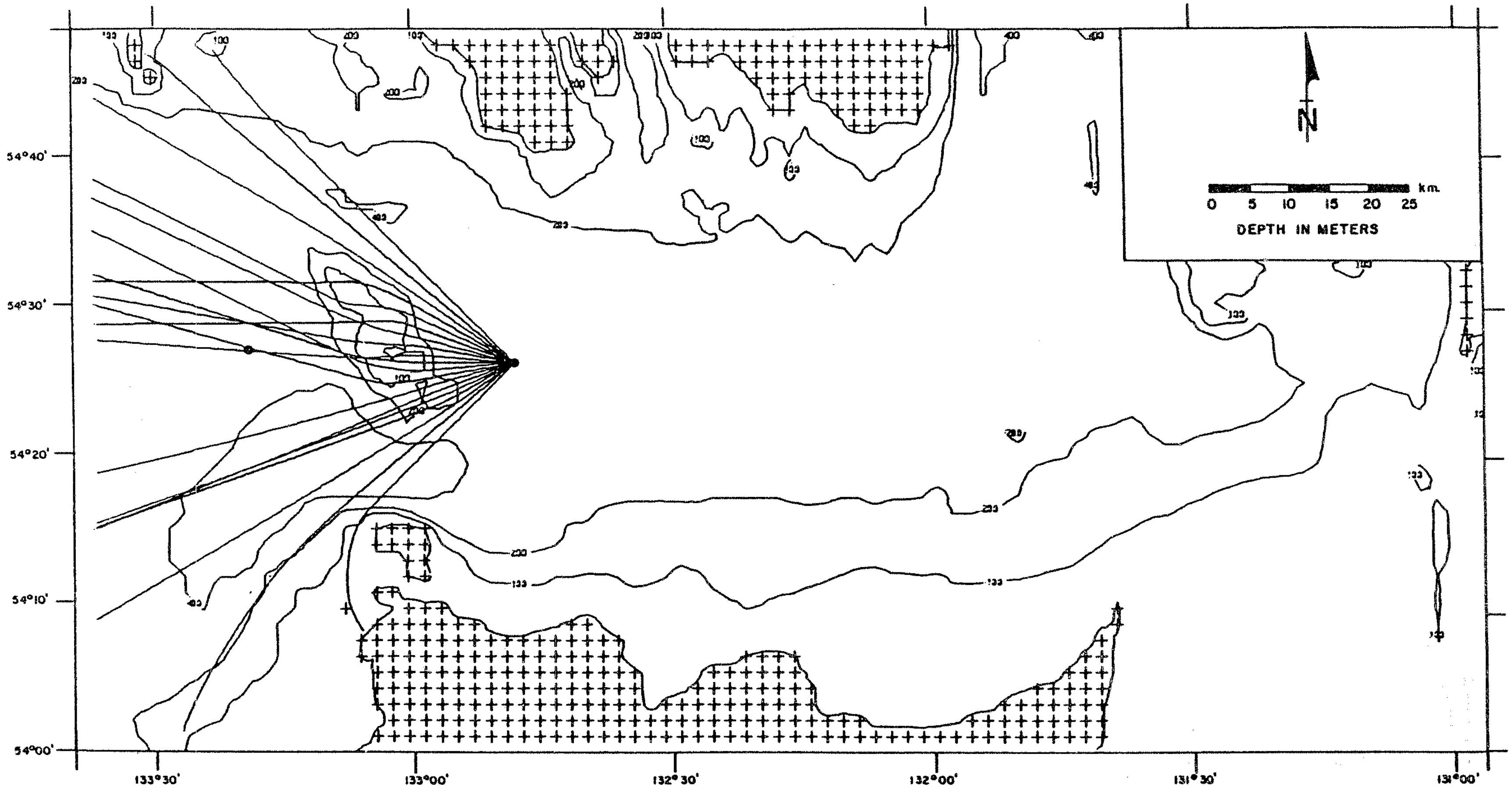

Fig. 3.3b Reverse ray patterns for Station 212 (Langara East) for a wave period of 18.3 s.

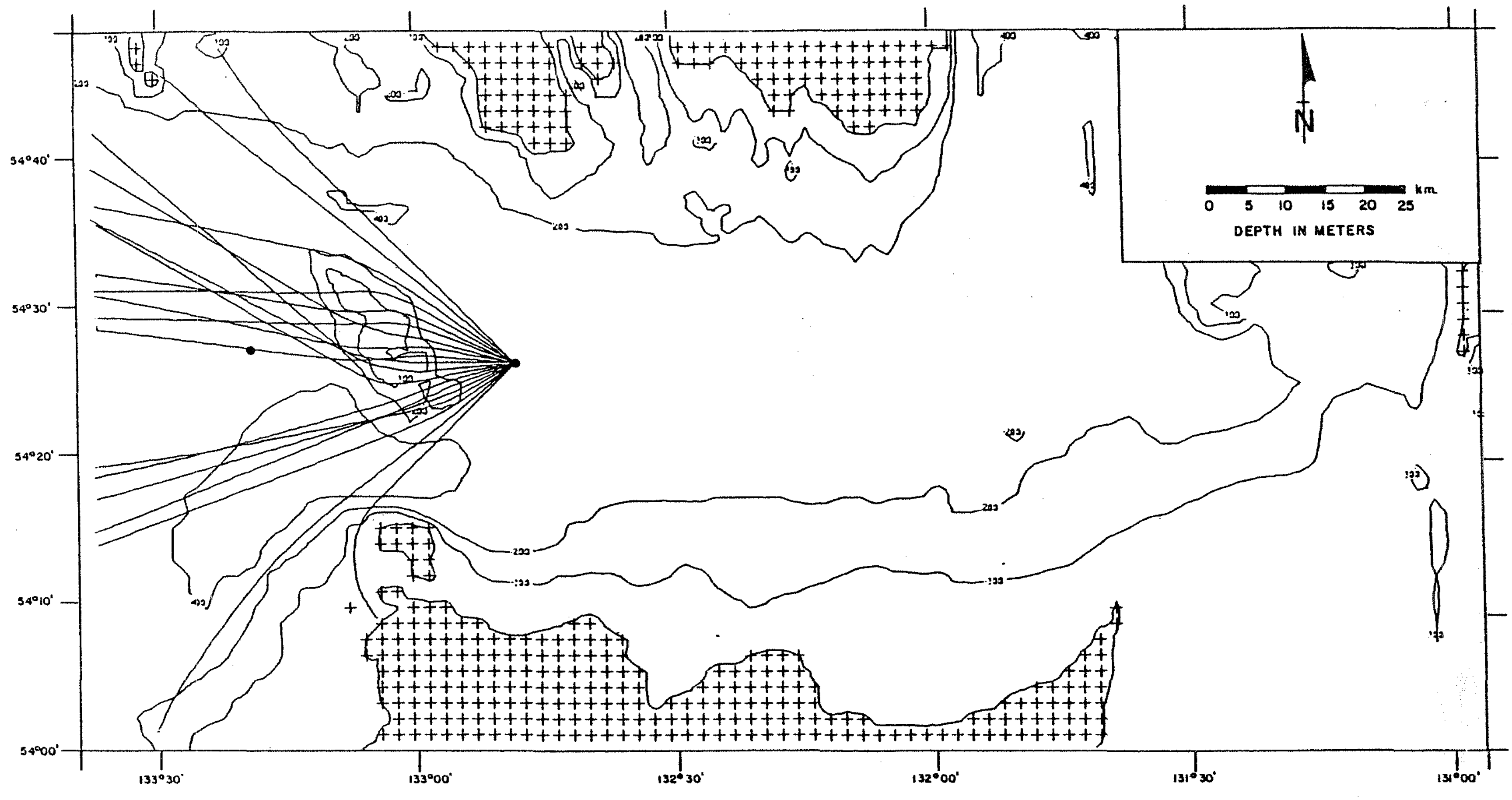

Fig. 3.3c Reverse ray patterns for Station 212 (Langara East) for a wave period of 21.3 s.

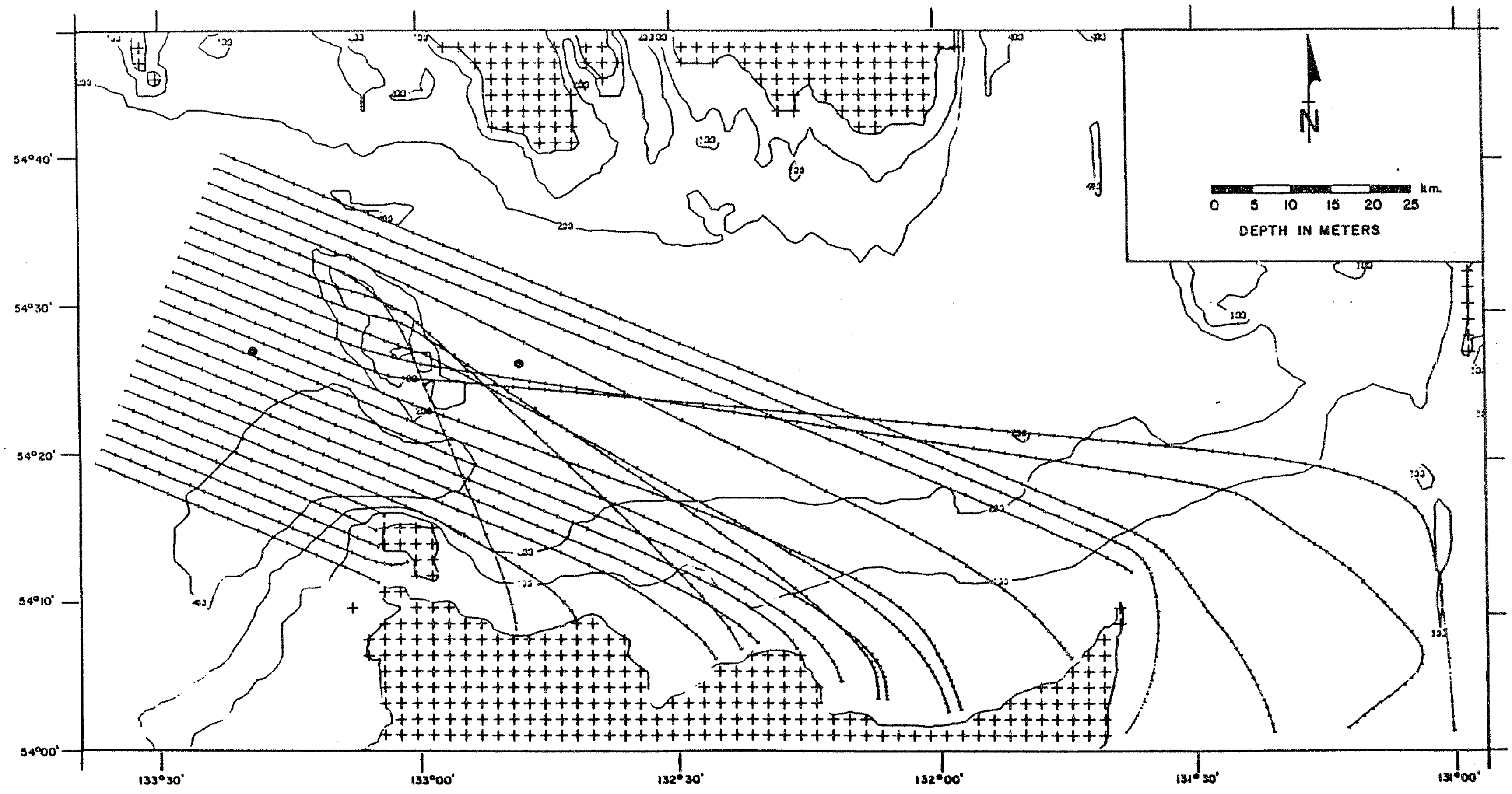

Fig. 3.4a Comparison of 16 s wave ray patterns over Learmonth Bank for WNW Swell.

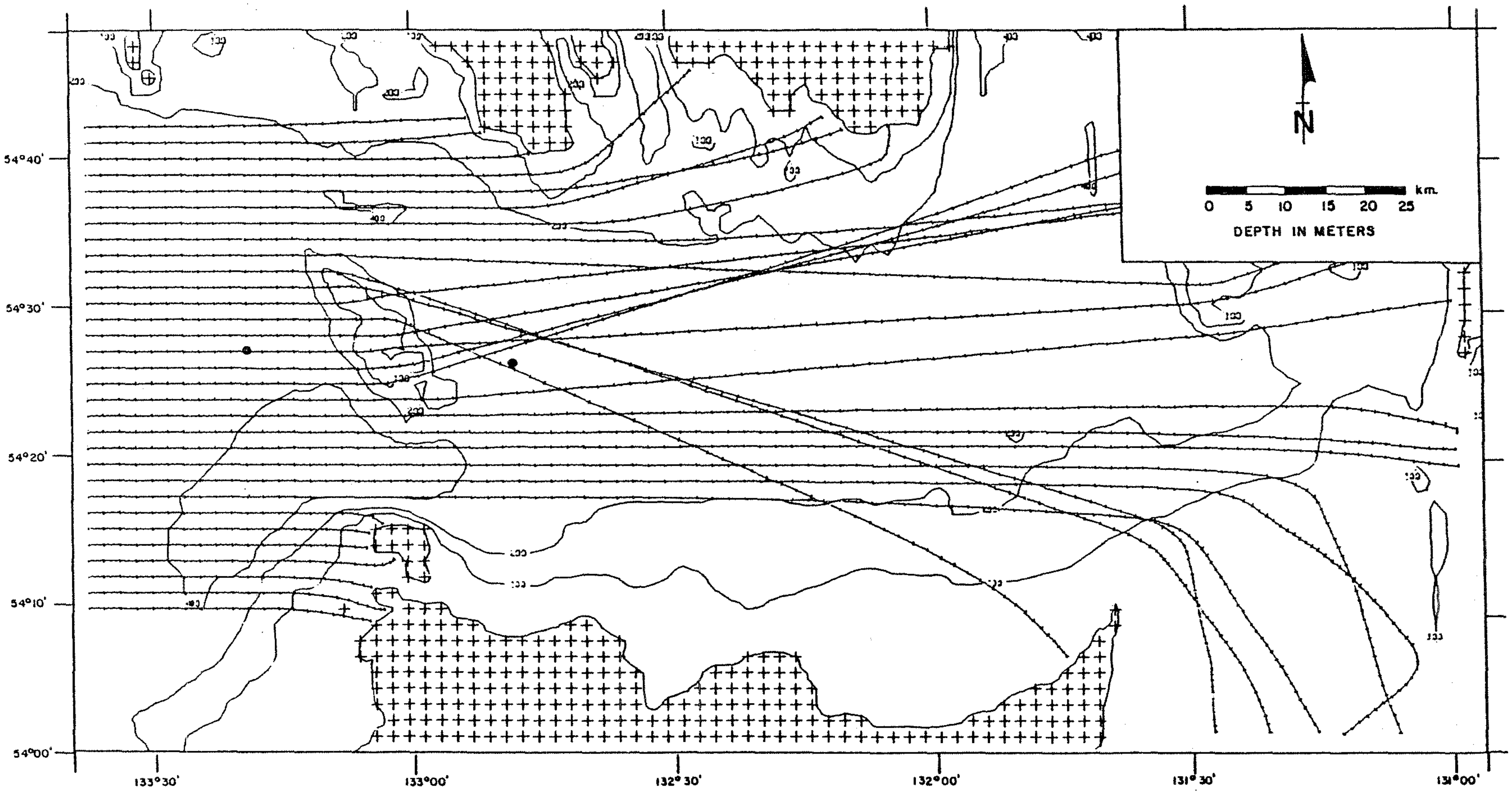

Fig. 3.4b. Comparison of 16 s wave ray patterns over Learmonth Bank for W swell.

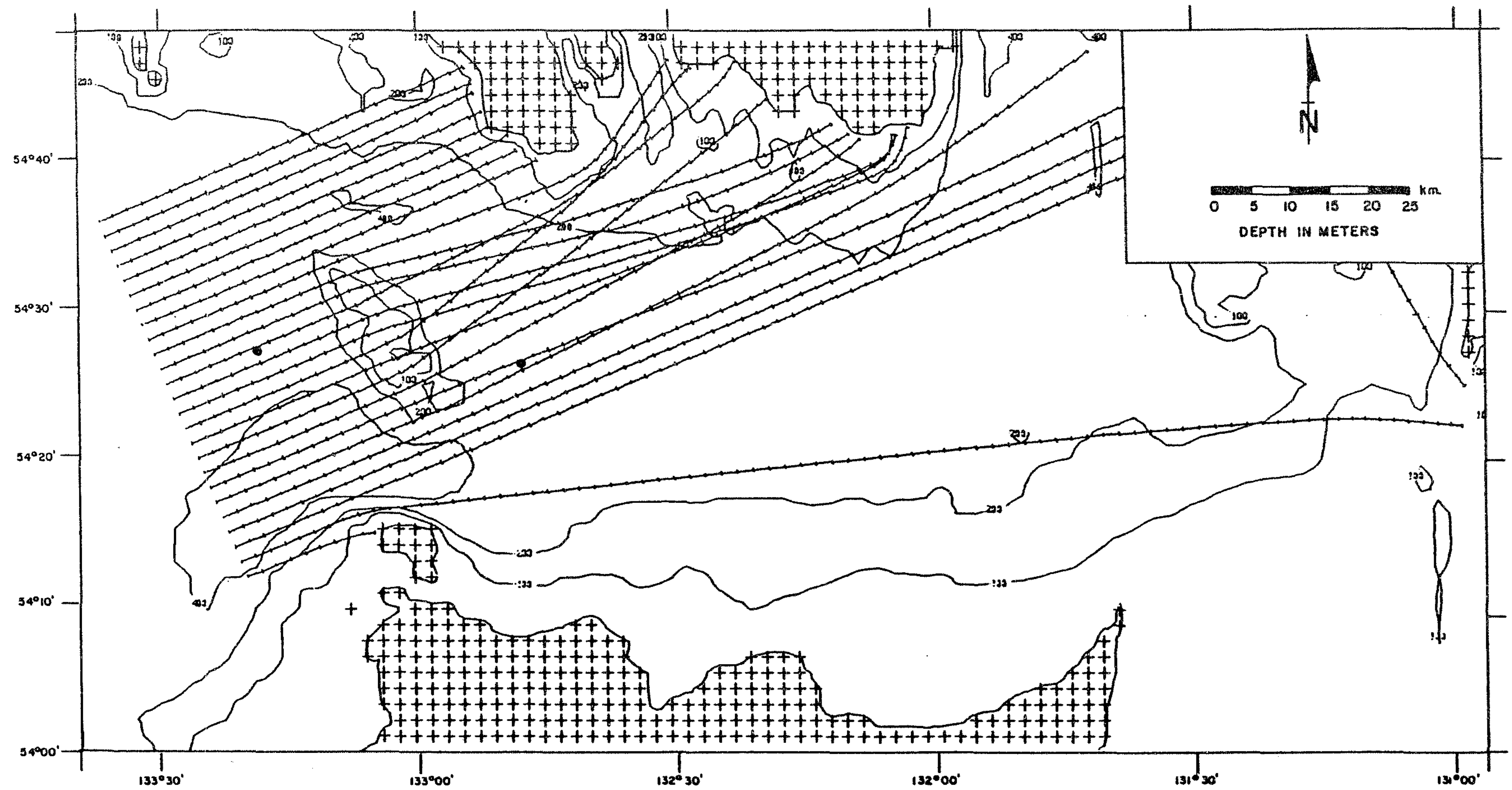

Fig. 3.4 c Comparison of 16 s wave ray patterns over Learmonth Bank for WSW swell.

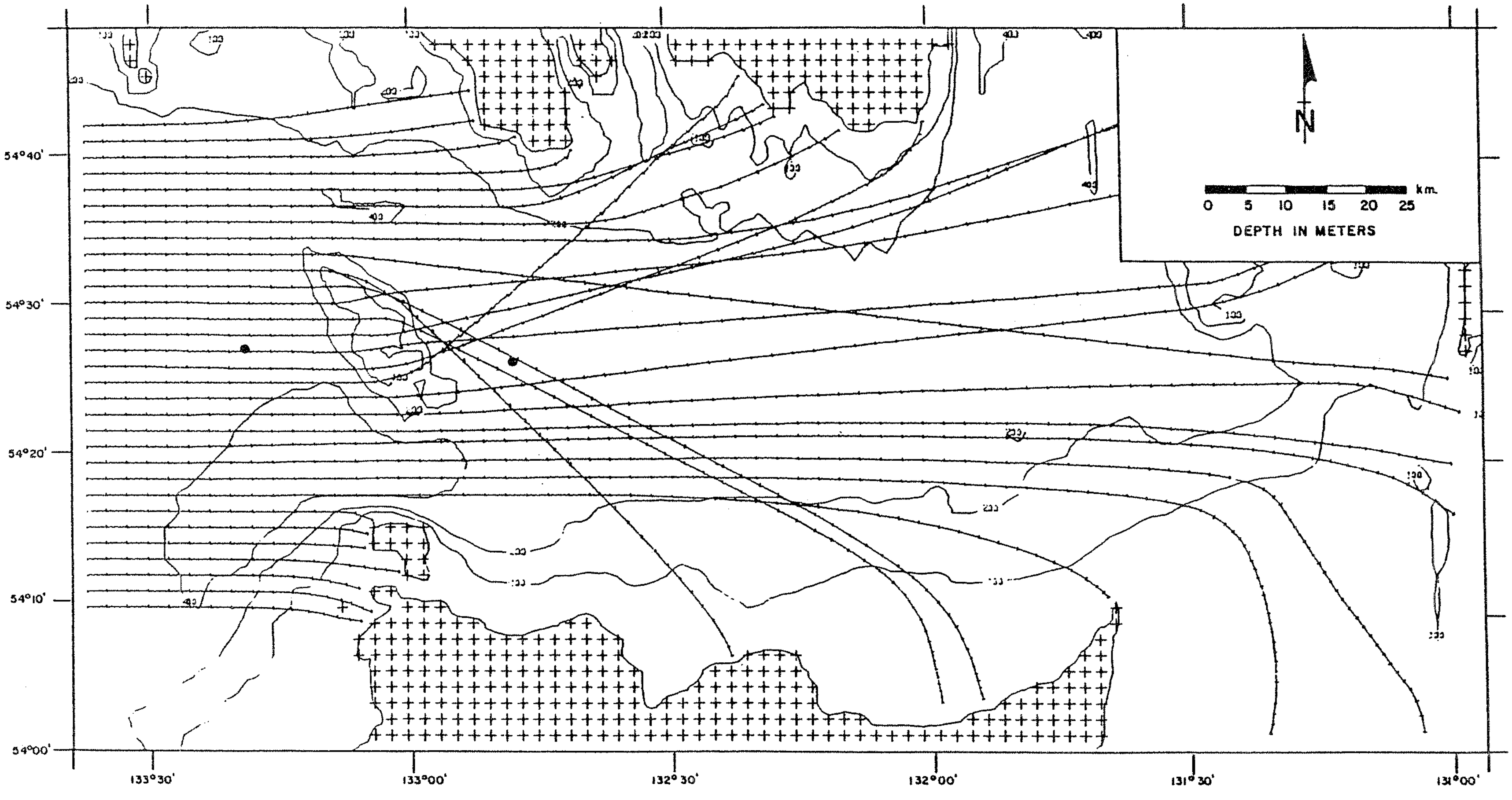

Fig. 3.5a Comparison of westerly wave ray patterns over Learmonth Bank for an 18.3 s wave period.

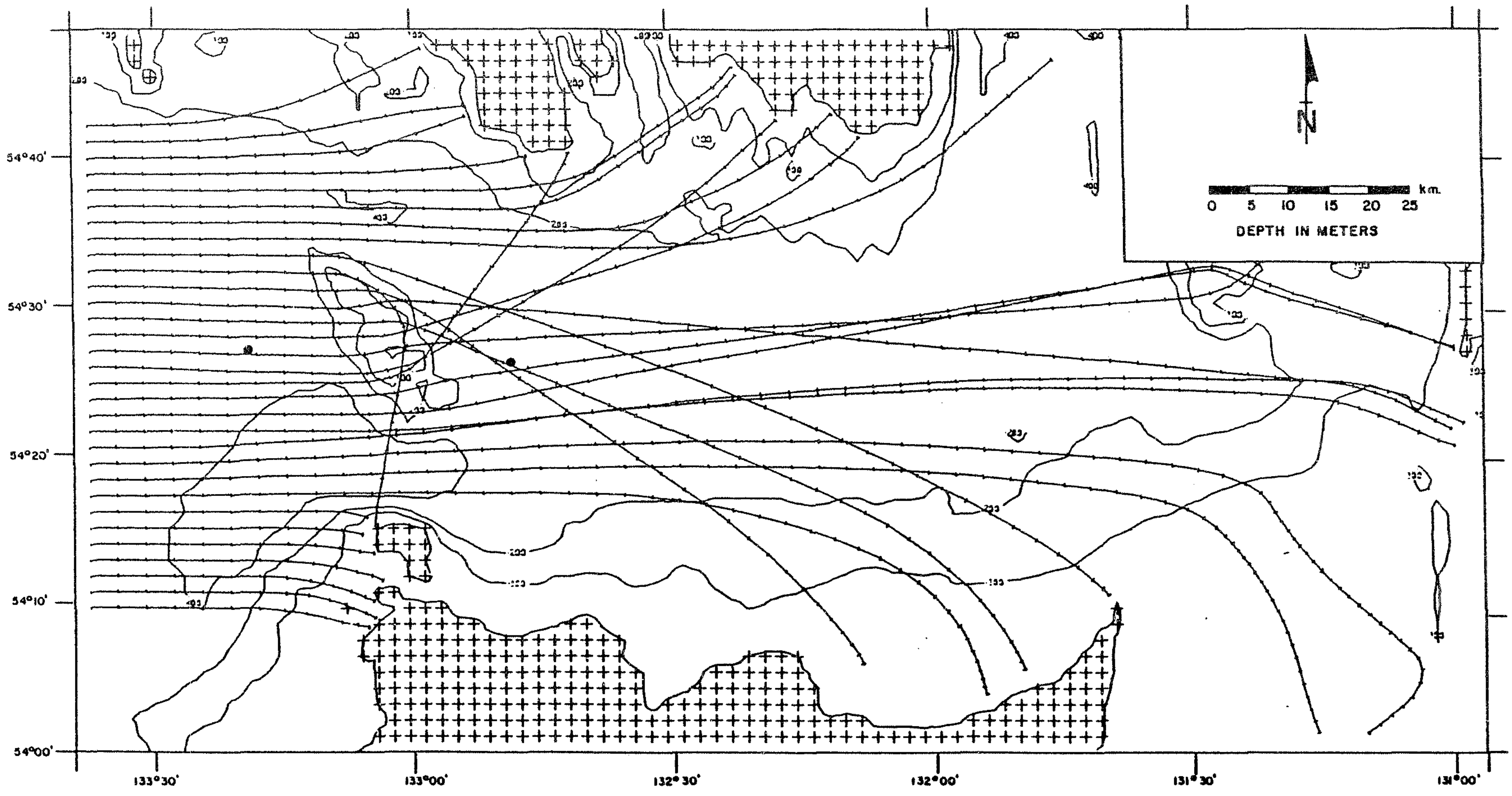

Fig. 3.5 b Comparison of westerly wave ray patterns over Learmonth Bank for a 21.3 s wave period.

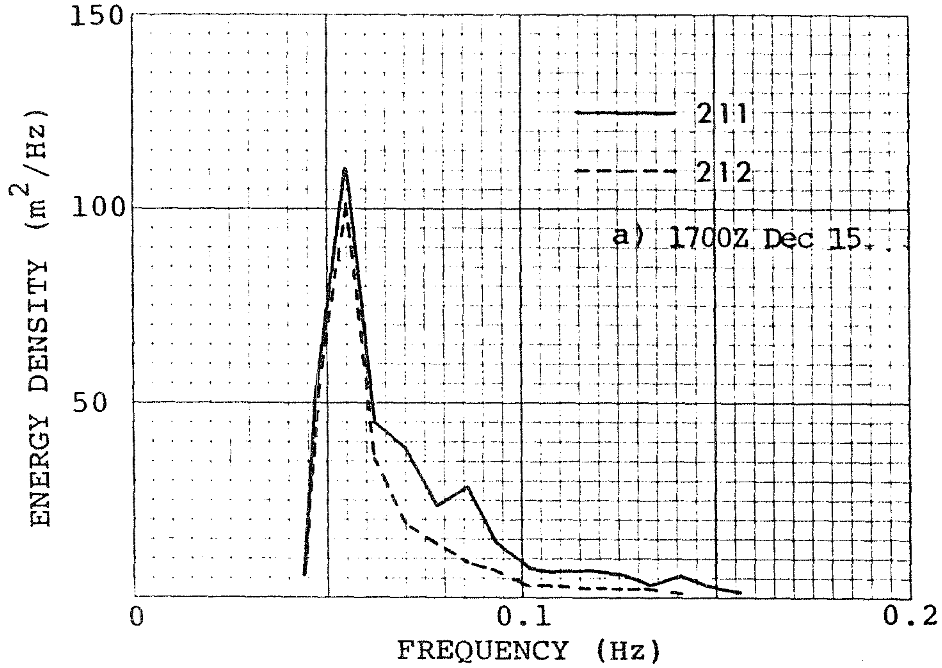

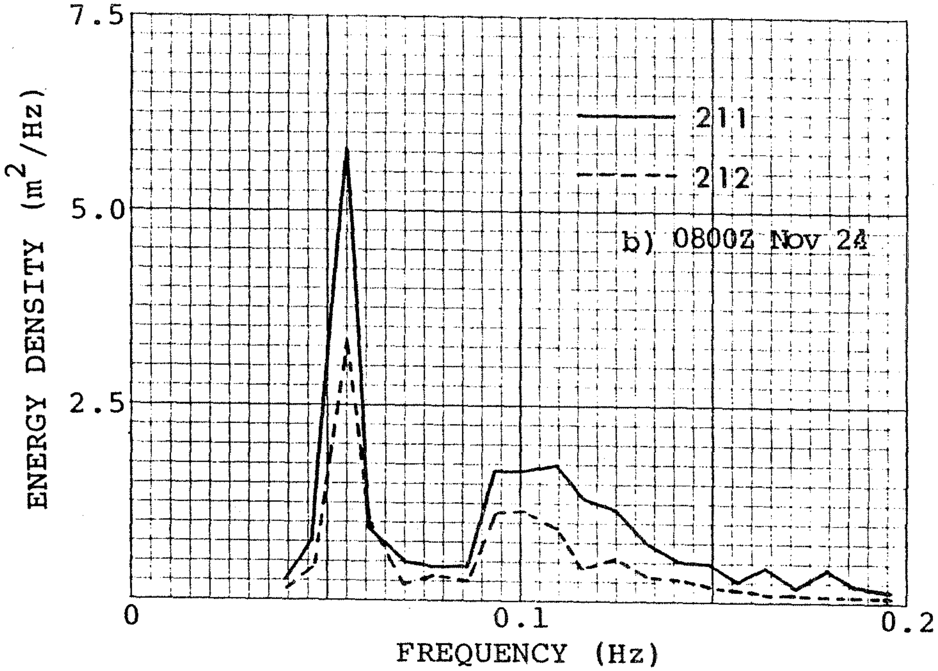

Fig. 3.6 Comparison of wave spectra for Langara West (211) and Langara East (212), located on either side of Learmonth Bank.

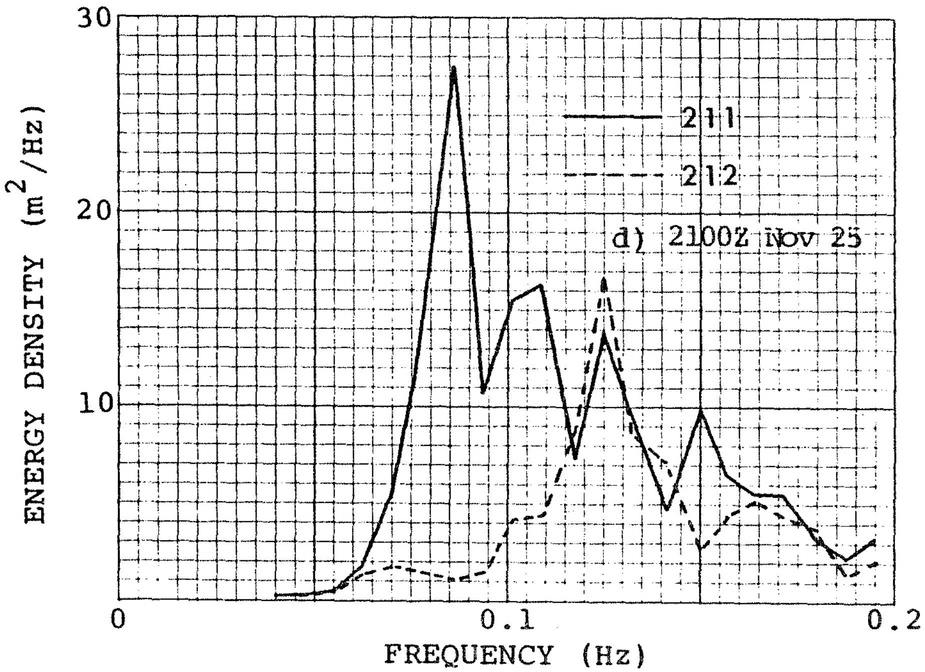

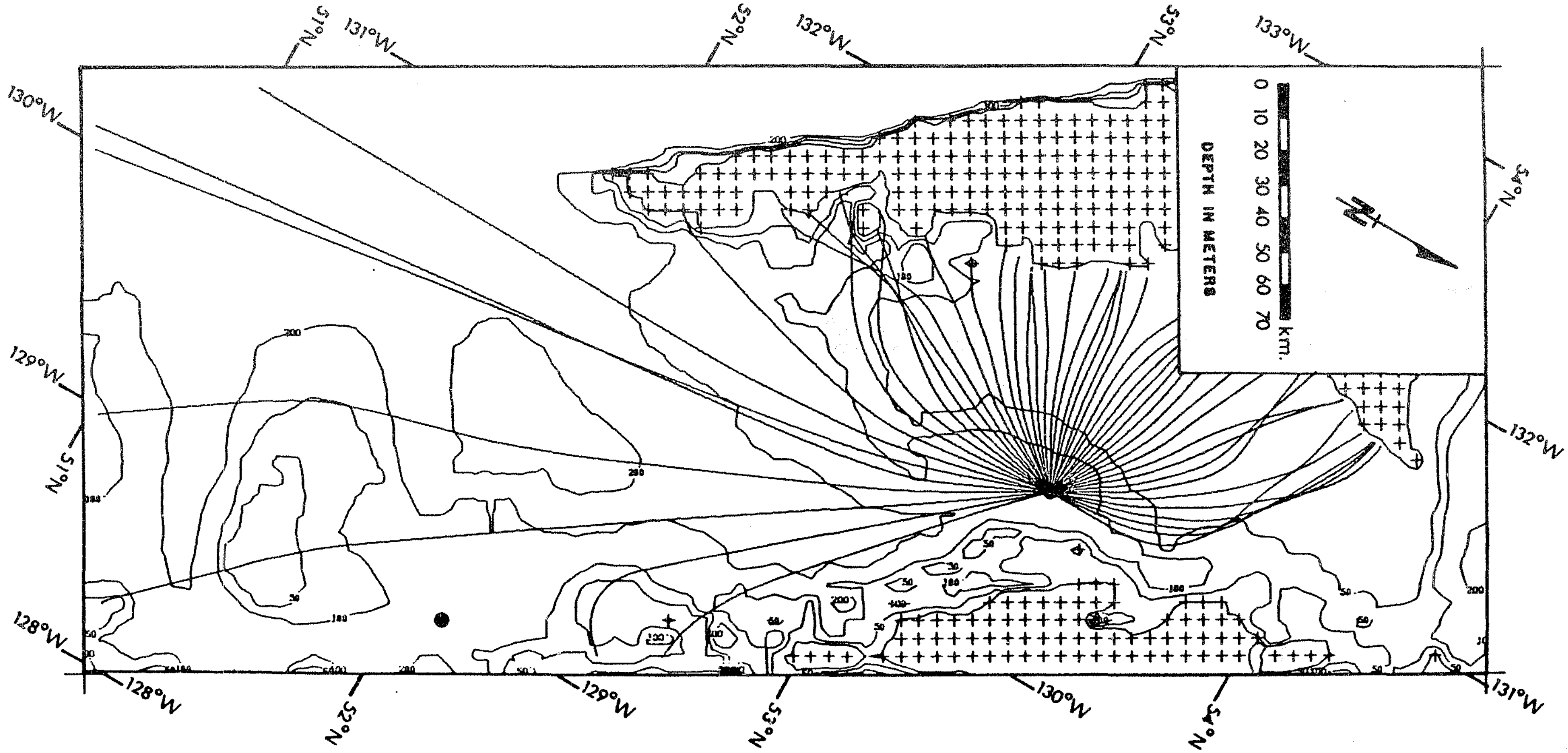

Fig. 3.7 Reverse ray refraction diagram for 16 s waves at Bonilla Island (Station 213).

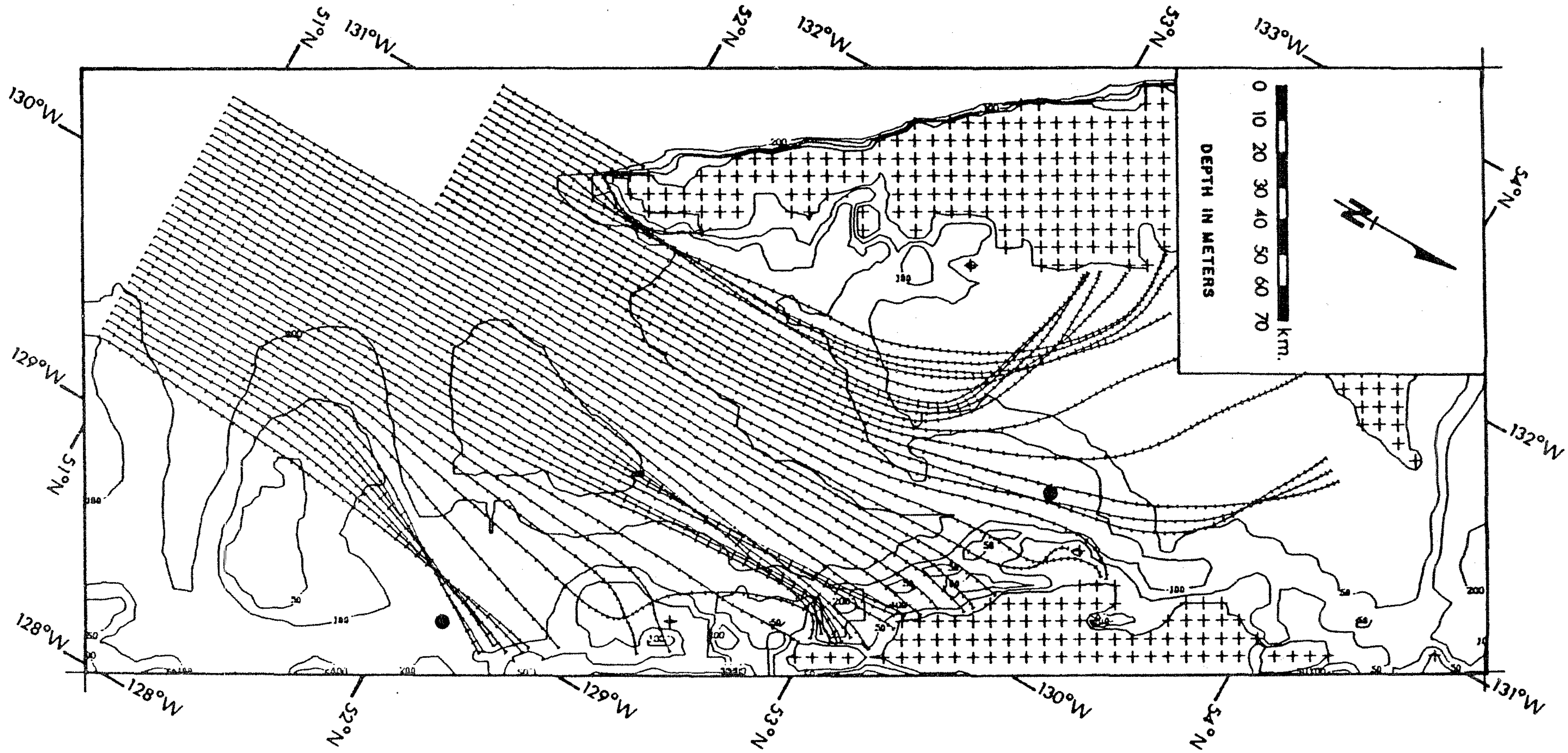

Fig. 3.8a Forward ray refraction diagrams for Queen Charlotte Sound - Hecate Strait for 16 s waves from S.

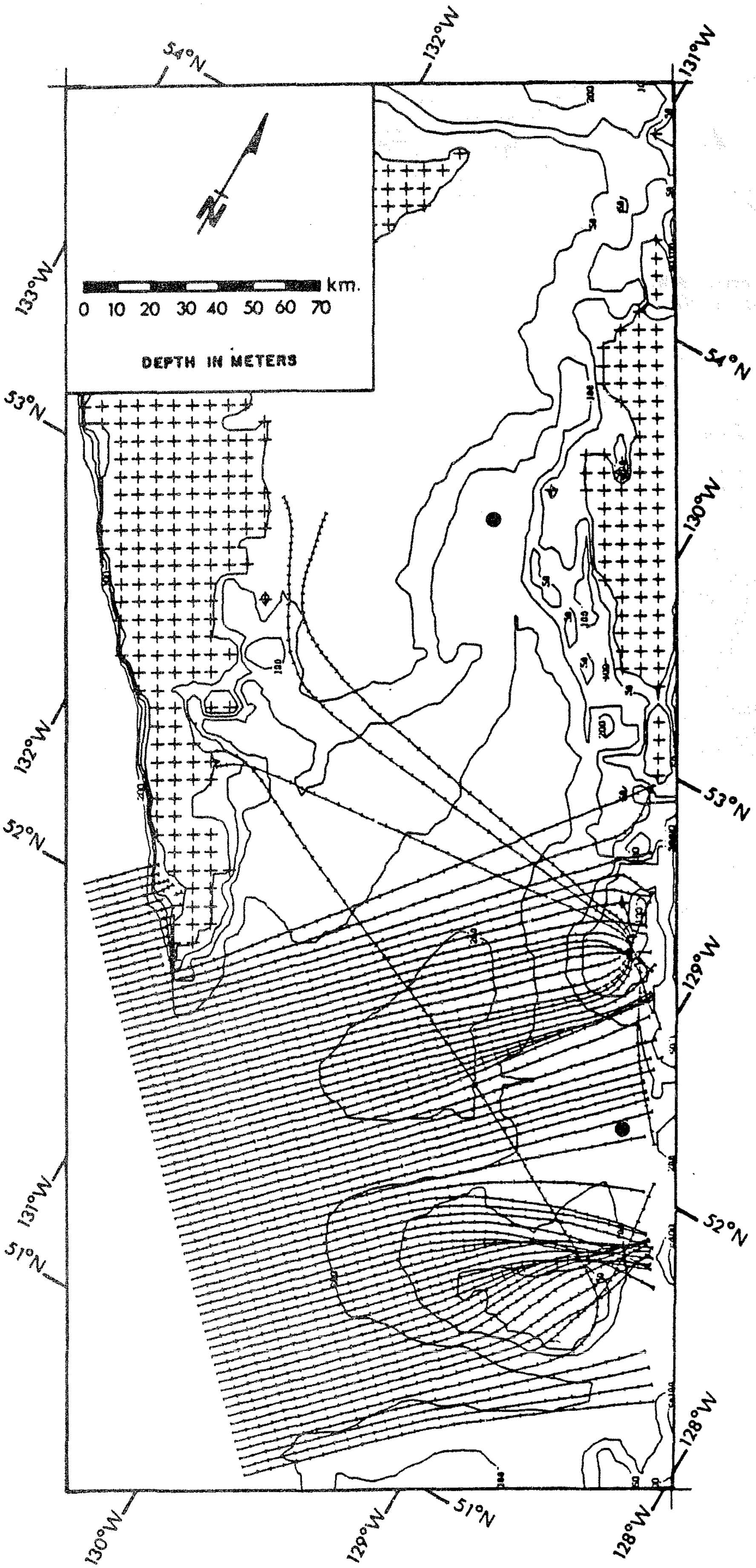

Fig. 3.8b As in Fig. 3.8a but for 16s waves from SW.

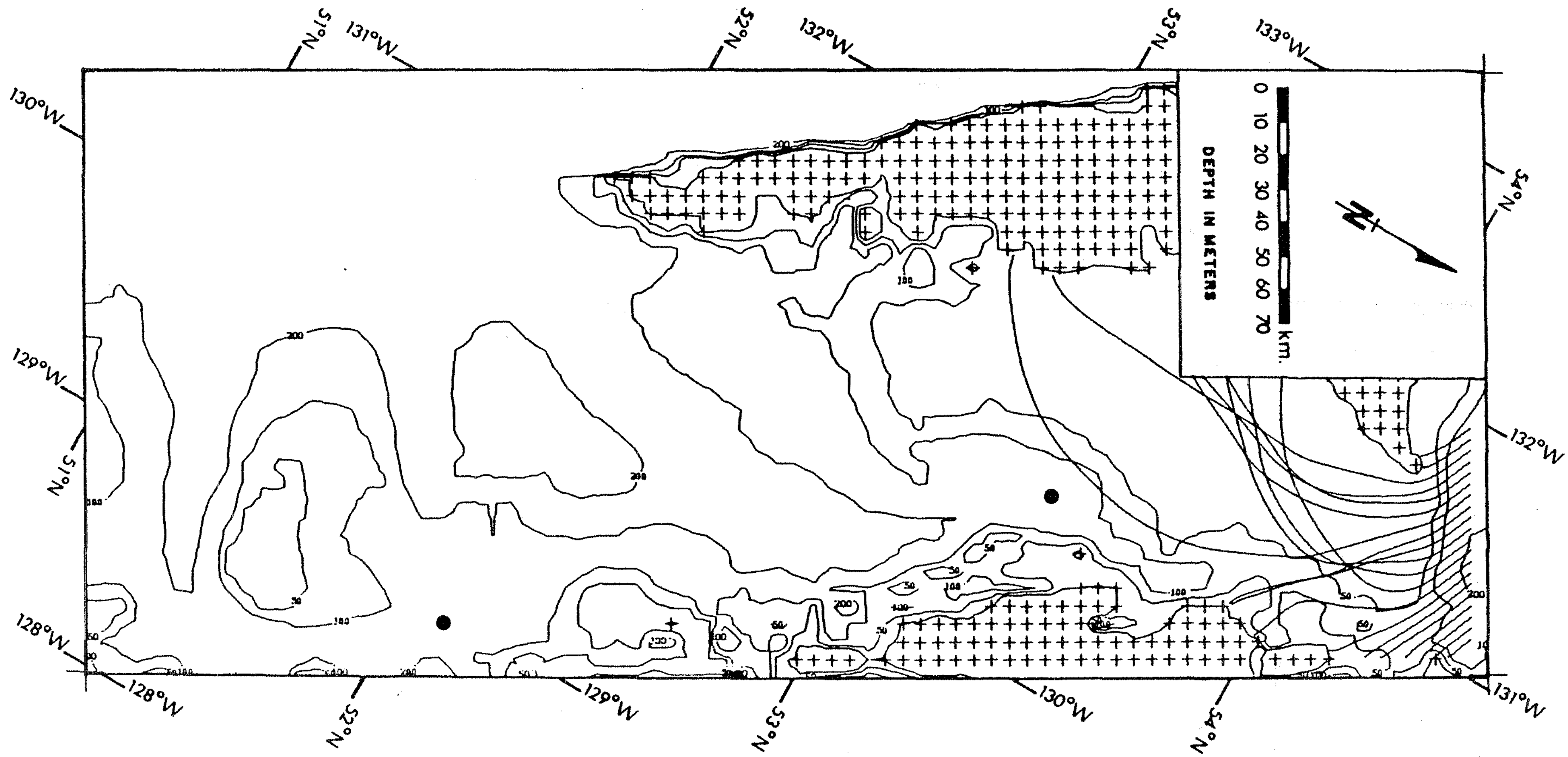

Fig. 3.9 Forward ray refraction diagram for 16 s waves originating in Dixon Entrance.

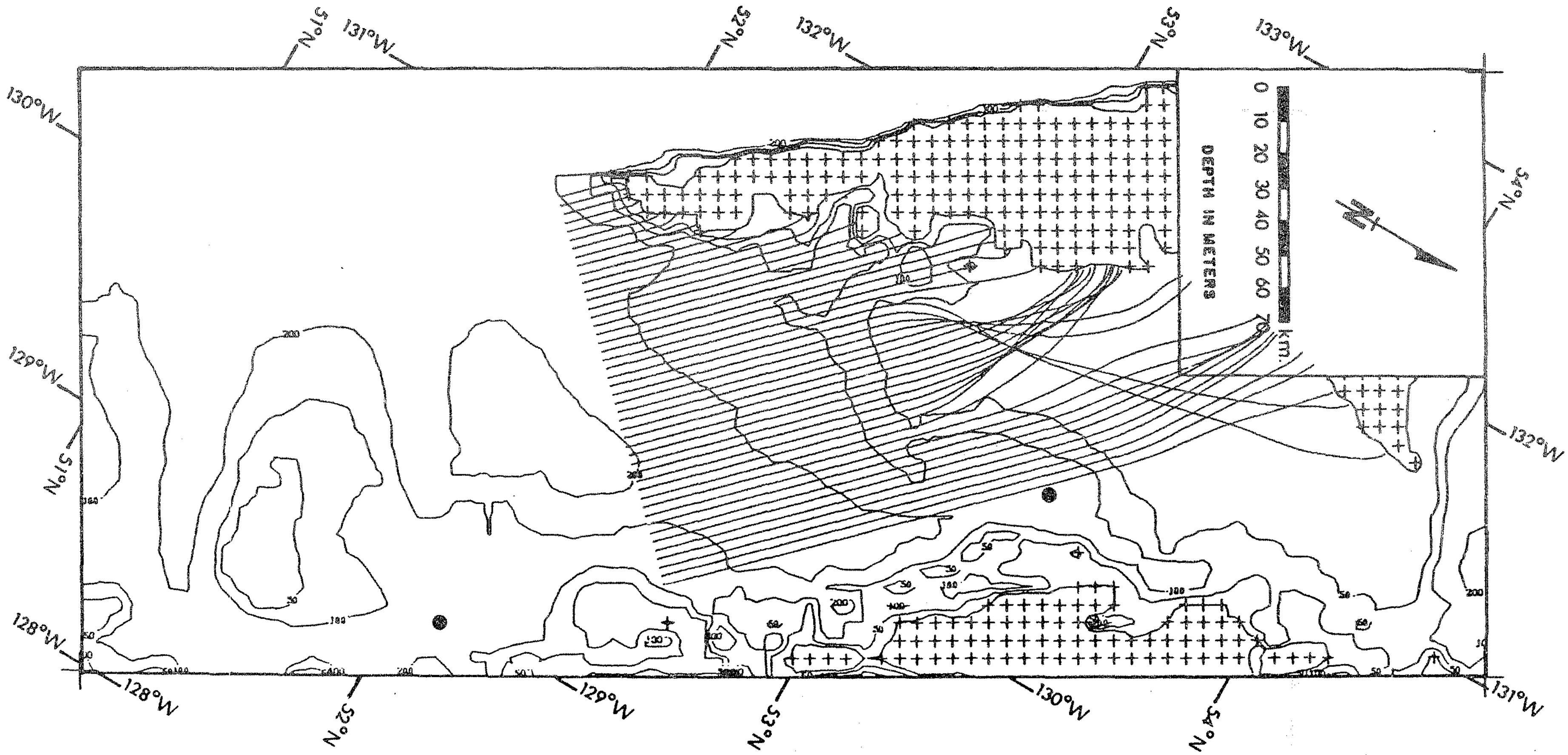

Fig. 3.10 Forward ray refraction diagram for Hecate Strait for SE 10 s waves originating in Queen Charlotte Sound.

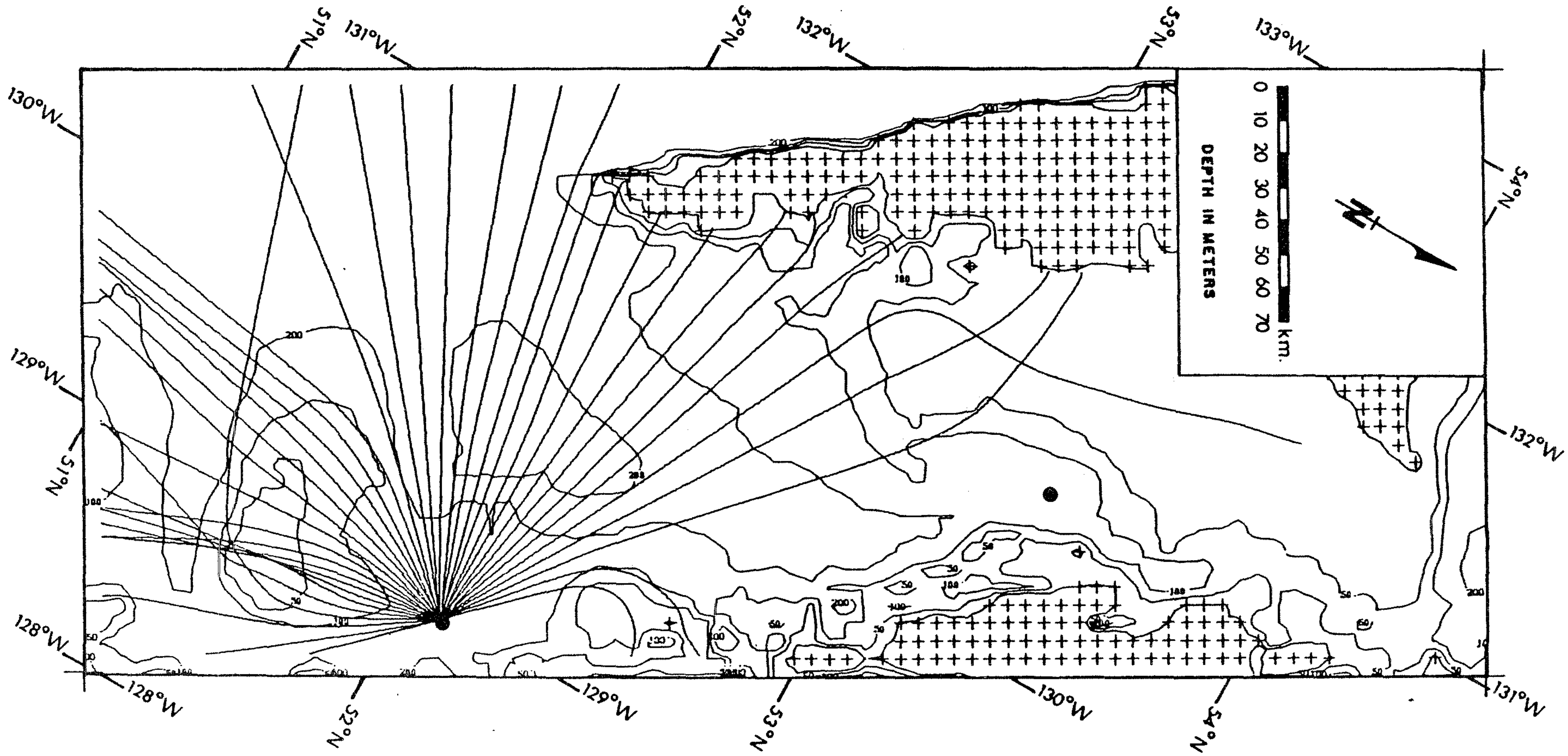

Fig. 3.11 Reverse ray refraction diagram for 16 s waves at McInnes Island (Station 214).

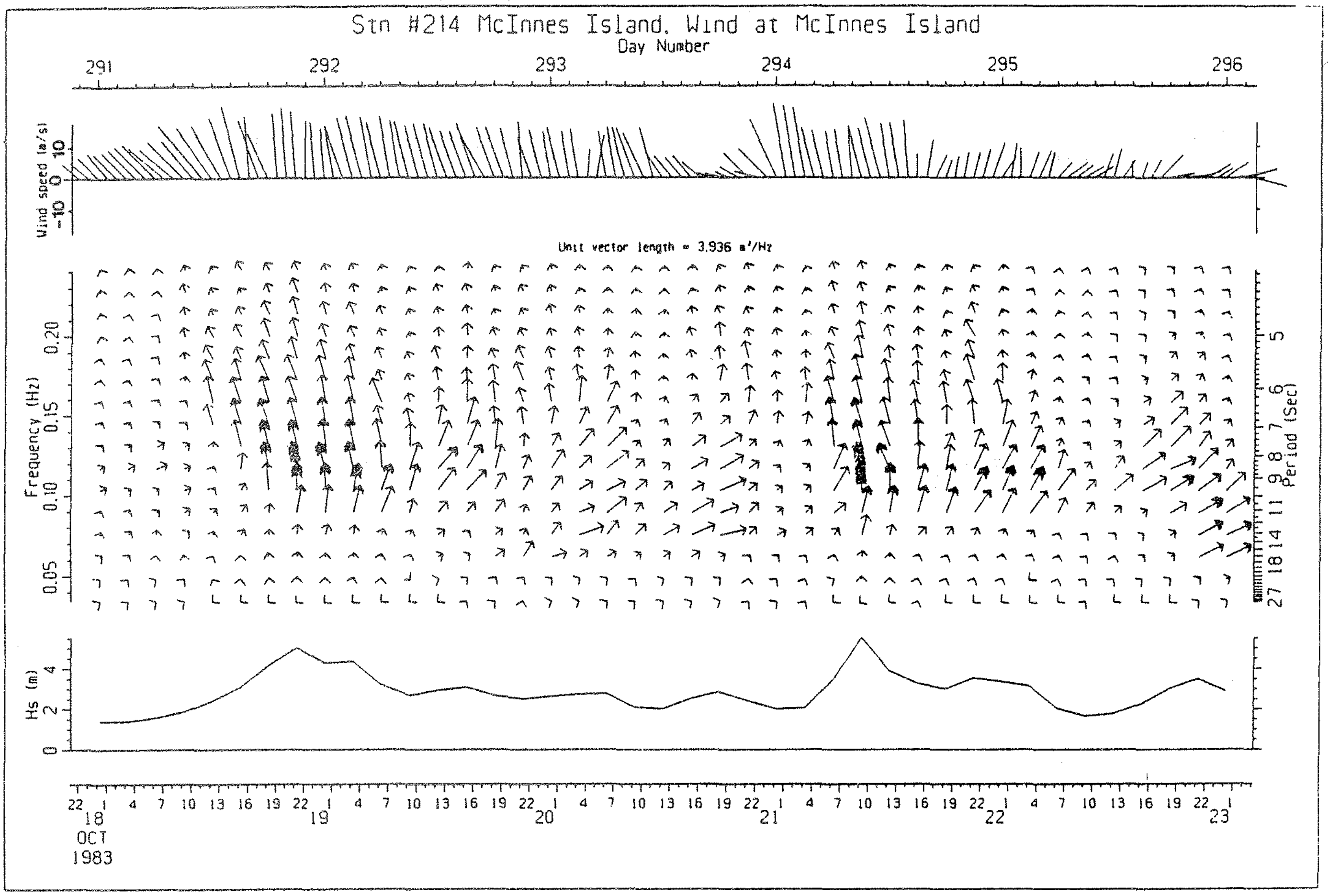

Fig. 3.12 Time series of hourly wind and three-hourly wave conditions at McInnes Island. Time axes are given in terms of calendar date (below) or cumulative day number (at the top). Vector direction is towards the direction of motion, with true north at the top of the page. Wind vector lengths are referred to the scale on the left hand side of the plot. Wave direction vectors feature multiple arrowheads. The spectral density value for a unit vector length given above the plot corresponds to a single-headed vector of maximal length. Each additional arrowhead indicates another multiple of that unit length.

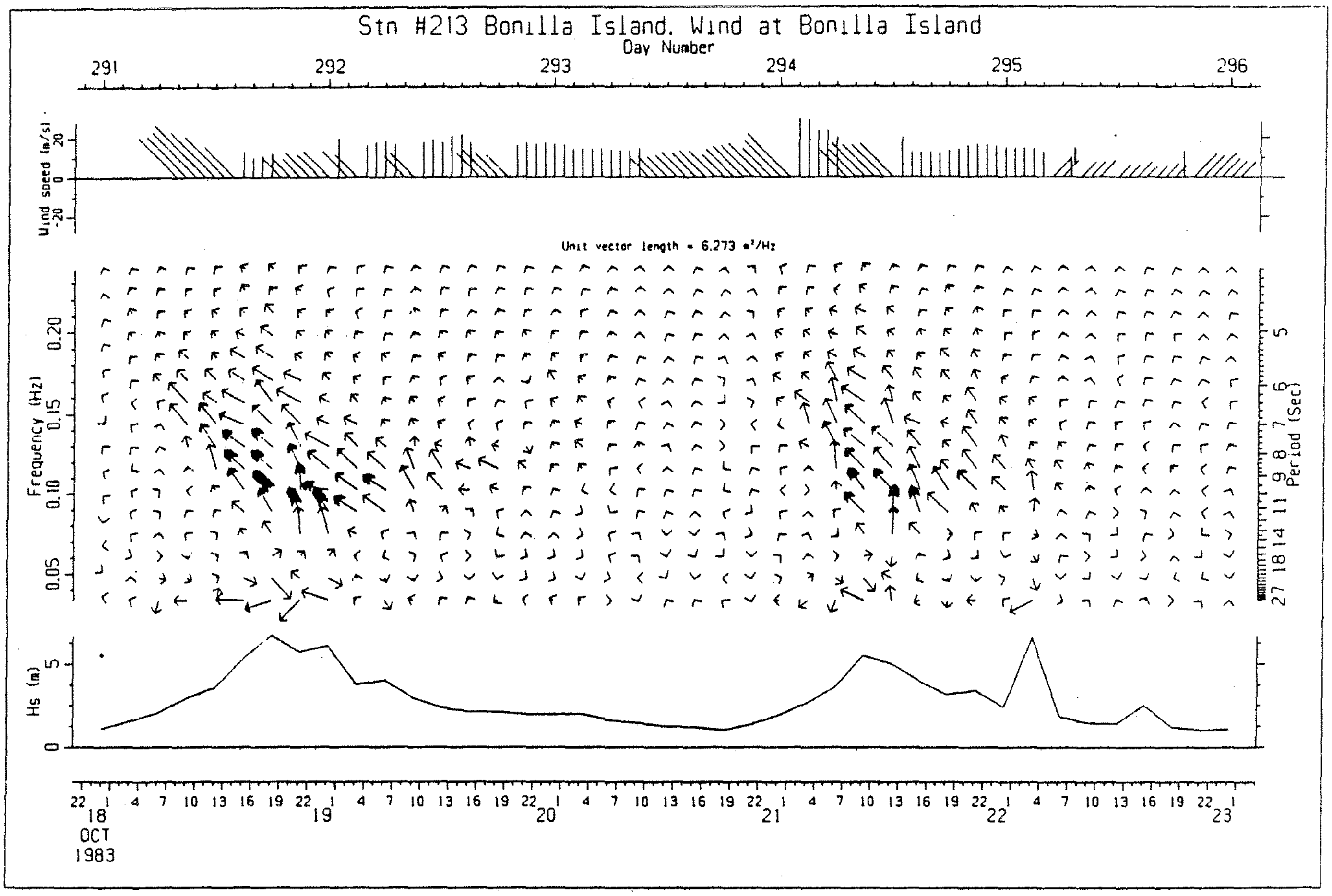

Fig. 3.13 Time series of hourly wind and three-hourly wave conditions at Bonilla Island. Time axes are given in terms of calendar date (below) or cumulative day number (at the top). Vector direction is towards the direction of motion, with true north at the top of the page. Wind vector lengths are referred to the scale on the left hand side of the plot. Wave direction vectors feature multiple arrowheads. The spectral density value for a unit vector length given above the plot corresponds to a single-headed vector of maximal length. Each additional arrowhead indicates another multiple of that unit length.

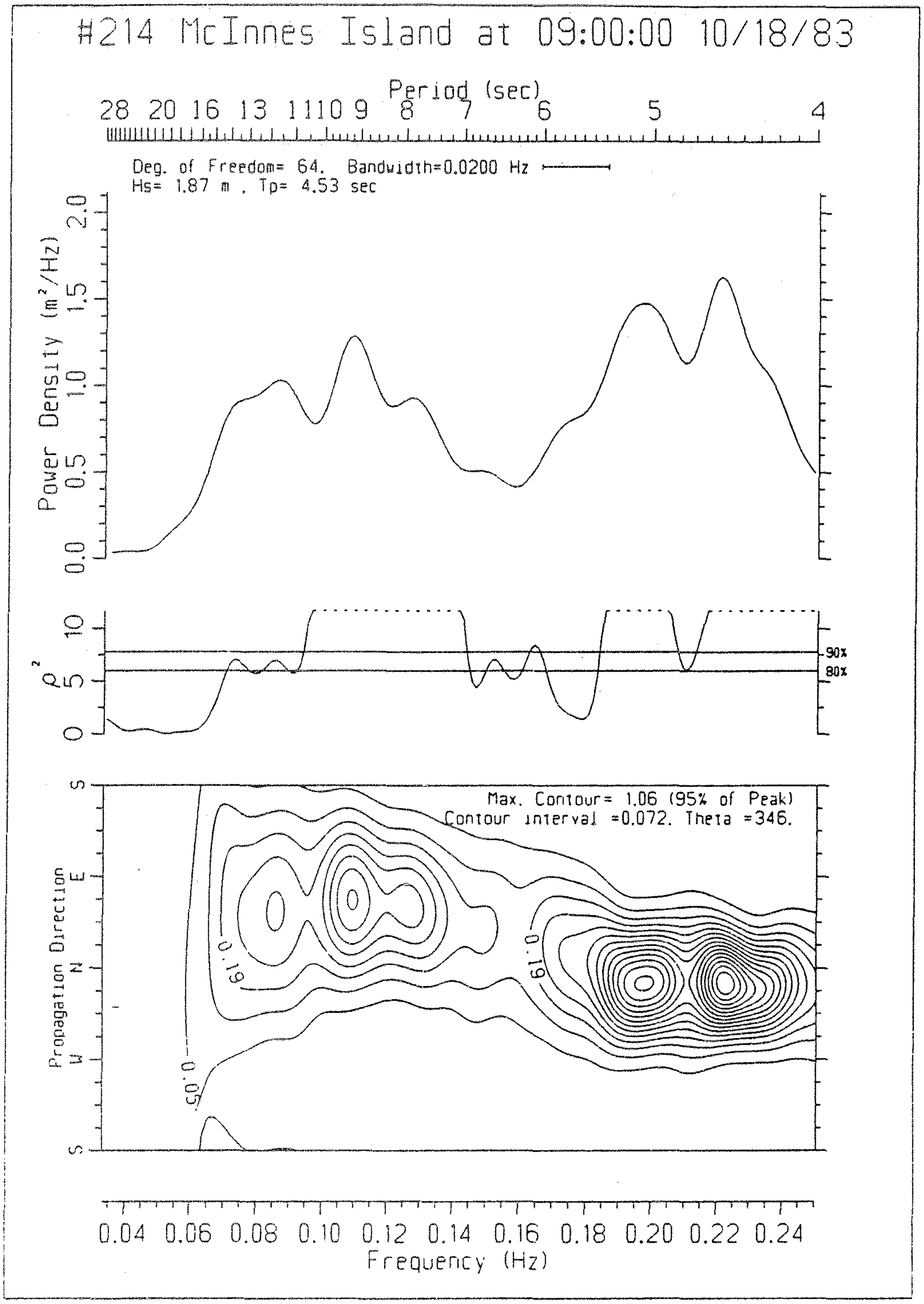

Fig. 3.14 Directional wave spectrum at McInnes Island for the times indicated. The top panel gives the power density; the number of degrees of freedom, the bandwidth, H_s and T_p are also shown. The middle panel shows the value of ρ^2, the error involved in fitting the directional spreading by a cosine-power model, using Long's (1980) method and the 80% and 90% confidence levels. Frequency ranges for which ρ^2 lies above the selected confidence level correspond to poor fits, for which the model should be rejected. The lower panel shows the directional spread of the waves as obtained from the model fitting techniques.

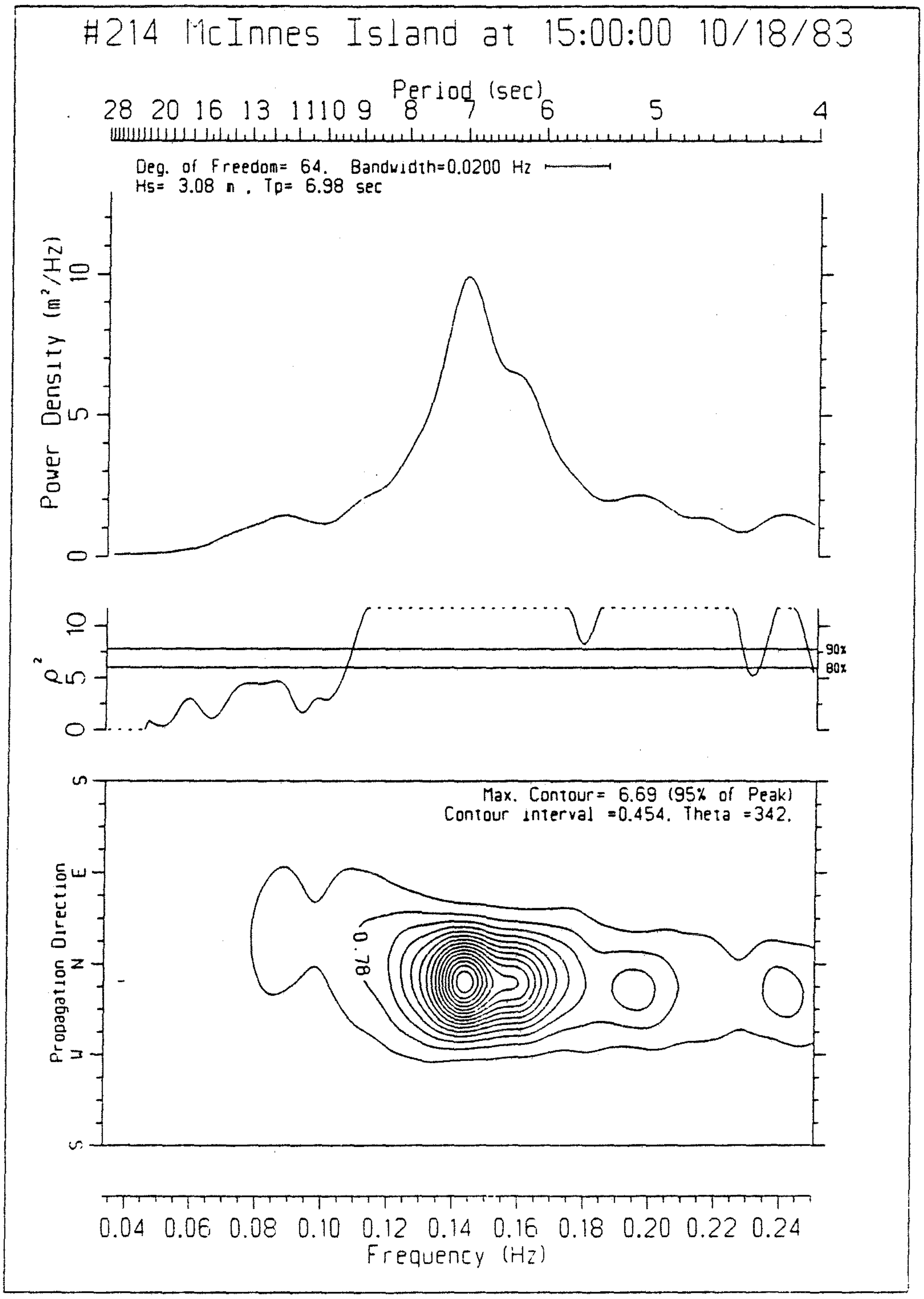

Fig. 3.14 continued

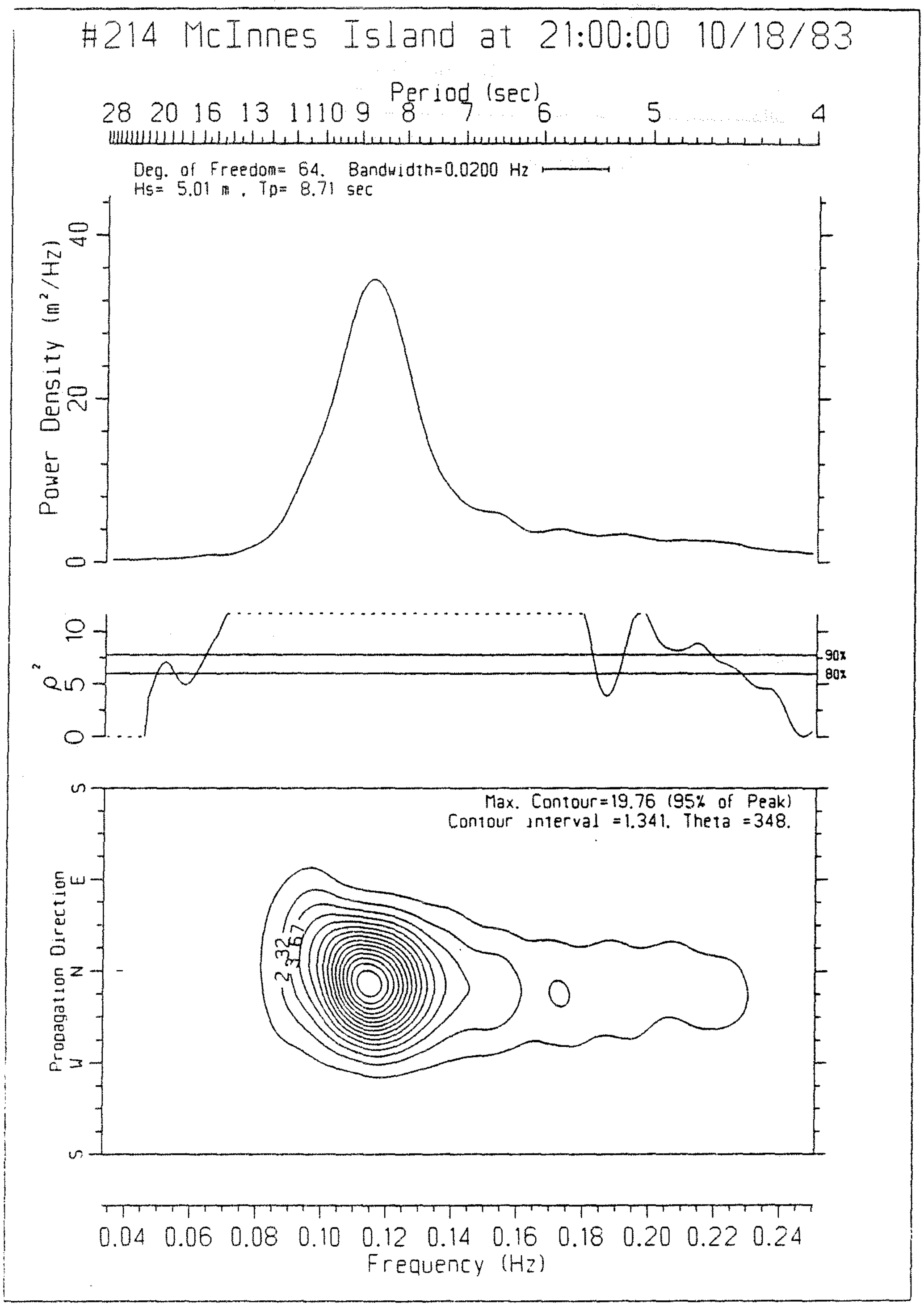

Fig. 3.14 continued

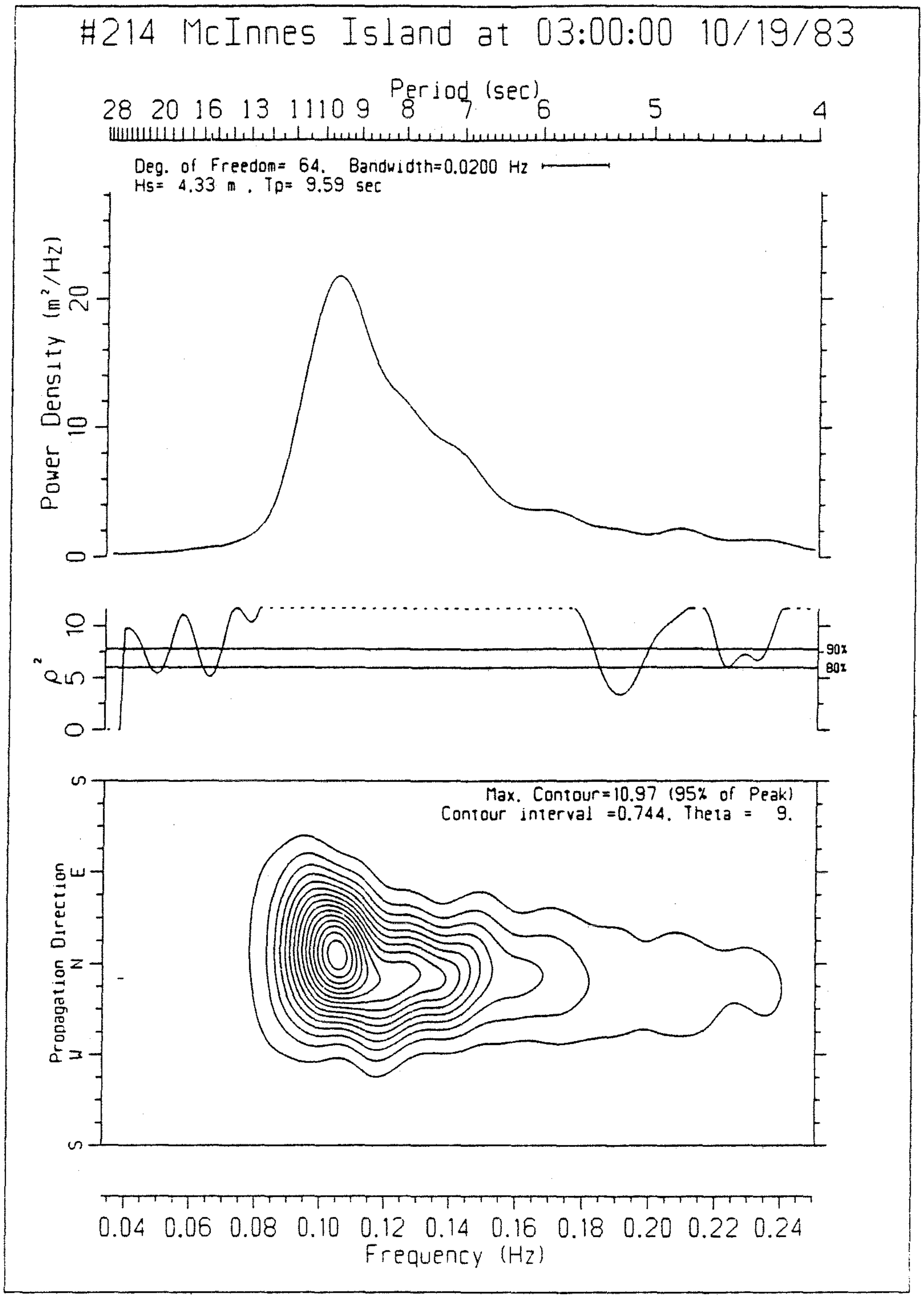

Fig. 3.14 continued

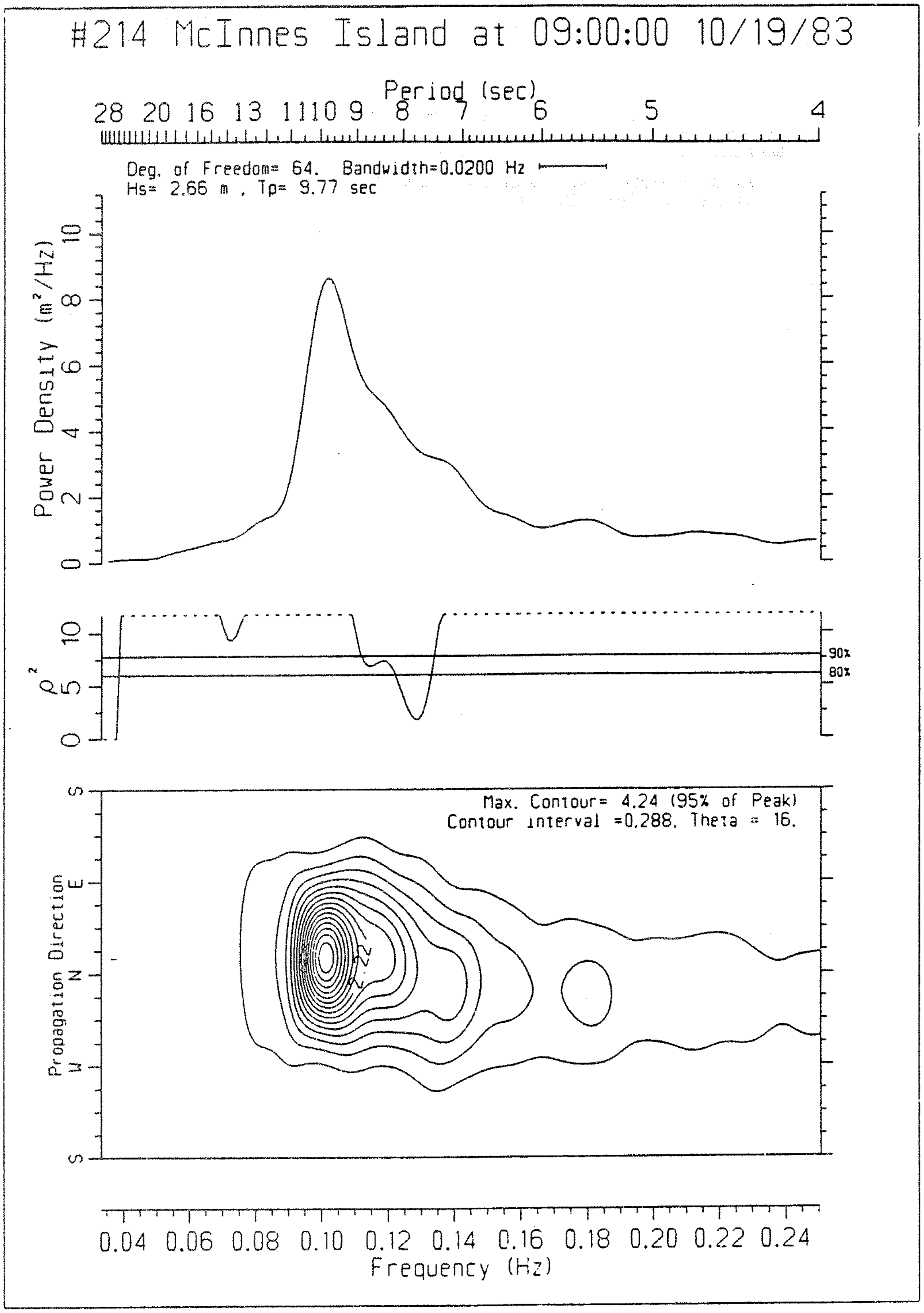

Fig. 3.14 continued

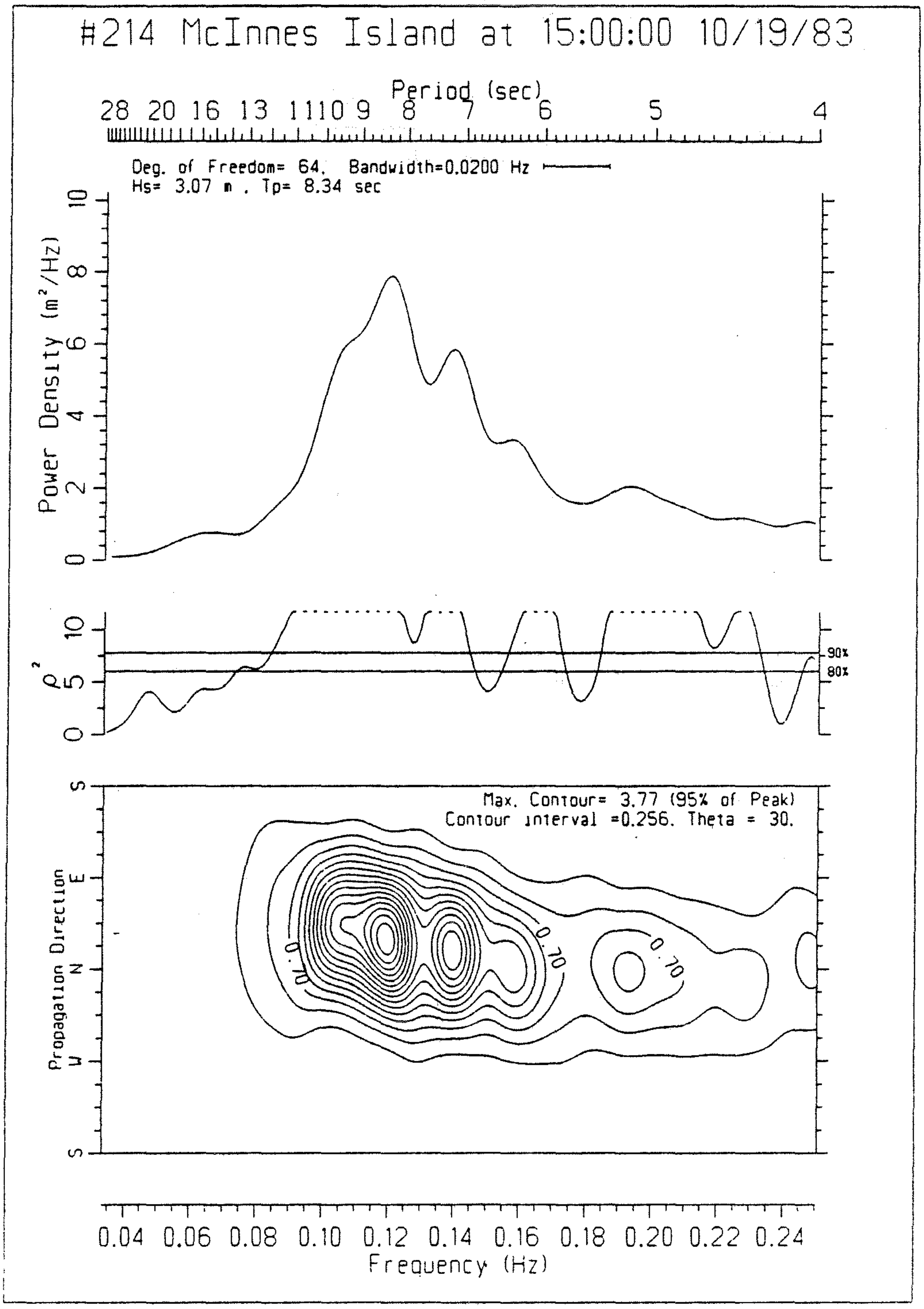

Fig. 3.14 continued

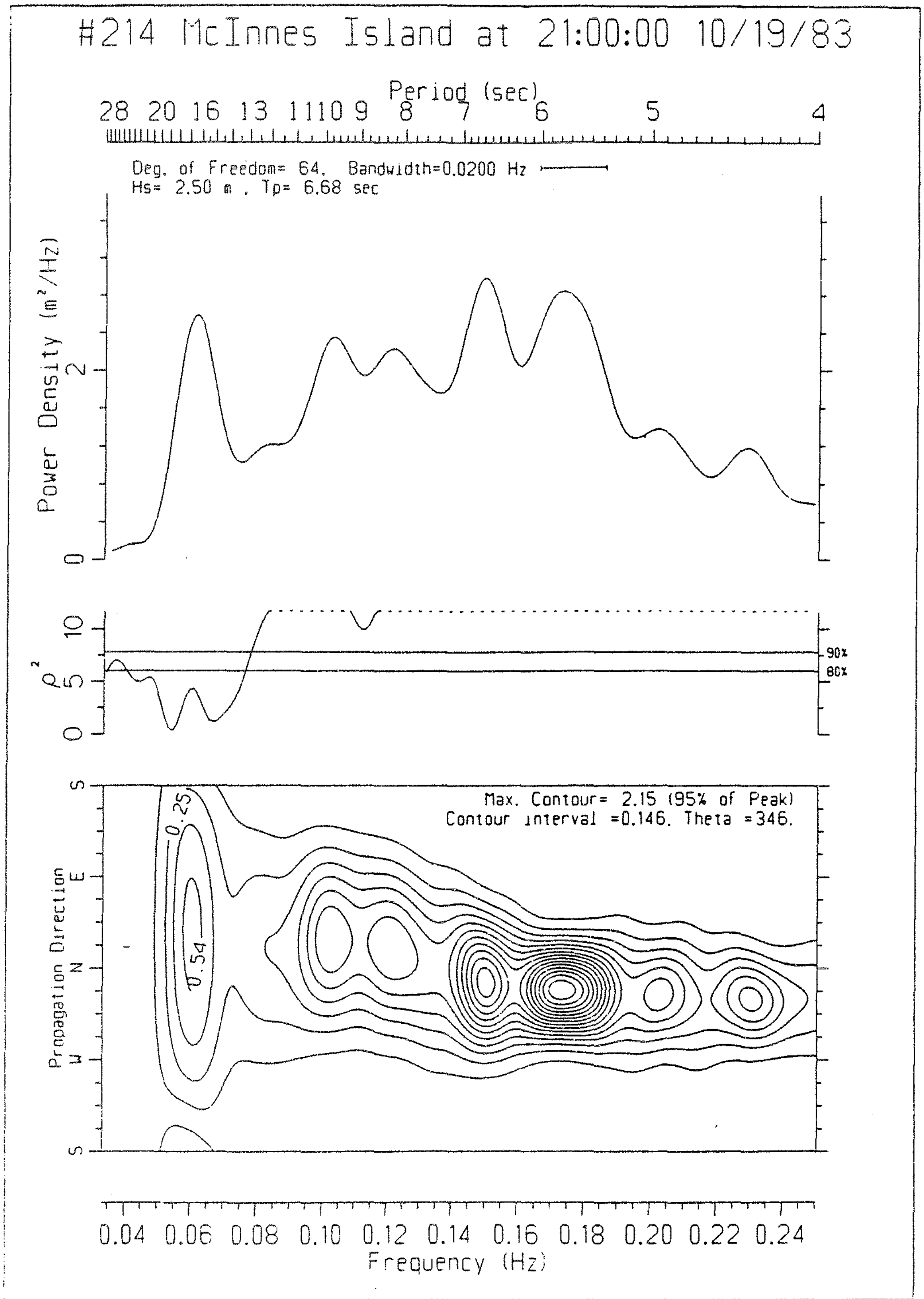

Fig. 3.14 continued

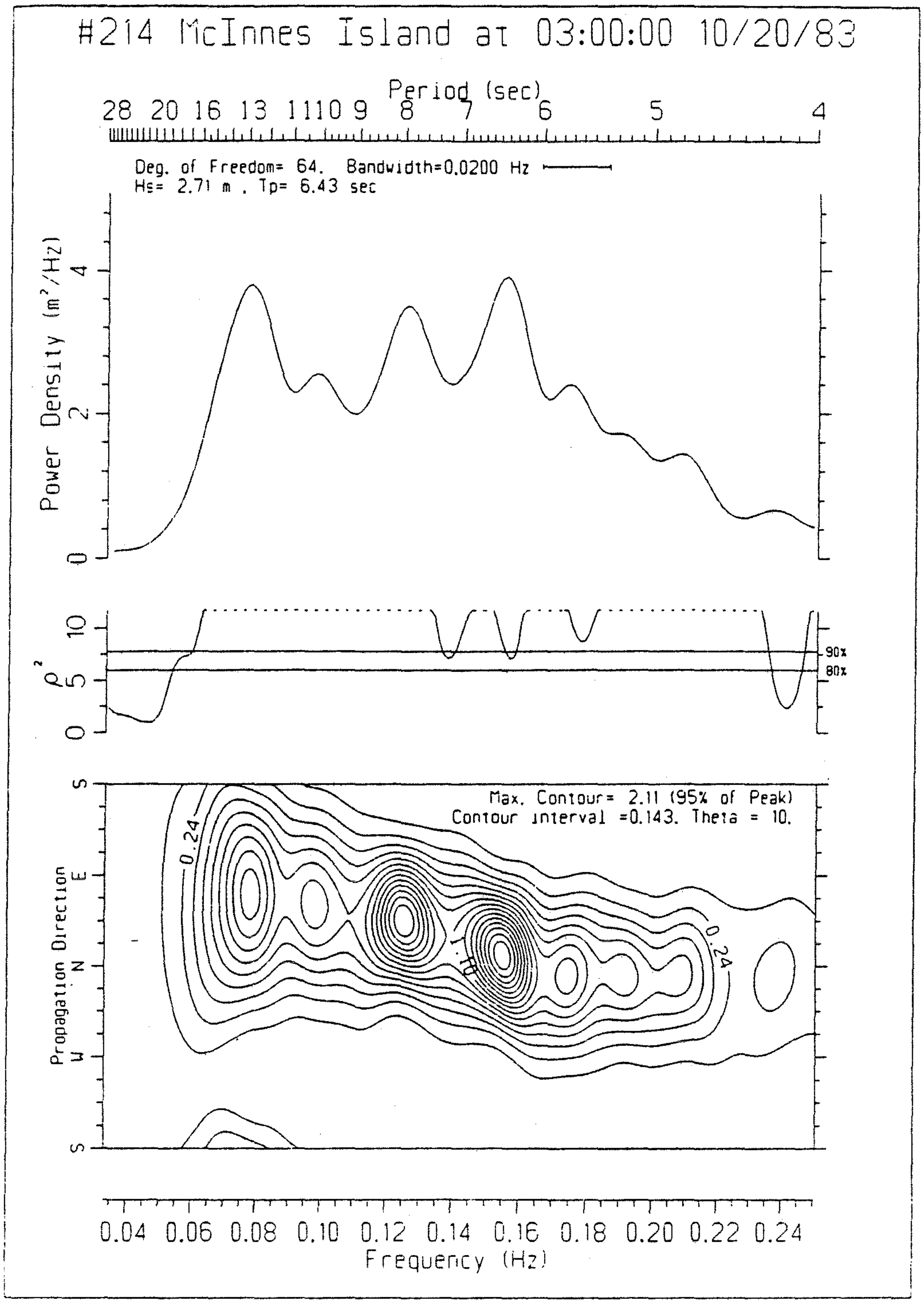

Fig. 3.14 continued

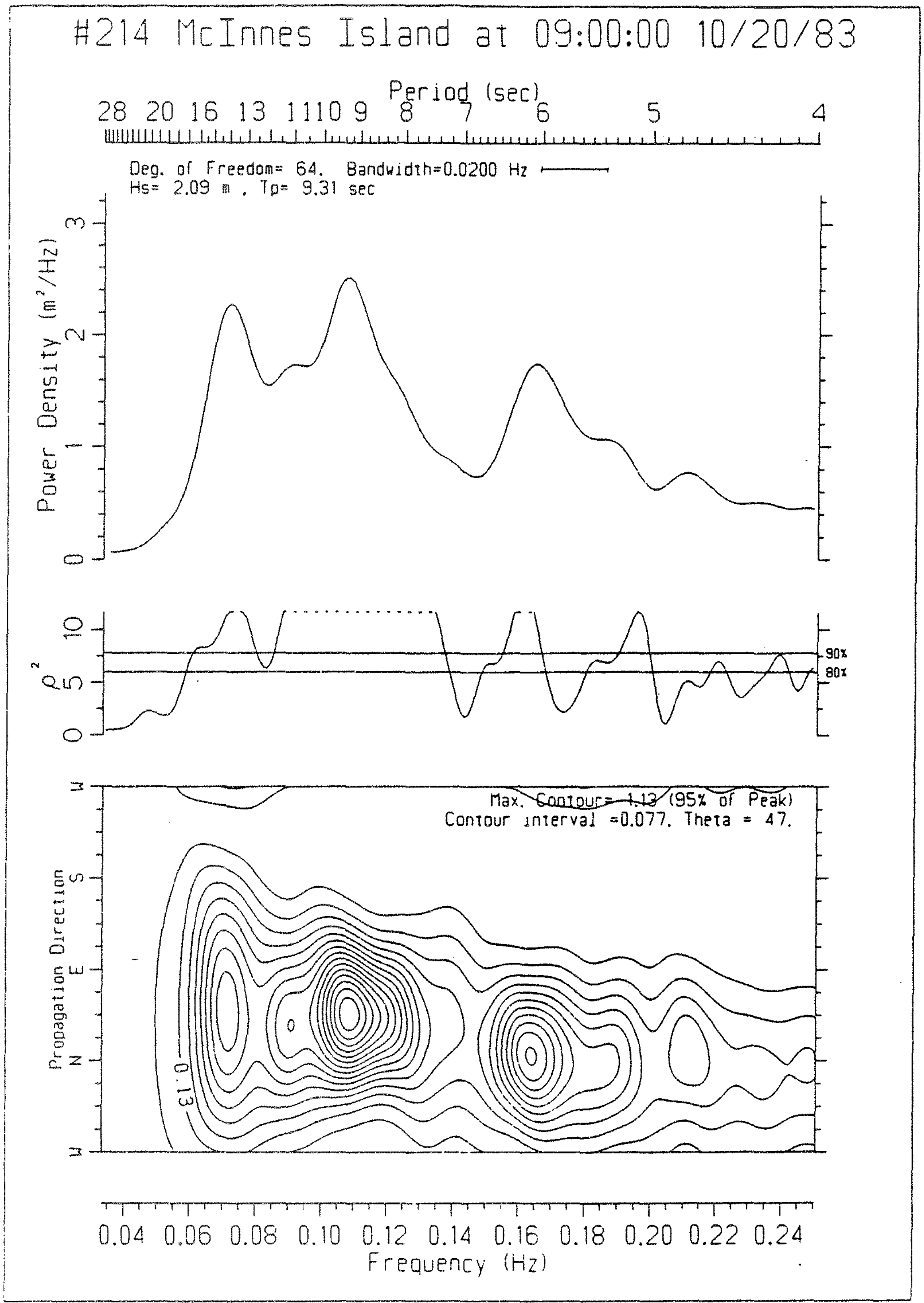

Fig. 3.14 continued

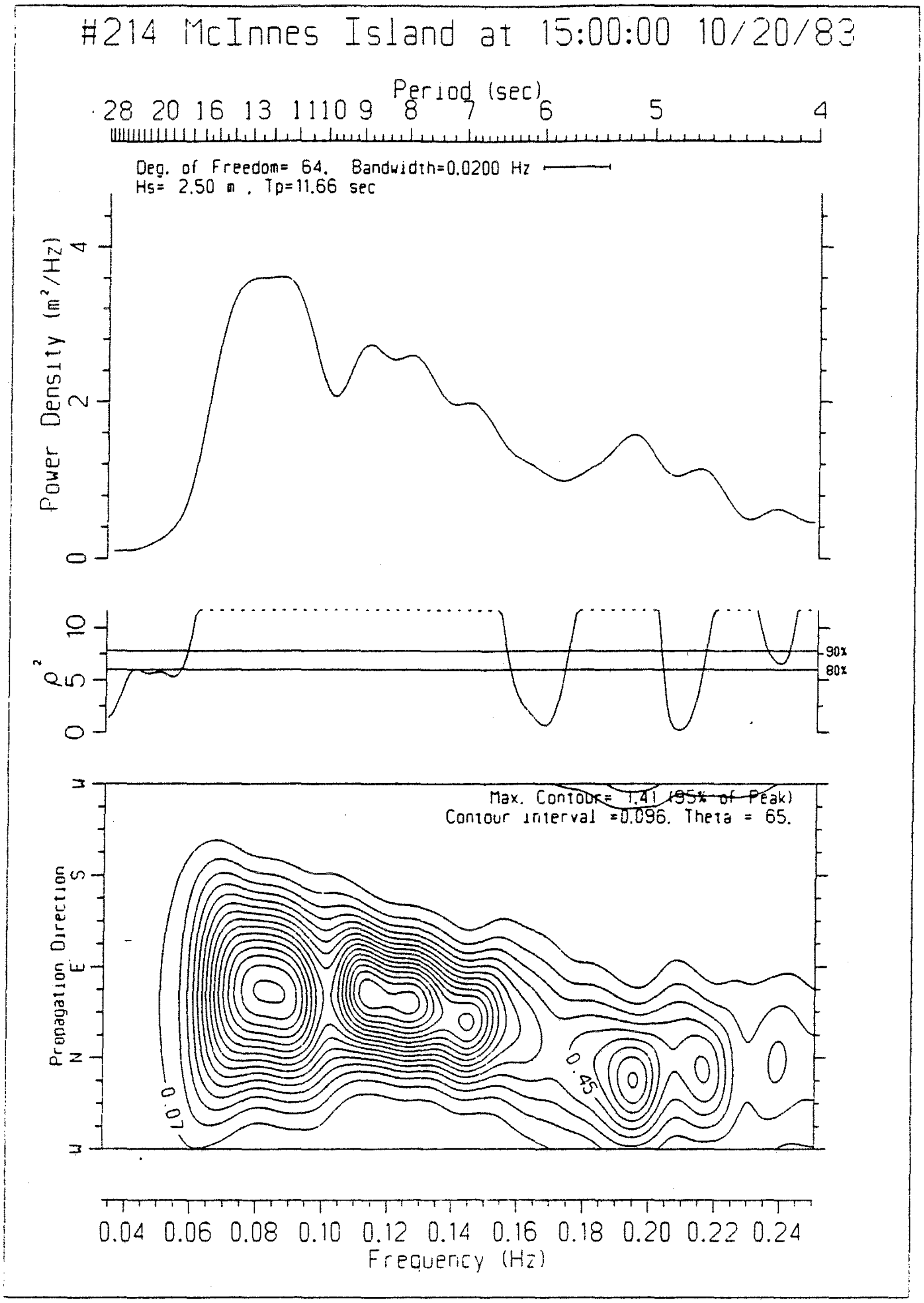

Fig. 3.14 continued

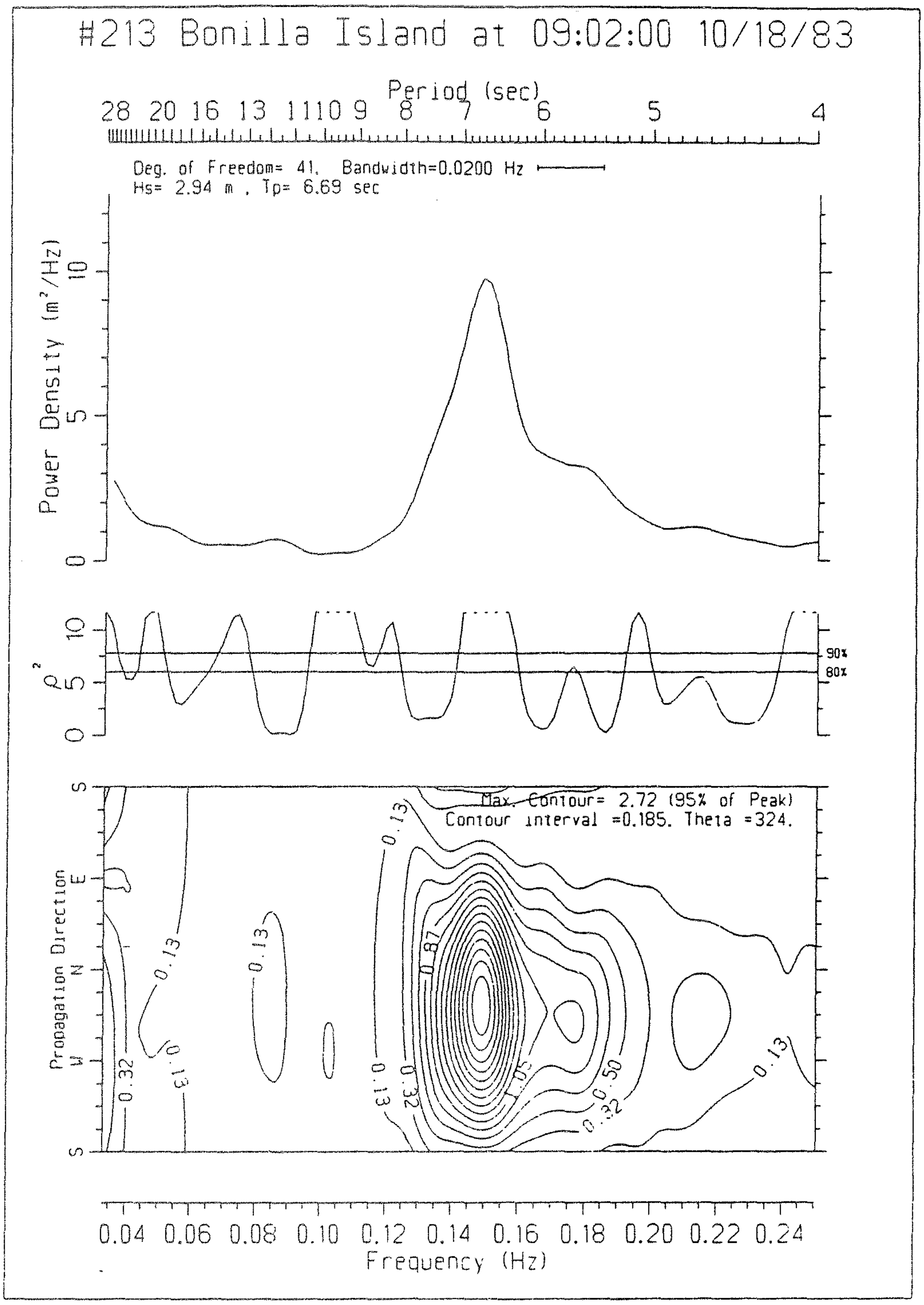

Fig. 3.15 Directional wave spectrum at Bonilla Island for the times indicated. The top panel gives the power density; the number of degrees of freedom, the bandwidth, H_s and T_p are also shown. The middle panel shows the value of ρ^2, the error involved in fitting the directional spreading by a cosine-power model, using Long's (1980) method and the 80% and 90% confidence levels. Frequency ranges for which ρ^2 lies above the selected confidence level correspond to poor fits, for which the model should be rejected. The lower panel shows the directional spread of the waves as obtained from the model fitting techniques.

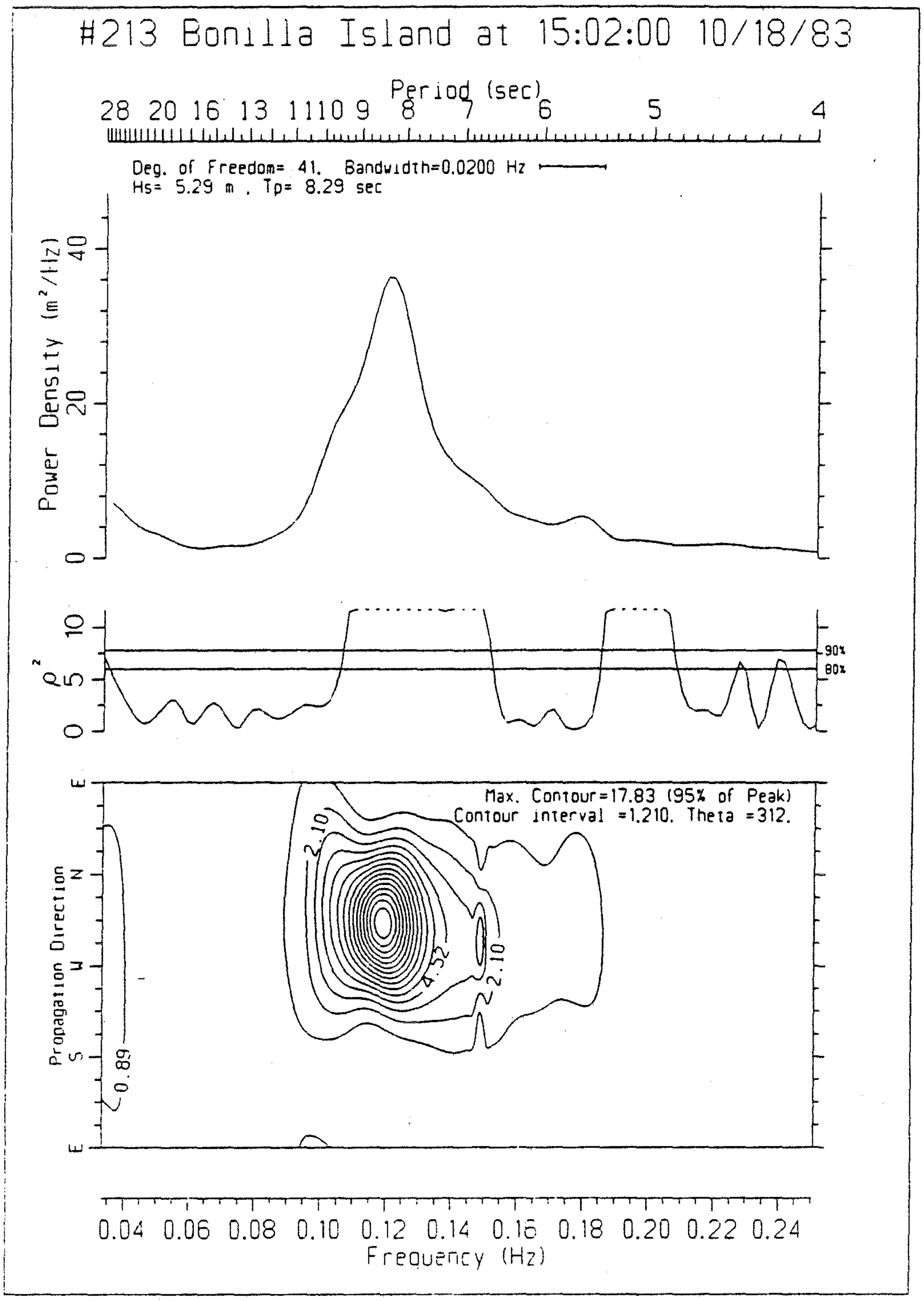

Fig. 3.15 continued

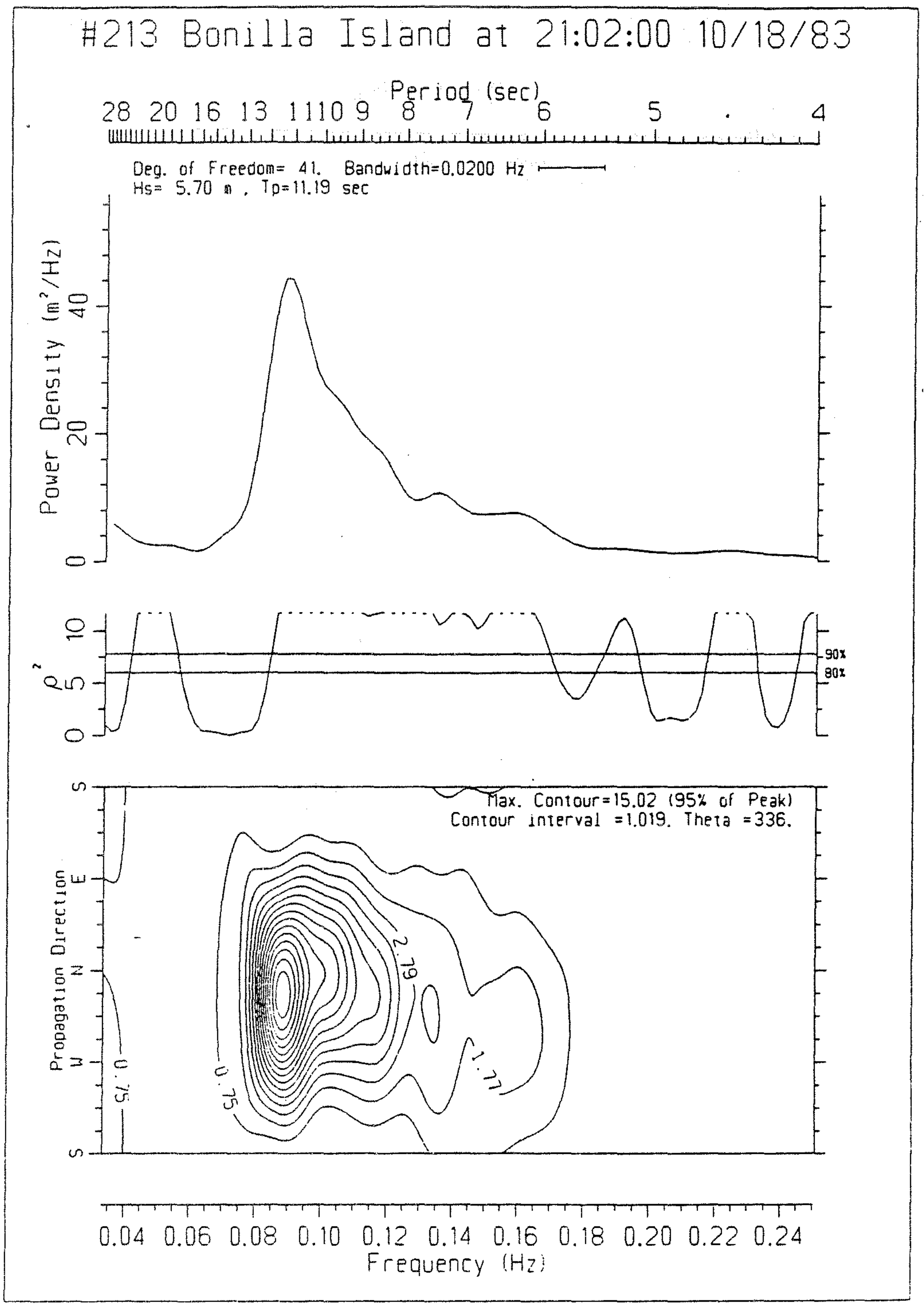

Fig. 3.15 continued

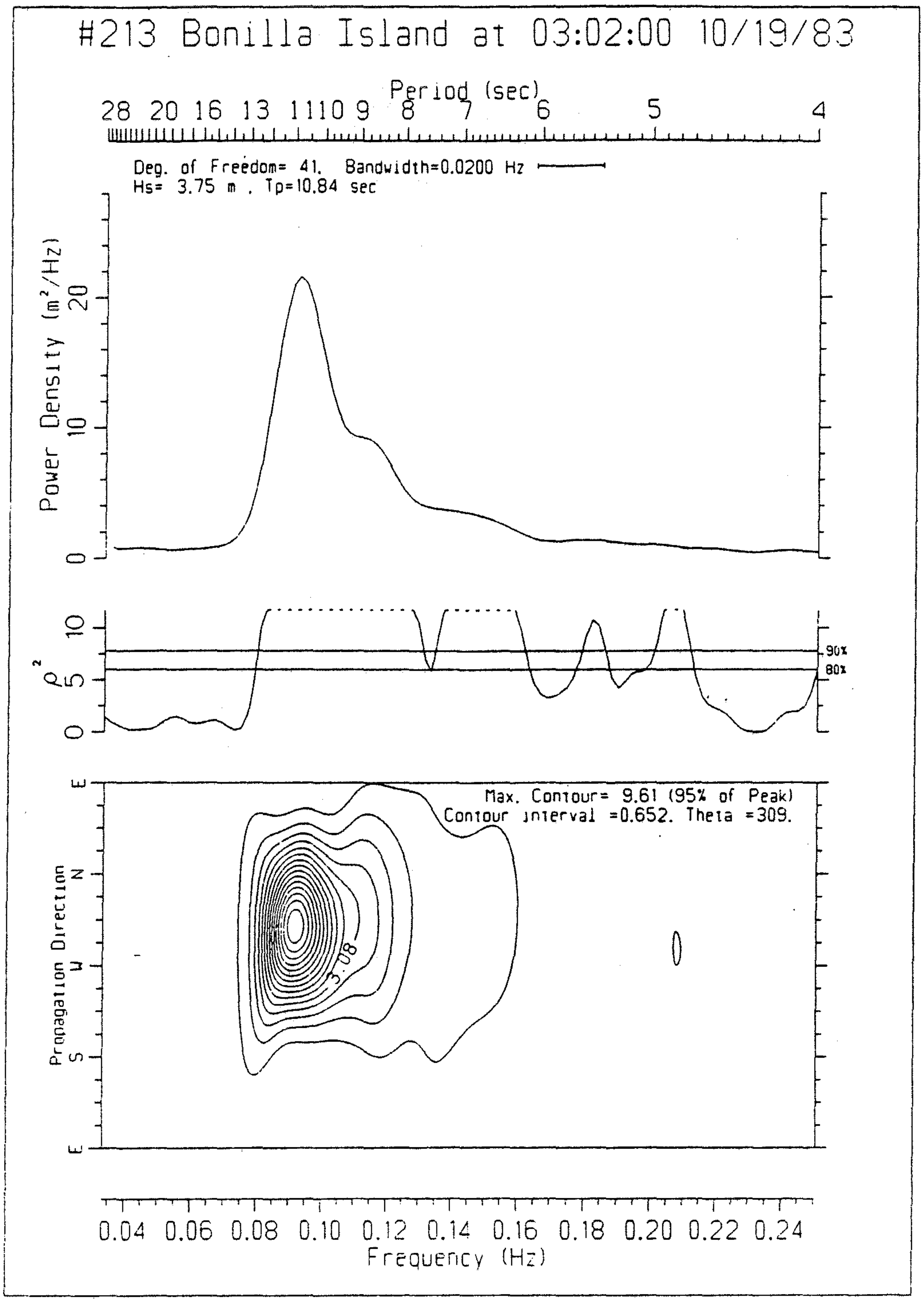

Fig. 3.15 continued

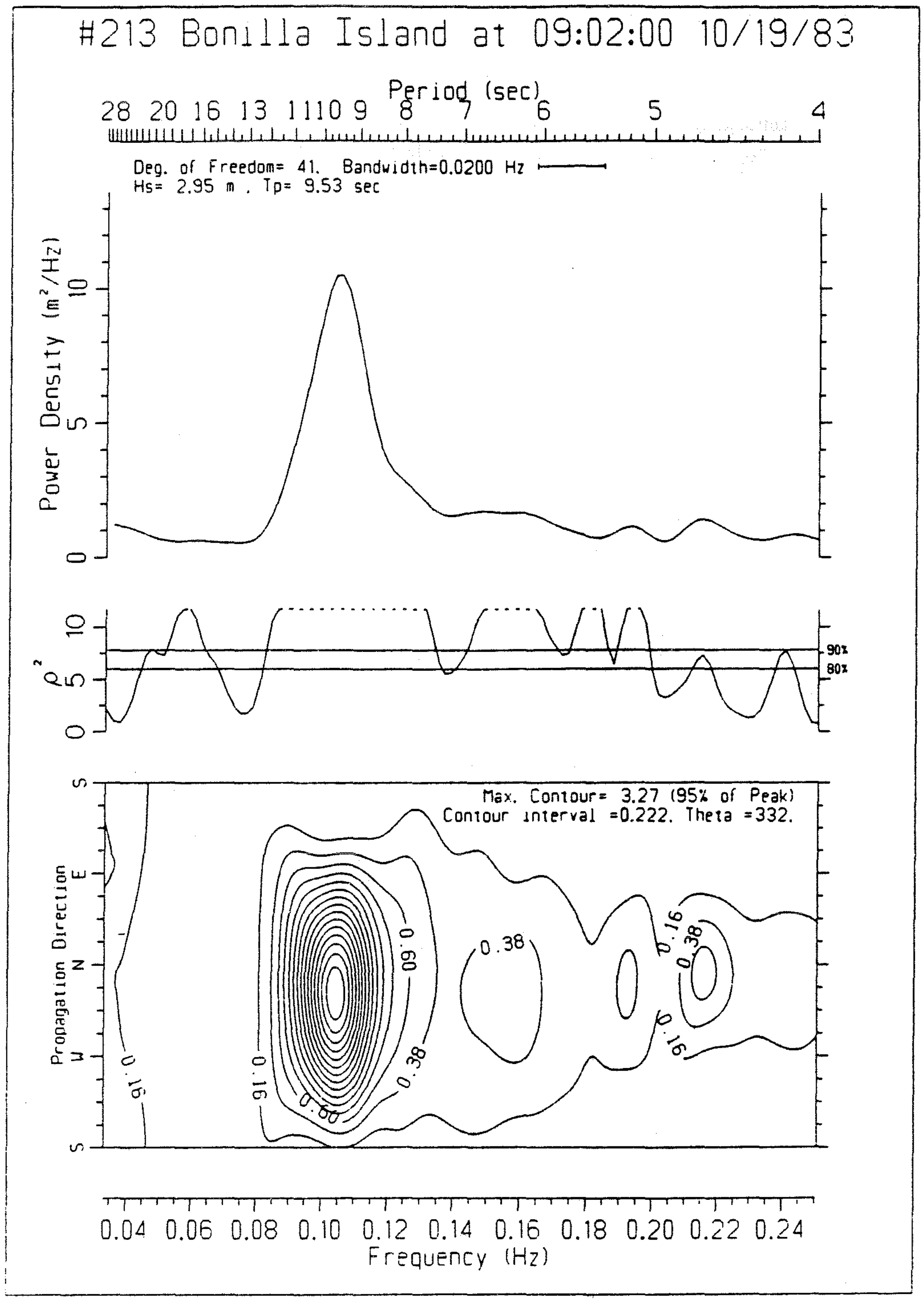

Fig. 3.15 continued

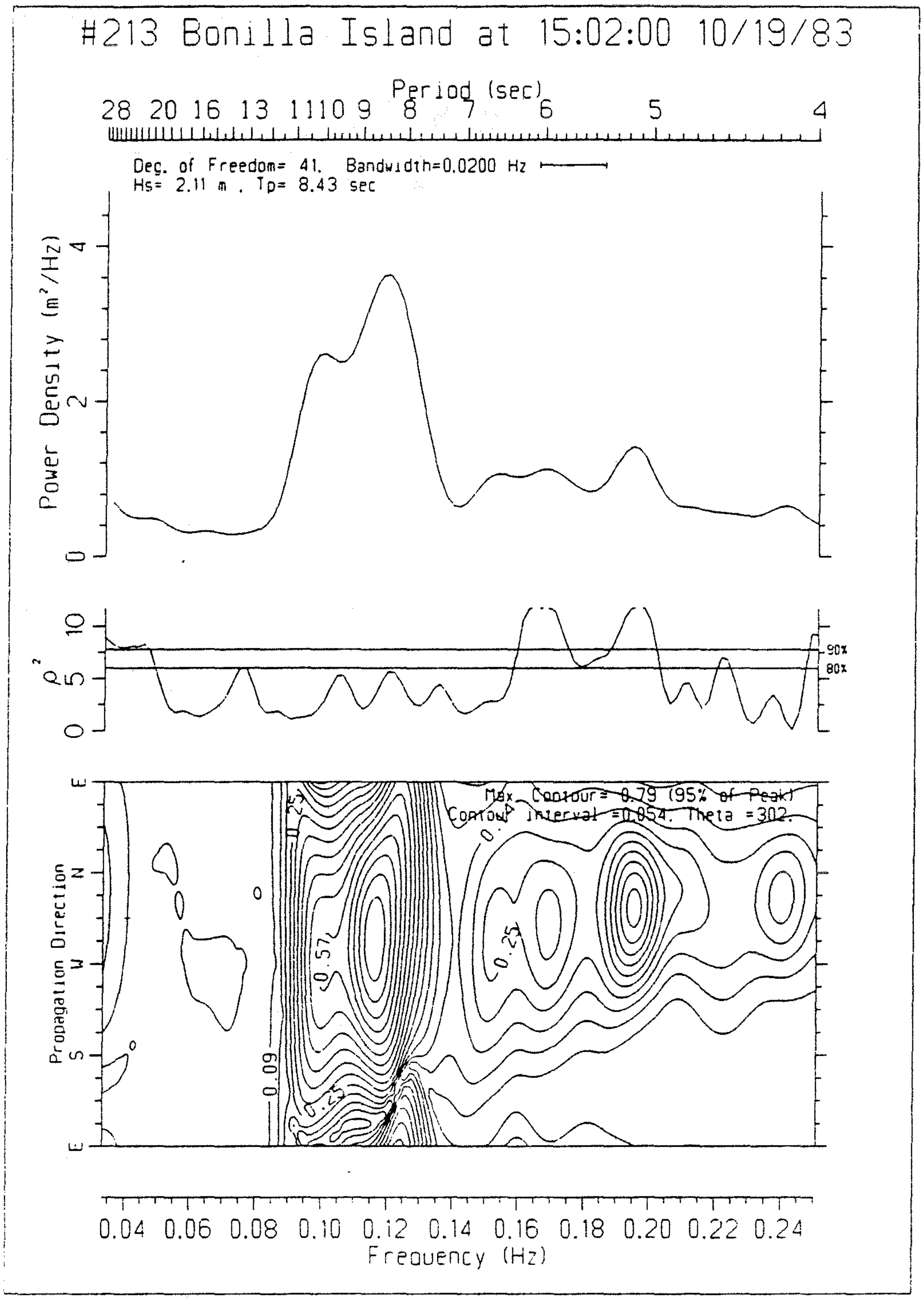

Fig. 3.15 continued

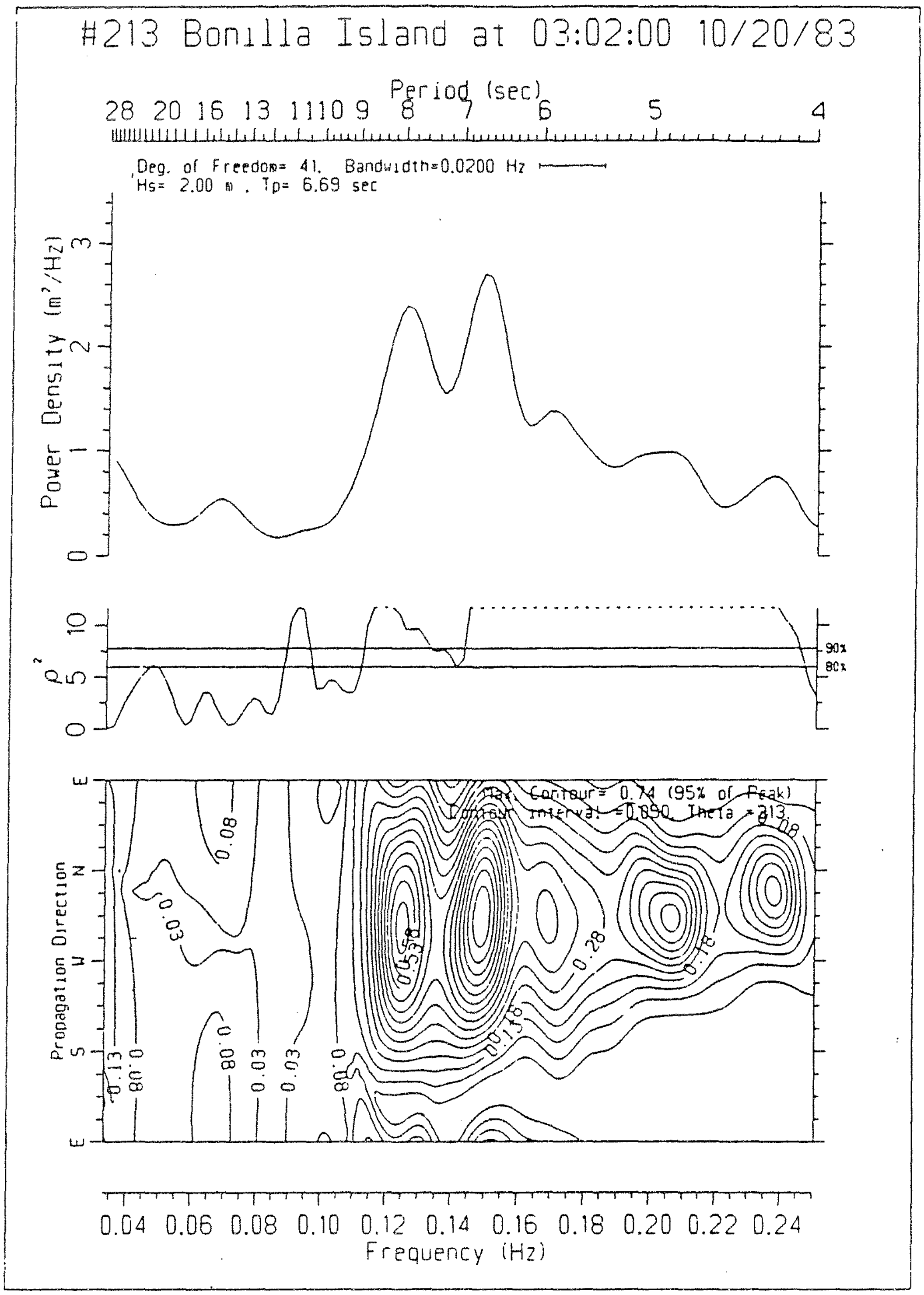

Fig. 3.15 continued

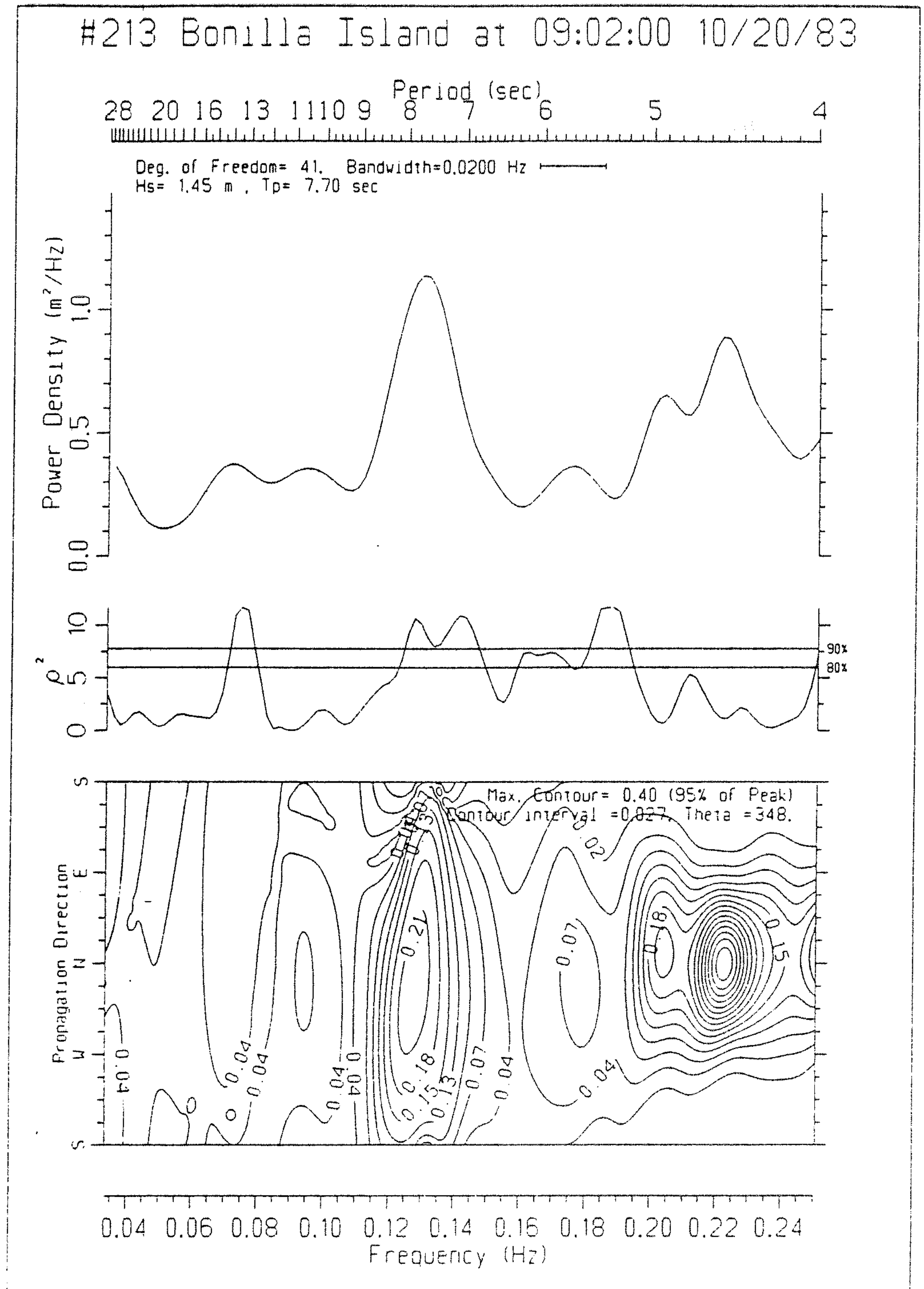

Fig. 3.15 continued

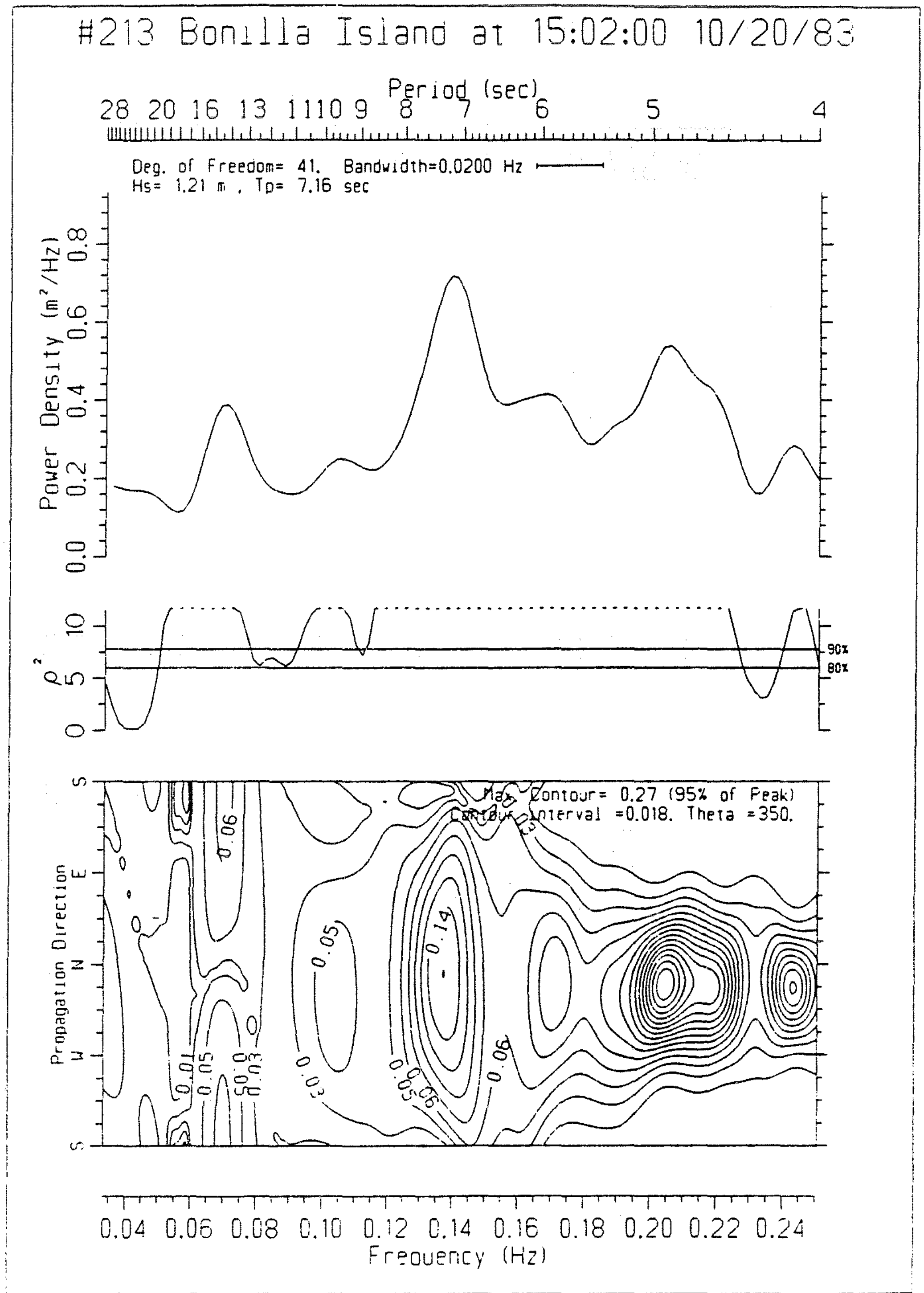

Fig. 3.15 continued

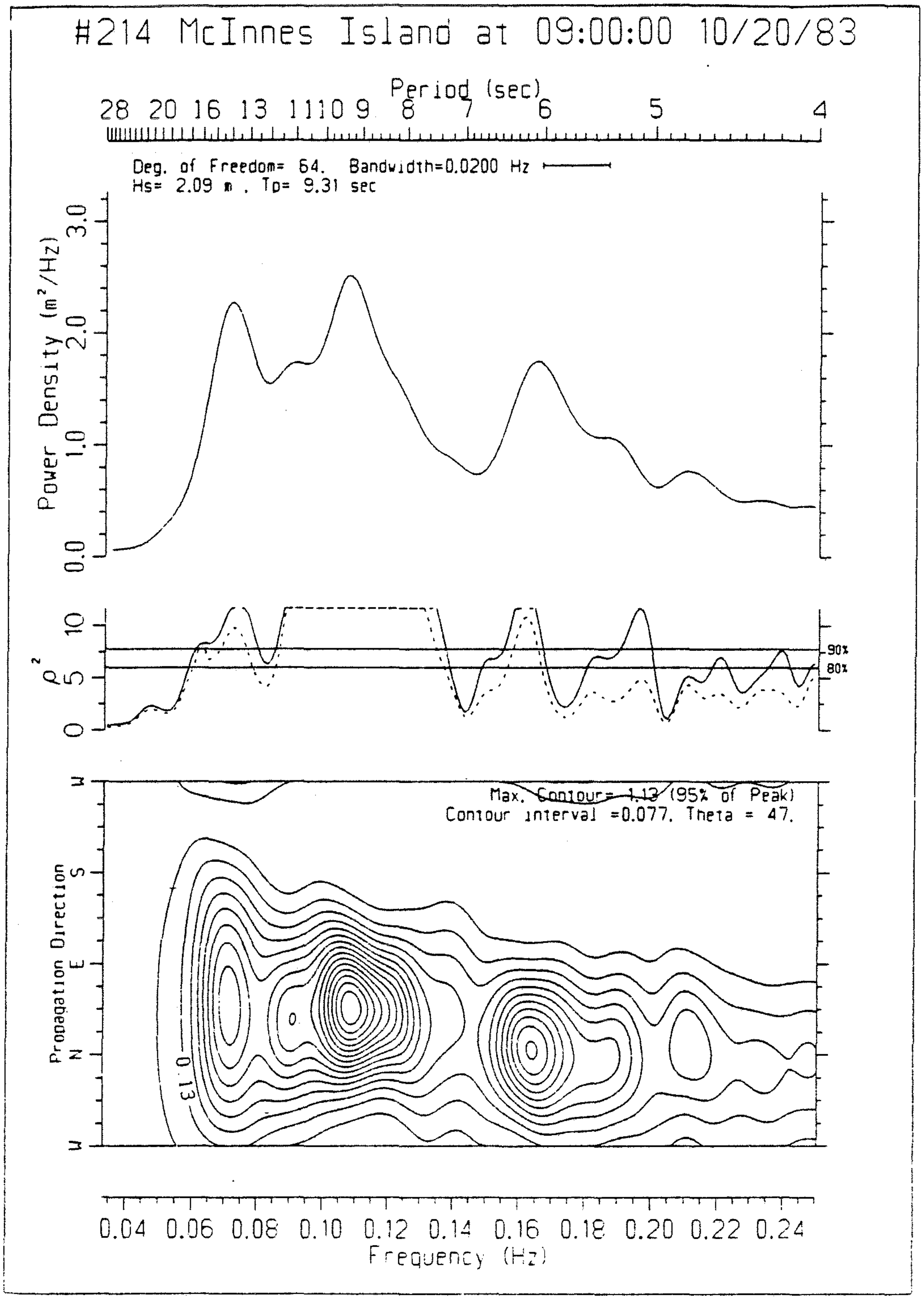

Fig. 3.16 Comparison of ρ^2 for one spectrum computed with Long's (1980) method (——) and the new optimization method of this study(----).

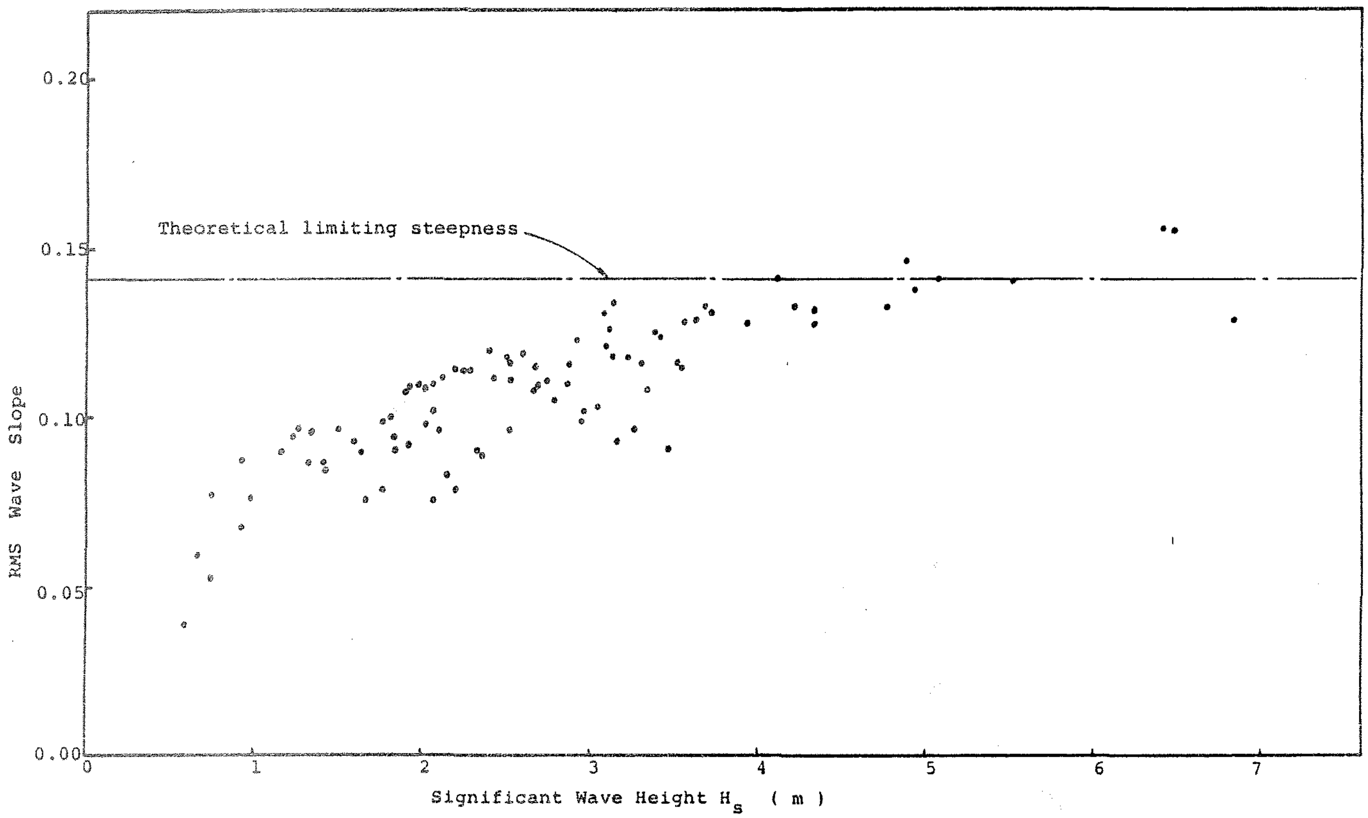

Fig. 3.17 Variation of the RMS wave slope Σ with significant wave height H_s.

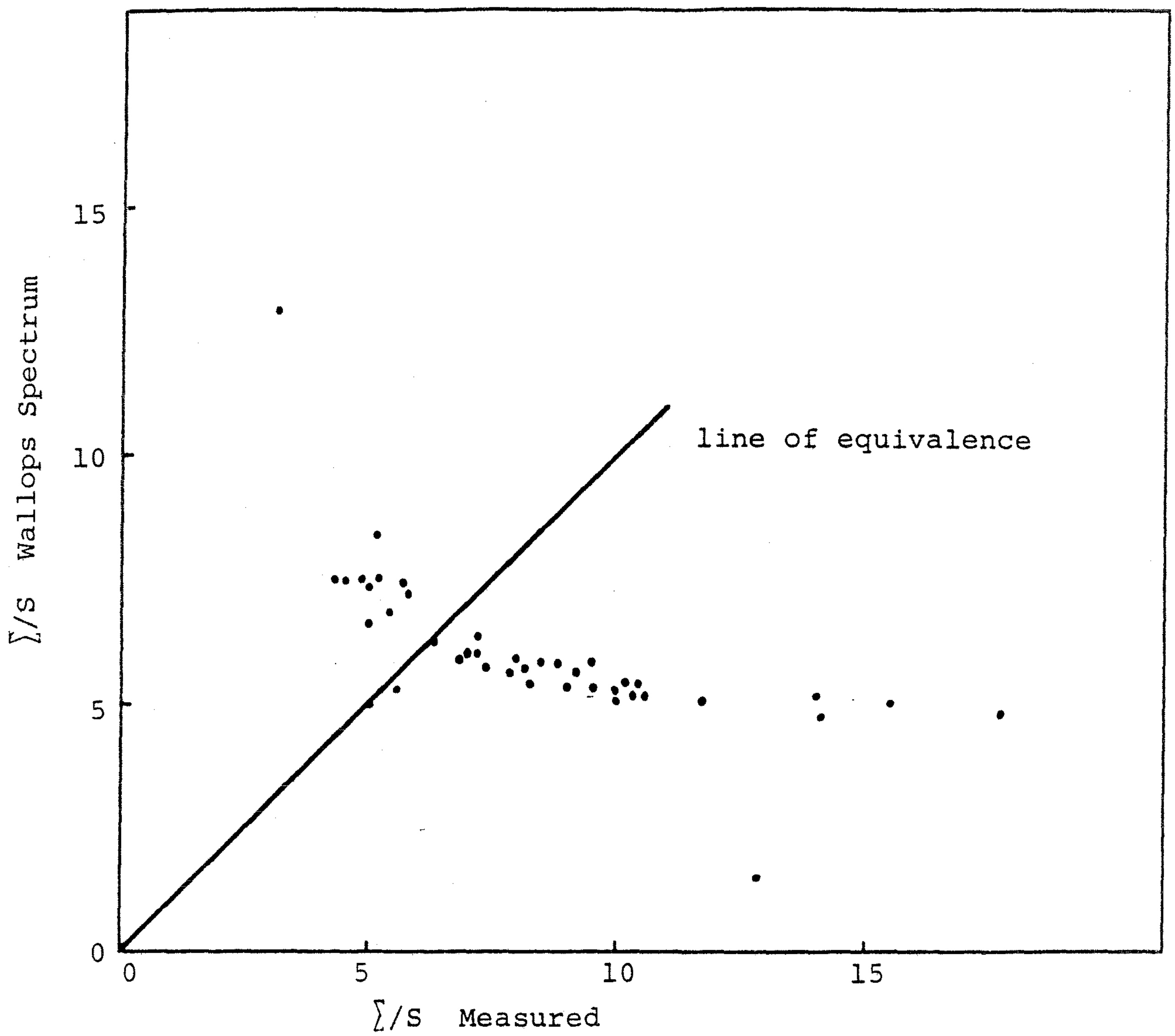

Fig. 3.18 Comparison of $\sum/S$ measured by the WAVEC with theoretical values from the Wallops spectrum.

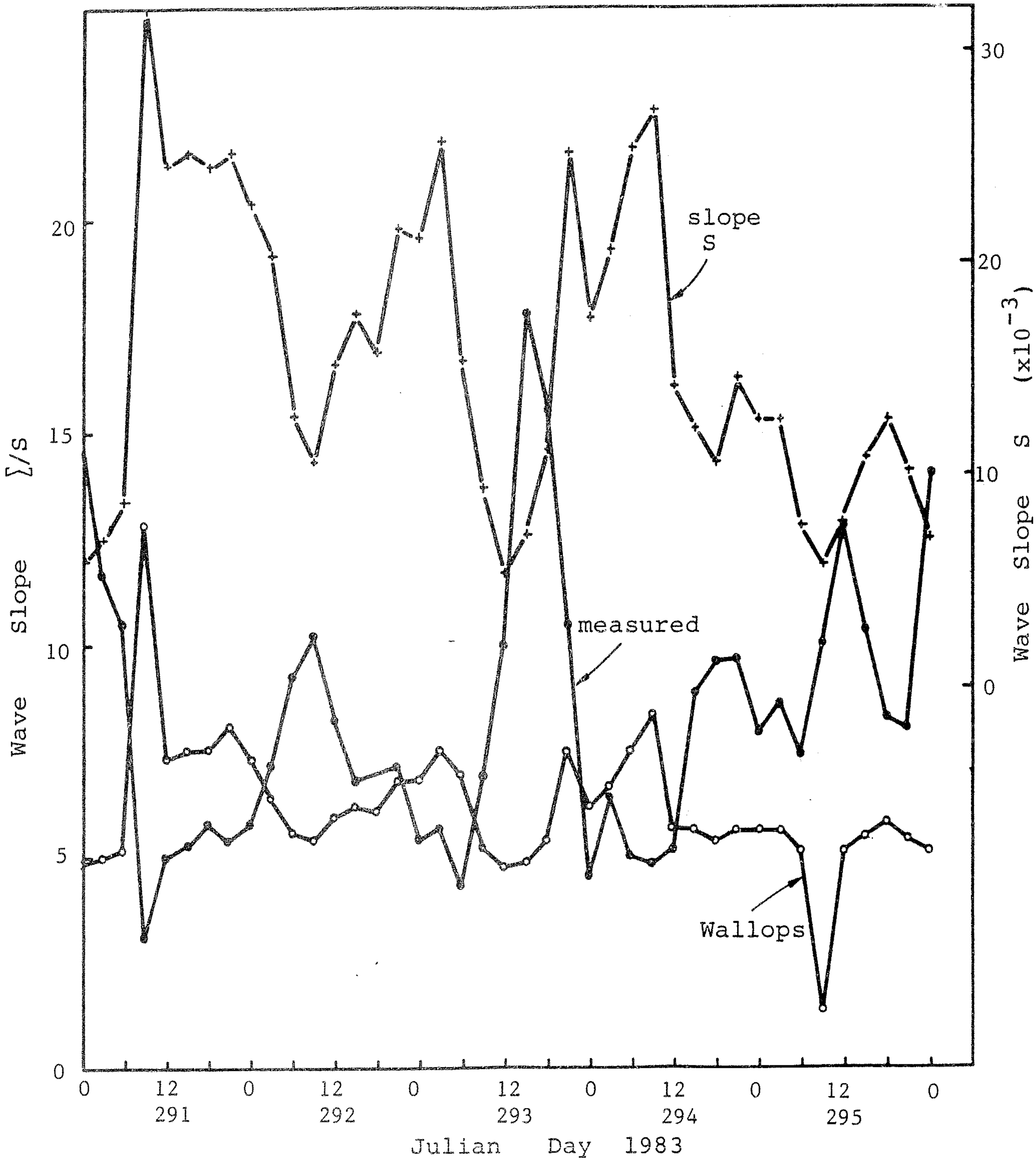

Fig. 3.19 Time series compairson of ∑/S - measured with ∑/S - Wallops spectrum.

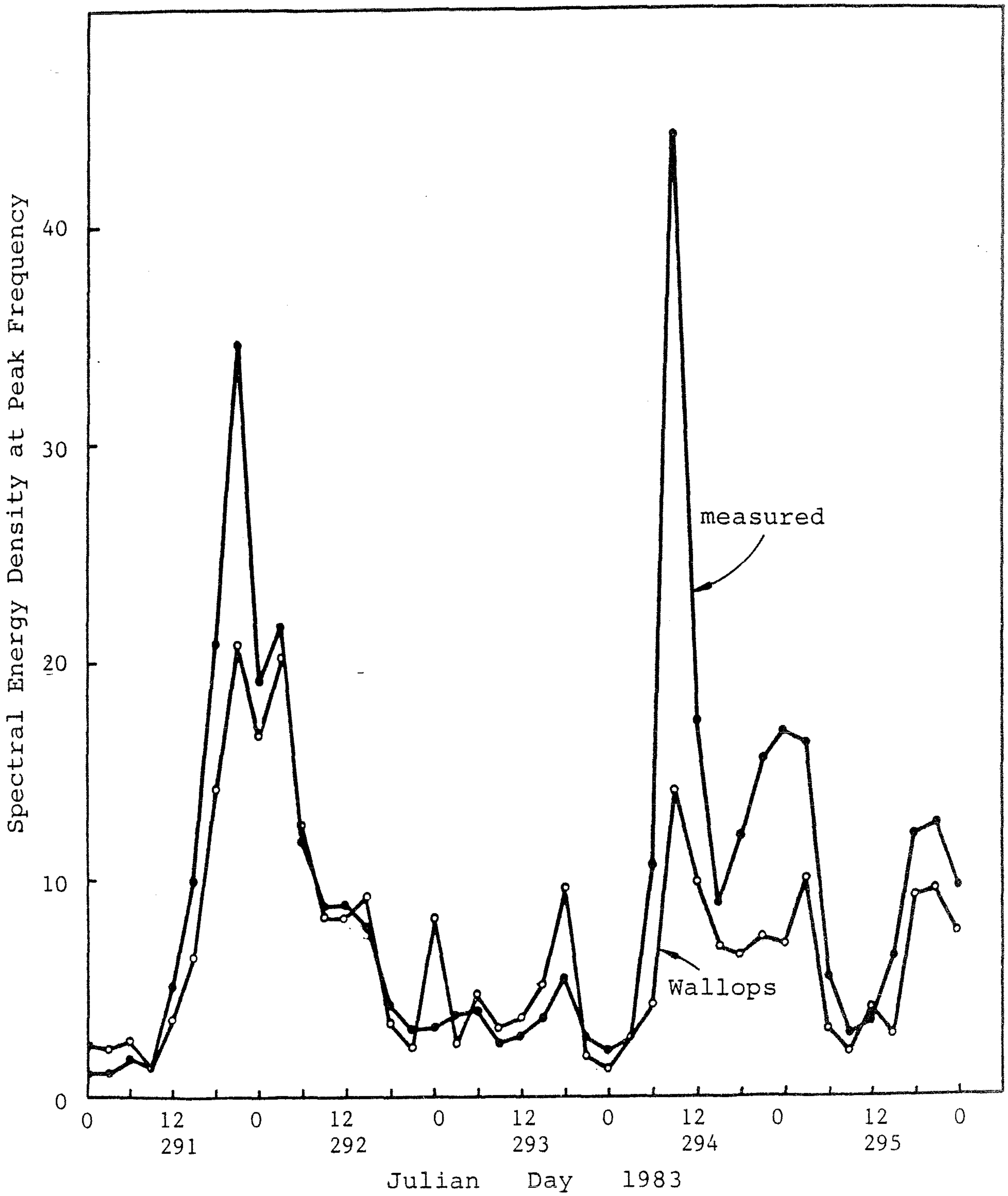

Fig. 3.20 Time series comparison of peak energy density, as measured with that predicted by the Wallops spectrum using the measured significant slope as input.

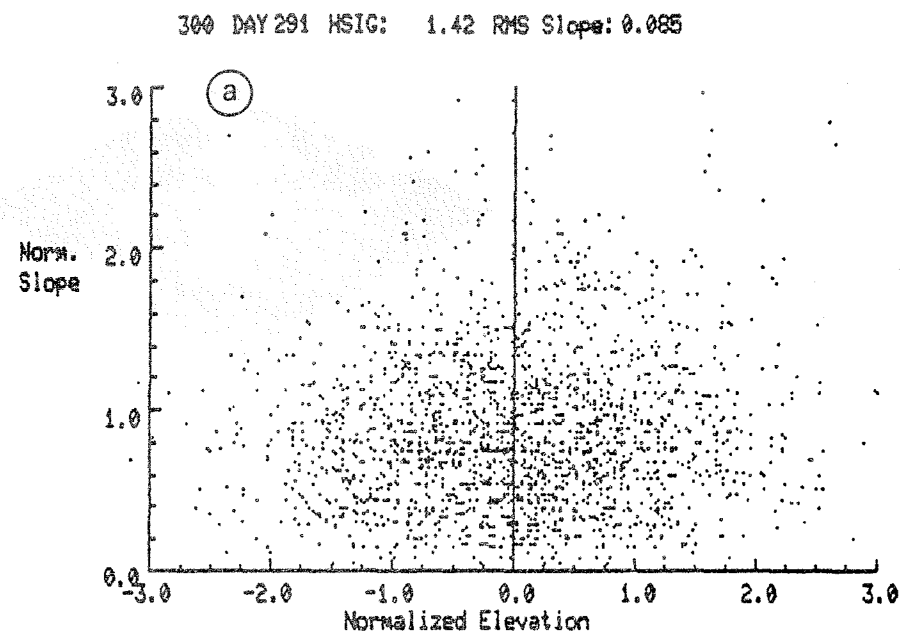

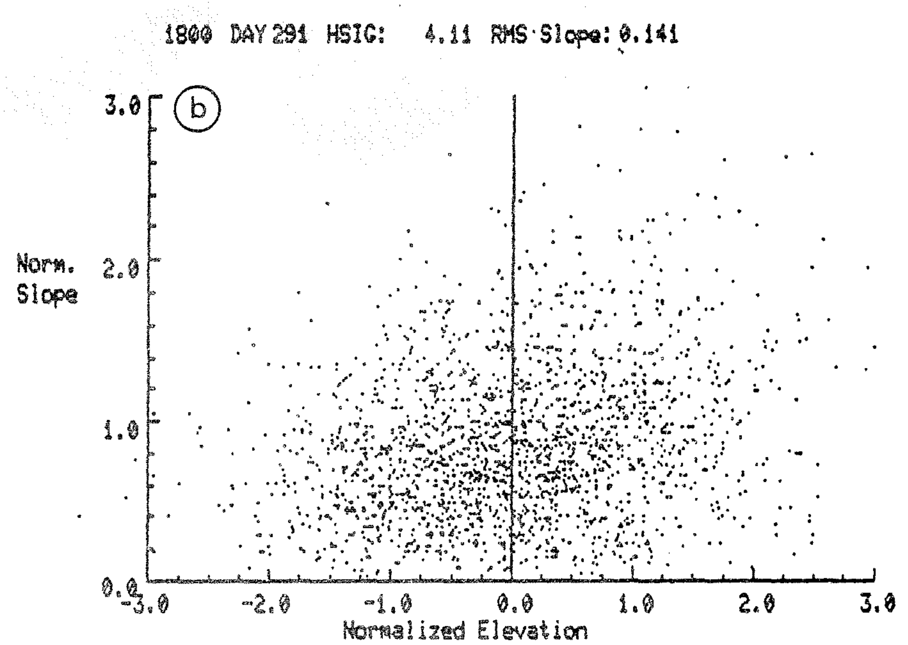

Fig. 3.21 Samples of the distribution of normalized wave slope with normalized surface elevation (measured at Station 214 with a WAVEC buoy).

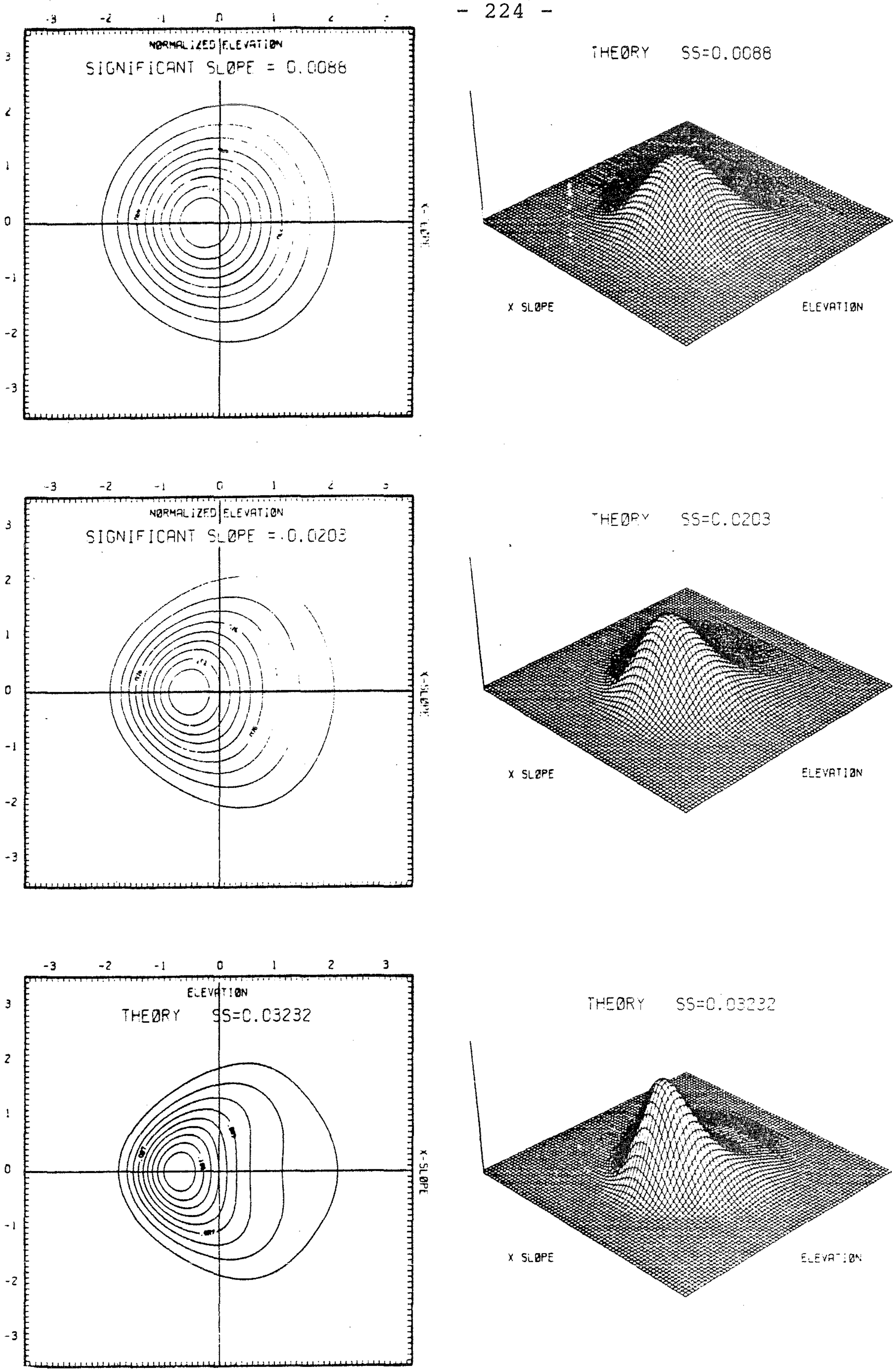

Fig. 3.22 Contour and perspective presentations of the theoretical joint probability density functions for low, medium and high significant slope values: S=0.0088 (contours from 0 to 0.1648 in steps of 0.01648), S=0.0203 (contours from 0 to 0.1906 in steps of 0.01906) and S=0.0323 (contours from 0 to 0.2435 in steps of 0.02435). (from Huang et al., 1984)

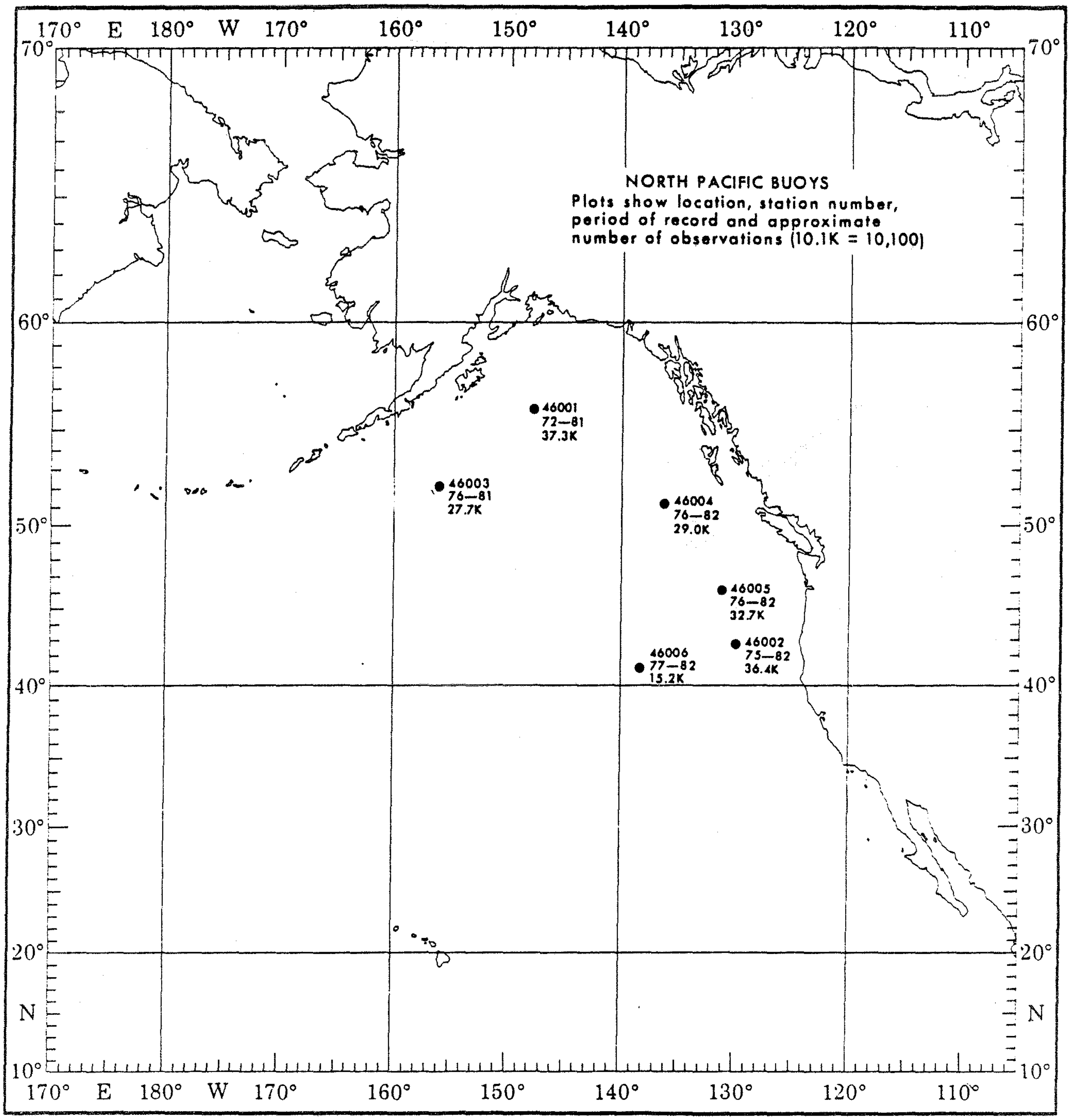

Fig. 4.1 Location of the United States NDBO wave buoys. Data from 46003, 46004 and 46005 were examined in the present study.

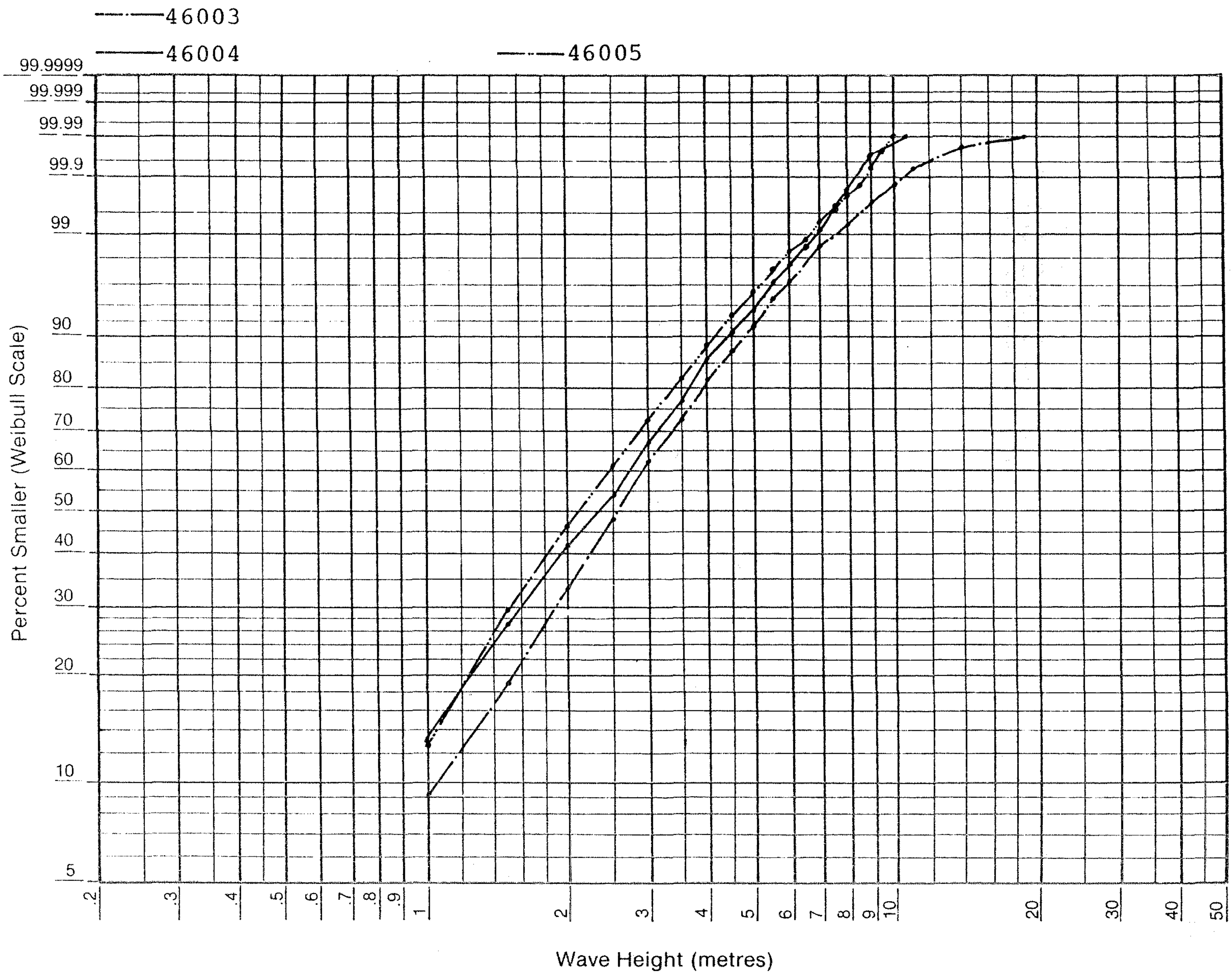

Fig. 4.2 Cumulative relative frequency curves for significant wave height in the Gulf of Alaska and Northwestern U.S. waters.

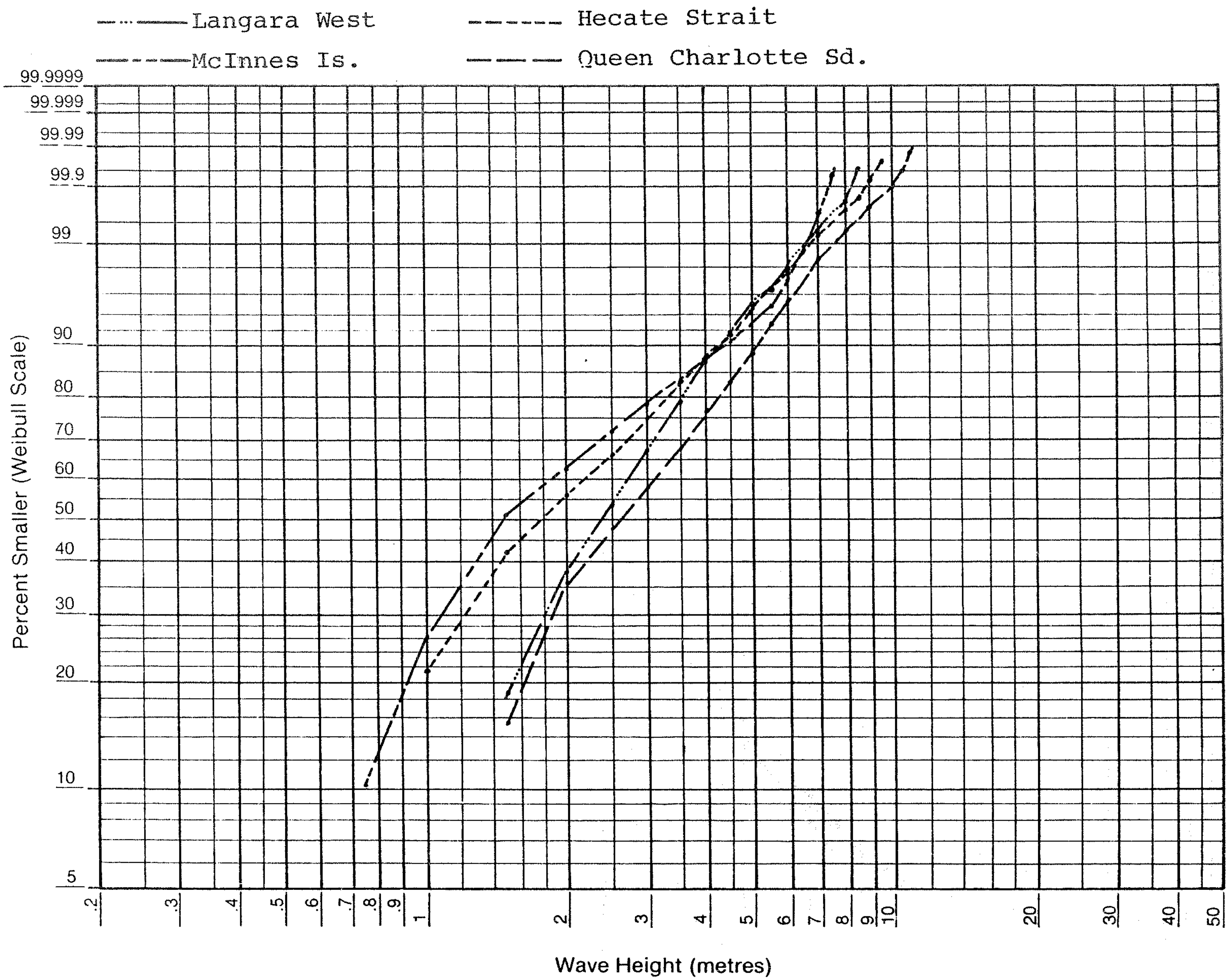

Fig. 4.3 Cumulative relative frequency curves for significant wave height in Queen Charlotte Sd., Hecate Strait and Dixon Entrance.

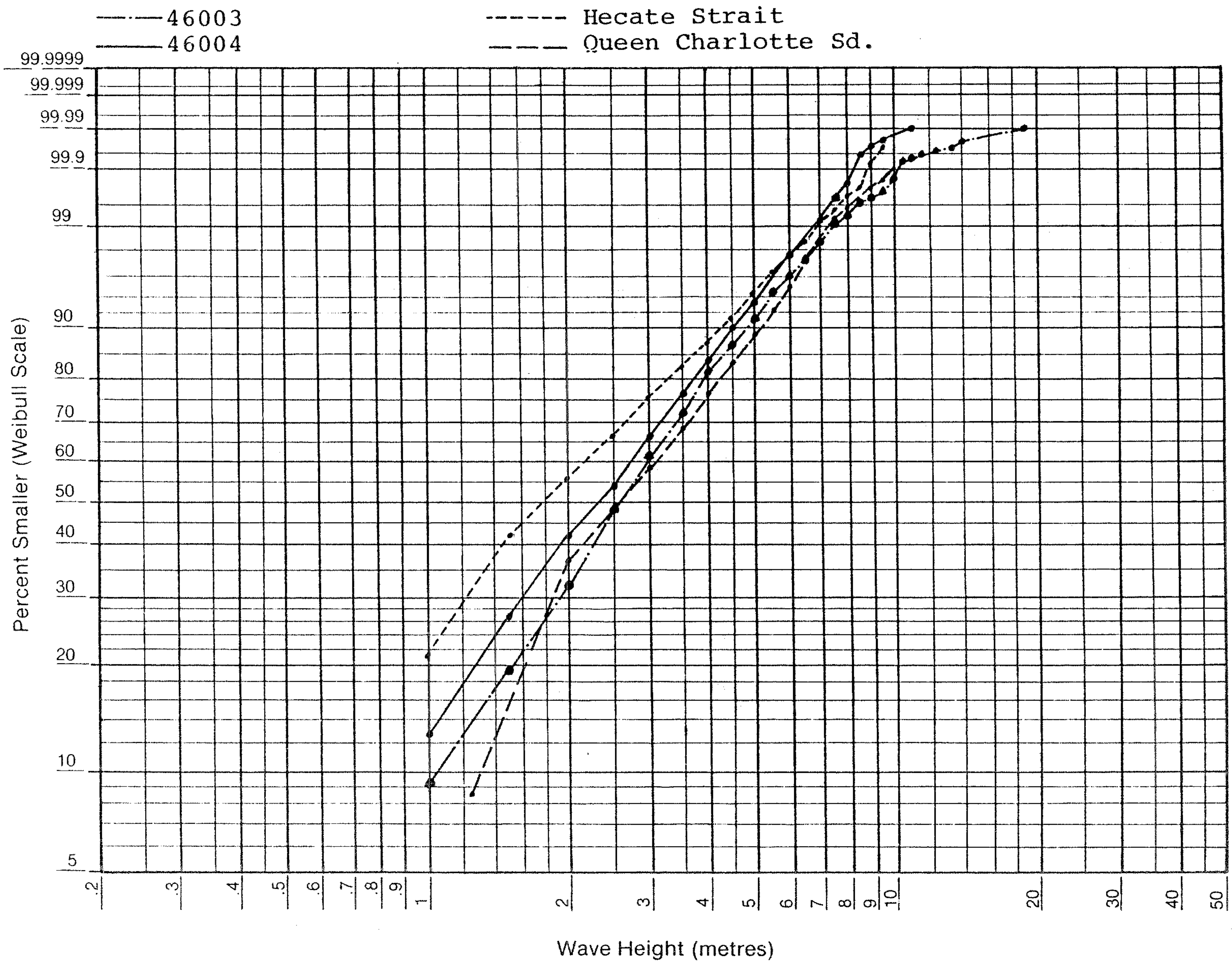

Fig. 4.4 Cumulative relative distributions for significant wave height at Queen Charlotte Sound, Hecate Strait, and Stations 46003 and 46004 in the Gulf of Alaska.

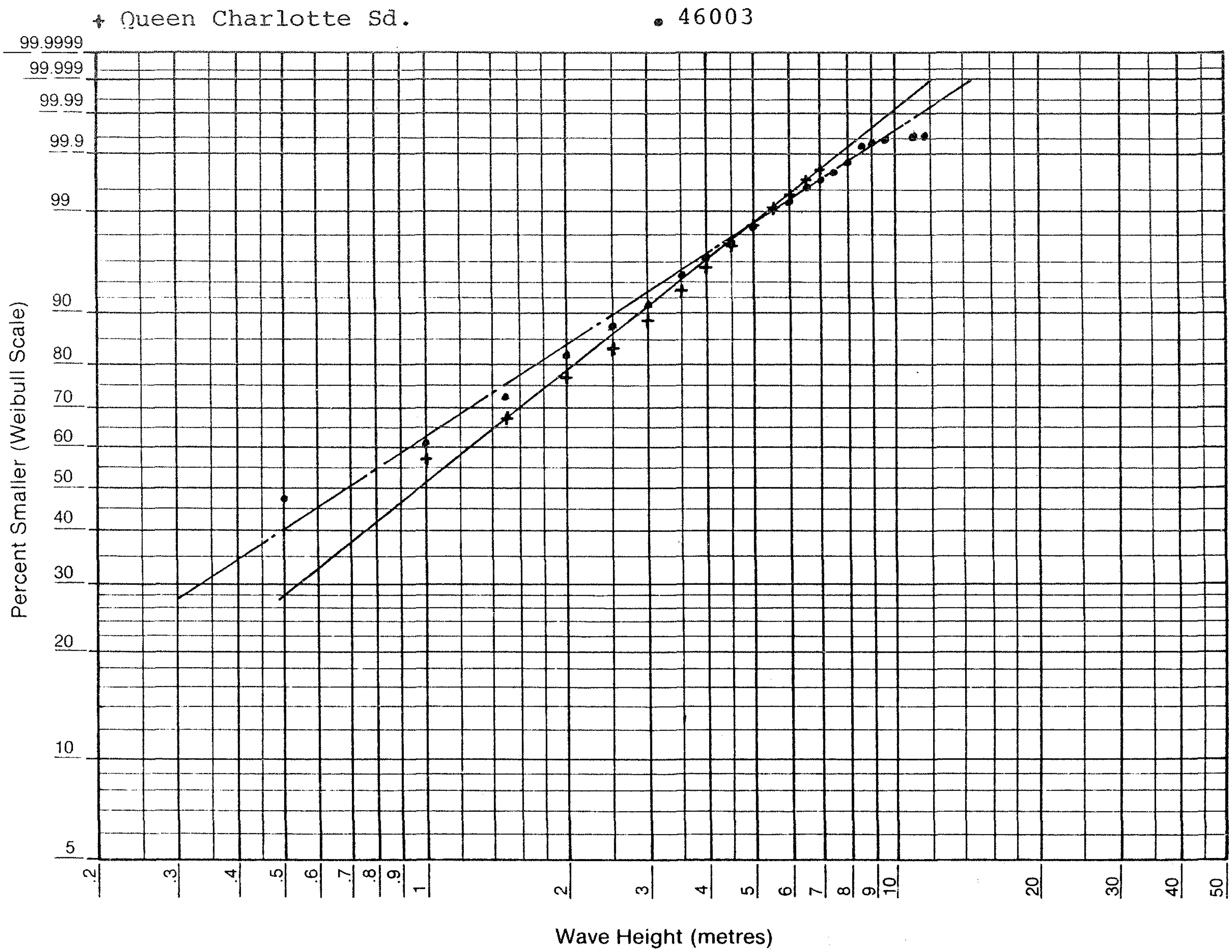

Fig. 4.5 Weibull distribution function fitted to significant wave height data with A=2.0m for 46003 and A=2.0m for Queen Charlotte Sd.

Fall McKenney Rock

Wind Direction

Wind Speed (m/s)	N	NNE	NE	ENE	E	ESE	SE	SSE	S	SSW	SW	WSW	W	WNW	NW	NNW	Sum
50																	0
																	0
45																	0
																	0
40																	0
																	0
35																	0
						1	1	1									3
30						2	4	1									7
						2	10	4									16
25						1	8	11	9								21
							14	15	8	1							38
20						4	59	26	13	1	1						104
	3					9	53	61	16	4			1	1			148
15	10	1	1		2	29	65	54	23	8	2	2		3	19	3	222
	13	10	10	1	11	46	43	57	29	19	10	4	4	7	34	30	328
10	30	16	5	6	49	61	58	31	39	44	29	11	13	35	60	43	530
	41	38	31	21	42	61	46	23	44	28	27	13	13	17	68	56	571
5	32	41	54	22	20	34	26	22	28	18	20	8	12	19	49	49	454
0	26	12	21	9	10	12	12	11	5	13	9	10	11	11	10	10	192
Sum	155	118	122	59	134	262	399	317	206	136	86	48	54	93	240	191	2832

Winter McKenney Rock

Wind Direction

Wind Speed (m/s)	N	NNE	NE	ENE	E	ESE	SE	SSE	S	SSW	SW	WSW	W	WNW	NW	NNW	Sum
50																	0
																	0
45																	0
																	0
40																	0
								1									1
35																	0
							2	1	1								4
30							1		1	1							3
							6	4									10
25						1	29	27	3	1		1					62
						4	40	38	9			1					88
20						10	69	67	8						1		158
			3	1		18	80	84	45	10	1	1			10	1	254
15	1	2	12	4	3	41	97	86	54	33	5	7	4	4	14		367
	9	14	18	3	25	89	124	62	47	47	28	18	3	5	15	20	525
10	49	81	32	7	54	135	72	40	49	55	30	12	9	9	25	32	685
	53	79	70	28	55	82	55	24	38	34	20	4	6	13	13	35	609
5	33	59	97	41	58	48	24	10	15	22	8	1	6	3	15	16	454
0	9	12	22	26	16	13	5	3	2	5	4	1	1	2	4	5	130
Sum	154	247	254	110	209	441	604	447	281	208	86	44	29	38	97	109	3346

Fig. 4.6 Joint histograms of wind speed versus wind direction at McKenney Rock (fall and winter seasons).

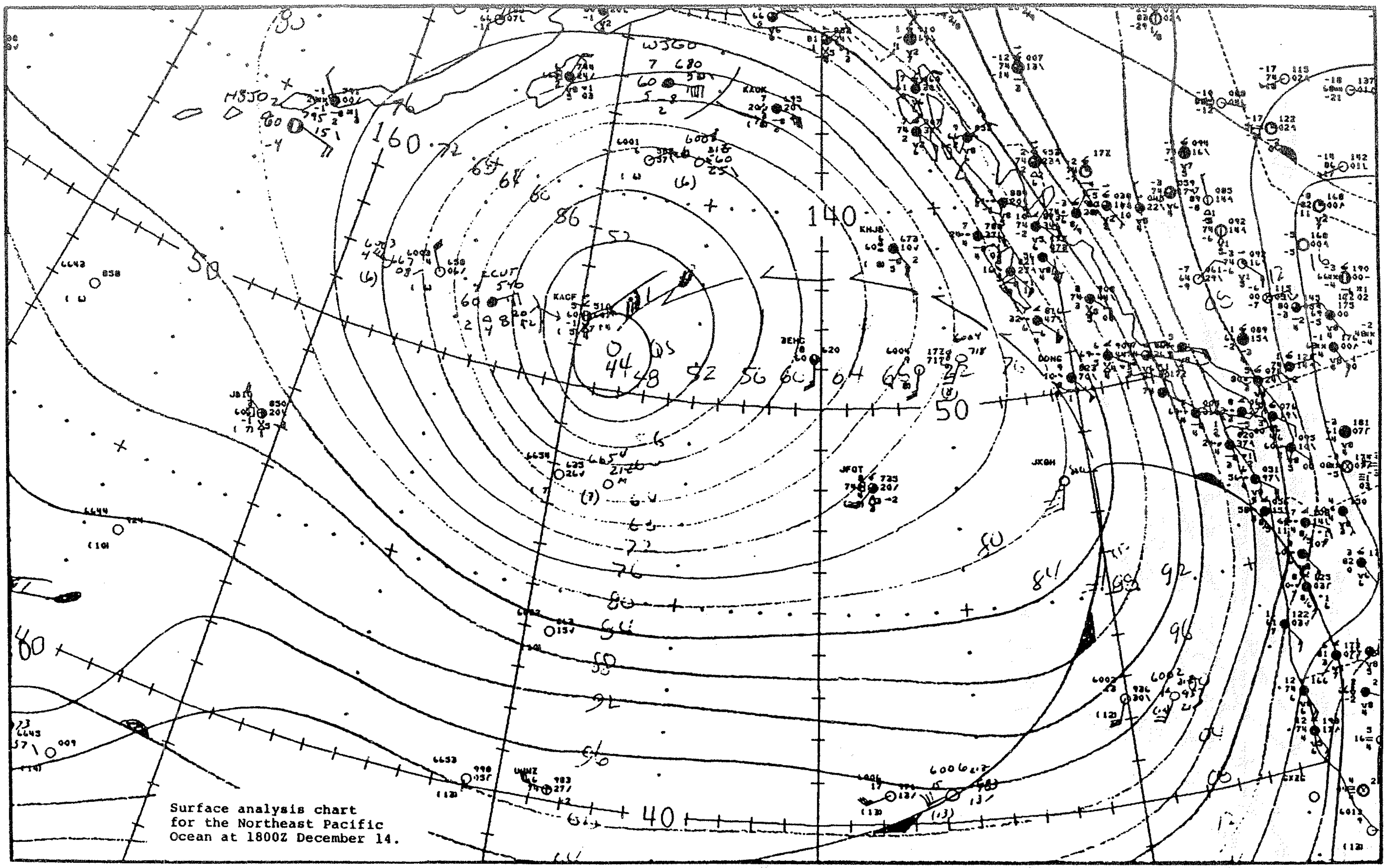

Fig. 4.7 Typical large-scale extratropical storm in the Gulf of Alaska.

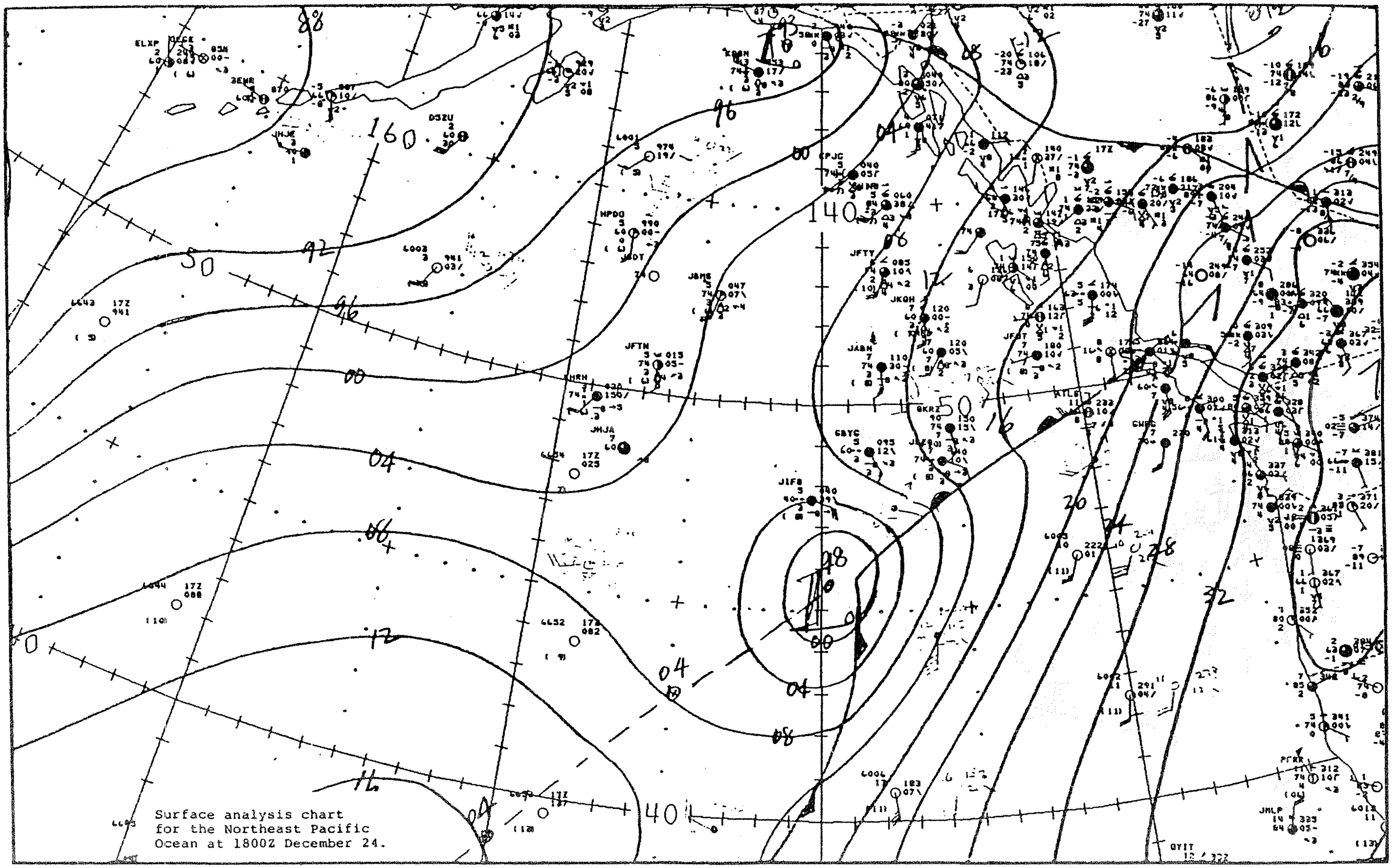

Fig. 4.8 Sequence of surface weather maps showing features of a typical small-scale storm impinging on Queen Charlotte Sound.

- 79 -

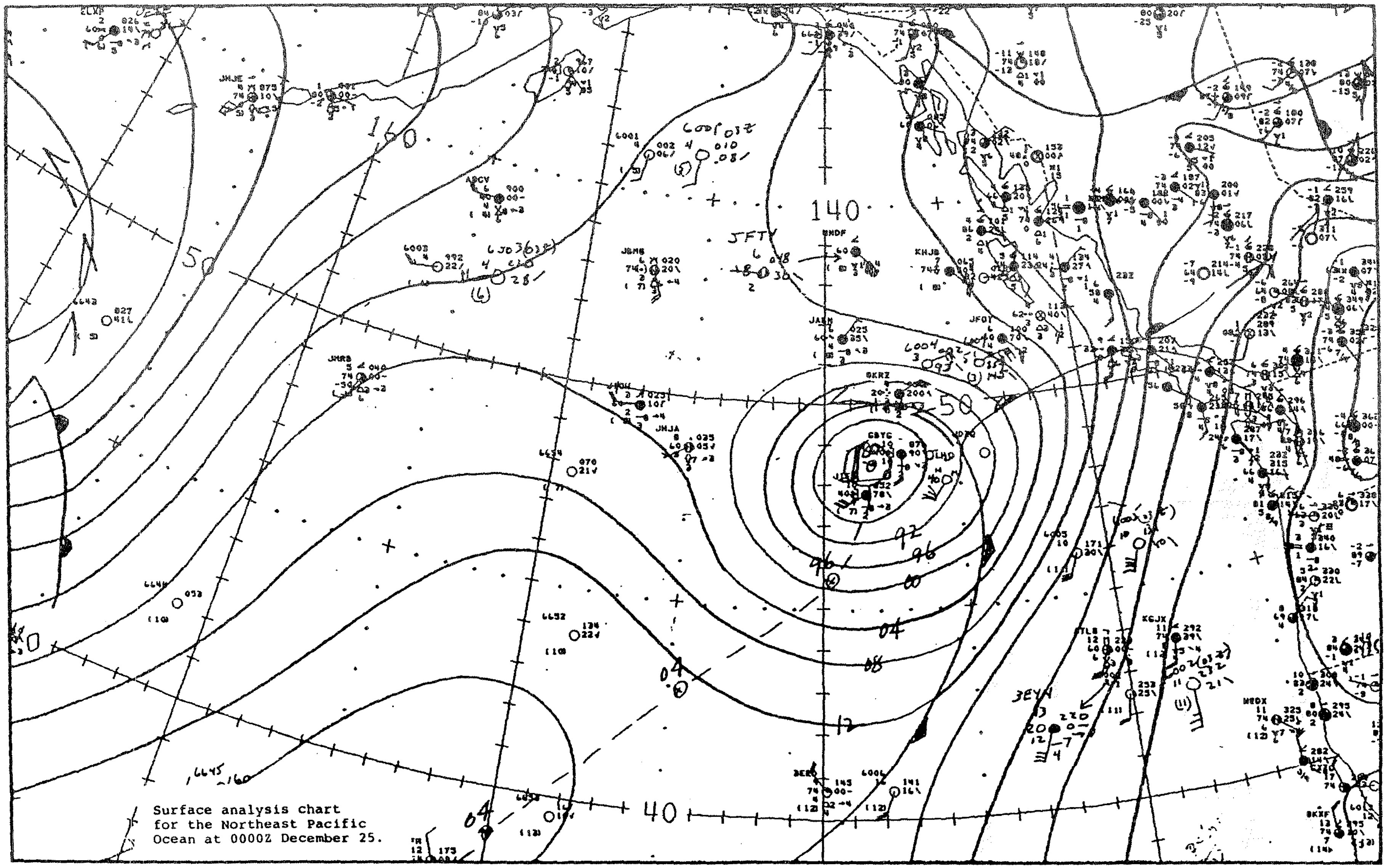

Surface analysis chart for the Northeast Pacific Ocean at 0000Z December 25.

Fig. 4.8 continued

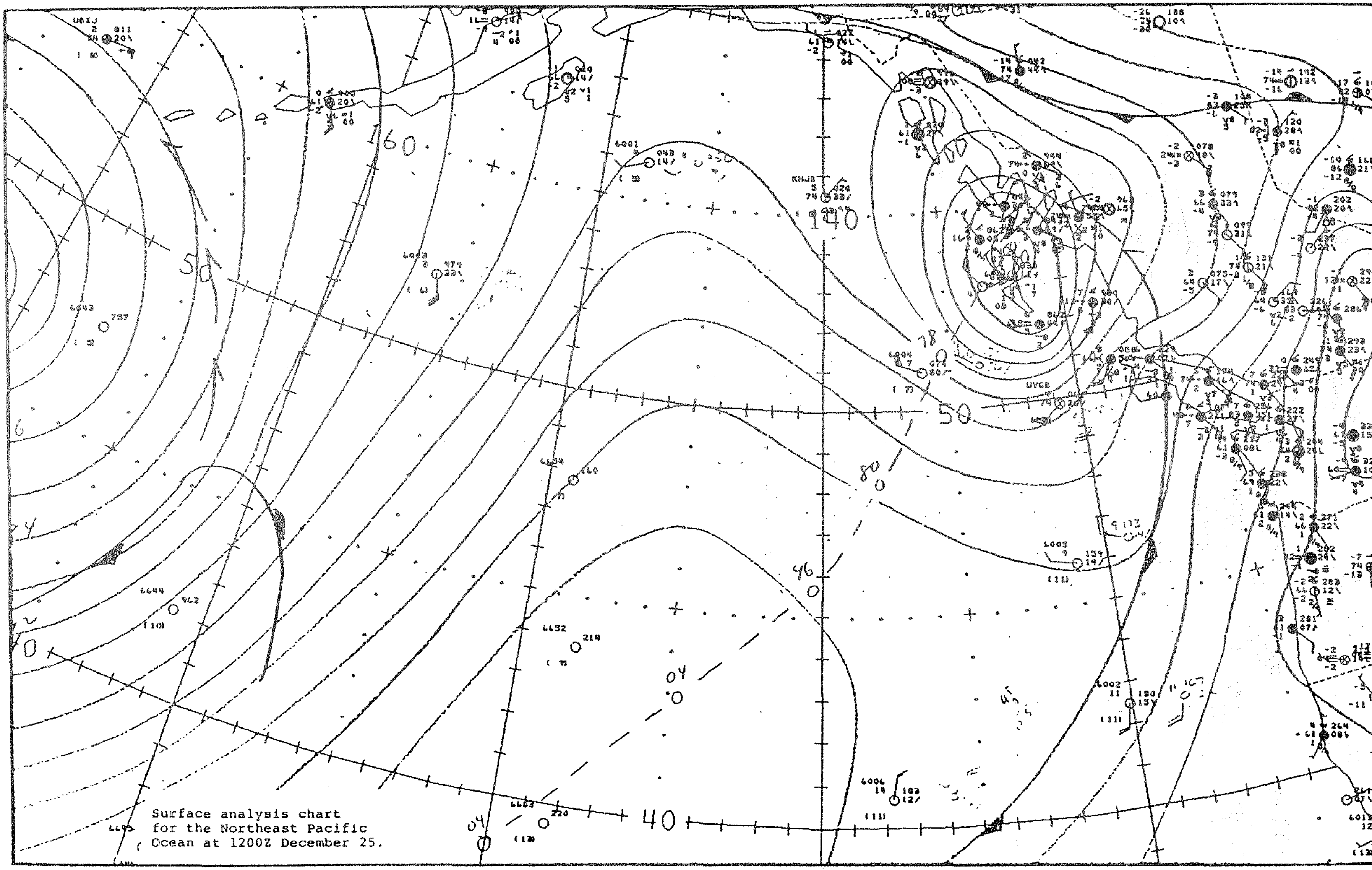

Fig. 4.8 continued

Spectrum measured at Station 216 08:10Z Nov. 15, 1982

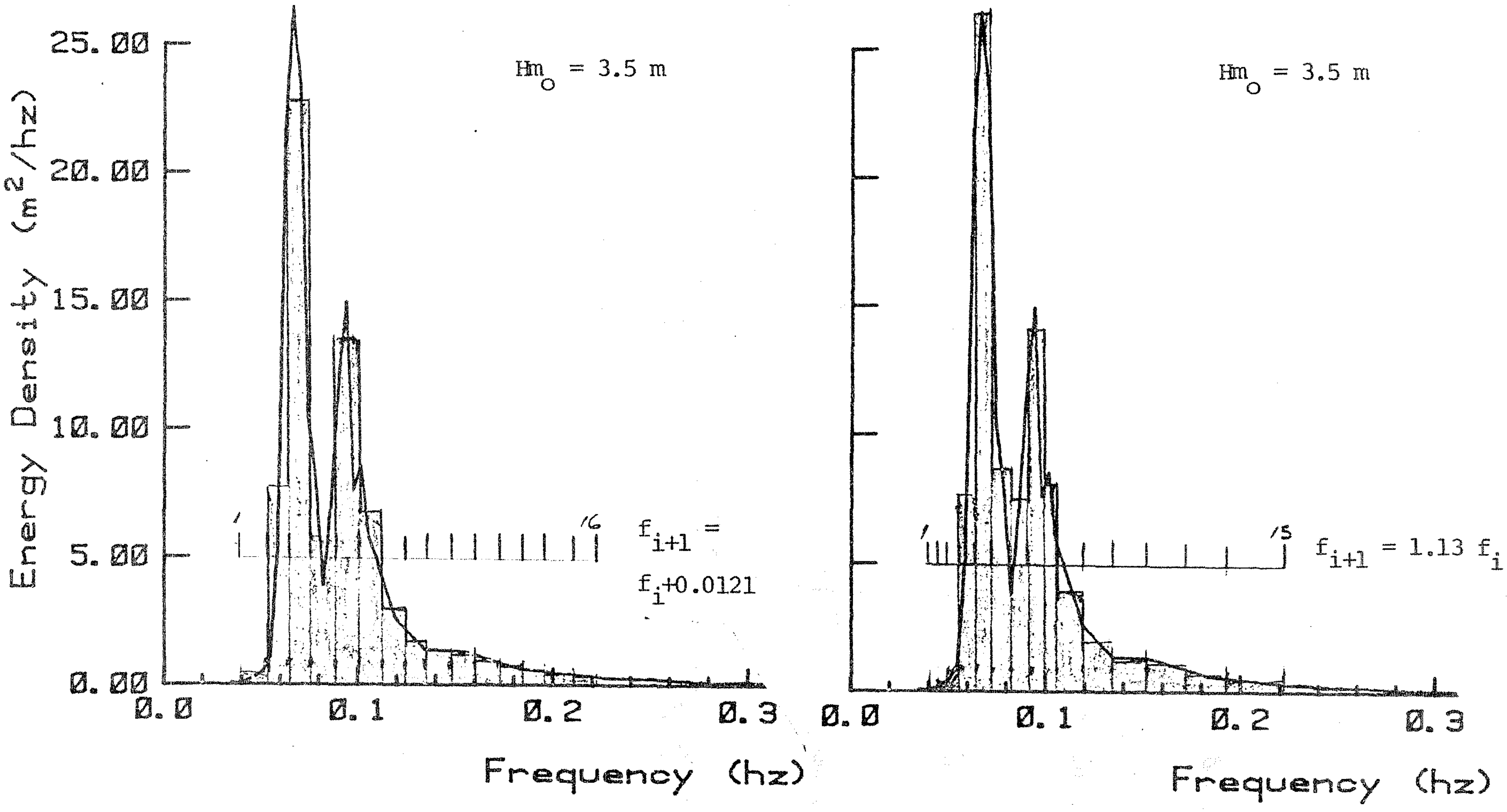

Equal Δf Equal f-ratio

Fig. 4.9 Comparison of alternative frequency discretization methods where swell makes an important contribution to the variance spectrum.

Spectrum measured at Station 215 16:57Z Oct. 4, 1982

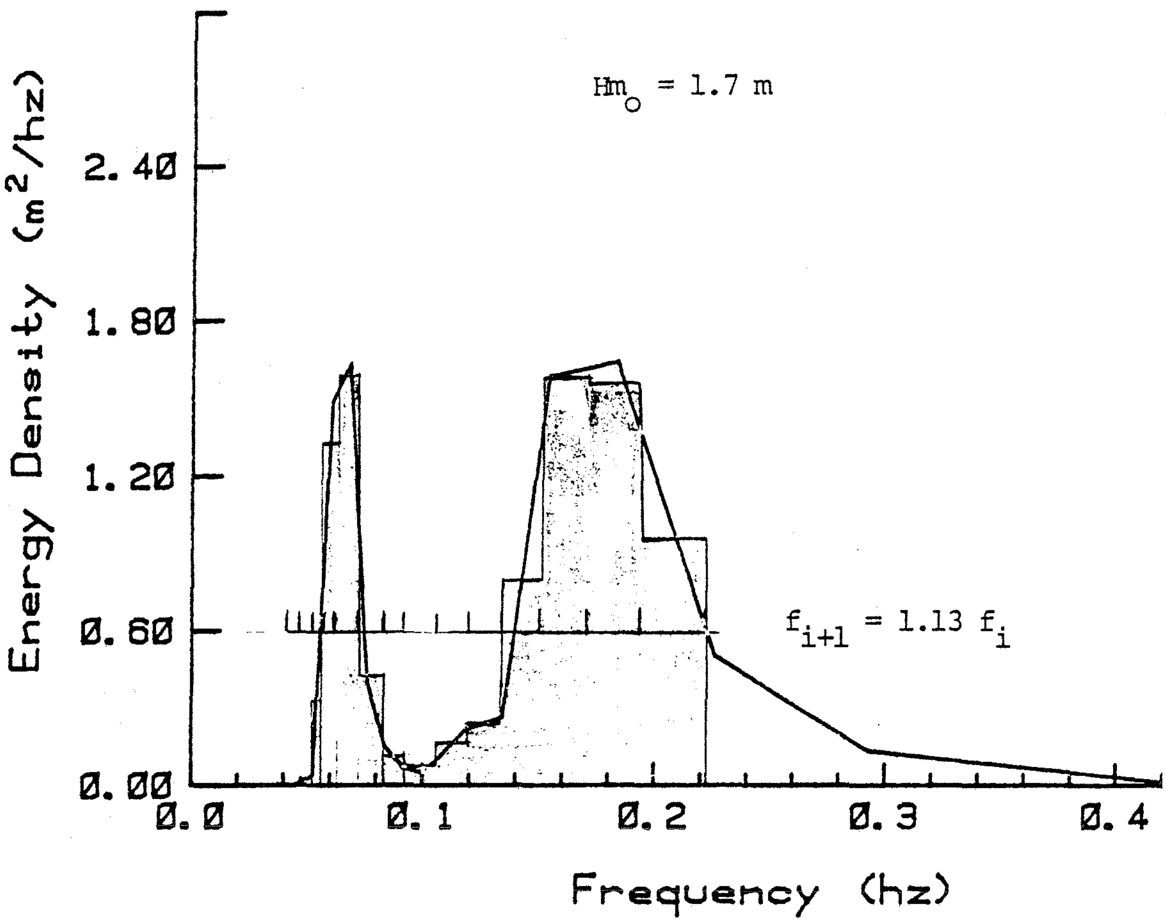

Equal f-ratio

Fig. 4.10 Illustration of frequency resolution of swell using a constant ration of successive frequencies.

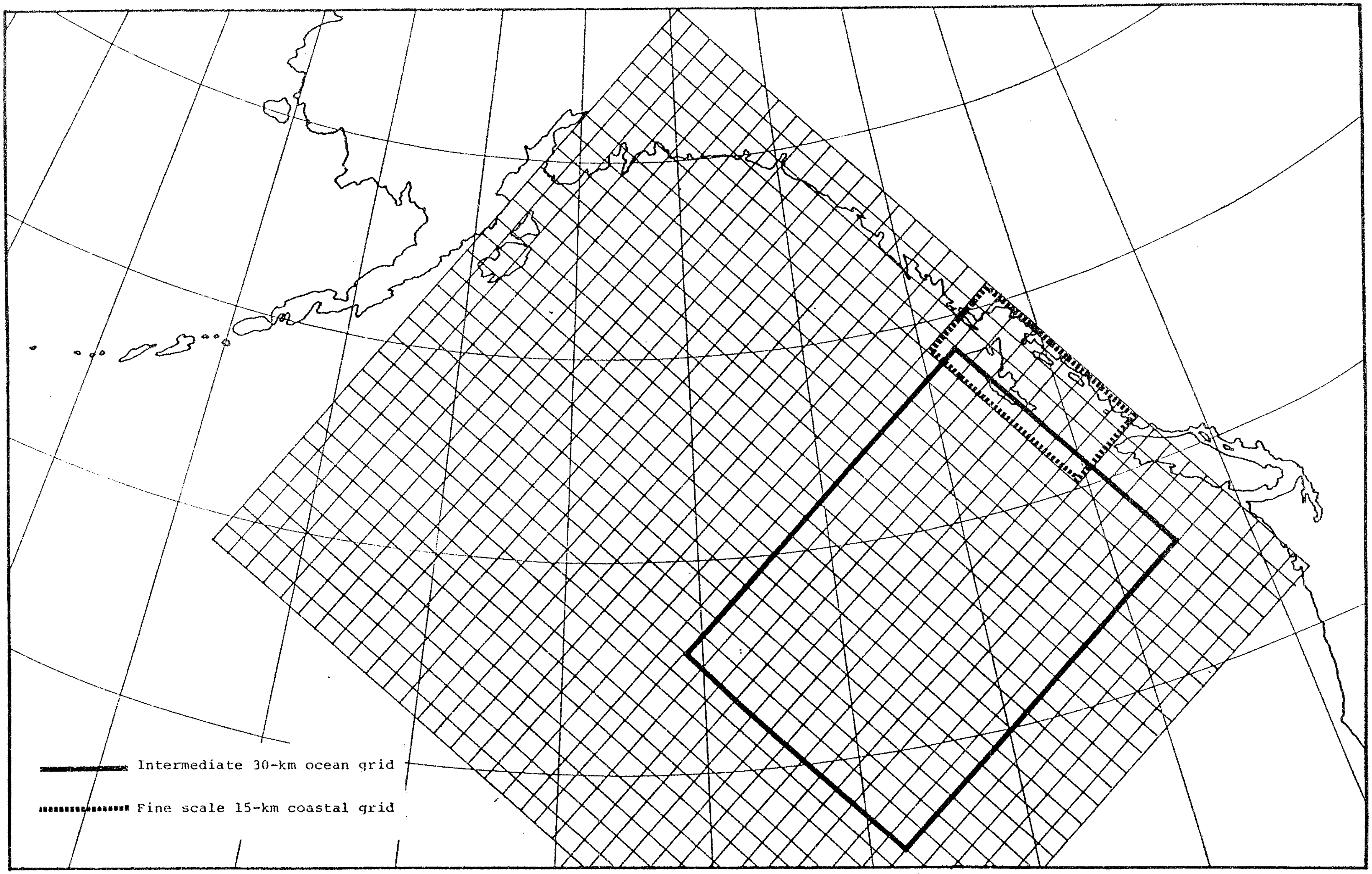

Fig. 4.11 Schematic diagram of one possible configuration of equally spaced nested grids for hindcasting small scale rapidly moving extratropical storms moving onto the British Columbia coast.